Development of Zwitterionic Chromophores and Nonlinear Optical Polymers for Electro-Optic and Near Infrared Chemosensor Applications

By

Wen Hui Hao

A thesis submitted to

the Faculty of Graduate and Postdoctoral Affairs

In partial fulfillment of the requirements for the degree of

Doctor of Philosophy in Chemistry

Carleton University

Ottawa, Ontario

July 2011

Your file Votre référence
ISBN: 978-0-494-83214-1
Our file Notre référence
ISBN: 978-0-494-83214-1

Abstract

To systematically understand the structure and property relationships and development of zwitterionic chromphores and non linear optical (NLO) polymers for applications in organic electro-optic (EO) materials and near infrared (NIR) fluorescent sensing, two series of zwitterionic chromphores, FDCNs (dicyanomethane-based) and PpQDMs (tricyanoquino-dimethane-based) and their corresponding NLO polymers were designed and synthesized. Incorporation of bulky groups onto the central part of FDCN chromophore was demonstrated as an effective strategy to minimize dipole-dipole molecular interaction. Efficient conjugated bridges were extended from dipyridylium donors and coupled with very strong 3CNQ electron acceptors to afford PpQDM chromophores with very large dipole moments and high hyperpolarizabilities. X-ray crystallographic data, negative solvatochromism, IR and NMR analysis confirm the charge-separated ground states of these two series of zwitterionic chromophores.

In addition, FDCN-MMA NLO polymers (**NA2**) were synthesized, in which the chromophore contents reached 14 wt % and exhibited high solubility, thermal stability and film-forming ability. PpQDM-based crosslinkable NLO polyimides were prepared through grafting the hydroxyl-containing PpQDM and BCBO crosslinking unit onto an acid-containing polyimide host. High chromophore loading (13.8 wt %) onto the polyimide was obtained. The T_g values of NLO polyimides were observed to vary due to different pendant groups and different PpQDM loading levels.

Thirdly, the poling conditions were optimized through investigations into various factors such as the molecular shape of the chromophores, the polarity of host polymers, poling voltage, and temperature. A large EO coefficient of 70 pm/V at the

telecommunication wavelength of 1550 nm has been obtained with a 5 wt % PpQDM-Ben doped PVP polymer using an *in situ* poling technique. A buffer layer (PEDOT: PSS/PVA) was first introduced into the double layer EO device, and improvement of the poling efficiency of NLO polymer systems was demonstrated.

Furthermore, PpQDMs are NIR fluorescent with large Stokes shifts and show high microenvironmental (pH, solvent polarity) sensitivity. PpQDM-Met (**M1**) is capable of selectively detecting metal ions (Fe^{2+}, Cu^{2+}) signaled by changes in the absorption and fluorescence. **M1**/copper complex was prepared and demonstrated to be the first high-contrast colorimetric and NIR fluorescence turn-on molecular probe for sensitive and selective detection of cysteine.

Acknowledgements

This thesis would not have been possible without the help and involvement of many people. First of all, I would like to express my deepest gratitude towards my supervisor, Dr. Zhi Yuan (Wayne) Wang, for providing me with such a great opportunity to work on an inspiring project, for his full support, trust and encouragement during my progress. My true appreciation and respect go to him for his knowledge and invaluable guidance in the accomplishment of my study and presentation of this thesis.

Second, my sincere appreciation to Dr. Jane Gao, for all her continuous direction, enthusiasm, expertise, and invaluable advice on various challenges over the last few years. Her devotion and encouragement motivated me during the completion of my Ph.D. study. Special thanks go to my defense committee members Dr. Jianfu Ding, Dr. Jeffrey Manthorpe, Dr. Christopher Boddy and Dr. Steven McGarry.

I wish to thank all my labmates in this project for their pioneer work and fruitful discussions, in particular: Dr. Naiheng Song, Mr. Andrew Beaudin, Dr. Yaowen Bai, Ms. Cara A. M. Weir, Dr. Ying Xiong, Dr. Kunli Wang, Ms. Sabrina Volland and Mr. Kirk M. Mulligan.

I also would like to particularly thank my colleagues, Dr. Gang Qian, Mr. Peter Mirtchev, Ms. Arran McBride and Ms. Skye McBride for your help, contributions and cherished friendships making this thesis work an enjoyable experience.

Many thanks are extended to everyone in Dr. Wang's group: Dr. Hongding Tang, Dr. Erin Todd, Dr. Xun Sun, Dr. Tayebeh Hadizad, Dr. Xianguo Wu, Dr. Shidi Xun, Dr. Geatan LeClair, Mr. Yuxing Cui, Ms. Fatima Hasanain, Mr. Huy Nguyen, Dr. Jia Zheng, Dr. Wenqiang Qiao, Mr. Mathieu Leyre, Dr. Xianzhen Li, Ms. Cathy Wang, Mr. David

Li, Dr. Ning Wang, Mr. Hana Abu and Mr. Sukanta Saha for providing excellent research environments.

I am thankful to Dr. Hooman Shadnia, for his help with the calculation of dipole moments and molecular hyperpolarizabilities, and Professor Jeff Smith, for his help with HRMS measurement. Thanks to Keith Bourque and Tony O'Neil, for all the help with NMR and IR measurements and to Jim Logan, for his help with computer and instrumental set-up for NLO measurement.

I am grateful to NSERC Canada Graduate Scholarship, Ontario Graduate Scholarship, Ontario Graduate Scholarship in Science and Technology and Carleton University for financial support.

Finally, I want to take this opportunity to appreciate my whole-hearted supportive family: my parents, my brother, my husband Xin Jun Cui and our son, David for their immeasurable love, tremendous support and understanding throughout my studies during the past few years.

Table of Contents

List of Tables

List of Figures

List of Schemes

List of Symbols and Abbreviations

β	Molecular first hyperpolarizability
$\chi^{(2)}$	Second-order susceptibility
ε	Dielectric constant
Φ_F	Fluorescent quantum yield
$[\eta]_{inh}$	Inherent viscosity
λ_{max}	Maximum absorption wavelength
μ	Dipole moment, Debye (10^{-18} esu/cm or 3.336×10^{-30} C/m)
r_{33}	Electro-optic coefficient in the poling field direction, pm/V
T_d	Decomposition temperature
T_g	Glass transition temperature
3CNQ	Tricyanoquinodimethane
AC	Alternate current
ACN	Acetonitrile
AIBN	Azobisisobutyronitrile
APC	Amorphous polycarbonate
BCBO	5-Aminobenzocyclobutenone
BLA	Bond-length-alternation
CAEM	2-Cyanoacetoxyethyl methacrylate
CT	Charge transfer
Cys	Cysteine
DBU	1,8-Diazabicyclo[5,4,0]undec-7-ene
DC	Direct current
DCC	Dicyclohexylcarbodiimide
DCM	Dichlomethane
DEMI	4-[1-Cyano-3-diethylamino-2-propenylidene]-2,5-cyclohexadiene-1-ylidenepropanedinitrile
DMAc	N, N-dimethylacetamide
DMAP	4-Dimethylaminopyridine
DMF	N, N-dimethylformide
DMSO	Dimethyl sulfoxide
DSC	Differential scanning calorimetry
EDC	1-(3-(Dimethylamino)propyl)-3-ethylcarbodiimide
EO	Electro-optic
esu	Electrostatic units
FRP	Fluorescence recovery percentage
GSH	L-glutathione
Hcy	Homocysteine

HOMO	Highest occupied molecular orbitals
HRMS	High resolution mass spectroscopy
HRS	Hyper-Rayleigh scattering
IR	Infrared
ITO	Indium-tin oxide
LHS	Left-hand-site
LTC	Leak through current
LUMO	Lowest unoccupied molecular orbitals
n	Refractive index
N-Acys	N-acetylcysteine
NIR	Near infrared
NLO	Nonlinear optical
NMR	Nuclear magnetic resonance
PEDOT	Poly(ethylene dioxythiophene)
PES	Polyethersulfone
PET	Photoinduced electron transfer
PL	Photoluminescence
PMMA	Poly(methylmethacrylate)
PQDM	β-[1-Substituted-4-pyridinium]-α-cyano-4-styryldicyanomethanide (trivial name: pyridinium tricyanoquinonedimethane)
PSS	Poly(styrenesulfonic acid)
PVA	Poly(vinyl alcohol)
PVP	Polyvinylpyrrolidone
RHS	Right-hand-site
TCF	Tricyanofuran
TCNQ	7,7,8,8-tetracyanoquinodimethane
TGA	Thermogravimetric analysis
THF	Tetrahydrofuran
TICT	Twisted intramolecular charge-transfer
UV-Vis	Ultraviolet-visible
Note:	Usual abbreviation are used for amino acids

Chapter 1 Introduction and Background

1.1 Introduction

Zwitterions are molecules, which contain both positive and negative charges at different locations but have an overall net charge of zero. Zwitterionic chromophores are an important type of the intramolecular charge-transfer (ICT) molecules, in which π-conjugated systems are terminated at opposite ends by donor and acceptor moieties ($D^{\delta+}$-π-$A^{\delta-}$; D, donor; A, acceptor; δ, degree of CT) (Figure 1.1). Zwitterionic chromophores have been investigated for their potential as functional materials for dyes, [1]nonlinear optics, [2] photovoltaic[3] and photochromic[4] materials, rectifiers, [5] and conductors.[6]

Many unique and interesting characteristics have been observed for zwitterionic molecules including highly charge-separated ground state, large dipole moment, large negative solvatochromism, and large negative first molecular hyperpolarizabilities (β) as well as small energy gap between the highest occupied molecular orbitals (HOMO) and the lowest unoccupied molecular orbitals (LUMO). In the last two decades, zwitterionic chromophores have found successful applications as nonlinear optical (NLO) chromophores and for molecular recognition.[7]

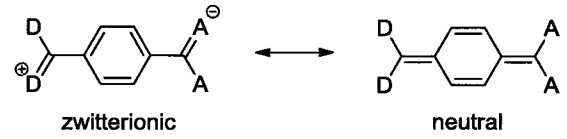

Figure 1.1. Schematic representation of zwitterionic chromophore.

The NLO properties of zwitterionic chromophores and their applications in telecommunications and optical information processing are being actively investigated. Their microscopic NLO efficiencies, characterized by their first molecular

hyperpolarizabilities (β), are related to the electronic ICT excitation between the ground and excited states of the molecules.[8]

The ground state and the first excited state of such molecules can be represented as linear combinations of neutral and zwitterionic limiting forms, and their contributions can be estimated through the use of structural parameters, prominent among which is bond length alternation (BLA),[9] defined as the difference between the average carbon-carbon single and double bond lengths in the polymethine backbone.

According to the "two-state"[10] and the BLA models, the increase of molecular β values comes from the decrease of HOMO-LUMO transition energies or reduction in the BLA of the entire conjugated system and the use of suitable electron donor and acceptor groups. These features facilitate electron delocalization therefore resulting in small optical gaps, occurring the near infrared (NIR) region, in zwitterionic chromophores.

Zwitterionic chromophores have been developed as solvent polarity indicators due to the large negative solvatochromic effect seen in solvents of increasing polarity. The longest wavelength ICT absorption band shifts in a wide range from the ultraviolet-visible (UV-Vis) to NIR region, but unfortunately they are not fluorescent.[11] Selective and sensitive NIR fluorescent dyes have attracted much attention in recent years because they offer distinct advantages in biological, clinical, and environmental analyte sensing. However, few zwitterionic chromophores with small band gap have been explored as NIR molecular fluorescent probes.

Distinctive properties of zwitterionic chromophores depend on the subtle interplay between several factors, such as the strength of the end groups and the connectivity of the π-electron bridge. Understanding the structure and property

relationships is clearly desirable for the successful design and development of new dipolar zwitterionic chromophores as potential NLO materials and NIR fluorescent probes.

The focus of this research is the development of dipolar zwitterionic chromophores and the corresponding polymers for applications as organic electro-optic (EO) materials and for NIR fluorescent sensing. The first major goal of this research was the synthesis and characterization of two new series of zwitterionic chromophores, dicyanodimethane-based (FDCN) and tricyanoquinodimethane-based (PpQDM) (Chapter **2**), their corresponding NLO polymers (Chapter **3**), and a study of their intrinsic electric properties. Additionally, the development of an understanding of the structure and property relationships of these zwitterionic chromophores through primary application in EO materials (Chapter **4**) as well as a study of the photoluminescence (PL) and NIR chemical sensing properties (Chapter **5**) for further successful design of new functional materials. This chapter provides background information on electro-optic materials and fluorescent chemosensors including the rationale for the design of new zwitterionic chromophores.

1.2 Electro-Optic Effect and Organic EO Materials

1.2.1 Basics to Electro-Optic Effect

NLO effects result from the polarization induced in a material by an intense electric field. Organic second-order NLO materials have attracted much attention in the past two decades due to their potential for use in telecommunications, optical data storage and digital signal processing, optical modulation, and many other applications as active

materials in photonic microdevices. [12]

The EO or Pockels effect is one of the most important NLO effects, and refers to the change of the optical properties of noncentrosymmetric materials in response to an applied electric field. Through the Pockels effect, the applied field can modulate the amplitude, phase, frequency, or direction of a light beam, which is one of the most widely used mechanisms in high-speed optical modulation and sensing devices, ultra-fast switches, and frequency-doubling devices. For optical communication technologies, EO modulators serve as the key components to encode high-speed electrical signals on an optical carrier wave.[13] An example of such signal transduction is the encoding of digital electronic computer data onto the optical or photonic internet. Various EO modulators made of inorganic crystals, such as KH_2PO_4 and $LiNbO_3$ have been experimentally demonstrated.[14]

In recent years, there has been growing interest in organic EO materials due to their potential applications in telecommunication, digital signal processing, THz generators, and photonic nano-micro devices.[15] Organic EO materials consist of many nonlinear optically active molecular units-NLO chromophores. NLO chromophores are molecules with extended π-electron conjugation system terminated at opposite ends by donor and acceptor moieties, in which the delocalized electron density can be polarized easily in response to an applied electric field (Scheme 1.1). These chromophores may be combined in pure form or dispersed in an optically inactive matrix such as a polymer.

Scheme 1.1. Typical structure of NLO chromophores.

In the case of an isolated chromophore, the application of a relatively weak electro-magnetic field induces a polarization (P) of electron density that is proportional or linear to the applied field,

$$P=P_0+\alpha_{ij}E_j \qquad \text{(eq.1)}$$

where P_0 represents the equilibrium polarization, α_{ij} denotes a particular tensor element of the linear polarizability, and E_j is a vector component of the applied electric field. In bulk materials, the field versus polarization description becomes:

$$P=P_0+\chi^{(1)}{}_{ij}E_j \qquad \text{(eq.2)}$$

where $\chi^{(1)}{}_{ij}$ represents linear susceptibility. When an optical field of a particular frequency interacts linearly with a material, the material exhibits a time varying polarization response proportional to its intensity. This response serves to alter the incident field as to create a new field that is of the same frequency, in which the propagating wave is phase-shifted in time with respect to the incident field. The magnitude of this phase shift is proportional to the index of refraction (n) of the material.

When a sufficiently intense optical field, such as laser radiation, interacts with the material, the description of the response needs to be expanded to include nonlinear (higher order) polarization terms. On the single molecule level and the bulk level, this is described by eq.3 and eq.4.

$$P=P_0+\alpha_{ij}E_j+\beta_{ijk}E_jE_k+\gamma_{ijkl}E_jE_kE_l \qquad \text{(eq.3)}$$

where β_{ijk} and γ_{ijkl} are the frequency dependent first and second molecular hyperpolarizabilities, respectively.

$$P=P_0+\chi^{(1)}{}_{ij}E_j+\chi^{(2)}{}_{ijk}E_jE_k+\chi^{(3)}{}_{ijkl}E_jE_kE_l \qquad \text{(eq.4)}$$

where $\chi^{(2)}_{ijk}$ and $\chi^{(3)}_{ijk}$ denote the first and second nonlinear susceptibilities, the subscripts *i, j* and *k* refer to a molecule-based coordinated system.

Unlike the linear case, time-varying nonlinear polarization effects give rise to new fields of altered frequency with respect to the incident radiation. This phenomenon results in second harmonic generation (SHG) in the case of $\chi^{(2)}_{ijk}$ and third harmonic generation (THG) in the case of $\chi^{(3)}_{ijk}$. In addition to frequency alternation in the form of SHG, first nonlinear susceptibility, $\chi^{(2)}_{ijk}$, gives rise to an electric field dependent effective combined susceptibility. This accounts for the Pockels effect in which control of electromagnetic susceptibility and refractive index is affected by application of a low-frequency electric field.

In a bulk material, nonzero even-order susceptibility $\chi^{(2)}$ can only come from noncentrosymmetric media. A bulk material consisting of many molecularly asymmetric chromophores, the need for overall noncentrosymmetry imposes the additional requirement of molecular alignment in order to achieve a finite macroscopic second-order nonlinear optical activity. $\chi^{(2)}_{zzz}(\omega)$ (the principle element of the nonlinear susceptibility tensor at frequency ω is related to the molecular parameters by:

$$\chi^{(2)}_{zzz}(\omega) = Nf\beta(\omega, \varepsilon) \langle \cos^3\theta \rangle \qquad \text{(eq.5)}$$

where N (molecules/cm^3) denotes the number density of active molecules that interact with the incident optical field, β_{zzz} is the hyperpolarizability tensor element coincident with the molecular symmetry axis, which is dependent on the wavelength (frequency, ω) of the incident light field, [16] and the dielectric permittivity (ε) of the electro-optic material.[17] θ is the angle between the field direction and the *z*-direction. The term of $\langle \cos^3\theta \rangle$ is the average molecular acentric order parameter denoting the extent of

chromophore alignment relative to the laboratory *z*-axis. The *z*-axis is parallel to the applied poling field, in electric field poled materials, as well as the field vectors of the optical and electrical operating fields in the case of an EO device. *f* is the local field factor taking into account the attenuation of applied electric field by the dielectric properties of the host.[18]

The EO effect is an electric field dependent change in refractive index utilized in many photonic device applications including EO modulators for electrical-to-optical signal transduction. EO modulators operate by impressing an electronic signal onto a laser beam, thereby altering the phase and amplitude of the light passing through it; it acts as an ultrafast shutter, blocking and unblocking the laser beam, thereby creating a signal. This control over the phase and frequency of an electromagnetic wave propagating through the material can be expressed by eq.6 in terms of applied field (E) and refractive index (n).

$$E = -2\Delta n/r_{33}n^3 \qquad \text{(eq.6)}$$

where Δn is the change in refractive index experienced by the propagating electromagnetic wave and r_{33}, the EO coefficient, denotes the magnitude of phase (refractive index, Δn) shift obtained for an applied low-frequency electric field and is given in units of pm/V. This EO coefficient is determined by the following equation:

$$r_{33} = -2\chi^{(2)}_{zzz}(\omega)/n^4 \qquad \text{(eq.7)}$$

where the subscript 3 indicates the poling field direction, z is the direction along which the molecular permanent dipole moment occurs and n is the refractive index of the EO material.

Therefore, the r_{33} of a noncentrosymmetric material can be related to the second-order susceptibility $\chi^{(2)}$ and the molecular β by combination of eq.5 and eq.7.

$$r_{33} = 2 < \chi^{(2)}_{zzz} > /n^4 = 2Nf < \beta(-\omega;\omega,0) > /n^4 = 2Nf\beta < cos^3\theta > /n^4 \quad \text{(eq.8)}$$

Equation 8 demonstrates the three most important factors in the optimization of $\chi^{(2)}_{zzz}(\omega)$ and in turn, $r_{33}(\omega)$: molecular first hyperpolarizability, chromophore number density, and acentric order need to be maximized simultaneously.

In the case of π-conjugated dipolar molecules, β_{zzz} is largely determined by molecular composition and can be tuned using synthetic chemistry; unfortunately, N and $<cos^3\theta>$ are not independent due to strong inter-chromophore electrostatic interactions. As the density of the highly dipolar chromophores increases, the average distance between them decreases and strong dipole-dipole interactions begin to compete with ordering forces such as the poling field. Therefore, the loading parameter N ($<cos^3\theta>$) must be optimized using molecular engineering approaches to control chromophore shape, lattice attachment geometry, solubility, etc. [19]

1.2.2 Molecular Hyperpolarizability

The first molecular hyperpolarizability, $\beta_{zzz}(\omega, \varepsilon)$ of dipolar NLO chromophores relies on the ground state electron density distribution asymmetry, which can be tuned through the asymmetric substitution of a π-electron-conjugated bridge with the appropriate donor and acceptor moieties. According to the simple two-state theoretical model by Oudar and Chemla, [20] the molecular β can be expressed as:

$$\beta_{zzz} \propto \frac{\Delta\mu_{eg}(\mu_{ge})^2}{E_{ge}^{\ 2}} \quad \text{(eq.9)}$$

where $\Delta\mu_{eg}$ represents the difference in dipole moment between the HOMO and the LUMO; μ_{ge} represents the transition dipole moment (oscillator strength) and E_{ge} represents the energy difference between ground (HOMO) and charge transfer excited states (LUMO).

Typically, stronger electron-density donors and acceptors as well as a longer conjugated bridging unit lead to a larger β_{zzz} (ω, ε). This rule works well for chromophores consisting of an aromatic bridge that partially energetically impedes polarization. However, the use of powerful donor/acceptor pairs or a particular conjugated interconnect, such as polyphenylene, does not necessarily lead to the realization of optimal β values, an optimal combination of donor and acceptor strengths has to be matched for maximization of the μβ value. [21]

This behaviour may be understood by another theory in terms of BLA, proposed by Gorman and Marder,[9] which correlates β with the degree of charge separation in the ground state (Figure 1.2) and in turn is dependent on the chemical structure and environment of the chromophore, due to the induced ground state polarization. [22] For dipolar molecules, BLA can vary from positive to zero and to negative, depending on the relative contributions of neutral and charge-separated resonance form to the ground state, which in turn depends on the donor and acceptor strengths. For the given donor and acceptor groups, the magnitude of BLA depends on the transition energy, which is dependent on the nature and the length of the π-conjugated bridge.[23]

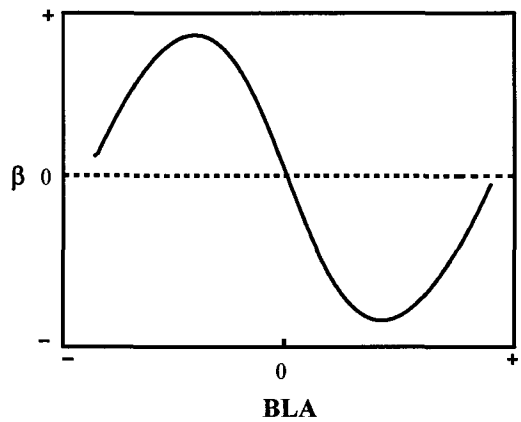

Figure 1.2. Relationship between molecular first hyperpolarizability and bond length alternation.

Two maximum β vales were predicted by BLA theory. A positive BLA value characterizes a neutral state where as a charge-separated (or zwitterionic) state is characterized by a negative BLA value. The negative sign of β for zwitterionic molecules indicates that the direction of ICT in these molecules is opposite to that in neutral molecules. If both resonances have an equal contribution, no BLA is observed and β becomes zero; this situation is referred to as the cyanine limit (Figure 1.3).

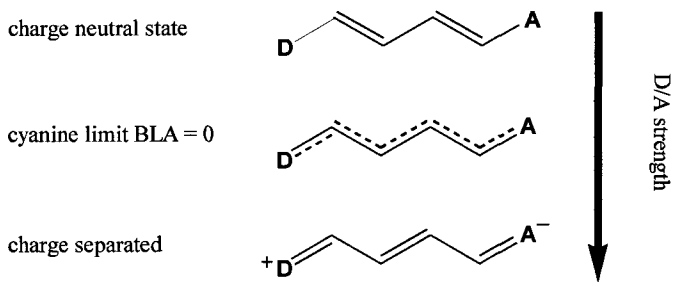

Figure 1.3. Ground state resonance forms of donor-acceptor polyene.

A large positive BLA and a small positive β value result for a chromophore which has weak donor and acceptor groups. In this case the neutral state dominates the ground state; upon increasing the strength of the donor and acceptor, the contribution of the

charge-separated state increases, resulting in a decreased BLA which passes through zero. As the strength of the donor and acceptor continue to increase eventually the charge-separated ground state dominates, leading to a reverse pattern with a negative BLA and a negative β value. Therefore, two local maximum β values can be found, in the positive region for neutral chromophores[24], and in the negative region for zwitterionic chromophores.[25]

1.2.3 Neutral Nonlinear Optical Chromophores

The past three decades have seen a large library of second order NLO chromophores developed and characterized with initial focus on simple para-substituted stilbenes (e.g., DANS in Figure 1.4).[26] These early systems did not lead to the expected high EO active materials; until 1990's, the BLA theory supported by the two-state model gave insight into the structure property relationship for both neutral and zwitterionic NLO chromophores. As a result, careful selection of donor, acceptor and conjugated bridge is crucial for a maximized molecular hyperpolarizability of a molecule.

1.2.3.1 Electron Donors

A large number donor groups capable of contributing electron density have been explored over the past decade. Although sulphur and oxygen based donors have also been explored, [27] the most successful type donor structure falls into the general class of alkyl and aryl amines as a result of their strong electron-donating properties and thermal stability.[28] Although no great difference between the alkyl and aryl amines has been reported, studies have indicated that a larger μβ value could result by using diarylamine than by using dialkylamine. [29] In the correct geometry, the energy level of the nitrogen

nonbonding lone pair is well matched to donate into the π^* orbital of the attached aromatic ring. This arrangement destabilizes the HOMO and reduces ionization potential creating a strong electron density donating effect. However, the degree of ground state polarization is not sufficient to maximize the β value due to the loss of the aromaticity in the charge-separated form upon polarization.

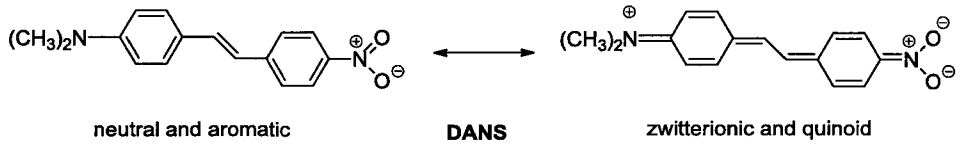

$\mu\beta \sim 500 \times 10^{-48}$ esu at 1.9 μm

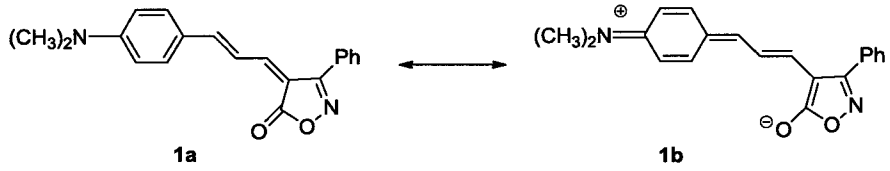

$\mu\beta = 1{,}202 \times 10^{-48}$ esu at 1.9 μm

Figure 1.4. Resonance forms of DANS and **1**.

An effective strategy to solve this problem was proposed in designing new dipolar chromophores with aromatic acceptors, in which the loss of aromatic stabilization in one part would be compensated by a gain in aromaticity in another part. In addition, this strategy can result in an increased ground state dipole moment (μ). For example, 3-phenyl-5-isoxazolone was introduced as the acceptor to chromophore **1**,[4a] the μβ value of **1** became much higher than that of DANS, which is similar in conjugation length to **1** (Figure 1.4).

Another approach to improve the μβ value is replacement of benzene rings in the π-bridge with heteroaromatics such as thiophene [30] (**2**, Table 1.1) and thioazole [31] (**4**,

Table 1.1). These heterocyclic rings have lower aromaticity energy than that of benzene, and as a result offer more contributions to the ground state, reduce the BLA and improve the thermostability of these chromophores.

Table 1.1. Chromophores contains thiophene and thioazole moieties

Name	Structure	$\mu\beta$ ($\times 10^{-48}$ esu) at 1.9 μm	Ref.
2	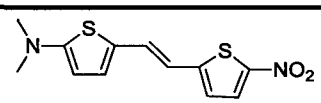	1040	30
3	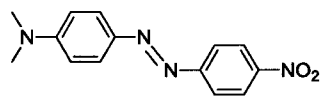	800	31
4	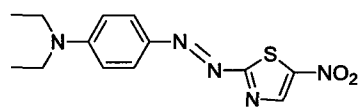	2190	31

As shown in Table 1.1, by replacing the benzene ring with thiophene, the μβ value increases from 500 × 10^{-48} esu for DANS to 1040 × 10^{-48} esu for chromophore **2**; and replacing the benzene ring with thioazole, the μβ value increases from 800 × 10^{-48} esu for **3** to 2190 × 10^{-48} esu for chromophore **4**. Both designs proved efficient in increasing the μβ values.

1.2.3.2 Electron Acceptors

Like electron donors, a large number of electron accepting groups with diverse chemical structures have been prepared over the past decade. More recently, the tricyanofuran-based (TCF) acceptor family, were developed and tested to be most promising due to the high chemical, thermal, and photostability with strong electron affinity.[32]

Table 1.2. Chromophores with modified acceptors

Name	Structure	$\mu\beta$ ($\times 10^{-48}$ esu) at 1.9 μm	Ref.
5	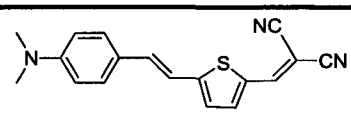	1300	33
6	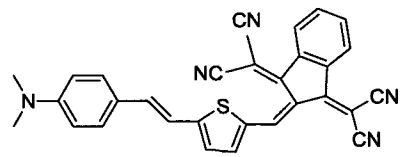	6100	33
FTC	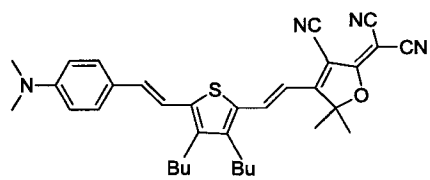	18000	34

Table 1.2 shows the examples (**5**, **6** and FTC) that have primarily the same donor and π-conjugate bridge but different acceptor groups. Increases in the μβ values of about 10 times are observed upon changing the dicyanovinyl electron acceptor for **5** [33] to more efficient TCF electron acceptor for FTC.[34]

Following the success of such materials based on the unfunctionalized TCF acceptor, [35] significant effort has been focused toward chemical modifications that improve electron affinity, allow secondary functionalization, or modify the shape of the chromophore. Several modified TCF structures are shown in Figure 1.5. Simple TCF (**A1**) is illustrated for comparison. In simple chromophores, switching the acceptor from TCF to CF3-TCF (**A3**) may significantly reduce the optical band gap ΔE_{ge} by as much as 0.3-0.5 eV and roughly double the β value. [36]

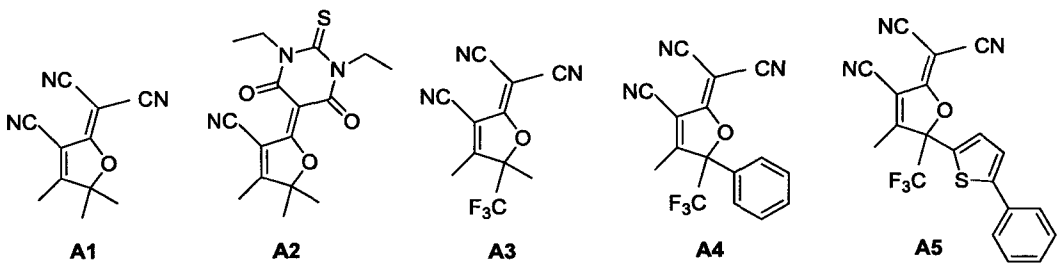

Figure 1.5. Modified electron acceptor structures of TCF class.

1.2.3.3 Bridges and Chromophores

A number of parameters must be satisfied when selecting a suitable conjugated bridge, including thermal and chemical stability, electronic character and maximizing β. Generally, an increase in conjugation length leads to an increase in observable molecular hyperpolarizabilty as seen in chromophores **7-10** (Table 1.3). For a given donor-acceptor chromophore, upon addition of one ethylene unit in the π-bridge, μβ value increases from 6700 × 10^{-48} esu for **7** to 9800 × 10^{-48} esu for **8**.[37] A doubling of μβ value for **9** was observed upon insertion of each additional ethylene unit into the π-bridge.[38] However, increasing the polyene length does not represent a practical approach to optimization of the molecular μβ value. First, beyond certain conjugation lengths the polarization saturates. Additionally, since the absorption show a bathochromic shift with increasing the length of conjugation, absorbance in the telecommunications wavelengths becomes an unfavourable possibility. Furthermore, increases in conjugation length can also lead to lowered chemical and thermal stabilities.[39]

Table 1.3. Effect of conjugation length on μβ value

Name	Structure	$\mu\beta$ ($\times 10^{-48}$ esu) at 1.9 μm	Ref.
7	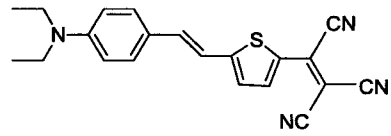	6700	37
8	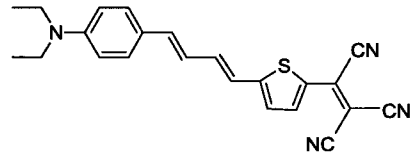	9800	37
9	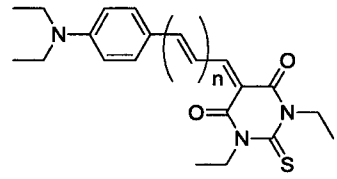	1457(n=1) 3945(n=2) 9831(n=3)	38
10	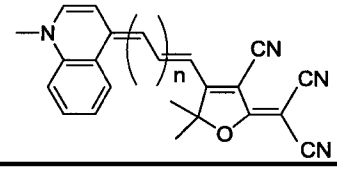	6820(n=0) 7112(n=1) 9384(n=2)	39

Incorporation of aromatic bridges usually leads to good thermal and photochemical stability due to the aromaticity of the ring lowers the energy of the HOMO consequently reducing the susceptibility of the chromophore to oxidation and chemical reaction; however, hyperpolarizability is reduced compared with the use of a polyene bridge. A compromise has been reached by using heterocyclics such as thiophenes, furans and pyroles, which offer lower delocalization energies when compared to aromatic rings and also better thermal stabilities when compared to the polyenes. [40]

Successful design is represented by the FTC (Figure 1.6, left), [41] thiophene-based bridges offer an attractive compromise between large β value and stability under a wide range of chemical synthesis conditions.

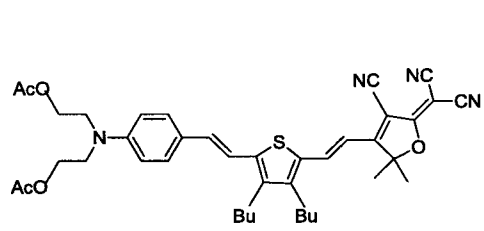

FTC (μ =12D)

$\mu\beta$ = 17,600 × 10^{-48} esu at 1.9μm

r_{33} = 55 pm/V (20 wt % in PMMA)

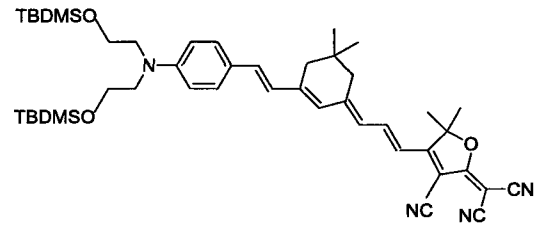

CLD (μ =13D)

$\mu\beta$ = 14,065 × 10^{-48} esu at 1.9μm

r_{33} = 92 pm/V (25 wt % in APC)

Figure 1.6. Two neutral benchmark chromophores FTC and CLD.

Recently, sterically protected (ring-locked) polyenes were successfully exploited in the π-bridging structures to increase the conjugation length and to produce high-μβ chromophores with good thermal stability.[42,43] A typical example is CLD, developed by Dalton and coworkers (Figure 1.6), in which the ring locked olefinic moiety is incorporated in the polyenes bridge to improve chemical and thermal stabilities, enforce a trans conformation of the polyene to increase an effective conjugation, and to change the shape of the chromophore reducing intermolecular interactions.[24]

FTC and CLD-type chromophores are two standard neutral chromophores, which have shown significant enhancement of the molecular μβ values (greater than 15000 × 10^{-48} esu at 1.9μm) and good thermostability has been demonstrated through optimization of the conjugation bridge structure and donor/acceptor pairing.

1.2.4 Zwitterionic Nonlinear Optical Chromophores

According to Marder's plot (Figure 1.2), two maxima of the β occur on either side of the cyanine limit, a positive β on the left-hand-site (LHS) refers to chromophores with neutral ground states, and a negative β on the right-hand-site (RHS) refers to

chromophores with zwitterionic ground states. Even though the absolute value of β is the only consideration, NLO chromophore synthesis has focused predominantly on traditional neutral push-pull systems, and little attention has been paid to zwitterionic chromophores. Zwitterionic dyes were developed initially as solvent polarity indicators due to their large negative solvatochromism. Compounds exhibiting solvatochromism are also of potential interest as materials that may exhibit the NLO property under the appropriate conditions. Recently, several zwitterionic dyes have found successful application as NLO chromophores due to their extremely large μβ values.[2c] Better-designed zwitterionic chromophores are developing since their electronic and structural properties are of considerable interest for new applications.

According to structure, some representative zwitterionic chromophores were classified and shown in Table 1.4 to Table 1.6. The charge-separated ground states of these chromophores are inferable from their strong negative solvatochromism and were demonstrated by the X-ray crystallography and theoretical modeling.[44, 45]

1.2.4.1 Betain Dyes and Merocyanine Dye

The first class is Betain dyes (**11, 12**) and merocyanine dyes (**13, 14**), which both show characteristically large negative solvatochromism (Table 1.4). Solvatochromism is the ability of a chromophore to exhibit a change in colour as a result of a change in solvent polarity. The absorption shifts results from a difference of dipole moments in ground and excited states of the chromophore. Negative solvatochromism refers to a hypsochomic (blue) shift occurring when the chromophore has a charge-separated ground state. Positive solvatochromism refers to a bathochromic (red) shift when the chromophore has a neutral ground state. In the case of negative solvatochromism, an

increase in solvent polarity stabilizes the ground state of zwitterionic chromophores, and an increase in the energy gap between the polar ground and non-polar excited states occur. This energy change in turn affects the absorbance and emission position as well as the shape of the resulting UV/Vis/NIR and PL spectra.

Table 1.4. Representative betain dyes and merocyanine dyes

Name	Structure	Properties	Ref.
11,12	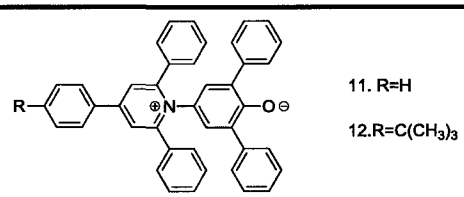 11. R=H 12.R=C(CH$_3$)$_3$	$\Delta\lambda_{max}$= -357 nm (λ_{water}-λ_{ether}) μ = 15D	11
13	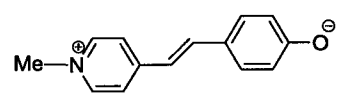	$\Delta\lambda_{max}$= -128 nm (λ_{MeOH}-λ_{CHCl3}) $\mu\beta$= -7600×10^{-48} esu	46
14	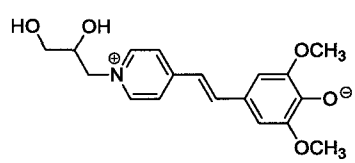	$\lambda_{NaOH\ aq}$ = 500 nm $\mu\beta_0$= -6914×10^{-48}esu [a]	47

[a] β_0: zero-frequency molecular first hyperpolarizability

In particular, **11** and its more lipophilic derivative **12** (soluble even in hydrocarbons) are the basis of the $E_T^{(30)}$ scale. Upon excitation, electron transfer occurs from the oxygen atom to the center of the aromatic system. The dipole moment is about 15 D in the ground state whereas it is nearly zero in the excited state.[11] The longest wavelength ICT absorption band is hypsochromically shifted by 357 nm on going from diphenyl ether (λ_{max}= 810 nm) to water (λ_{max}= 453 nm).

1.2.4.2 Polyphenylenes Bridge /Tricyanofuran-Based Acceptor

The second class is phenylpolyenes end-capped with aromatic donor and the strong tricyanofuran-based (TCF) acceptor groups (**15, 16**), which exhibit large μβ values through complicated syntheses (Table 1.5).

Table 1.5. Zwitterionic chromophores containing polyphenylenes bridge /TCF acceptor

Name	Structure	Properties $\mu\beta_0$ ($\times 10^{-48}$ esu)	Ref.
15	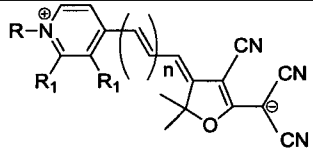 a:R=CH_3;R1=H;n=1 b:R=CH_3;R1=H;n=2 c:R=CH_3;R1=H;n=3	a: λ_{DMF} = 570 nm; $\mu\beta_0$ = -2213 b: λ_{DMF} = 600 nm; $\mu\beta_0$ = - 6444 c: λ_{DMF} = 615 nm; $\mu\beta_0$ = -8900	25a
16	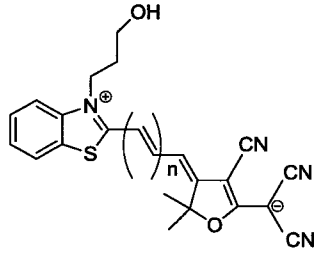 a:R=CH_3;R1=H;n=1 b:R=CH_3;R1=H;n=2 c:R=CH_3;R1=H;n=3	a: λ_{DMF} = 605 nm; $\mu\beta_0$ = -2496 b: λ_{DMF} = 705 nm; $\mu\beta_0$ = -3354 c: λ_{DMF} = 810 nm; $\mu\beta_0$ = N/A	25a

1.2.4.3 Heteroaromatic Ring Containing π-Bridge

The third class are molecules containing heteroaromatics (e.g., thiophene) in the π-bridge, whose reduced ring aromaticity relative to benzene leads both to an increased transition moment and to a change in dipole moment (Figure 1.7).[48]

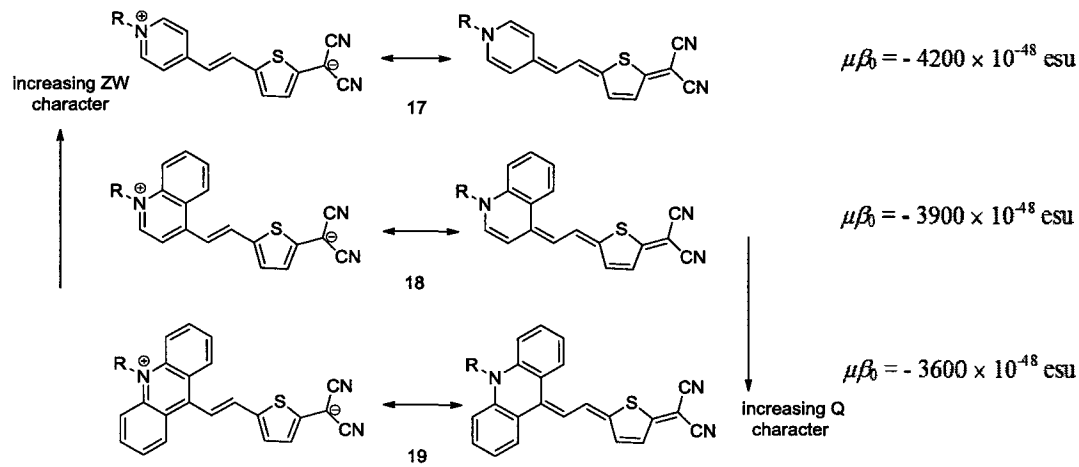

Figure 1.7. Zwitterionic chromophores containing heteroaromatic ring in the π-bridge.

In comparison with neutral chromophores of comparable sizes (e.g. **5**: $\mu\beta_{1.9\mu m}$ = 1300 × 10^{-48} esu), zwitterionic chromophores (**17-19**) containing thiophene in the bridge exhibit much larger μβ value and the increased dipole moment (e.g., **17**: μ = 20 D in dioxane; **7**: μ = 6 D)

Also the μβ values are dramatically influenced by large orders of magnitude, by a consecutive annelation of the pyridyl ring of these chromophores (pyridine-quinoline-acridine) and medium polarity. In polar media, the ground states of these chromophores can be described as linear combinations of zwitterionic and quinoid forms. Figure 1.7 clearly shows that, the importance of the zwitterionic form sequentially decreases, and the quinoid form simultaneously increases, ongoing from pyridine **17** to quinolone **18** to acridine **19**. The main reason is that the pyridine ring loses aromaticity in the right-hand side formula and the acridinium ring can better sustain a quinoid character due to the restored full aromaticity of the two benzene side rings. In less polar media, negative β values were obtained only in **17**, and become positive and increase from **18** to **19**. The

annelation effect explains the reasons behind why quinolone and acridine rings have hardly been used in designing new dyes with optimized β values.

1.2.4.4 D^+–π–A^- Tertiary Amine/ 3CNQ-Based Zwitterionic Chromophores

The fourth class are D^+–π–A^- tertiary amine/ tricyanoquinodimethane-based (3CNQ) zwitterionic chromophores, which have been extensively studied of their NLO properties (Table 1.6).

Table 1.6. D^+–π–A^- tertiary amine/3CNQ adducts

Name	Structure	Properties	Ref.
DEMI	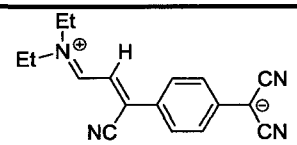	λ_{DMF} = 693 nm $\mu\beta_0$ = - 9450×10^{-48} esu	4b
PQDM	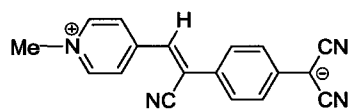	λ_{DMF} = 694 nm $\beta_{1.06\ \mu m}$ = -1270×10^{-30} esu	3
QQDM	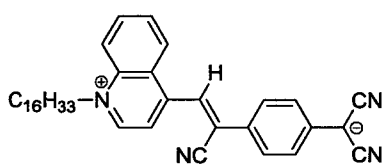	λ_{MeCN} = 712 nm $\chi^{(2)}_{zzz}$ = 180 pm/V	49

3CNQ is one of the best acceptors known to date, where the gain in aromatic stability from a one electron reduction is the large driving force behind this powerful acceptor. The 3CNQ acceptor is based on the electron acceptor 7,7,8,8-tetracyanoquinodimethane (TCNQ), which was first reported in 1960[50] and is well known to form semi-conducting salts since TCNQ readily accepts an electron to form stable anion radicals. TCNQ has also been shown to react with tertiary amines such as triethyl amine and 2- or 4-methylquinoline to form stable zwitterionic molecules, DEMI and

PQDM, respectively. These TCNQ derivations have also shown multifunctional properties as molecular rectification[5a] and photochromic behaviour.[51]

DEMI has displayed very large μβ value at zero frequency when compared to push-pull systems of similar length due to the aromatic stability gained by the 3CNQ acceptor when in the charge-separated state. Due to the low requirement for extensive conjugations in yielding large μβ values, zwitterionic chromophores are typically easier to be prepared than neutral chromophores.

However, despite the large μβ values and ease in preparation, DEMI suffers from very low solubility due to its very planar structure, and a strong tendency to form anti-parallel aggregates. Furthermore, the olefinic interconnect is very sensitive to both heat and light. To be usable in practical EO applications, the donor moiety of this class of zwitterionic chromophores must be optimized to meet the required properties. Considering the pyridium-based analogue PQDM, although no μβ value were reported, comparative studies by Cross and co-workers [52] indicated a larger β_0 (-1270×10^{-30} esu) for PQDM than that for DEMI ($\beta_0 = -350 \times 10^{-30}$ esu) and predicted a large EO coefficient will be realized in a suitable polymer host.

Most recently, Marks' group[2c] reported the development of TMC twisted intramolecular charge transfer (TICT) chromophores consisting of a conjugated donor-bridge-acceptor π-electron system, which provides rotation about the CT axis. Unlike the planar π-electron system of most dipolar zwitterionic chromophores, the π-electron conjugation is broken in the twisted biaryl molecules. Theoretical studies have predicted that the degree of rotation modulates the π-orbital overlap resulting in electric field induced nonlinear polarization is maximized at an optimum dihedral angle of $\theta \approx 70°$-$85°$.

TICT chromophores reported so far consist of substituted biaryl compounds characterized by charge-separated ground states (Figure 1.8), whose calculated β and μβ values (~70,000 × 10^{-48} esu) can be two orders of magnitude larger than that of DANS.

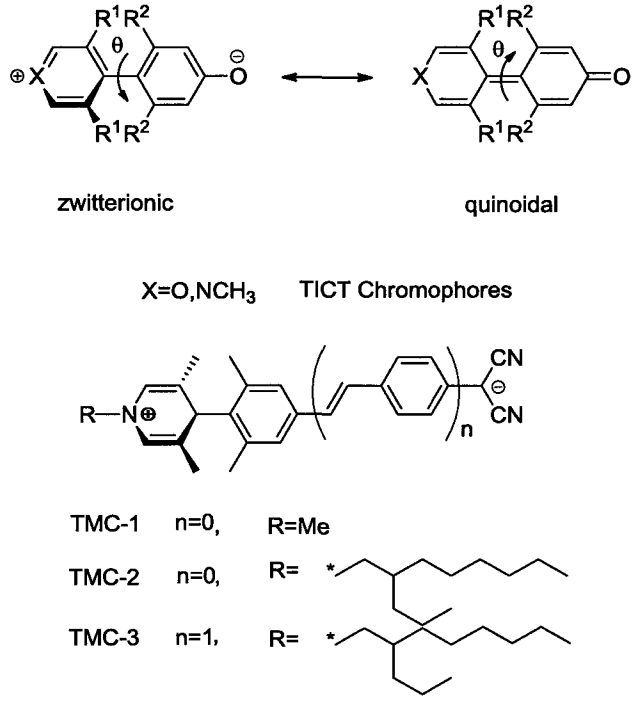

Figure 1.8. TICT and TMC chromophore strucutrs.

The new generation TMC chromophores have large twist angles and exhibit extremely large μβ value. For example, the twist angle (θ) in TMC-2 is 89.6° determined by X-ray diffraction. The hyperpolarizability and dipole moment for extended conjugated molecule TMC-3 was measured as $\mu\beta$ = -488, 000 × 10^{-48} esu (λ_{exp} = 1.907 μm) using the electric field induced second harmonic generation method (EFISH), which is much larger than that of CLD ($\mu\beta$ = 35, 000 × 10^{-48} esu, EFISH, λ_{exp} = 1.907 μm).

Unlike the conventional planar chromophores, TICT chromophores with large optical nonlinearity can be simple compounds consisting of two substituted arene rings

such as TMC-1. Therefore, they exhibit good thermostability and enhance the resistance to photochemical/oxidative degradation. TMC-3 possesses a ground state dipole moment as large as 50.6 D (calculated by DFT method). This large dipole moment, combined with the reduced solubility typically displayed by zwitterionic chromophores, causes this type of chromophore to aggregate aggressively. EO coefficient of TMC-3 was measured to be 330 pm/V in a polar polyvinylphenol host, using the Teng-Man technique under an applied poling field of 100 V/μm. However, this extraordinarily high r_{33} value has so far only been measured by *in situ* (constant poling bias) methods.[4c]

To reduce aggregation, two strategies must be taken into account in preparing EO materials containing TICT chromophores either by synthetic modification of the TICT molecule or by choosing an appropriate polymer hosts.

1.2.5 Development of Nonlinear Optical Polymers

Polymers containing NLO active chromophores have emerged as a promising class of EO materials.[53,54] These materials are typically made from organic chromophores with high microscopic molecular hyperpolarizabilities, incorporated into polymer matrixes, and poled with an external applied electric field at or near the glass transition temperature (T_g) to achieve a noncentrosymmetric dipole alignment.

The polymeric NLO materials have received increasing interests in EO applications because of their high NLO susceptibility, low dielectric constant, fast response time, small dispersion in refractive index, structural flexibility, and ease of material processing. The most striking advantage of poled polymers results from their unique EO mechanism that arises mainly from electronic excitations in individual

nonlinear molecules by the displacement of electrons not ions, as in inorganic materials, so polymer can provide a much large bandwidth in high frequency operations.[54]

The development of NLO polymers depends on the successful incorporation of the NLO chromophores into a polymer matrix, the poled polymers can be classified into two systems: 1) guest-host systems, where the NLO chromophores (guests) are doped into a polymer (host), 2) substituted systems, where the organic chromophores are covalently bound to a polymer backbone.

1.2.5.1 Guest-Host Polymers

Guest-host systems are the simplest approach to screen NLO chromophores and EO materials, where the chromophores are physically incorporated into a polymer host. They facilitate the combination of different polymer matrixes and chromophores without any complicated chemistry, but suffer from several drawbacks including 1) low concentration of chromophores that can be doped in the polymer without aggregation. Aggregation changes the spectroscopic properties, increases the scattering losses, and limits the mobility of the chromophores, hence, usually reducing the EO response of the system; 2) low temporal stability of the orientation. In general, the stability depends strongly on the local environment provided by the polymer matrix. For practical application, the T_g of a guest-host NLO polymer should be at least 100 ^{o}C higher than the ultimate operating temperature. Recently, a few thermally stable guest-host systems were successfully established by doping NLO chromophores into higher glass transition temperature polymers, such as amorphous polycarbonate (APC), polyethersulfone (PES), polyquinolines and polyimide. [55,56]

1.2.5.2 Side-Chain and Crosslinkable NLO Polymers

The most traditional way to increase chromophore concentration and the temporal stability of the orientation is to covalently attach the chromophores onto the polymers. Side-chain NLO polymers where the chromophore is attached as a side-chain to the backbone, and main-chain NLO polymers where the chromophore is incorporated into the backbone itself are two examples. Main-chain NLO polymers receive relatively little attention because the preparation highly depends on the purity of chromophore-containing monomer, also the expected large dipole moment cannot be obtained due to the chain entanglements[57], and poling is much more difficult due to the hard large segmental motions of the polymer backbones.

Compared to main-chain NLO polymers, side-chain polymers represent a more versatile approach to chromophore-linked systems. First, there is significant flexibility in optimization of properties for side-chain NLO polymers through modification of backbone structures, adding side groups, and introduction of crosslinking functionalities. Second, the additional distance that separates the chromophores from the backbones due to the pendent nature of these systems allows for better alignment during the poling process. The restricted mobility improves the stability and helps to reach higher concentrations without aggregation. Furthermore, side-chain NLO polymers can be synthesized either by copolymerizing chromophore-containing monomers or through a post-functionalization, which allows various types of NLO chromophores can be grafted into the polymer under mild conditions, and for the preparation of host polymer capable of undergoing further modifications.

Good thermal stability of poling-induced dipole order of side-chain NLO polymers can be achieved by grafting NLO chromophores into high-T_g polymers such as polyurethane, [58] and polyimide.[59]

Polyimides are the most promising high T_g polymers for EO study due to their good mechanical strength, low optical loss, good compatibility with highly polar NLO chromophores, (e.g., PQDM)[60] and can be easily modified by using different polymerizing monomers. The preparation of NLO polyimides typically involves various post-functionalizations and addition polymerization.[61] First side-chain NLO polyimide was prepared by condensation of hydroxyl-functionalized polyimide with the acid-containing CLD chromophore.[62] A high chromophore loading (25 wt %) and a high EO coefficient (71 pm/V) at 1.3 μm were achieved.

Another way to improve the stability is crosslinking. The crosslinking can be done either before or after the orientation process. However, reduced EO activity was often observed because that spontaneous crosslinking and poling process often proceed together making it difficult to align the dipolar chromophores efficiently. Recently, Jen's group demonstrated an effective strategy to improve the poling efficiency by employing a new cross-linkable system based on the thermally reversible Diels-Alder reaction, the polymer crosslinking while cooling after the poling process. A good temporal stability (~80% of the original r_{33} value) of the cross-linkable NLO polymer was obtained.[63]

1.3 Chemosensor Chemistry and Near Infrared Fluorescent Sensors

1.3.1 Basics to Chemosensor

Selective and sensitive chemosensors are molecules specifically designed for the qualitative and quantitative monitoring of analytes. A chemosensor can be regarded as "a receptor that interacts with an analyte producing a detectable change in a signal".[64] The changes in physical properties of a chemosensor such as absorption and/or fluorescence spectra have been widely used in biological and analytical chemistry, in medicine and environmental sciences. These types of sensors are extensively used for the analysis of cations, anions and even molecules due to fast and convenient detection. Although electrochemical techniques have also been used, [65] this short introduction will focus on optical sensors since they will be mainly studied in the next chapters.

The most common types of chemosensors consist of three components for molecular recognition and signal transduction: a receptor (responsible for the selective analyte binding), an active signalling unit (whose properties should change upon the formation of a complex, e.g., fluorescence can be either quenched or enhanced based on molecule or ion recognition) and a spacer that can change the geometry of the system and tune the electronic interaction between these moieties.[66]

1.3.2 Fluorescent Molecular Sensors of Cations

Fluorescent molecular sensors are molecules that undergo a change in fluorescent property, intensity or color, upon recognition of target molecules or experiencing an environmental change. Among the versatile chemosensors, fluorescent molecular sensors have distinct advantages for chemosensing and bioimaging due to their high sensitivity,

selectivity, short response time, local observation (e.g. by fluorescence imaging spectroscopy), low cost and easy fabrication. Moreover, remote sensing is possible by using optical fibers (Scheme 1.2). [67]

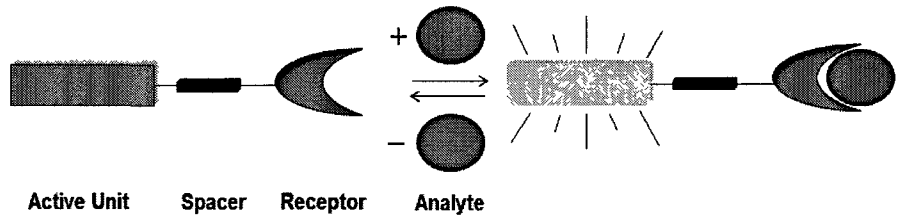

Scheme 1.2. Schematic representation of a fluorescent chemosensor.

The development of fluorescent molecular sensors for metal ions, especially for cations with biological interest such as K^+, Ca^{2+},Cu^{2+}, etc. has always been of particular interest, since some of them are present in biological systems in trace amounts and as environmental pollutes in uncontrolled amounts. Additionally, organometallic complexes were used to construct indicator displacement assays (IDAs) for the detection of peptides, amino acids and nucleotides. [68]

In the design of fluorescent molecular sensors for metal ions, special requirements should be met in order to fulfil the criteria of affinity and selectivity. In the design of the metal binding unit (fluoroionophore), the most critical factor is the characteristics of the ionophore moiety i.e. the ligand topology and the number and nature of the complexing heteroatoms or groups, which should match the characteristics of the cation, such as ionic diameter, charge density, coordination number, intrinsic nature (soft, hard, etc.). The considerable changes in the fluorescence of a fluorophore depends on the interaction of cations and ionophores, photoinduced processes including electron transfer (PET), charge transfer (PCT), energy transfer, excimer formation, etc.

1.3.2.1 Fluorescent Molecular Sensors with Open-Chain Receptor

Receptor containing only one aliphatic amine group

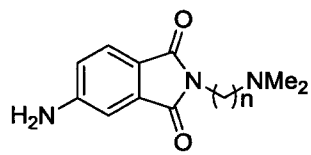

F1 n=2

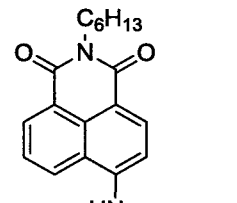

F2

F1[69] and **F2** are the simplest molecules appending the fluorophore to the amine by an alkyl chain. A significant fluorescence enhancement (30 times for **F1**) can be observed in acetonitrile solutions upon metal complexation with many transition metal ions, including those ions that usually quench fluorescence, such as Fe^{3+}, Co^{2+}, Ni^{2+} and Cu^{2+}. The proposed mechanism is that complexation prevents the PET to occur, and that leads to an enhancement of the fluorescence. **F2** was reported[70] to have a similar effect, but with a greater selectivity for Cu^{2+}, where the fluorescence of the chemosensors (10 mM) is only by much higher concentrations (10-100 ppm) of Ni^{2+}, Mn^{2+}, Zn^{2+} and Ca^{2+}.

Chemosensors composed of polyamine and achelator receptors

The pH dependence of the fluorescence intensity changes in the presence of Cu^{2+}, Ni^{2+} and Zn^{2+} in acetonitrile/water solutions of **F3** which composed of polyamine receptors and an anthracene fragment was reported.[71]A decrease of the intensity is observed at lower pH for copper ions, since metal ion complexation in these conditions leads to the deactivation of the excited state via an energy transfer process from the chromophore to metal centred states.

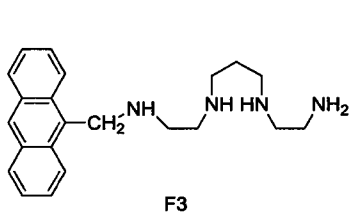

F3

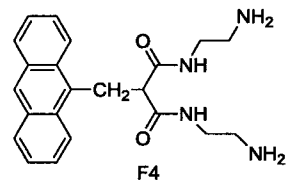

F4

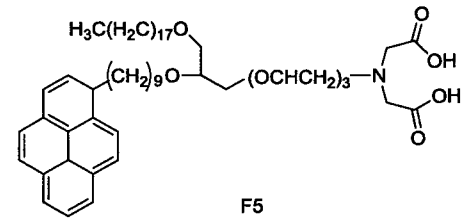

F5

A well-known category of ligands, dioxo-tetraamines were reported to signal the presence of Ni^{2+} and Cu^{2+}, when connected to chromophores such as anthracene (**F4**).[72] The complexation mechanism involves the deprotonation of the two amide groups. This process can occur only with Ni^{2+} and Cu^{2+} ions, which profit by a large ligand field stabilization. **F5** is a representative sensor containing chelators with carboxylic groups[73], it is known to efficiently bind divalent hard metal ions like Ca^{2+} and Mg^{2+}, but show a remarkably high affinity for Cu^{2+}. Complexation with copper is fast and reversible, and a detection limit of 5 nM for Cu^{2+} was reported.

1.3.2.2 Fluorescent Molecular Sensors with Cyclic Receptor

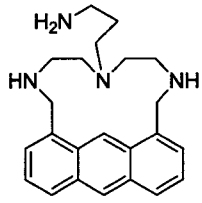

F6

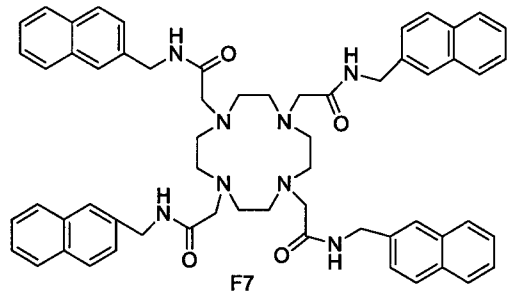

F7

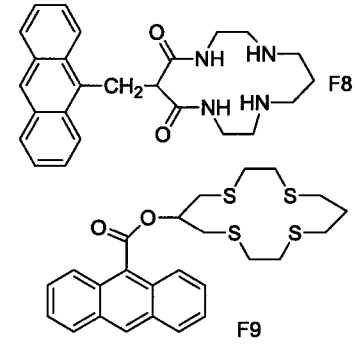

F8 F9

F6 [74] shows a very high selectivity towards Cu^{2+} and Hg^{2+}. In water solution at pH7, this compound displayed chelation-enhanced quenching effects with only these two ions, with overall emission changes of 18-fold and four fold, respectively. **F7** [75, 76] is based on the cyclen receptor and on the naphthalene chromophore. Cu^{2+} ions leads to a fluorescence decrease of 95% by the heavy atom effect. **F8**, [72] possessing a dioxocyclam

receptor shows a similar behaviour to the open-chain analogue **F4**, complexing both Cu^{2+} and Ni^{2+} ions, and exhibiting the same qualitative behaviour. However, the pH interval available for selective titration (in which the two ions can be discriminated) is reduced due to the macrocyclic effect. The tetrathia-macrocycle **F9**, [77] contains a crown which does not contain nitrogen atoms but four sulfur atoms and is known for its strong affinity towards Cu^{2+} in the presence of other 3d metal ions. Copper binding leads to an efficient quenching of the chromophore luminescence centred at 470 nm through PET from anthracene to the metal ion. However, Ag^{+} ions are shown to compete in ethanol with Cu^{2+} ions, forming a stable complex.

1.3.3 Organometallic Complex-Based Optical Chemosensors

Intrinsic chemosensors

These sensors feature the receptor unit as part of the chromophore/fluorophore.[66a] The interaction between the bound substrate and the dye (chromophore or fluorophore) leads directly to the modification of its emission properties.

A typical example of such sensor developed by D'Souza *et al.*, the neutral zinc porphyrin (**F10**), which was tested as a fluorescencent sensor for nicotine (Figure 1.9).[78] The molecular recognition of **F10** upon binding nicotine in toluene solution was observed by both UV-Vis and fluorescence spectroscopy. The result implied that the pyridyl nitrogen of nicotine axially ligates the zinc ion and the pyrrolidine nitrogen hydrogen bonding to the carboxylic acid group. A bathochromic shift of visible bands of **F10** and a decrease in the intensity of the emission bands at 605 nm and 650 nm were observed.

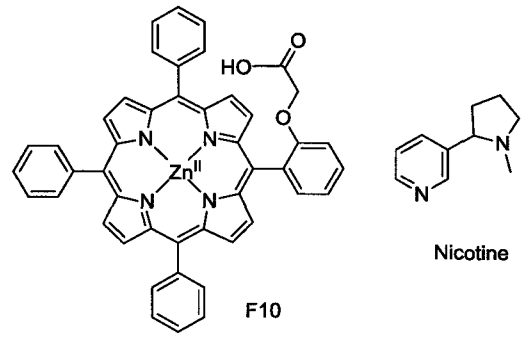

Figure 1.9. A neutral zinc porphyrin complex **F10** designed to bind nicotine.

This kind of chemosensor is relatively easy to make, but the development and optimization of these sensors has been proven difficult, because they are intrinsically rigid as they have to be designed around the substrate, any modification of the binding site to modify its selectivity or affinity may change the emission properties of the dye.

Self-Assembled Chemosensors

The chemosensing ensemble is an easy and convenient strategy that has been developed only in last ten years based on a competition assay. In a metal-based indicator-displacement assay, the receptor is composed from a metal ion or ions coordinated by ligands. A chromophore/fluorophore is introduced into the system as an indicator to coordinate with the metal center and, eventually, the ligand(s), which results in optical changes that can be measured to derive the binding affinity. Zinc (II), copper (II) and rhodium [79] complexes have been widely used for this approach and can operate in highly polar solvents (aqueous ethanol or pure water) as well as display strong affinity towards analytes.

This strategy was applied initially by the Fabbrizzi's group for the detection of histidine in water.[80] Receptor **F11** was designed to incorporate two copper ions in order to gain affinity for analytes (Figure 1.10). Eosine was one of the fluorescent indicators

with emission wavelengths in the visible region, and has a carboxylate group in the molecular structure. Eosine is bound through noncovalent interactions to **F11**, which quenches its emission; the added analytes displace the Eosine indicator, which was released to the solution restoring its fluorescence. Results showed that **F11** binds to histidine better than glycine, phenylalanine, valine, leucine, and proline due to histidine possessing an imidazole residue which coordinates to dicopper centres resulting in higher selectivity.

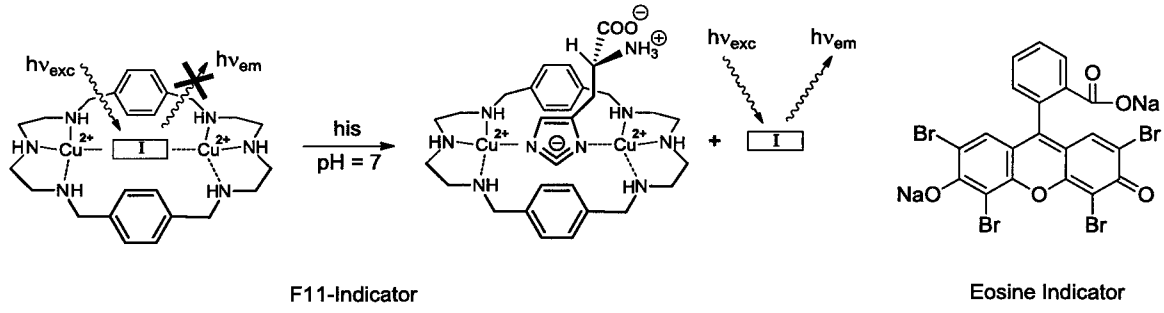

Figure 1.10. A chemosensing ensemble for histidine.

1.3.4 NIR Fluorescent Molecular Sensors

Although visible fluorescent molecules play important roles in various research areas, optical imaging of molecular processes in living organisms has stimulated interest in the development of molecular probes for use in the NIR region (typically 700- 900 nm). In this spectral window, many intrinsic tissue chromophores and macromolecules have low light absorption, low auto fluorescence and low light scattering. In addition, the NIR light can penetrate much deeper into tissue, which is suitable for therapeutic applications[81] and can be used as tags or stain for bio-imaging.[82]

1.3.4.1 NIR Fluorescent Cyanine Dyes

New NIR imaging methods and molecular probes (Figure 1.11) have received considerable interests and development in the last decade. The dye indocyanine green (ICG) is a gold standard for in vivo optical imaging due to its excellent NIR emission properties and suitability for use in humans. Several ICG derivatives have also been prepared for subsequent conjugation with peptides, antibodies, and other biologically relevant molecules.[83] However, a major problem with these probes is the occasional lag time between uptake in target tissue and clearance from surrounding tissue.

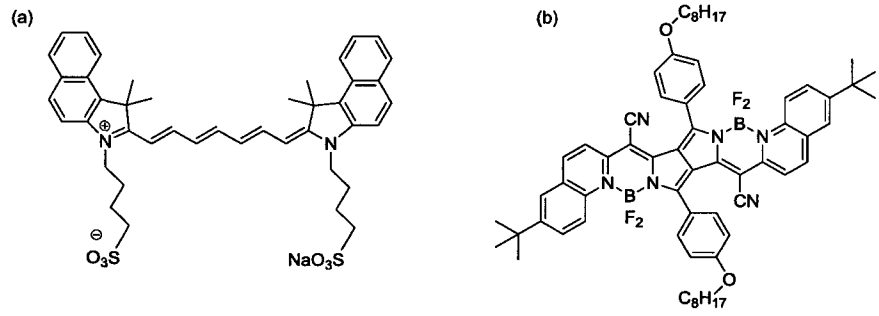

Figure 1.11. Chromophores of the NIR-fluorescent carbocyanine dye ICG (a) and diketopyrrolopyrrole cyanine dyes (b)

Development of active NIR probes, which only emit fluorescence in response to a specific molecular event is necessary. However, earlier polymer-based responsive probes have shown limited access to intracellular enzymes and the slow enzyme-dependent fluorescent enhancement.[84] Therefore, development of small molecular NIR probes with small HOMO-LUMO gaps for biochemical analytes (amino acids, coenzymes, carbohydrates, etc.) is clearly desirable.

1.3.4.2 NIR Zwitterionic Fluorophores

The optical and electronic properties of organic molecules are determined by their energy gap, which is the energy difference between the HOMO and LUMO. Narrowing this energy gap is an effective way to obtain a red shift in absorption and emission spectra. Common strategies to reduce the energy gap include 1) extending the conjugation length, 2) introduction of a strong electron donor and a strong electron acceptor, 3) lowering the bond length alternation of π-conjugated chromophores.[85]

Approaches 1) and 2) have been extensively investigated to tailor the opto-electronic properties of monomeric chromophores in a D-π-A system. However, the extent of π-electron delocalization in polyene-type polymers is limited by distortion of the polymer backbones that results in finite energy separations between the valence molecular orbitals. The disadvantages are extensive tedious synthesis for screening new electron donors and acceptors. Recently, adjusting the BLA of zwitterionic chromophores has become a promising strategy to recognize small optical band gap.

In 2006, two hyperpolarizable merocyanines (I and II) showing the strongest PL emission bands at 565 nm and 640 nm in 9:1 ethanol-methanol solvent was first reported by Smith's group (Figure 1.12).[86] More recently, Marks' group [4c] reported their studies on the TICT-TMC chromophore aggregation in solution by optical absorption and fluorescence spectroscopies (Figure 1.8). Although TMC-3 has the longest conjugated bridge in the new twisted zwitterionic chromophores, the maximum emission at 485 nm in CH_2Cl_2 is still in the visible region. Moreover, the fluorescent sensitivity of these dyes to solvent polarity is not reported yet.

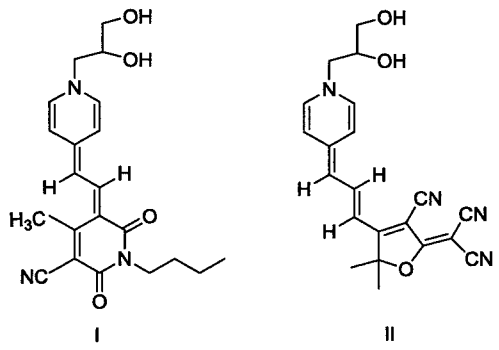

Figure 1.12. Structures of merocyanines I and II.

In 2010, novel donor/ acceptor substituted cross-conjugated carbocycles based on quinoids (**Q1**) or expanded quinoids (**Q2**) were prepared for reducing HOMO-LUMO gaps. X-ray diffraction shows that these push-pull quinoids have significant charge-separated ground states (Figure 1.13). The maximum absorption of **Q1** is around 695 nm; extending the conjugation by an additional quinodimethane ring gives **Q2** two major absorptions, one is located in the visible region (λ_{max}= 610 nm), and the other broad absorption is located in the NIR region (λ_{max}= 845 nm).[87] However, the fluorescent property of these new zwitterionic chromophores was not reported.

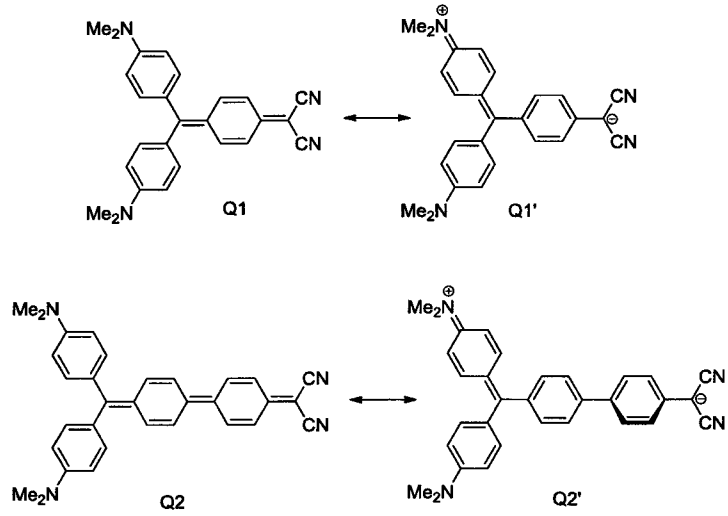

Figure 1.13. Contribution of charge-transfer aromatization to ground state of **Q1** and **Q2**.

D^{+}-π-A^{-} type of zwitterionic dyes derived from a tertiary amine and TCNQ [3,4b] show great potential to be NIR fluorophores because they possess a low-energy resonance structure of quinoid having the effectively reduced BLA. In addition, the hybridization of the energy levels of the donor and acceptor also gives rise to a smaller HOMO-LUMO gap. With the similar structures, PeQDM was found recently by our group to exhibit NIR PL (λ_{max}= 850 nm) and have potential application for pH indicator.[88]

1.4 Rationale and Objectives

The field of NLO materials for EO applications and chemosensors has been rapidly growing over the last years.

A wide range of NLO chromophores with very large μβ values has recently been prepared according to the established theories, especially for the synthesis and functionalization of neutral chromophores. However, among many requirements for practical EO devices, high macroscopic nonlinearity, which requires a high microscopic molecular nonlinearity of NLO chromophores and an efficient dipole alignment induced by applying an electric field, is still the most important issue to be addressed. Additionally, other critical problems such as thermal stability, photochemical stability, optical transparency, and processability in a given chromophore are followed. Moreover, polymer matrices with good thermal stability and appropriate polarity to host chromophores to meet effective poling and device processing conditions are still required.

There is already a wide choice of fluorescent molecular sensors for particular applications. However, there is still a need for sensors with improved selectivity and minimum perturbation to the microenvironment to be probed during the analysis.

Moreover, the shortcoming of current used NIR probes was addressed by the development of simpler small molecular NIR probes with small HOMO-LUMO gaps for biological and biochemical analytes (e.g., amino acids) and in vivo use.

This research is particularly interested in development of dipolar zwitterionic chromophores for a variety of applications. Compared with the multi-step synthesis of the extensive conjugations for neutral chromophores, zwitterionic chromophores are typically easier to be prepared and have advantages in chemical and thermal stabilities. They are distinguished as solvent polarity indicators for their large negative solvatochromic effect. In addition, their large hyperpolarizabilities provide NLO properties for EO application, their relatively small sizes and large dipole moments are also of great importance for the efficient electric poling. Moreover, small band gap and NIR fluorescence properties make them potential NIR molecular fluorescence probes.

Zwitterionic chromophore PQDM was first successfully synthesized with high yield by our group, the EO activities were studied and low EO coefficient was obtained (r_{33} = 21pm/V) in a guest-host polymer with low loading density.[89] A higher r_{33} of 45 pm/V was obtained in a side-chain polyimide system[56] and was improved to 65 pm/V in a hyperbranched PQDM doped polymer.[90] In order to reduce the intermolecular aggregation, PeQDMs were developed later by introducing an ester group to the acceptor moiety. However, r_{33} values are still much less than the theoretical prediction [52] (210 pm/V) and a tradeoff of number density and macroscopic nonlinearity were observed, indicating that the material still have strong aggregation. [91]

We have maintained an interest in this class of chromophore. To realize the full potential application of zwitterionic chromophores, it is required to better understand the

structure-property relationship regarding the strength of donor, acceptor and conjugated length, two series of zwitterionic chromophores based on PQDM were designed and proposed as being ideal for achieving highly efficient poling.

To reduce the molecular aggregation and increase the EO coefficient, the first approach is "controlling the chromophore structure" through control of the size and shape of the chromophores, by introducing different groups from **R1** to **R4** to obtain increased molecular size and a spherical shape of the chromophores. The second approach is applying the "site-isolation principle", [92] to minimize undesirable dipole-dipole interactions in any polymer system that contains such compounds. Dicyanovinyl and 3CNQ were chosen as acceptors because particularly large molecular hyper-polarizabilities were found when they were present in reported NLO chromophores. Figure 1.14 shows the strategies to modify the PQDM chromophores.

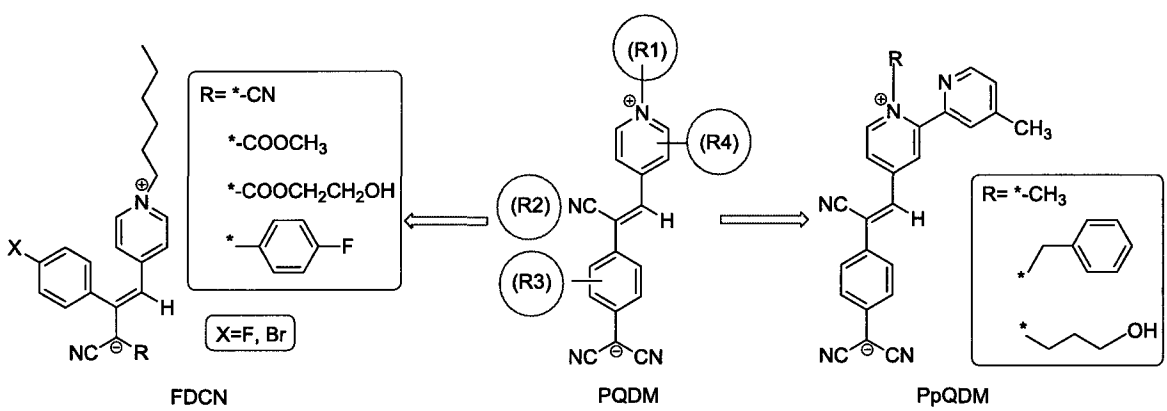

Figure 1.14. Potential modifications of PQDM and two new series of chromophores.

FDCN chromophores were designed based on the pyridinium donors, with a shorter conjugation to experimentally evaluate the dipole moment, and at the same time, lessen the structural complexity of the molecules. Aromatic bulk group was introduced to

the central moiety to reduce the π-π stacking. Halides on the aromatic rings were added (e.g., F, Br) to make the central part more bulky, and finally long aliphatic chains on the donor were used to help improve the solubility.

For chromophores PpQDM, dipyridylium was chosen as the donor to increase the donor size and reduce molecule symmetry and longer conjugation with stronger acceptor 3CNQ was expected to enlarge the μβ value. Careful selection of the hydroxyl alkyl halide is necessary to control the physical properties of the chromophore when grafted into a host polymer. For example, the length of the alkyl chain will determine the ability of the chromophore to orientate during poling since the alkyl chain represents the polymer chromophore spacer. These chromophores allow for functionalization at the donor side of the molecule for increasing solubility, for grafting, and/or for cross-linking, and improve the highly desirable NLO properties. All of the above features make these two series of chromophores very promising for NLO applications.

Another specific characteristic of FDCN and PpQDM chromophores is that the two cyano groups in dicyanovinyl and 3CNQ make them not only strong acceptors which contributes to the optical response, and also can function as ligands to coordinate to metal ions unlike the common optical chemosensors, which need communication between a binding site and a chromophore in a molecule.[93] This allows zwitterionic dyes, which consists of a binding site in the chromophore to be promising molecular probe candidates to recognize specific guests through binding sites and produce a direct change in optical properties (absorption or fluorescence). PpQDM chromophores are expected to exhibit NIR fluorescent property due to their longer conjugation length.

According to the above rationale, the main objectives of this research were as following:

1) In the first part of this work, we synthesized two new series of zwitterionic chromophores and their corresponding NLO chromophore-polymers.

2) In the next part, we systematically studied the relationship between the structure of these zwitterionic chromophores and their EO properties.

3) Finally, we investigated the NIR fluorescent property of the PpQDM chromophores, and then whether the PpQDM chromophores can form organometallic complexes to realize selective NIR biochemical sensing.

1.5 References

(1) Bell, N. A.;Crouch, D. J.;Simmonds, D. J.; Goeta, A. E.; Gelbrich, T.; Hursthouse, M. B. *J. Mater. Chem.* **2002**, *12*, 1274.

(2) (a)Marder, S. R.; Gorman, C. B.; Meyers, F.; Perry, J. W.; Bourhill, G.; Bredas, J.-L.; Pierce, B. M. *Science* **1994**, *265*, 632. (b)Szablewski, M.; Thomas, P. R.; Thornton, A.; Bloor, D.; Cross, G. H.; Cole, J. M.; Howard, J. A. K.; Malagoni, M.; Meyers, F.; Bredas, J.-L.; Wenseleers, W.; Goovaerts, E. *J. Am. Chem. Soc.* **1997**, *119*, 3144. (c)Kang, H.; Facchetti, A.; Jiang, H.; Cariati, E.; Righetto, S.; Ugo, R.; Zuccaccia, C.; Macchioni, A.; Stern, C. L.; Liu, Z.; Ho, S.-T.; Brown, E.C.; Mark A. Ratner, M. A.; Marks, T. J. *J. Am. Chem. Soc.* **2007**, *129*, 3267.

(3) Higashino, K.; Nakaya, T.; Ishiguro, E. *J. Photochem. Photobiol. A: Chem.* **1994**, *79*, 81.

(4) Ashwell, G. J. *Thin Solid Films* **1990**, *186*, 155.

(5) (a)Metzger, R. M.; Chen, B.; Hopfner, U.; Lakshmikantham, M. V.; Vuillaume, D.; Kawai, T.; Wu, X.; Tachibana, H.; Hughes, T. V.; Sakurai, H.; Baldwin, J. W.; Hosch, C.; Cava, M. P.; Brehmer, L.; Ashwell, G. J. *J. Am. Chem. Soc.* **1997**, *119*, 10455. (b)Metzger, R. M. *Acc. Chem. Res.* **1999**, *32*, 950.

(6) Neilands, O. *Mol. Cryst. Liq. Cryst.* **2001**, *355*, 331.

(7) (a)Andreu, R.; Garin, J.; Orduna, J.; Alcala, R.; Villacampa, B. *Org. Lett.* **2003**, *5*, 3143. (b)Kay, A. J.; Woolhouse, A. D.; Zhao, Y.; Clays, K.; *J. Mater. Chem.* **2004**, *14*, 1321. (c)Schmidt, J.; Schmidt, R.; Wurthner, F. *J. Org. Chem.* **2008**, *73*, 6355.

(8) Wolf, J. J.; Wortmann, R. *Adv. Phys. Org. Chem.* **1999**, *32*, 121.

(9) (a)Marder, S. R.; Perry, J. W.; Bourhill, G.; Gorman, C. B.; Tiemann, B. G.; Mansour, K. *Science* **1993**, *261*, 186. (b)Gorman, C. B.; Marder, S. R. *Proc. Natl. Acad. Sci. USA* **1993**, *90*, 11297.

(10) Oudar, J. L.; Chemla, D. S. *J. Chem. Phys.* **1977**, *66*, 2664.

(11) Reichardt, C. *Chem. Rev.* **1994**, *94*, 2319.

(12) (a) *Nonlinear Optics of Organic Molecules and Polymers*; Nalwa, H. S.; Miyata, S., Eds.; CRC Press: Boca Raton, 1997. (b)Burland, D. M.; Miller, R. D.; Walsh,

C. A. *Chem. Rev.* **1994**, *94*, 31. (c)Kajzar, F.; Lee, K. S.; Jen, A. K-Y. *Adv. Polym. Sci.* **2003**, *161*, 1. (d)Luo, J. D.; Zhou, X.; Jen, A. K.-Y. *J. Mater. Chem.* **2009**, *19*, 7410.

(13) (a)Lee, M.; Katz, H. E.; Erben, C.; Gill, D. M.; Gopalan, P.; Heber, J. D.; McGee, D. J. *Science* **2002**, *298*, 1401. (b)Liu, A. S.; Jones, R.; Liao, L.; Samara-Rubio, D.; Rubin, D.; Cohen, O.; Nicolaescu R.; Paniccia, M. *Nature*, **2004**, *427*, 615.

(14) Kaminov, I. P.; Turner, E. H. Proc. IEEE **1966**, *54*, 1374.

(15) (a)Ma, H.; Liu, S.; Luo, J. D.; Suresh, S.; Liu, L.; Kang, S. H.; Haller, M.; Sassa, T.; Dalton, L. R.; Jen, A. K.-Y. *Adv. Funct. Mater.* **2002**, *12*, 566. (b)Dalton, L. R.; Sullivan, P.; Bale, D. H. *Chem. Rev.* **2010**, *110*, 25.

(16) (a)Prasad, P. N.; Williams, D. J. *Introduction to Nonlinear Optical Effects in Molecules and Polymers*; John Wiley and Sons: New York, 1991. (b) Singer, K. D.; Kuzyk, M. G.; Sohn, J. E. *J. Opt. Soc. Am. B* **1987**, *4*, 968.

(17) (a)Bourhill, G.; Bredas, J. L.; Cheng, L.-T.; Marder, S. R.; Meyers, F.; Perry, J. W.; Tiemann, B. G. *J. Am. Chem. Soc.* **1994**, *116*, 2619. (b)Brown, E. C.; Marks, T. J.; Ratner, M. A. *J. Phys. Chem. B* **2008**, *112*, 44. (c)Di Bella, S.; Marks, T. J.; Ratner, M. A. *J. Am. Chem. Soc.* **1994**, *116*, 4440.

(18) Kuzyk, M. G.; Dirk, C. W. *Characterization Techniques and Tabulations for Organic Nonlinear Optical Materials*; Marcel Dekkar: New York, 1998.

(19) (a)Dalton, L. R.; Harper, A. W.; Robinson, B. H. *Proc. Natl. Acad. Sci. U.S.A.* **1997**, *94*, 4842. (b) Robinson, B. H.; Dalton, L. R. *J. Phys. Chem. A* **2000**, *104*, 4785.

(20) (a)Kanis, D. R.; Ratner, M. A.; Marks, T. J. *Chem. Rev.* **1994**, *94*, 195. (b) Oudar, J. L. *J. Chem. Phys.* **1977**, *67*, 446.

(21) (a)Cheng, L. T.; Tam, W.; Marder, S. R.; Stiegman, A. E.; Rikken, G.; Spangler, C. W. *J. Phys. Chem.* **1991**, *95*, 10643. (b)Cheng, L. T.; Tam, W.; Stevenson, S. H.; Meredith, G. R.; Rikken, G.; Marder, S. R. *J. Phys. Chem.* **1991**, *95*, 10631.

(22) Kippelen, B.; Peyghambarian, N.; *Adv. Polym. Sci.* **2003**, *161*, 87.

(23) Marder, S. R.; Kippelen, B.; Jen, A. K.-Y.; Peyghambarian, N. *Nature*, **1997**, *388*, 845.

(24) Zhang, C.; Dalton, L. R.; *Chem. Mater.* **2001**, *13*, 3043.

(25) Kay, A. J.; Woolhouse, A. D.; A. D.; Zhao, Y.; Clays, K.; *J. Mater. Chem.* **2004**, *14*, 1321.

(26) Davydov, B. L.; Derkacheva, L. D.; Dunina, V. V.; Zhabotinskii, M. E.; Zolin, V. K.; Kreneva, L. C.; Samokhina, M. A. *JEPT Lett.* **1970**, *12*, 16.

(27) Rao, V. P.; Cai, Y. M.; Jen, A. K.-Y. *J. Chem. Soc. Chem. Comm.* **1994**, 1689.

(28) (a)Staub, K.; Levina, G. A.; Barlow, S.; Kowalczyk, T. C.; Lackritz, H. S.; Barzoukas, M.; Fort, A.; Marder, S. R. *J. Mater. Chem.* **2003**, *13*, 825. (b) Twieg, R. J.; Burland, D. M.; Hedrick, J. L.; Lee, V. Y.; Miller, R. D.; Moylan, C. R.; Volksen, W.; Walsh, C. *Mater. Res. Soc. Symp. Proc.* **1994**, *328*, 421.

(29) Jen, A. K.-Y.; Cai, Y. M.; Bedworth, P. V.; Marder, S. R. *Adv. Mater.* **1997**, *9*, 132.

(30) Jen, A. K.-Y.; Rao, V. P.; Wong, K. Y.; Drost, K. J. *J. Chem. Soc. Chem. Commun.* **1993**, 90.

(31) Dirk, C. W.; Katz, H. E.; Schilling, M. L.; King, L. A. *Chem. Mater.* **1990**, *2*, 700.

(32) Melikian, G.; Rouessac, F. P.; Alexandre, C. *Synth. Commun.* **1995**, *25*, 3045.

(33) (a)Dalton, L.; Harper, A.; Ren, A.; Wang, F.; Todorova, G.; Chen, J.; Zhang C.; Lee, M. *Ind. Eng. Chem. Res.*, **1999**, *38*, 8. (b)Hua, J.; Luo, J. D.; Qin, J.; Shen, Y.; Zhang, Y.; Lu, Z. *J. Mater. Chem.* **2002**, *12*, 863.

(34) Robinson, B. H.; Dalton, L. R.; Harper, A. W.; Ren, A.; Wang, F.; Zhang, C.; Todorova, G.; Lee, M.; Aniszfeld, R.; Garner, S.; Chen, A.; Steier, W. H.; Houbrecht, S.; Persoons, A.; Ledoux, I.; Zyss, J.; Jen, A. K.-Y. *Chem. Phys.* **1999**, *245*, 35.

(35) Shi, Y.; Zhang, C.; Zhang, H.; Bechtel, J. H.; Dalton, L. R.; Robinson, B. H.; Steier, W. H. *Science* **2000**, *288*, 119.

(36) (a)Luo, J. D.; Haller, M.; Ma, H.; Liu, S.; Kim, T.-D.; Tian, Y.; Chen, B.; Jang, S.-H.; Dalton, L. R.; Jen, A. K.-Y. *J. Phys. Chem. B* **2004**, *108*, 8523. (b)Liao, Y.; Eichinger, B. E.; Firestone, K. A.; Haller, M.; Luo, J. D.; Kaminsky, W.; Benedict, J. B.; Reid, P. J.; Jen, A. K.-Y.; Dalton, L. R.; Robinson, B. H. *J. Am. Chem. Soc.* **2005**, *127*, 2758. (c)Kim, T.-D.; Kang, J.-W.; Luo, J. D.; Jang, S.-H.; Ka, J.-W.;

Tucker, N.; Benedict, J. B.; Dalton, L. R.; Gray, T.; Overney, R. M.; Park, D. H.; Herman, W. N.; Jen, A. K.-Y. *J. Am. Chem. Soc.* **2007**, *129*,488.

(37) Cai, C.; Liakatas, I.; Wong, M.-S.; Busch, M.; Bosshard, C.; Gunter, P.; Concilio, S.; Tirelli, N.; Suter, U. W. *Org. Lett.* **1999**, *1*, 1847.

(38) Prasad, P.; Williams, D. *Nonlinear Optical Effects in Molecules and Polymers*; John Wiley and Sons: New York, 1991.

(39) (a)Cheng, L. T.; Tam, W.; Marder, S. R.; Steigman, A. E.; Rikken, G.; Spangler, C. W. *J. Phys.Chem.***1991**, *95*, 10643. (b)Ahlheim, M.; Barzoukas, M.; Bedworth, P. V.; Blanchard-Desce, M.; Fort, A.; Hu, Z.; Marder, S. R.; Perry, J. W.; Ruser, C.; Staehelin, M.; Zysset, B. *Science* **1996**, *271*, 335.

(40) (a)Albert, I. D. L.; Marks, T. J.; Ratner, M. A. *J. Am. Chem. Soc.* **1997**, *119*, 6575. (b)Rao, V. P.; Jen, A. K.-Y.; Chandrasekhar, J.; Namboothiri, I. N. N.; Rathna, A. *J. Am. Chem. Soc.* **1996**, *118*, 12443. (c)Raposo, M. M. M.; Sousa, A. M. R. C.; Kirsch, G.; Ferreira, F.; Belsley, M.; De Matos Gomes, E.; Fonseca, A. M. C. *Tetrahedron* **2005**, *61*, 11991.

(41) (a)Chen, D.; Fetterman, H. R.; Chen, A.; Steier, W. H.; Dalton, L. R.; Wang, W.; Shi, Y. *Appl. Phys. Lett.* **1997**, *70*, 3335. (b)Mingqian, H.; Leslie, T. M.; Sinicropi, J. A. *Chem. Mater.* **2002**, *14*, 4662.

(42) Zhang, C.; Ren, A. S.; Wang, F.; Zhu, J.; Dalton, L. R. *Chem. Mater.* **1999**, *11*, 1966.

(43) Shu, C. F.; Shu, Y. C.; Gong, Z. H.; Peng, S. M.; Lee, G. H.; Jen, A. K.-Y. *Chem. Mater.* **1998,** *10*, 3284.

(44) Metzger, R. M.; Heimer, N. E.; Aswell, G. J. *Mol. Cryst. Liq. Cryst.* **1984**, *107*, 133. (b)Bell, N. A.; Crouch, D. J.; Simmonds, D. J.; Goeta, A. E.; Gelbrich, T.; Hursthouse, M. B. *J. Mater. Chem.* **2002**, *12*, 1274.

(45) (a)Broo, A.; Zerner, M. C. *Chem. Phys.* **1995**, *196*, 407. (b)Broo, A.; Zerner, M. C. *Chem. Phys.* **1995**, *196*, 423.

(46) (a)Dulcic, A.; Flytzanis, C. *Opt. Commun.* **1978**, *25*, 402. (b)Benson, H. G.; Murrell, J. N. *J. Chem. Soc., Faraday Trans.2* **1972**, *68*, 137.

(47) Kay, A. J.; Woolhouse, A. D.; Gainsford, G. J.; Haskell, T. G.; Barnes, T. H. *J. Mater. Chem.* **2001**, *11*, 996.

(48) Abbotto, A.; Beverina, L.; Bradamante, S.; Facchetti, A.; Klein, C.; Pagani, G. A.; Redi- Abshiro, M.; Wortmann, R. *Chem. Eur. J.* **2003**, *9*, 1991.

(49) Ashwell, G. J. *Organic Materials for Nonlinear Optics*; Ashwell, G. J.; Bloor, D. Eds; Royal Soc. Of Chem.: Cambridge, 1993.

(50) (a)Acker, D. S.; Harder, R. J.; Hertler, W. R.; Mahler, W.; Melby, L. R.; Benson, R. E. ; Mochel, W. E. *J. Am. Chem. Soc.* **1960**, *82*, 6408. (b)Acker, D. S.; Hertler W. R. *J. Am. Chem. Soc.* **1962**, *84*, 3370.

(51) Akhtar, S.; Tanaka, J.; Metzger R. M.; Ashwell, G. J. *Mol. Cryst. Liq. Cryst.* **1986**, *139*, 353.

(52) Cross, G. H.; Hackman, N. A.; Thomas, P. R.; Szablewski, M.; Palsson, L. O.; Bloor, D. *Opt. Mater.* **2002**, *21*, 29.

(53) Burland, D. M.; Miller. R. D.; Walsh, C. A. *Chem. Rev.* **1994**, *94*, 31.

(54) (a)Shuto, Y.; Anmno, M.; Kaino, T. *Jpn. J. Appl. Phys.* **1991**, *30*, 320. (b)Chen, D.; Fetterman, H.; Chen, A.; Sterier, W.; Dalton, L. *Appl. Phys. Lett.* **1997**, *77*, 3335.

(55) Jen, A. K.-Y.; Wong, K. Y.; Rao, V. P.; Drost, K. *J. Electron. Mater.* **1994,** *23*, 653.

(56) Cai, Y. M.; Jen, A. K.-Y. *Appl. Phys. Lett.* **1995**, *117*, 7295.

(57) Xu, C.; Wu, B.; Becker, M. W.; Dalton, L. R.; Ranon, P. M.; Shi, Y.; Steier, W. H. *Chem. Mater.* **1993**, *5*, 1439.

(58) Moon, K.-J.; Shim, H.-K.; Lee, K.-S.; Zieba, J.; Prasad, P. N. *Macromolecules* **1996**, *29*, 861.

(59) Yoon, C. B.; Shim, H. K. *J. Mater. Chem.* **1999**, *9*, 2339.

(60) Song, N. H.; Men, L.; Gao, J. P.; Bai, Y. W.; Beaudin, A. M. R.; Yu, G. M.; Wang, Z. Y. *Chem. Mater.* **2004,** *16,* 3708.

(61) (a)Zhu, P.; Wang, P.; Wu, W.; Ye, C. *J. Non. Opt. Phys. Mater.* **1999**, *8*, 461. (b) Qin, A.; Yang, Z.; Bai, F.; Ye, C. *J. Polym. Sci.: Part A: Polym. Chem.* **2003**, *41*, 2846.

(62) Luo, J. D.; Haller, M.; Li, H.; Tang, H. Z.; Jen, A. K.-Y.; Jakka, K.; Chou, C. H.; Shu, C. F. *Macromolecules* **2004**, *37*, 248.

(63) Luo, J. D.; Haller, M.; Li, H.; Kim, T.-D.; Jen, A. K.-Y. *Adv. Mater.* **2003**, *15*, 1635.

(64) Anslyn, E. V. *J. Org. Chem.* **2007**, *72*, 687.

(65) Beer, P. D.; Cadman, J. *Coord. Chem. Rev.* **2000**, *205*, 131.

(66) Bissel, R. A; De Silva, A. P.; Gunaratne, H. Q. N.; Lynch, P. L. M.; Maguire, G. E. M.; Sandanayake, K. R. A. S. *Chem. Soc. Rev.* 1992, 187.

(67) De Silva, A. P.; Nimal Gunaratne, H. O.; Gunnlaugusson, T.; Huxley, A. J. M.; McCoy, C. P.; Rademacher, J. T.; Rice, T. E. *Chem. Rev.* **1997**, *97*, 1515.

(68) Nguyen, B. T.; Anslyn, E. V. *Coord. Chem. Rev.* **2006**, *250*, 3118.

(69) Ramachandaram, B.; Samanta, A. *Chem. Commun.* **1997**, 1037.

(70) Mitchell, K.A.; Brown, R. G.; Yuan, D.; Chang, S.-C.; Utecht, R. E.; Lewis, D. E. *J. Photochem. Photobiol. A: Chem.* **1998**, *115*,157.

(71) Fabbrizzi, L.; Licchelli, M.; Pallavicini, P.; Perotti, A.; Taglietti, A.; Sacchi, D. *Chem. Eur. J.* **1996**, *2*, 75.

(72) Fabbrizzi, L.; Licchelli, M.; Pallavicini, P.; Perotti, A.; Sacchi, D. *Angew. Chem. Int. Ed. Engl.* **1994**, *33*, 1975.

(73) Sasaki, D. Y.; Shnek, D. R.; Pack, D. W.; Arnold, F. H. *Angew. Chem. Int. Ed. Engl.* **1995**, *34*, 905.

(74) Ohler, J. Y. N. E.; Vance, D. H.; Aumiller, W. D.; Czarnik, A. W. *Tetrahedron Lett.* **1997**, *38*, 3845.

(75) Parker, D.; Williams, J. A. G. *J. Chem. Soc. Perkin Trans. 2* **1995**, 1305.

(76) Beeby, A.; Parker, D.; Williams, J. A. G. *J. Chem. Soc. Perkin Trans. 2* **1996**, 1565.

(77) De Santis, G.; Fabbrizzi, L.; Licchelli, M.; Mangano, C.; Sacchi, D.; Sardone, N. *Inorg. Chim. Acta* **1997**, *257*, 69.

(78) Deviprasad, G. R.; D'Souza, F. *Chem. Comm.* **2000**, 1915.

(79) Hilderbrand, S. A.; Lim, M. H.; Lippard, S. J. *J. Am. Chem. Soc.* **2004**, *126*, 4972.

(80) Hortala, M. A.; Fabbrizzi, L.; Marcotte, N.; Stomeo, F.; Taglietti, A. *J. Am. Chem. Soc.* **2003**, *125*, 20-21.

(81) Richards-Kortum, R.; Sevick-Muraca, E. *Annu. Rev. Phys. Chem.*, **1996**, *47*, 555.

(82) (a)Patonay, G.; Antoine, M. D. *Anal.Chem.***1991**, *63*, 321. (b)Stoyanov, S. *Pract. Spectrosc.* **2001**, *25*, 35.

(83) (a)Achilefu, S. *Technol. Cancer Res. Treat.* **2004**, *3*, 393. (b)Hilderbrand, S. A.; Weissleder, R. *Curr. Opin. Chem. Biol.* **2010**, *14*, 71.

(84) Achilefu, S. *Angew. Chem. Int. Ed.* **2010**, *49*, 9816.

(85) (a)Perepichka, D. F.; Bryce, M. R. *Angew. Chem. Int. Ed.* **2005**, *44*, 5370. (b) Roncali, J. *Chem. Rev.* **1997**, *97*, 173.

(86) Smith, G. J.; Dunford, C. L.; Kay, A. J.; Woolhouse, A. D. *J. Photochem. Photobiol. A: Chem.* **2006**, *179*, 237.

(87) Wu, Y. L; Bures, F; Jarowski, P. D.; Schweizer, W. B.; Boudon, C.; Gisselbrecht, J-P; Diederich, F. *Chem. Eur. J.* **2010**, *16*, 9592.

(88) Ying Xiong "Development of Zwitterinic Chromophores for Electro-Optic Applications", *Ph.D. Thesis*, Carleton University, **2008.**

(89) Beaudin, A. M. R.; Song, N. H.; Bai, Y. W.; Men, L.; Gao, J. P.; Wang, Z. Y.; Szablewski, M; Cross, G.; Wenseleers, W. Campo, J.; Goovaerts, E. *Chem. Mater.* **2006,** *18,* 1079.

(90) Bai, Y. W.; Song, N. H.; Gao, J. P.; Sun, X; Wang, X. M.; Yu, G. M.; Wang, Z. Y. *J. Am. Chem. Soc.* **2005**, *127*, 2060.

(91) Xiong, Y.; Tang, H.; Zhang, J.; Wang, Z.Y.; Campo, J.; Wenseleers, W.; Goovaerts, E. *Chem. Mater.* **2008,** *20,* 7465.

(92) Luo, J. D.; Liu, S.; Haller, M.; Liu, L.; Ma, H.; Jen, A. K.-Y. *Adv. Mater.* **2002**, *14*, 1763.

(93) Czarnik, A. W. *Acc. Chem. Res.* **1994**, *27*, 302.

Chapter 2 Synthesis and Characterization of Zwitterionic Chromophores

2.1 Introduction

According to the BLA model, [1] LHS chromophores with neutral ground states have positive β values; while RHS zwitterionic chromophores with charge-separated ground states have negative β.[2] Although the absolute value of β is the only consideration for NLO chromophores for EO application, predominant efforts focus on the exploration of neutral chromophores and less attention has been paid to zwitterionic chromophores despite the considerable advantages displayed by zwitterionic chromophores including 1) ease of synthesis, 2) good thermal stability, 3) high ground state dipole moment and 4) larger nonlinearity than the neutral push-pull system of similar conjugation length. [3]

Among the many types of zwitterions, derivatives of TCNQ such as β-[4-pyridinium]-α-cyano-4-styryldicyano-methanide, (trivial name: pyridinium tricyanoquinonedimethane, PQDM) (Scheme 2.1), which was first reported by Metzger and Ashwell[4] and calculated to have a large static hyperpolarizability of 1270×10^{-30} esu.[5] The stabilization gained in the charge-separated state due to the increase in aromaticity of the negatively charged 3CNQ acceptor represents a huge driving force for these chromophores used in EO applications. This stabilization has been confirmed by X-ray crystallography, infrared (IR), and nuclear magnetic resonance (NMR) spectroscopy.[6] However, these highly crystalline chromophores have no functional groups, which makes it very difficult to chemically incorporate them into a polymer host.

Our group is particularly interested in functionalization of PQDM due to the desirable figures of merits, 1) large β values, comparable to some well-studied neutral ground state chromophores, such as FTC ($\mu\beta = 18{,}000 \times 10^{-48}$ esu); 2) large dipole

moment (43 ± 8 D); [7] 3) relatively small size, which can be easily prepared via short synthetic routes; 4) good solubility in common organic solvents and good thermal stability (e.g. > 250 °C). These advantages make PQDM the most promising candidate of zwitterionic chromophores for NLO applications.

The first reported synthesis of PQDM involved the condensation reaction between picolinium halide and lithium TCNQ adduct or TCNQ with low reaction yields (e.g., 6 - 30%) and long reaction time (5-14 days). [8] In 2003, our group reported a drastic improvement in reaction time and yield (97%) for the PQDM synthesized from two equivalents of lithium TCNQ adduct with one equivalent of picolinium halide in refluxing acetonitrile with the presence of two equivalents of a strong organic base (1,8-diazabicyclo[5.4.0] undec-7-ene, DBU) (Scheme 2.1). [9]

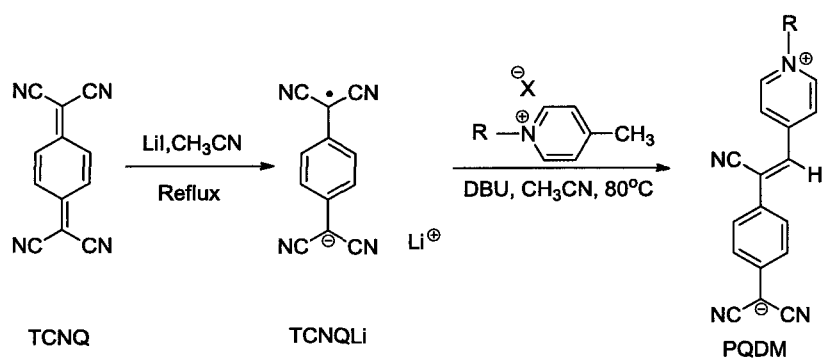

Scheme 2.1. Synthesis of PQDM.

Following the successful synthesis of PQDM, a series of hydroxyl-containing PQDM derivatives with different R groups, such as hydroxypropyl and hydroxyhexyl were synthesized by our group in 2006 (e.g., PQDM-C3OH in Chart 2.1). These chromophores were successfully covalently bonded to the polyimide as side chains. However, the functionalization of PQDM has mainly focused on introducing different substituents on the pyridinium ring (donor part), [10] and no significant contribution on

increasing the β values was found in the modified PQDM. The poling efficiency and EO coefficient values of these polymer systems were still much lower than the theoretical prediction. The limitation of the above EO device is generally considered to be due to the strong intermolecular dipole-dipole interactions since dipolar chromophores are closely packed, poling-induced non-centrosymmetric alignment of these chromophores is very limited. [11]

In 2008 we developed a new series of functionalized zwitterionic picolinium dicyano-esterquinodimethane (PeQDM) chromophores (e.g., PeQDM-Ben in Chart 2.1), aiming to reduce the chromophore-chromophore interaction by introducing an ester group into the acceptor part. The high molecular hyperpolarizability was unexpectedly maintained, or even increased in comparison to the PQDM chromophores, despite the fact that the ester group is considered to be a weaker electron acceptor than the cyano group in PQDM.[12]

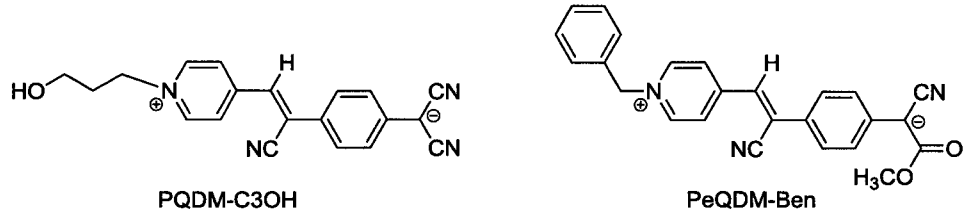

PQDM-C3OH PeQDM-Ben

Chart 2.1. Chemical structures of PQDM-C3OH and PeQDM-Ben.

In order to understand the structure-property relationship of zwitterionic chromophores and realize the full potential of PQDM chromophores, this chapter describes the synthesis and structural characterization of two series of functionalized FDCN (Scheme 2.2) and PpQDM chromophores (Scheme 2.6) based on the design rationale described in Chapter **1**, as well as the X-ray crystallographic analysis,

thermostability, negative solvatochromism, acid sensitivity, and microscopic NLO properties of these two series of chromophores.

2.2 Results and Discussion

2.2.1 Synthesis and Characterizations of FDCN Chromophores

2.2.1.1 Synthesis of FDCN Chromophores

Using 4-fluorophenylacetonitrile (or 4-bromophenylacetonitrile) and 4-pyridine-carboxaldehyde as starting materials, the synthesis of FDCN chromophores is depicted in Scheme 2.2. The pyridinium moiety with 6-carbon aliphatic chain in FDCN is considered to be a donor, whereas the acceptor part contains a cyano group and is chosen as the site of structural modification.

The crucial pyridinium salt donor intermediate **2** was prepared by alkylation of intermediate **1** and then the central cyano group of **2** was substituted with different acceptors. The target chromophores including a bromo-cyanide containing chromophore (BrDCN) and four fluoro-cyanide containing chromophores, with different aliphatic and aromatic groups as the acceptor, were prepared with high yield (60%). Among the FDCN chromophores, hydroxyl-containing chromophore (FCNOH) is considered to be the potential monomer for making side-chain NLO polymers (UV spectra of FDCNOH in DMF and chloroform in Appendix B, Figure S2.7). The general procedure for the synthesis of 2-hydroxyethyl cyanoacetate[13] was undertaken by esterification of cyanoacetic acid with 2-hydroxyethyl alcohol in benzene in the presence of TsOH as a catalyst; the molar ratio of cyanoacetic acid to the alcohol was 1:1 to 1:1.05 (Scheme 2.3).

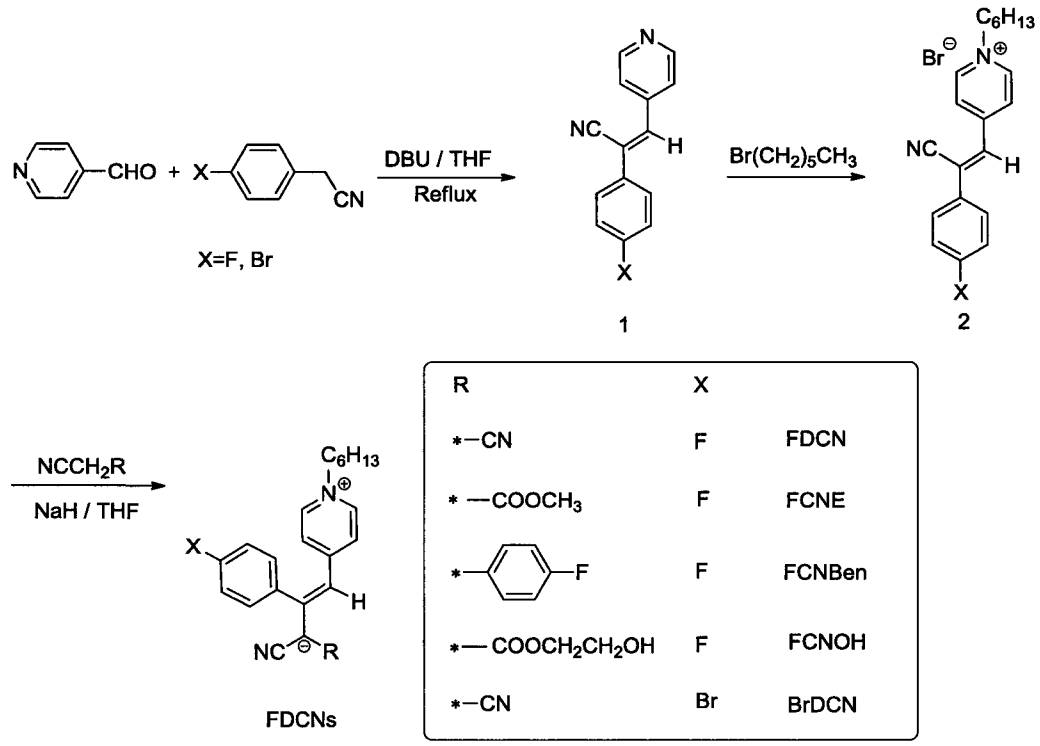

Scheme 2.2. Synthesis of crucial intermediate **2** and FDCN chromophores.

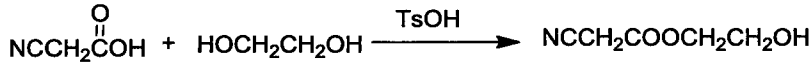

Scheme 2.3. Synthesis of 2-hydroxyethyl cyanoacetate.

2.2.1.2 Characterizations of FDCN Chromophores

All of the FDCN chromophores were fully characterized by ^{1}H NMR, ^{13}C NMR, IR and mass spectrometry.

Figure 2.1 shows the ^{1}H NMR spectrum of FDCN with assigned peaks. In the spectrum, proton resonances (ppm) at 7.81 (2H, d, J = 7.1 Hz), 7.36 (2H, d, J = 8.7 Hz), 7.32 (2H, d, J = 8.7 Hz), 6.34 (2H, d, J = 7.1 Hz), 5.88 (1H, s), 3.92 (2H, t), 1.22 (6H, m) and 0.83 (3H, t) were observed and are consistent with the zwitterionic structure of FDCN.

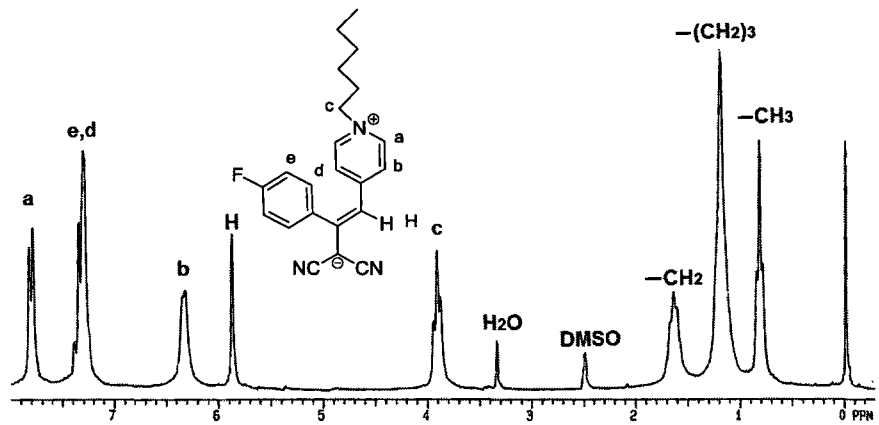

Figure 2.1. ^{1}H NMR spectrum (300 MHz) of FDCN in DMSO-d_6.

Figure 2.2 displays the IR spectrum of FDCN. The cyano group is observed at 2192 cm^{-1}, and the intensity of the peak is strikingly high, which is characteristic of the cyano group connected to an electron-rich group with a negative charge. The IR data accurately supports the zwitterionic structure of FDCN. Additionally, in the MS spectrum of FDCN (Appendix B, Figure S2.3), the molecular ion peak at m/z 347.1793, 348.1776 $[M+H]^+$ and 370.1608 $[M+Na]^+$ were observed and further support the structural characterization.

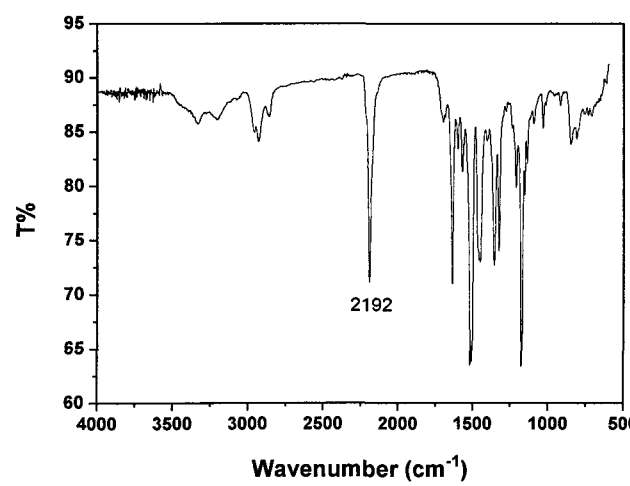

Figure 2.2. IR spectrum of FDCN (KBr pellet).

In order to illustrate the extent of ground-state charge separation, selected IR data of **2**, FDCN, FCNE and other model compounds are listed in Table 2.1. Since the stretching frequency of the cyano groups is sensitive to the vicinal electron density, it is a good probe for the ground-state charge transfer. The bond strength and therefore the vibrational frequency of CN groups are reduced by the presence of increased vicinal electron density, which interacts with the π^* orbital of the CN group. [14]

Table 2.1. Selected IR data for **2**, FDCN, FCNE

Compound	ν_{CN} (cm^{-1})
$Li^+[C(CN)_2Ph]^-$	2178 [17a]
TCNQ	2226 [17b]
2	2224
FDCN	2192
FCNE	2180
PQDM	2173[12]
PeQDM	2146[14]

For reference, the stretching frequency, ν_{CN} = 2178 cm^{-1}, for lithium dicyano-phenylmethanide ($Li^+[C(CN)_2Ph]^-$) models a full formal vicinal negative charge; while the stretching frequency, ν_{CN} = 2226 cm^{-1}, for TCNQ serves as a model without formal vicinal charge.[15] The CN stretches at 2220 cm^{-1} and 2224 cm^{-1} for intermediate compounds **1** and **2**, respectively, point to a small formal charge at the corresponding dicyanovinyl sites. On the other hand, the lower values for FDCN (ν_{CN} = 2192 cm^{-1}) and FCNE (ν_{CN} = 2180 cm^{-1}) imply considerable CT character in the ground state. The smaller $\nu_{C\equiv N}$ frequency for FCNE indicates that more aromatization was gained from ICT than FDCN. Similar comparison of the smaller $\nu_{C\equiv N}$ frequency of PeQDM (2146 cm^{-1}) with that of PQDM (2173 cm^{-1}) indicate that PeQDM with one cyano and one ester group

at the acceptor part gain more aromatization stabilization than PQDM, which shows that PeQDM has a higher molecular hyperpolarizability and larger EO coefficient than PQDM.

2.2.1.3 Structure Characterization by X-ray Crystallograph

Further evidence for the formation of zwitterionic chromophores is provided by X-ray crystallography. Although it is often difficult to grow single crystals of highly dipolar dyes, crystal of FDCN suitable for crystallographic structure analysis and can be obtained by slow crystallization from a hexane/acetone solution at room temperature. Important crystallographic data for FDCN are collected in Appendix A. The molecular structure of FDCN and selected bond lengths of the crystal are shown in Figure 2.3 and Table 2.2, respectively.

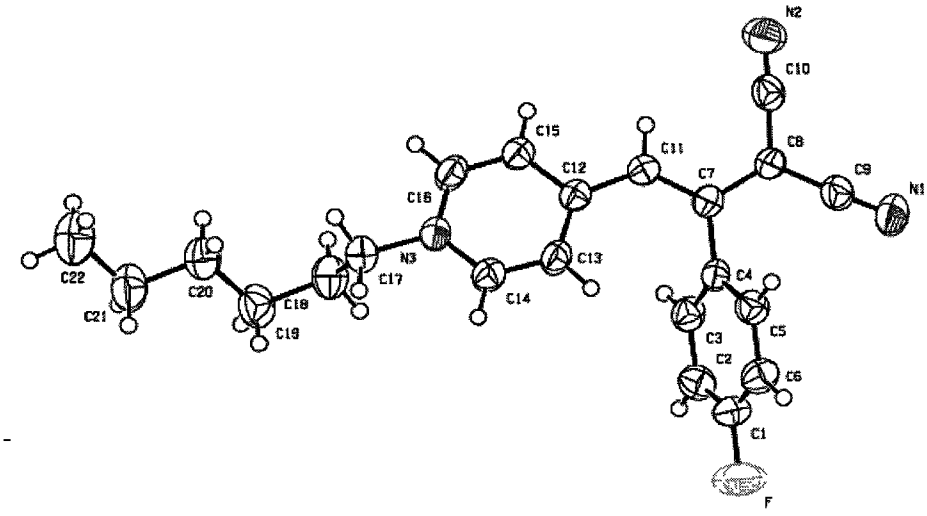

Figure 2.3. ORTEP drawing of the structure of FDCN in the crystal with atomic number. Hydrogen atoms were omitted for clarity.

Despite of the considerable number of bulky substituents, an almost undisturbed π-conjugated system, which is nearly coplanar, is observed and reveals significant bond

length equilibration within the conjugated path. The central C7-C11 bond has a bond length of 1.384 Å, very similar to the length of a C=C double bond is maintained (standard C-C single bond and double bond values are 1.46 Å and 1.34 Å, respectively.[16]), indicating a significant displacement of electron density (or charge transfer) from the donor to the acceptor moieties, corresponding to a large contribution of the zwitterionic resonance structure in FDCN. This conclusion is also supported by additional bond lengths shown in Table 2.2.

However, single bond character is observed between C7 and C8 (1.408 Å) also evident from the observed C-CN bond (1.411 Å and 1.420 Å in FDCN vs 1.427 Å in typical TCNQs), indicating substantial negative charge localization within the $-C(CN)_2$ group, and elongated CN (1.151 Å and 1.147 Å) bond compared to that in typical TCNQs (1.144 Å) [17] indicating a result of charge resonant stabilization via the two CN groups.

Table 2.2. Selected bond distances for FDCN in the crystal[a]

Atom1	Atom 2	Å	Atom1	Atom 2	Å
C4	C7	1.487(2)	C16	N3	1.352(1)
C7	C11	1.384(4)	C14	N3	1.349(2)
C7	C8	1.408(2)	C17	N3	1.480(1)
C11	C12	1.416(2)	C8	C9	1.411(2)
C12	C13	1.409(2)	C8	C10	1.420(2)
C12	C15	1.413(2)	C9	N1	1.147(2)
C13	C14	1.352(2)	C10	N2	1.151(2)
C15	C16	1.349(2)	C1	F	1.362(4)

[a] Esd's in parentheses refer to the last digit.

For comparison, the well-known Brooker dye 4-{2-[1-methyl-4-(1*H*) pyridylidene] ethylidene}cyclohexa-2,5-dien-1-one (Scheme 2.4), which has a similar conjugated backbone and a length of the central bond of 1.35 Å in the solid state, is considered as the

prototype of a zwitterionic merocyanine dye, with an estimated degree of 81.8% for the zwitterionic form. [18] The longer central bond, 1.384 Å, in FDCN indicated that less than 80% of the zwitterionic form in its ground state. Compared to the central bond length of PeQDM (1.354 Å, double bond character), FDCN has a lower degree of charge transfer in ground state than that of PeQDM.

Although the bond lengths in the conjugated bridge and acceptor part clearly demonstrated a zwitterionic molecular structure of FDCN, the bond length of the pyridinium ring is quinoidal rather than aromatic. Similar phenomena have also been reported for other zwitterionic molecules such as DEMI [19] and PeQDM.[12] Therefore, the best description of the ground state structure of such chromophores is the combination of the two limiting forms (Scheme 2.4), zwitterionic, and neutral forms with predominantly zwitterionic structure. The zwitterionic character is also verified by the negative solvatochromism of FDCN (Table 2.4 in Section 2.2.4).

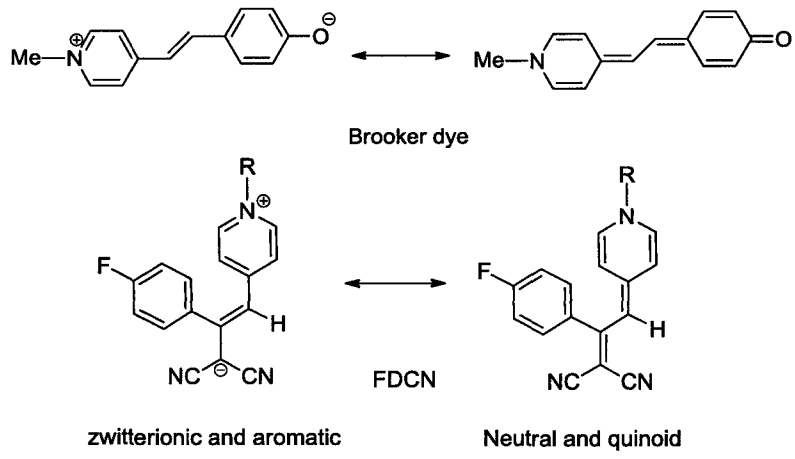

Scheme 2.4. Resonance structures of Brooker dye and FDCN.

The solid-state packing diagram of FDCN is shown in Figure 2.4 (left). Even in the presence of central bulky fluorophenyl substituents, a centrosymmetric unit of two

FDCN is observed in the crystal cell, arrayed in an antiparallel fashion with an intermolecular distance of 4.0645 Å between the aromatic backbones. Antiparallel overlap with respect to each other and a smaller slip angle (θ = 48.8°) than that in PeQDM-Ben (θ = 64.5°) is observed which indicated that there is no H-aggregation between two chromophores. The intermolecular distance (d) is considerably larger than the sums of van der Waals radii between planar cofacial π-electron systems (~ 3.50 Å)[20] and result in the difficulty in close face-to-face packing of the aromatic rings in these central bulky molecules. Therefore, incorporation of bulk groups onto the central moiety is an effective strategy to minimize molecular interaction. The weak electrostatic interactions between FDCN (compared to PQDM and PeQDM) make this kind chromophore soluble not only in polar solvents such as DMF, acetonitrile (ACN) and methanol, but also moderately soluble in less polar solvents such as chloroform, tetrahydrofuran (THF) and benzene.

However, π-π stacking formed between the substituted fluorophenyl rings (distance of 3.5 Å between these two π systems) is observed. Further increase the size of the central part of zwitterionic chromophore with bulky substituted group may effectively decrease the intermolecular distance.

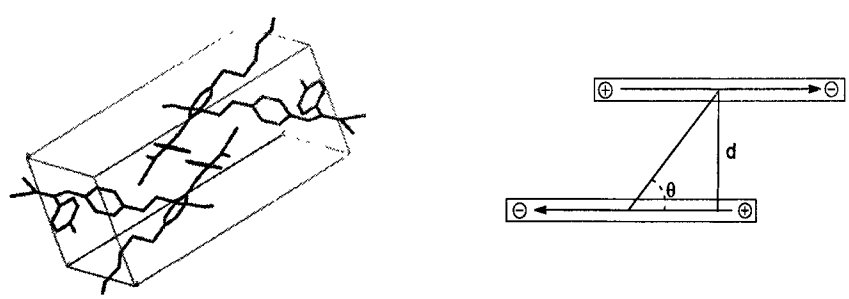

Figure 2.4. Crystal packing diagrams of chromophore FDCN (the hydrogen atoms are omitted for clarity (left) ; Model for a centrosymmetric dimer of two dipolar dyes, θ is the slip angle of the dimer, d is the distance between the π-π systems (right).

2.2.1.4 Thermal Analysis

For EO application, thermal stability of the chromophore is a key parameter for the selection of host polymer and poling temperature. The thermal properties of FDCN and BrDCN were measured by thermogravimetric analysis (TGA) under nitrogen and onset temperatures for 5% weight loss were found at 312 °C and 323 °C, respectively (Figure 2.5 left), such a thermal stability is higher than that of PQDM (Decomposition temperature ,T_d = 287 °C) [10] and PeQDMs (215 °C-287 °C). [12]

Differential scanning calorimetry (DSC) studies of FDCN and BrDCN showed typical phase transition (Figure 2.5 right). Crystallization occurs at 130 °C and 120 °C respectively before the chromophores melt at 167 °C and 196 °C. Cooling with rates of 10 °C/min does not lead to crystallization of these chromophores but to formation of amorphous solids. The propensity for glass formation was utilized on organic photorefractive materials based on merocyanine dyes.[21]

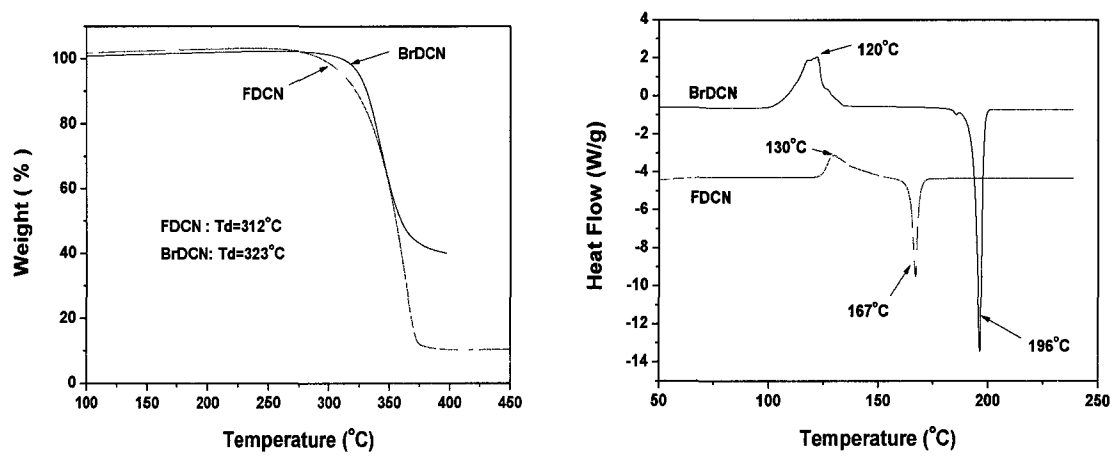

Figure 2.5. TGA (left) and DSC (right) traces of FDCN and BrDCN.

2.2.2 Synthesis and Characterizations of PpQDM Chromophores

2.2.2.1 Synthesis of PpQDM Chromophores

Using a strong electron-withdrawing group, 3CNQ, as the acceptor and dipyridylium with the different functional groups as the donor moieties, a new series of PpQDM chromophores were synthesized. The incorporation of a bulky side group is deemed to reduce the molecular symmetry and alleviate anti-parallel aggregation as well as improve solubility of these highly dipolar molecules. For further incorporation of the resulting chromophores into a polymer, (either by doping or grafting) and for comparison with the PQDM and PeQDM, the dipyridylium salts should be functionalized with some simple alkyl, benzyl and hydroxyl groups. In selecting the bromo alcohols, the rigidity and length of the spacer between the hydroxyl group and the core structure of PpQDM are considered and a flexible spacer (e.g., 3-carbon aliphatic chain) was proved to be appropriate. Using 4, 4'-dimethyl-2, 2'-dipyridyl as a starting material, the functionalized dipyridylium salts were typically prepared by refluxing the dipyridyl with corresponding alkyl halides at a high yield (Scheme 2.5).

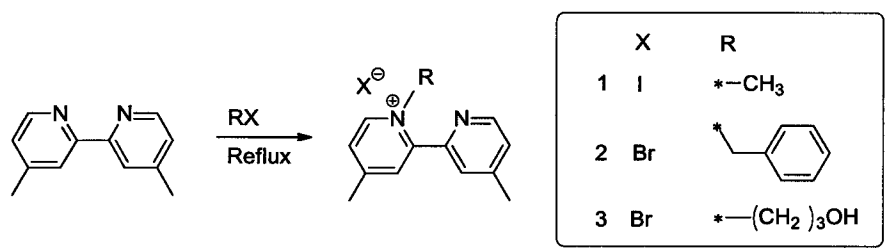

Scheme 2.5. Synthesis of dipyridylium halides.

To improve the synthesis of PpQDM chromophores, the reaction conditions were studied. First, lithium TCNQ salt was prepared by reaction of TCNQ and lithium iodide according to the literature method.[22] Using 2 molar equivalent of lithium TCNQ adduct, one molar equivalent of dipyridylium halide in methanol, and in presence of 1-

piperidineethanol as the base, three target PpQDM chromophores (PpQDM-Met, PpQDM-Ben, and PpQDM-C3OH) were successfully obtained in yields of 45-65% (Scheme 2.6).

The reaction was monitored by UV-Vis spectra of aliquots of the reaction mixture in DMF (Figure 2.6). The very intense peaks of lithium TCNQ salt at 422 nm, 747 nm and 848 nm decreased gradually when the dipyridylium halides and the base catalyst were added; the charge transfer peak of the resulting chromophore at around 690 nm started forming when half molar equivalent of catalyst was added, then it became much stronger than that of the radical anion peaks of TCNQLi after the other half of the catalyst was added.

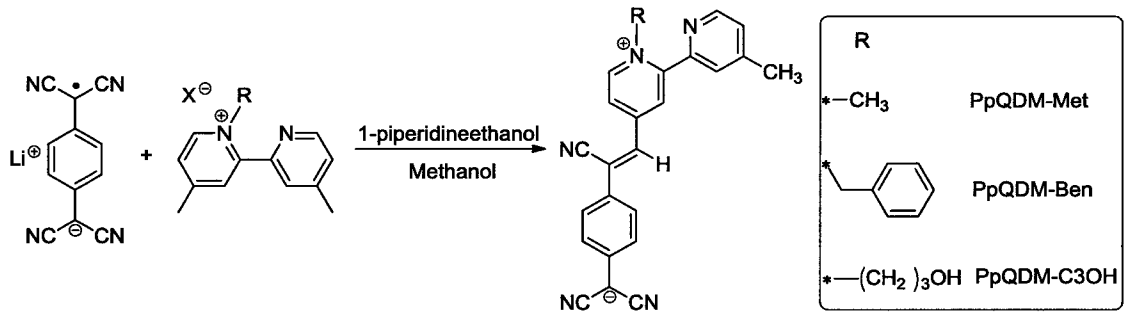

Scheme 2.6. Synthesis of PpQDM chromophores.

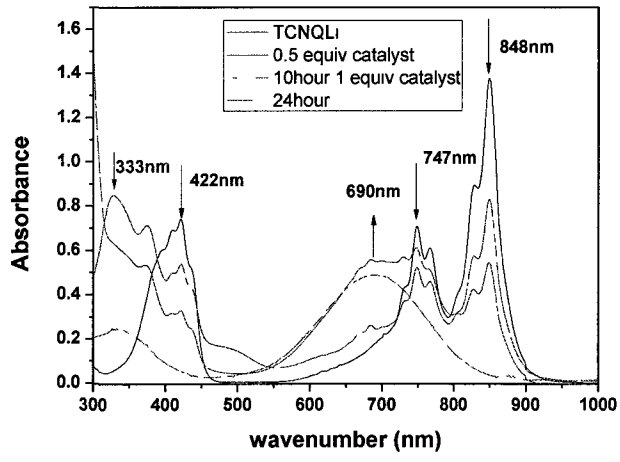

Figure 2.6. The formation of PpQDM-C3OH monitored by UV-Vis spectroscopy.

2.2.2.2 Characterizations of PpQDM Chromophores

All of the PpQDM chromophores were purified by simple filtration and washing with methanol, and the structures have been fully characterized by ^{1}H NMR, ^{13}C NMR, IR and HRMS spectrometry (Appendix B, Figure S2.13).

As shown in IR spectrum of PpQDM-Met (Figure 2.7), two different stretching frequencies of the cyano groups were found. The first one at 2226 cm^{-1}, belongs to the vinylcyano group which connects to the central carbon-carbon double bond, as in TCNQ (ν_{CN} = 2226 cm^{-1}); another group was at low wavenumber (2173 cm^{-1} and 2137 cm^{-1}) due to a large formal vicinal charge at the corresponding dicyanovinyl site, indicated a considerable charge separation in the ground state of PpQDM-Met. The smaller ν_{CN} frequency for PpQDM-Met might be due to the two fold aromatization (both donor and acceptor rings) gained from ICT.

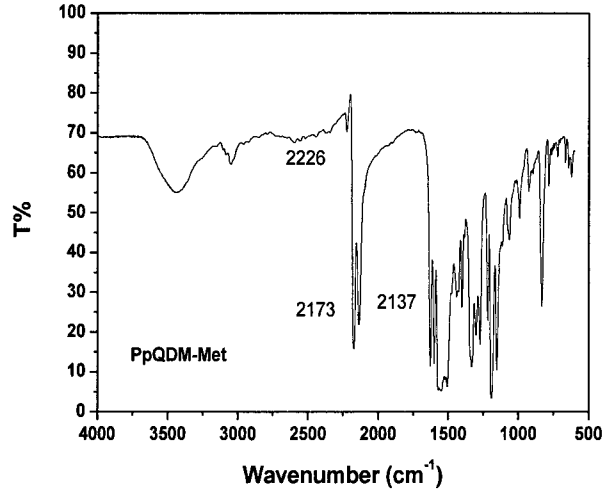

Figure 2.7. IR spectrum of PpQDM-Met (KBr pellet).

Figure 2.8 shows the ^{1}H NMR spectrum of PpQDM-Met with peaks assigned to the structure. ^{1}H NMR (2D COSY) spectrum of the aromatic protons of PpQDM-Met

and ^{13}C NMR spectrum are shown in the Appendix B (Figures S2.11 and S2.12) and are consistent with the desired structure.

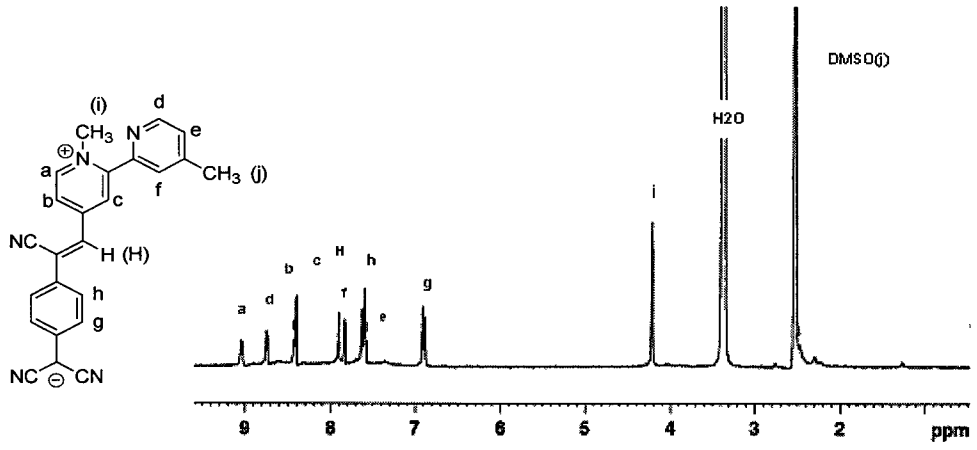

Figure 2.8. ^{1}H NMR spectrum of PpQDM-Met in DMSO-d_6.

To illustrate the extent of ground state charge separation, selected ^{1}H NMR data of FDCN and FCNE, PpQDM-Ben and PeQDM-Ben, PpQDM-C3OH, PeQDM-C3OH, and PQDM-C3OH in DMSO are listed in Table 2.3.

Table 2.3. Selected ^{1}H NMR data for FDCN, FCNE, PpQDM-Ben, PeQDM Ben, PpQDM-C3OH, PeQDM-C3OH and PQDM-C3OH

Compound	δ1 (ppm)[a]	δ2 (ppm)[b]
FDCN	7.81	3.92
FCNE	7.72	3.88
PpQDM-Ben	9.15	5.94
PeQDM-Ben	9.05	5.75
PpQDM-C3OH	9.06	4.62
PQDM-C3OH	8.94	4.57
PeQDM-C3OH	8.93	4.57

[a] The ^{1}H NMR chemical shifts of protons on methine carbon of pyridium ring

[b] Protons of the methyl attached to the tertiary nitrogen

The extent of downfield shifts of the ^1H NMR resonance of the protons on the methine carbon of pyridium ring is in accordance with the findings from CN vibration analysis. Additionally, H_g and H_h exhibit signals at 6.87 ppm and 7.58 ppm, the appearance of these proton signals in the aromatic region, downfield from the olefinic region, further supports the reduced quinoid character in the ground state, due to ICT aromatization.

In the expanded π-conjugated systems, the larger downfield shift of the methine protons in PpQDM-C3OH (9.06 ppm), PQDM-C3OH (8.94 ppm) and PeQDM-C3OH (8.93 ppm) suggests a significant degree of charge separation in the ground state, as compared to FDCN (7.81 ppm) and FCNE (7.72 ppm). The larger downfield shift of the methine protons in PpQDM-Ben (9.15 ppm) compared to that of PeQDM-Ben (9.05 ppm) indicates a greater degree of ground state charge separation due to the composition of stronger acceptor (3CNQ) and dipyridylium donor. Therefore, PpQDMs are expected to have larger μβ values than PeQDM chromophores and improve the NLO properties.

2.2.2.3 Thermal Stability of PpQDM Chromophores

The PpQDM chromophores are quite thermally stable, as measured by TGA, a high onset temperature for 5% weight loss was found at 310 °C, 304 °C and 283 °C for PpQDM-Met, PpQDM-Ben and PpQDM-C3OH, respectively (Figure 2.9). PpQDM-Met containing methyl group shows the highest T_d, which is almost 25 °C and 100 °C higher than that of PQDM and PeQDM, respectively. The enhanced thermal stability of PpQDM chromophores might be ascribed to the addition of the methyl pyridine ring on the aromatic donor. Such a thermal stability of PpQDM meets the requirements for most material processing and device fabrications.

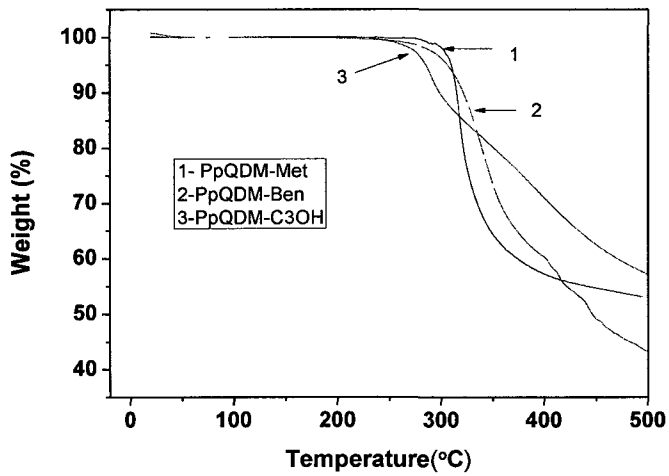

Figure 2.9. TGA trace of PpQDM-Met in nitrogen with a heating rate of 10 °C min^{-1}.

2.2.3 UV-Vis-NIR Absorption

The absorption characteristics of FDCN and PpQDM chromophores were measured in DMF (Figure 2.10). All of the two series of chromophores exhibit intense optical absorption in the UV-Vis-NIR region with extinction coefficients as large as 33,300 M^{-1} cm^{-1}.

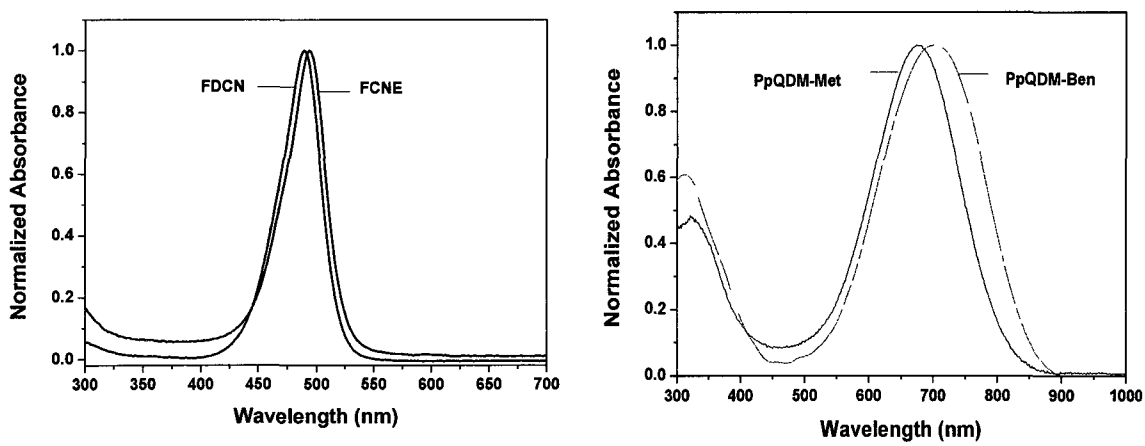

Figure 2.10. Optical absorption spectra of FDCN (left) and PpQDM (right) chromophores in DMF solution.

The FDCN and FCNE optical absorption spectra are selected and show maximum absorption wavelength (λ_{max}) at 489 nm and 493 nm, respectively, assignable to ICT excitation in Figure 2.10 (left), pyridinium intra-subfragment excitation is expected to be at higher energy [23] and overlap with the solvent cut-off.

In the UV spectral region (Figure 2.10 right), the PpQDM spectrum also features an intense band at 330 nm, assigned to pyridinium and phenyl subfragment high-energy intra-ring excitations; the strong long-wavelength absorption band at 680 nm (PpQDM-Met) and 690 nm (PpQDM-Ben) with a molar extinction coefficient of 26,000-27,000 $mol^{-1}cm^{-1}$ is due to CT from the negatively charged dicyanomethanide group to the positively charged nitrogen in pyridium.[24] CT band of PpQDM-Met blue shifts (10 nm) compared to bulky phenyl-functionalized PpQDM-Ben due to stronger antiparallel centrosymmetric dimer formation as has also been reported in merocyanine dye aggregation studies. [20] All of the PpQDM chromophores are readily soluble in polar aprotic solvents such as DMF, DMSO and NMP, but moderately soluble in polar solvents such as ACN, methanol and acetone and essentially insoluble in less polar solvents such as chloroform, THF and benzene.

2.2.4 Negative Solvatochromism

To investigate the solvatochromism of FDCN and PpQDM chromophores, the maximum optical absorption wavelengths of FDCNs and PpQDMs in various solvents were measured and the selected results are summarized in Table 2.4, while representative absorption spectra of PpQDM-Met are presented in Figure 2.11.

Table 2.4. Optical absorption (λ_{max}, nm) data for FDCN and PpQDM chromophores

Compound	λ_{max}(nm)					
	THF 7.6[a],37.4[b]	Acetone 20.7,42.2	Methanol 32.7,55.4	DMF 36.7,43.2	ACN 37.5,45.6	DMSO 46.7,45.1
FDCN	495	487	480	485	483	484
FCNE	502	495	486	493	490	492
PpQDM-Met	810	713	647	680	673	655
PpQDM-Ben	830	737	678	691	689	683

[a] Solvent Dielectric Constant (ε) (Lide D. R. *Handbook of chemistry and physics* 76th edition, P8-64, 1995-1996) [b] Reichardt $E_T^{(30)}$ values

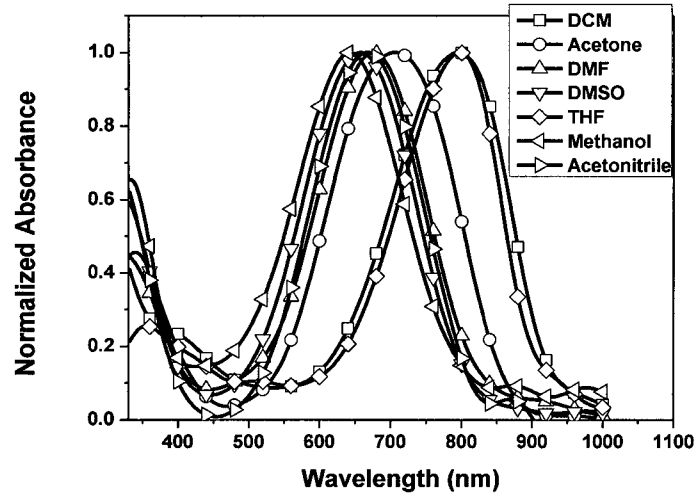

Figure 2.11. UV-Vis-NIR spectra of PpQDM-Met in different solvents.

In this experiment the relative polarity of the solvents was firstly determined based on their dielectric constants (ε): THF < Dichloromethane (DCM) < Acetone < Methanol < DMF < ACN < DMSO. The UV-Vis-NIR absorptions of PpQDM-Met in these solvents show the corresponding blue shift with increasing solvent polarity, with the exception of methanol. Considering solute/solvent interactions, another empirical parameter of solvent polarity, $E_T^{(30)}$ was employed to determine the relative polarity of the solvents. $E_T^{(30)}$ is a well selected strongly solvent-dependent spectral absorption

parameter,[25] and the values are based on the negative solvatochromic betaine dye (pyridinium N-phenolate) as a probe molecule (Structure in Chapter **1**, Table 1.4), and they are defined as the molar electronic transition (ET) energy of the dissolved dye. By using the $E_T^{(30)}$ parameter as the index of solvent polarity, the above solvents have a polar order: THF < DCM < Acetone < DMF < ACN < DMSO < Methanol and the order is consistent with the UV-Vis-NIR spectral results of PpQDM-Met.

From the solvatochromism data presented in Table 2.4 and Figure 2.11, two major points are apparent, 1) the direction of the solvatochromic shift and 2) the magnitude of the solvatochromic shift ($\Delta\lambda_{max}$). It can be seen that the CT band of PpQDM-Met exhibits strong negative solvatochromic effect - a large blue shift with increasing solvent polarity (the spectra were recorded in the concentration range where aggregation is not significant). The CT band of PpQDM-Met is blue shifted from 810 nm in the less polar THF to 647 nm in the polar methanol. This represents a shift of ~163 nm, and is comparable to the largest solvatochromic effects reported in heavily studied merocyanine derivatives, [20] approximately a third that of the Reichardt betaine dye.[25] The negative solvatochormism result indicates that the charge-separated resonance form of PpQDM-Met is more dominant in the ground state than the excited state ($\mu_g > \mu_e$) (Scheme 2.7). Consequently, greater stabilization of the zwitterionic form occurs in high polarity solvents than in low polarity solvents, leading to higher energy absorption maximum in high polarity solvents. FDCN chromophores also show a blue shift in their absorption maxima in going from non-polar to polar solvents and are therefore good examples of zwitterionic chromophores, which is consistent with the conclusion obtained from IR and X-ray crystallographic results.

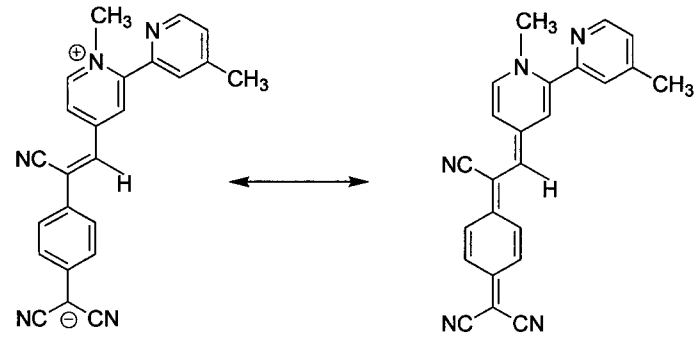

Zwitterionic Form
(Ground state)

Neutral Form
(Exited state)

Scheme 2.7. Resonance structures of PpQDM-Met.

With respect to the second observation, the magnitude of the solvatochromic shift in the PpQDM chromophores (on average 157 nm) is larger than the solvatochromic shift in the FDCN chromophores (on average 15 nm). This can be explained by the magnitude of the gain in resonance stabilization energy upon aromatization of the two donor and acceptor units. The gain in aromaticity for the FDCN chromophores is expected to be less than in the case of PpQDMs due to the combination of a weaker acceptor and shorter conjugated bridge. Therefore, in comparison to the charge-separated forms of PQDM (a blue shift as large as 125 nm), PpQDMs chromophores are more stabilized in high polarity media, meaning the first hyperpolarizabilities and dipole moments of the PpQDM chromophores will be larger than those observed for the PQDM chromophores.

Few TCNQ-based chromophores have been described in terms of their solvent polarity indicating abilities. DEMI was extensively studied in terms of solvatochromic effects and shows a very limited response when compared to the Reichardt betaine dye. [26] Thus PpQDMs appear to be one of the novel $D^{\delta+}$–π–$A^{\delta-}$ solvatochromic systems.

2.2.5 Fluorescence Properties of FDCN and PpQDM Chromophores

The sensitivity of betain dyes to solvent polarity is exceptionally high; however, they are not fluorescent. Polarity-sensitive fluorescent dyes offer distinct advantages especially in biological studies. The fluorescence properties of FDCN and PpQDM chromophores in DMF were studied, and the results are summarized in Table 2.5 with the optimal concentration for PL measurement to be 2×10^{-5} M. The emission spectra of dilute solutions of FDCN and PpQDM-Met chromophores excited at 470 nm and 670 nm are presented in Figure 2.12. The strongest emission bands of FDCN and PpQDM-Met have maxima at 530 nm and 875 nm, respectively. Further, the fluorescence spectra associated with the lowest excited singlet states display mirror image relationships to the corresponding absorption bands with Stokes shifts of between 45 nm (1388 cm^{-1}) and 195 nm (3277 cm^{-1}) which are typical of dipolar, monomeric molecules in polar solvents. [27]

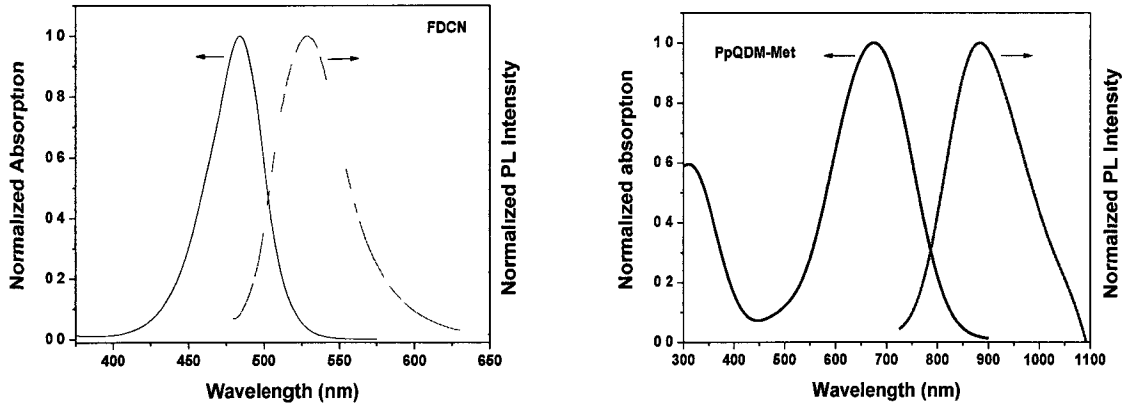

Figure 2.12. The normalized absorption and emission spectra of FDCN (left) and PpQDM-Met (right) in DMF.

Stokes shift (the gap between the maximum of the first absorption band and the maximum of the fluorescence spectrum, expressed in wavenumbers, $\Delta\bar{\nu} = \bar{\nu}_a - \bar{\nu}_f$)

indicates the difference in the properties and the structure between the ground S_0 state, and the first exited S_1 state. The values of Stokes shift of FDCN is relative smaller around 1760 cm^{-1} (shift between the maximum of emission and maximum of the absorption $\Delta\lambda = \lambda_F - \lambda_A = 40 \sim 45$ nm) than that of PpQDM which are in the 2950-3277 cm^{-1} region ($\Delta\lambda = \lambda_F - \lambda_A = 190 \sim 195$ nm), due to its shorter conjugated bridge and smaller relative dipole moment compared with PpQDMs. The larger Stokes shift of PpQDM is in accordance with other investigations on PQDM and PeQDM derivatives. Compared with other known zwitterionic compounds, such as DEMI, whose Stokes shift is only 1505 cm^{-1} ($\Delta\lambda$ = 770-690 = 80 nm), indicate that the dipyridium donor is a key determinant in making the PpQDM-Met into an extended delocalized π-electron system.

Table 2.5. Optical properties of the band of CT of FDCNs and PpQDMs in DMF

Compound	λ_A (nm)[a]	λ_F (nm)	$\lambda_F - \lambda_A$ (nm)	Φ_F (%)
FDCN	485	520[b]	45	0.40[d]
FCNE	493	533[b]	40	0.27[d]
PpQDM-Met	680	875[c]	195	0.20[e]
PpQDM-Ben	705	890[c]	185	0.19[e]

[a] Measured in DMF at a concentration of 2×10^{-5} M. [b] Measured in DMF at a concentration of 2×10^{-5} M. Excitation wavelength = 470 nm. [c] Measured in DMF at a concentration of 2×10^{-5} M. Excitation wavelength = 670 nm. [d] Fluorescence quantum yield, relative to Rhodamin 6G (Φ_F = 0.88 in Ethanol). [e] Fluorescence quantum yield, relative to IR-125 (Φ_F = 0.13 in DMSO).

In this work, both FDCN and PpQDM-Met as the representatives of the two new series of chromophores were evaluated as polarity-sensitive fluorescent dyes. In 2008, PeQDM-Ben was found to exhibit NIR photoluminescence at ~860 nm in DMF solution when being excited at 650 nm,[28] and it has potential application as a pH sensor. PpQDM chromophores show tuneable NIR fluorescence (e.g., 875 to 890 nm) longer than that of

PeQDM by changing the strength of donor through introducing different substituted groups on the nitrogen of the dipyridium ring, which indicated that the stronger charge transfer occurred in PpQDM than that in PeQDM, therefore, PpQDM were expected to show stronger fluorescence sensitivity to the polarity of the environment.

First, the sensitivity of the FDCN fluorescence to solvent polarity was investigated; the results are summarized in Table 2.6. As seen in Figure 2.13, a series of fluorescence spectra of FDCN show the blue shift with increasing solvent polarity, the spectral maxima extending from 524 nm (in methanol) to 539 nm (in 1,4- dioxane). This is the first report of zwitterionic chromophores showing potential application as polarity-sensitive fluorescent dyes in the visible region.

Table 2.6. Optical properties of the CT band of FDCN in different solvents

Solvent	Dielectric constant (ε)	λ_A (nm)	ε ($Lmol^{-1}cm^{-1}$)	λ_F (nm)	$\lambda_F - \lambda_A$ (nm)
1,4-Dioxane	2.2	498	75,498	539	41
THF	7.6	495	97,380	538	43
DCM	8.9	498	102,300	535	37
Acetone	20.7	487	96,224	531	44
Methanol	32.7	480	104,540	520	44
DMF	36.7	484	64,400	529	45
ACN	37.5	483	95,340	526	43
DMSO	46.7	485	106,320	528	43

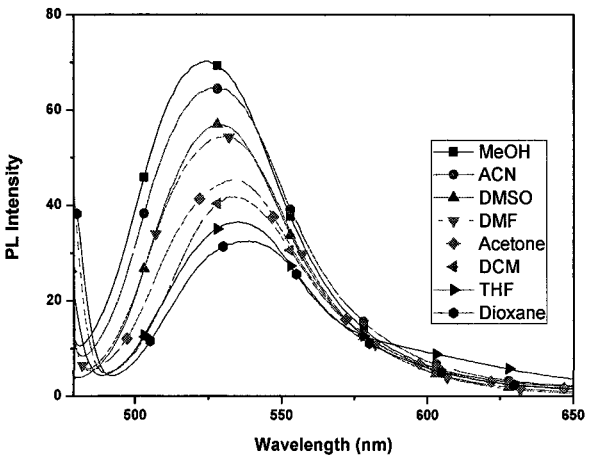

Figure 2.13. Fluorescence spectra of FDCN solutions excited at 460 nm. The successive maxima correspond to methanol, ACN, DMSO, DMF, acetone, DCM, THF and 1, 4-dioxane. The heights do not reflect relative fluorescence yield.

Compared with FDCN, PpQDM-Met offers outstanding sensitivity of fluorescence to the changes in solvent polarity. The fluorescence spectra show the remarkable blue shift with increasing solvent polarity, which extends from 840 nm (in methanol) to 930 nm (in DCM). Table 2.7 shows the maximum fluorescence and absorption data of PpQDM-Met in various solvents. The shift of the absorption peaks with solvent polarity ($\Delta\lambda_A$= 148 nm from THF to methanol) are more pronounced than the shifts of emission peaks ($\Delta\lambda_F$ = 75 nm). This indicates that $\mu_g > \mu_e$, dipole moment of the chromophore decreases upon excitation. The increase in the Stokes shift from 1649 cm^{-1} in THF to 3693 cm^{-1} in DMSO is very large. The increased Stokes shift in polar solvents can be attributed to the higher degree of solvent stabilization effect on the ground state energy than on the excited state. This indicates that the ground state dipole moment of PpQDM-Met is significantly larger than the one in the excited state, leading to pronounced solvatochromism of fluorescence. The larger shift between the emission and absorption of PpQDM in polar solvents offers the most important additional

advantage for PpQDM chromophores - application as a novel environmentally sensitive single molecule fluorophore. [29]

As shown in Table 2.7, the emission yields of PpQDM-Met shows large variations depending strongly on the polarity of the solvent, with values in the range of 0.058-0.7. Figure 2.14 presents the dependence of the quantum fluorescence yield on the dielectric constant of the solvents. The maximum yields are found in solvents of higher polarity, with a several-fold decrease in low polar solvents.

Table 2.7. Optical properties of the CT band of PpQDM-Met in different solvents

Solvent	Dielectric constant (ε)	λ_A (nm)	λ_F (nm)	$\lambda_F - \lambda_A$ (nm)	Stokes shift (cm^{-1})	Φ_F (%)[a]	Δf [b]
THF	7.6	795	915	120	1649	0.058	0.210
DCM	8.9	805	930	125	1669	0.073	0.219
Acetone	20.7	713	885	172	2726	0.088	0.287
Methanol	32.7	647	840	193	3550	0.137	0.308
DMF	36.7	680	875	195	3277	0.20	0.276
ACN	37.5	673	870	197	3356	0.32	0.304
DMSO	46.7	655	864	209	3693	0.70	0.265

[a] Fluorescence quantum yield, relative to IR-125 ($\Phi_F = 0.13$ in DMSO).
[b] The orientational polarizability of the solvents.

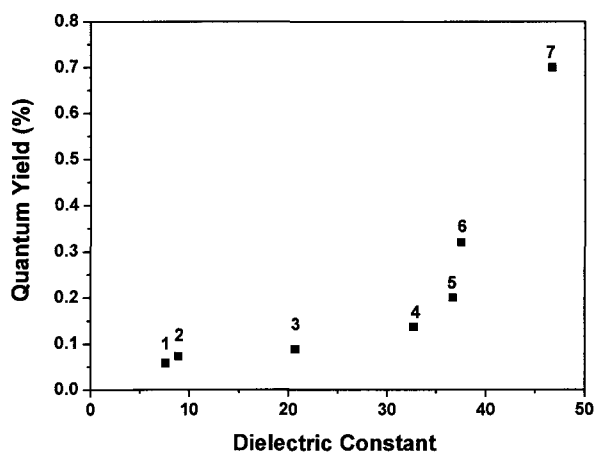

Figure 2.14. Fluorescence quantum yields (Φ_F) of PpQDM-Met vs. the solvent dielectric constant (ε) THF (1), DCM (2), acetone (3), MeOH (4), DMF (5), ACN (6), DMSO (7).

The Stokes shifts against the orientational polarizability of the solvent was also shown in Table 2.7, the orientational polarizability of the solvent is defined by eq.1, [30] where n is the refractive index of the solvent and ε is its dielectric constant. Inspection of Table 2.7 shows that at similar values of Δf (compare methanol and ACN, both close to $\Delta f = 0.3$), the aprotic solvent ACN produce considerably smaller Stokes shifts than those which can form a hydrogen bond by acting as proton donors. Similar effects have been noted for other studied fluorophores. [31]

$$\Delta f = \frac{\varepsilon - 1}{2\varepsilon + 1} - \frac{n^2 - 1}{2n^2 + 1} \quad \text{(eq.1)}$$

Solvatochromic shift of the emission spectra is often applied to determine the dipole moment difference $\Delta\mu$ between the first excited electronic state and the ground state of chromophores. The larger $\Delta\mu$ of PpQDMs than PQDMs and PeQDMs were proven by the larger solvatochromic shift of their emission spectra. The fluorescent property of PpQDMs will be further discussed in Chapter **5**, together with NIR fluorescent probes application.

2.2.6 Dipole Moment and Molecular Hyperpolarizability

The dipole moments of a molecule in the ground and excited states are different due to changes in electron densities in these states. A change in solvent is accompanied by a change in polarity, dielectric constant or a change in polarizability of the surrounding medium. Thus, a change of solvent affects the ground and excited states differently. A prior knowledge of the dipole moments of electronically excited species is often useful in the design of NLO materials.

The dipole moment of FDCN and FCNE were measured by the most common method based on dielectric and refractive index measurements according to Debye's theory. The changes in the dielectric constant and the refractive index of solutions of the chromophores in nonpolar solvent, chloroform, are measured and a dipole moment of 21.6 D for FDCN and 11.39 D for FCNE were obtained.

The calculation of the dipole moment of PpQDM chromophores was performed as a result of their lower solubility in nonpolar solvents. Structures of these chromophores were sketched and energy minimized using PM6 Method. The dipole moments were calculated using B3LYP/6-31+G (d) method and the results were shown in Table 2.8.

To be useful for EO applications, potential chromophores need to possess large NLO responses ($\mu\beta_0$) greater than 2000×10^{-48} esu. [32] Molecular first hyperpolarizability measurements can be carried out by a number of techniques including EFISH, Hyper-Rayleigh scattering (HRS), etc. Among of these techniques, HRS is the most straight forward techniques, since it is based on the incoherent SHG obtained directly from randomly oriented chromophores in a dilute solution.

As a collaborative work, HRS measurements were carried out on two chromophores from the PQDM and PeQDM series [10,12] by a physics group at the University Antwerpen in Belgium, yielding extremely large dynamic first hyperpolarizabilities of $\beta_{zzz} = 1865 \times 10^{-30}$ esu for PQDM-Met and $\beta_{zzz} = 1797 \times 10^{-30}$ esu for PeQDM-Ben. These values correspond to β_0 value of 595 and 670×10^{-30} esu, respectively, which are in agreement with theoretical predictions. In this work, dynamic β values of FDCN and FCNE were measured by the same HRS method in DMF solution at 1.07 μm wavelength, and are represented as the β_{zzz} component, assuming all other

components are negligible (i.e. an idealized linear chromophore is assumed). The β values of PpQDM chromophores were calculated from Gaussian 98, results based on the above experimental data and known standards (e.g., DEMI, 27 D, $\mu\beta_0$ value of 9500 × 10^{-48} esu). [33] All of the experimental and theoretical results are summarized in Table 2.8.

Table 2.8. Physical properties of FDCN and PpQDM chromophores, in comparison to the PQDM and PeQDM chromophores

Chromophore	μ (D)	β (× 10^{-30} esu)	β_0 (× 10^{-30} esu)
FDCN	21.6[a]	-320[c]	45[d]
FCNE	11.39[a]	-495[c]	57[d]
PpQDM-Met	50.0[b]	-1918[b]	697
PpQDM-Ben	47.0[b]	-1942[b]	752
PQDM-Met	40.5[36]	-1865[c]	595[5]
PeQDM-Ben	--	-1797[c]	670[12]

[a] experimental value measured in $CHCl_3$; [b] calculated value; [c] experimental value measured in DMF at 1070 nm; [d]β_0 (static hyperpolarizability) was derived from the simple two-level model as described in eq. 2: [35]

$$\beta = \beta_0 \frac{\lambda^4}{(\lambda^2 - \lambda_{max}^2)(\lambda^2 - 4\lambda_{max}^2)} \qquad \text{(eq.2)}$$

λ is the wavelength of the optical field (1.07 μm) and λ_{max} is the wavelength of the CT band. PQDM-Met: λ_{max} = 654 nm in DMF;[11] PeQDM-Ben: λ_{max} = 691 nm in DMF[13]; PpQDM-Met: λ_{max} = 680 nm in DMF and PpQDM-Ben: λ_{max} = 690 nm in DMF.

The results from Table 2.8 show that PpQDM chromophores have larger hyperpolarizabilities than PQDM and PeQDM chromophores. The β values of PpQDM chromophores are almost 4 times higher than that of FDCNs, which are attributed to an increase in conjugation leading to a gain in stability from the aromatized negatively charged acceptor; when compared to DEMI ($\mu\beta_0$ = 9500 × 10^{-48} esu), the significant enhancement of hyperpolarizabilities (e.g., $\mu\beta_0$ = 34,850 × 10^{-48} esu for PpQDM-Met) are due to the stronger aromatic donor. By taking the dipole moment of PpQDM-Met (μ = 50

D), an extraordinary large μβ value of $-95{,}900 \times 10^{-48}$ esu was obtained, which is much larger than that of the benchmark chromophore, FTC ($\mu\beta = 18{,}000 \times 10^{-48}$ esu).

2.2.7 Acid Sensitivity

In the previous study, PQDM and PeQDM were found to be sensitive to acids such as H_2SO_4, HCl and acetic acid, but fairly stable in basic media at room temperature. Due to the longer "push-pull" backbone, PpQDMs show a stronger CT absorption band at 680 nm to 690 nm in DMF (Figure 2.15) and give a bright blue color. The pronounced negative halochromism of PpQDM-Met can be demonstrated by a test-tube experiment: upon addition of water, the absorption of PpQDM-Met in DMF shifted to shorter wavelengths and causes a distinct color change from blue (λ_{max} = 680 nm) to purple (λ_{max} = 580 nm, $\Delta\lambda$ = -100 nm) at a (H_2O/DMF) volume ratio of 5:1. When an excess of acid is present, the blue color solution of PpQDM-Met turned colorless immediately, the visible absorption band disappears on the protonation of the negative carbon atom, while the intra-ring excitation band at 330 nm is unaffected. Subsequent addition of DMF to the acid containing solution moved the absorption back to 680 nm.

This reversible color-changing process is believed to be due to the protonation of the chromophore by acid and deprotonation by base at the acceptor moiety (Scheme 2.8). To further investigate the mechanism of the halochromism, P-PpQDM-Met (protonated PpQDM-Met) was prepared by introducing an excess of dry HCl to the solution of PpQDM-Met and precipitated from ethyl ether.

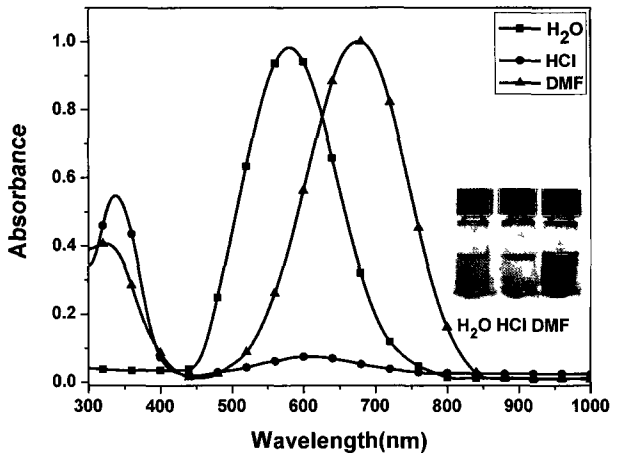

Figure 2.15. UV-Vis spectra of PpQDM-Met in DMF, H_2O and HCl.

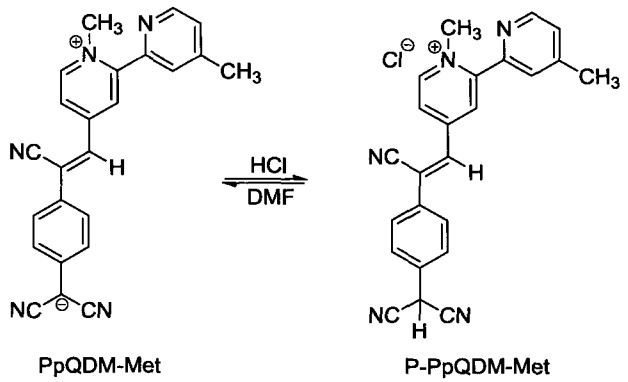

Scheme 2.8. Protonation of PpQDM-Met and deprotonation of P-PpQDM-Met.

The results from Figure 2.16 show that the position and intensity of $\nu_{C\equiv N}$ at the acceptor of PpQDM-Met changed noticeably after protonation. Before protonation, $\nu_{C\equiv N}$ was at a lower frequency (2173 cm^{-1} and 2137 cm^{-1}) with high intensity due to the adjacent negative carbon center -$C(CN)_2$; after protonation, $\nu_{C\equiv N}$ moved to higher frequency (2248 cm^{-1}) with a much smaller intensity, which is typical for C≡N group connected to the neutral saturated carbon atom. The vinylcyano group at the central part of the chromophore (2226 cm^{-1}) did not show any difference after the protonation. This indicated that the negatively charged part of PpQDM-Met can function as a binding site

to proton due to the presence of the negative charge. The strong dipyridium donor and –C $(CN)_2$ negative carbon center make PpQDM-Met a promising molecular probe to further investigate the spectra response upon binding with metal ions or neutral organic molecules. The application of this colorimetric and fluorescence molecular probe for sensitive and selective detection of metal ions and amino acids will be discussed in Chapter **5**.

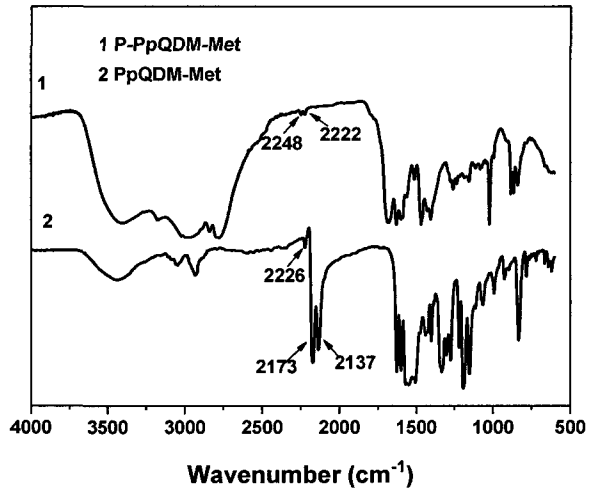

Figure 2.16. IR spectra of PpQDM-Met and P-PpQDM-Met.

2.3 Conclusions

Two series of novel zwitterionic chromophores FDCNs and PpQDMs have been designed and synthesized in moderate yields (40 - 60%). Optimal synthetic conditions have been established for both series of chromophores. Hydroxyl-containing FDCN and PQDM chromophores have been synthesized for covalent coupling with polymers. X-ray crystallographic data, negative solvatochromism, IR and ^{1}HNMR and ^{13}CNMR data analysis confirm the highly charge-separated ground state of these two series of zwitterionic chromophores. These chromophores show good solubility in common organic solvents and high thermal stability.

X-ray crystallographic data of FDCN demonstrated that incorporation of bulk groups onto central part of the chromophore is an effective strategy to minimize dipole-dipole molecular interaction; higher solubility of FDCN in low polarity solvents makes it a good zwitterionic chromophore for experimental measurements of dipole moment and first hyperpolarizability, and these accurate experimental values were employed as internal standards for theoretical calculation for that of PpQDMs chromophores.

PpQDM chromophores with a stronger donor (dipyridylium), longer conjugation bridge and stronger acceptor 3CNQ were found to have large dipole moment and very large molecular hyperpolarizability, which demonstrates the great potential of this type of chromophores for NLO applications.

The solvent dependence of the fluorescence of PpQDM chromophores has been investigated. PpQDMs chromophores are NIR fluorescent with large Stokes shift (3839 cm^{-1} in polar solvent) and show high microenvironmental (e.g., pH and solvent polarity) sensitivity, which make them an interesting new class of NIR fluorescent polarity probes and promising candidates for NIR fluorescent chemosensor applications.

2.4 Experimental Section

Materials. TCNQ was purchased from Aldrich Chemical Canada. Lithium TCNQ salt was prepared according to the literature procedure.[22] DMF was dried and distilled over CaH_2 under an atmosphere of dry nitrogen. 4-Bromophenylacetonitrile, 4-pyridinecarboxaldehyde, DBU, 1-bromohexane, malononitrile, fluorophenylacetonitrile, methyl cyanoacetate, cyanoacetic acid, hydroxyethyl cyanoacetate, 4,4'-dimethyl-2,2'-dipyridyl, benzyl bromide, 3-bromo-1-propanol and all other reagents and solvents were purchased from Aldrich and used as received.

General Methods. ^{1}H and ^{13}C NMR spectra were recorded on a Varian 300 MHz (300 and 75 MHz for ^{1}H and ^{13}C NMR, respectively) or a Bruker AMX 400 MHz spectrometer using tetramethylsilane (TMS; δ = 0 ppm) as an internal standard. The Fourier transform infrared (FTIR) spectra were recorded on a Perkin-Elmer1600 or a Bomen Michelson 120 FTIR spectrometer in the regions of 4000-400 cm^{-1}. Mass spectra were measured with a Micromass Quattro LC ESI mass spectrometer (EI and TOF-ESI). The melting points were determined using a Fisher-Johns melting point apparatus. Standard differential scanning calorimetric analysis was carried out in nitrogen on a TA DSC Q100 with a heating rate of 10 ^{o}C min^{-1}. Thermogravimetric analysis was carried out in nitrogen on a Hi-Res TGA 2950 thermogravimetric analyzer with a heating rate of 10 ^{o}C min^{-1}. The UV-Vis-NIR spectra were recorded on a Perkin-Elmer Lambda 900 UV-Vis-NIR spectrometer at room temperature. The solvatochromism study was conducted using organic solvents across a range of dielectric constants (ε): THF, DCM, acetone, methanol, DMF, ACN and DMSO. Due to the poor solubility of PpQDM-Met in THF, the THF solution was prepared by adding 20 μL of PpQDM-Met in DMF (2×10^{-5} M) into 1.98 mL of THF. Fluorescence emission spectra were measured on a PTI fluorescence system. The absorption and fluorescence emission spectra of all the samples were taken in DMF/MeOH solution in a quartz cuvette with a path length of 10.0 mm.

Single Crystal X-ray Diffraction. All diffraction measurements were carried out on a Bruker SMART APEX CCD diffractometer with graphite-monochromated Mo-Kα (λ = 0.71073 Å) radiation. Data were collected using the Bruker SMART detector, processed using the SAINT Plus package from Bruker. The structures were solved by direct methods (SHELXS-97) and expanded using Fourier techniques (SHELXL-97). All

calculations were performed using the Bruker SHELXTL97 crystallographic software package.

Quantum yields measurement

The fluorescence emission spectra were measured with a PTI spectrofluorometer. The fluorescence emission spectra of FDCNs and PpQDMs (2×10^{-5} M) were measured at 25 °C, with excitation at 470 nm and 670 nm. The fluorescent quantum yield (Φ_F) of FDCNs and PpQDMs were evaluated using a relative method with reference to luminescence standards, Rhodamin 6G (Φ_F = 0.88 in ethanol) [36] and IR-125 (Φ_F = 0.13 in DMSO), [37] respectively. The quantum yield of FDCNs and PpQDMs can be expressed by eq. 3.[38] Φ is the quantum yield (subscript "r" stands for the reference and "x" for the sample), A is the absorbance at the excitation wavelength, I (λ) is the relative intensity of the exciting light at wavelength λ, n is the refractive index of the solvent for the luminescence, and D is the area (on an energy scale) of the luminescence spectra. The samples and the reference were excited at the same wavelength. The sample absorbance at the excitation wavelength was kept as low as possible to avoid fluorescence errors (A_{exc} < 0.1).

$$Q_x = Q_r\left(\frac{A_r(\lambda_r)}{A_x(\lambda_x)}\right)\left(\frac{I(\lambda_r)}{I(\lambda_x)}\right)\left(\frac{n_x^2}{n_r^2}\right)\left(\frac{D_x}{D_r}\right) \quad \text{(eq.3)}$$

Synthesis of FDCN Chromophores

2-(4-Bromophenyl)-3-pyridine-4-yl-acrylonitrile (1)

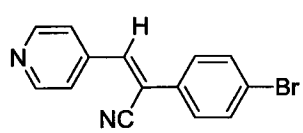

Under anhydrous and oxygen-free conditions, to a 250 mL round-bottomed flask, 4-bromophenylacetonitrile (5.9 g, 30.0 mmol), 4-pyridinecarboxaldehyde (3.0 mL, 30.0 mmol), 80 mL of dry THF, and 1mL of DBU were added. The mixture was heated to reflux for 18 h and then cooled to room temperature. The solvent was removed under reduced pressure; the red residue was washed with methanol (30 mL), filtered and dried. The final product was an off-white crystalline collected in 3.9 g (95% yield); m.p:138-140 °C; ^{1}HNMR (300 MHz, DMSO-d_6, TMS, ppm): δ 8.75 (2H, d), 8.15 (1H, s), 7.81 (6H, m); IR (KBr, cm^{-1}): 2217 (C≡N), 1645(C=N), 1594,1588 (C=C); UV-Vis: λ_{max} = 312 nm (DMF) ; MS (EI, m/z): 284 [M$^+$], 286 [M+2]$^+$.

2-(4-Bromophenyl)-3-pyridine-4-yl-acrylonitrile bromide salt (2)

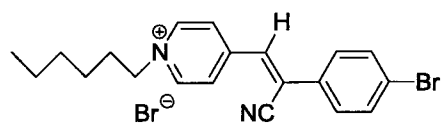

A mixture of compound **1** (0.350 g, 1.23 mmol), 1-bromohexane (2.8 mL, 20.0 mmol) and 2 mL of benzonitrile was refluxed for 18 h. The reaction mixture was cooled and the precipitate was filtered. The crude product was dissolved in 10 mL of hot acetonitrile then added into 50 mL of hot ether, and the precipitate was filtered. The final product was a yellow amorphous powder collected in 0.30 g (66% yield); ^{1}H NMR (300 MHz, DMSO-d_6, TMS, ppm): δ 9.22 (2H, d, J = 8.4 Hz), 8.48 (2H, d, J = 8.4 Hz), 8.44 (1H, s), 7.86 (4H, m), 4.64 (2H, t), 1.95 (m, 2H), 1.32 (6H, m), 0.89 (3H, t); IR (KBr, cm^{-1}): 2219 (C≡N), 1637(C=N), 1604,1583 (C=C); MS (ESI, acetonitrile, m/z): 369 (M$^+$, 100); UV-Vis: λ_{max} = 347 nm (DMF).

Synthesis of BrDCN

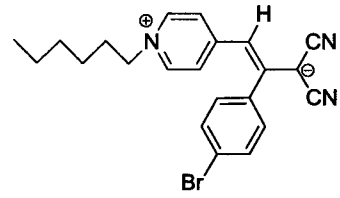

Under anhydrous and oxygen-free conditions, to a 25 mL round-bottomed flask, malononitrile (0.027 g, 0.40 mmol), sodium hydride (0.024 g, 60%, 0.60 mmol) and compound **2** (0.1 g, 0.2 mmol) were ad ded at 0 °C. After 30 min, the insoluble inorganic salt was removed by filtration, and the filtrate solution was concentrated under reduced pressure. The residue was purified by mixture of acetone and hexane (1:1). The final product was an orange-red crystal (0.059 g, 65%). m.p 196 °C; ^{1}H NMR (400 MHz, DMSO-d_6): δ 7.81 (2H, d, J = 7.1 Hz), 7.36 (2H, d, J = 8.7 Hz), 7.32 (2H, d, J = 8.7 Hz), 6.34 (2H, d, J = 7.1 Hz), 5.88 (1H, s), 3. 92 (2H, t), 1.22 (6H, m), 0.83 (3H, t); IR (KBr, cm^{-1}): 2190 ($\upsilon_{C\equiv N}$ of cyano groups), 1640 ($\upsilon_{C=N}$ of picolinium moiety), 1571, 1450 ($\upsilon_{C=C}$ aromatic ring); MS (EI, m/z): 407 $[M]^+$, 409 $[M+2]^+$; UV-Vis: λ_{max} = 486 nm (DMF); TGA: T_d = 323 °C.

2-(4-Fluorophenyl)-3-pyridine-4-yl-acrylonitrile (3)

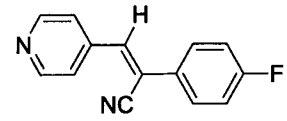

Under anhydrous and oxygen-free conditions, to a 250 mL round-bottomed flask 4-fluorophenylacetonitrile (4.05 g, 30.0 mmol), 4-pyridinecarboxaldehyde (3.2 g, 30.0 mmol), 90 mL of dry THF and 1mL of DBU were added. The mixture was heated to reflux for 18 h and then cooled to room temperature. The solvent was removed under reduced pressure and the red residue was washed with methanol (30 mL), filtered and

dried. The final product was an off-white crystalline collected in 3.4 g, 55% yield. m.p: 166-167 °C; ^{1}H NMR (400 MHz, DMSO-d_6): δ 8.75 (d, 2H), 8.15 (s, 1H), 7.81 (m, 6H); IR (KBr, cm^{-1}): 2216 (C≡N), 1592, 1543(C=C); MS (EI, m/z): 224 (M^+, 100%); UV-Vis: λ_{max}=319 nm (DMF).

2-(4-Fluorophenyl)-3-pyridine-4-yl-acrylonitrile bromide salt (4)

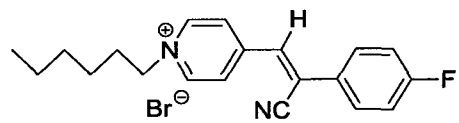

A mixture of compound **3** (1.75 g, 7.80 mmol), 1-bromohexane (20.0 mL, 143.0 mmol) and 3 mL of benzonitrile was refluxed for 18 h. The reaction mixture was cooled and the precipitate was filtered. The crude product was dissolved in 40 mL of hot acetonitrile then added into 250 mL of hot ether, the precipitated was filtered, a yellow amorphous powder collected in 2.4 g, yield 80% yield. ^{1}H NMR (300 MHz, DMSO-d_6): δ 9.23 (2H, d, J = 8.4 Hz), 8.49 (2H, d, J = 8.4 Hz), 8.45 (1H, s), 7.87 (4H, m), 4.64 (2H, t), 1.95 (m, 2H), 1.32 (6H, m), 0.88 (3H, t); IR (KBr, cm^{-1}): 2224 (C≡N), 1637 (C=N), 1597,1557 (C=C); MS (ESI, acetonitrile, m/z): 309 (M^+,100); UV-Vis: λ_{max} = 341 nm (DMF).

Synthesis of FDCN

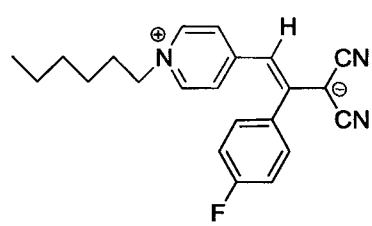

Under anhydrous and oxygen-free conditions, to a 50 mL round-bottomed flask malononitrile (0.50 g, 7.4 mmol), sodium hydride (0.30 g, 60%, 7.5 mmol) and

compound **4** (1.0 g, 2.6 mmol) in 20 mL of THF were added at 0 °C. After 30 min, the insoluble inorganic salt was removed by filtration, and the filtrate solution was concentrated under reduced pressure. The residue was purified by mixture of acetone and hexane (1:1). The final product was an orange-red crystal: 0.56 g, 63% yield; m.p:167 °C; ^{1}H NMR (400 MHz, DMSO-d_6): δ 7.81 (2H, d, J = 7.1 Hz), 7.36 (2H, d, J = 8.7 Hz), 7.32 (2H, d, J = 8.7 Hz), 6.34 (2H, d, J = 7.1 Hz), 5.88 (1H, s), 3.92 (2H, t), 1.22 (6H, m), 0.83 (3H, t); ^{13}C NMR (100 MHz, DMSO-d_6): 161.2, 151.4, 139.8, 133.7, 130.0, 129.9, 119.8, 119.2, 118.2, 116.6, 116.4, 101.7, 56.7, 30.4, 29.8, 24.9, 21.8, 13.7; IR (KBr, cm^{-1}): 2192 ($\upsilon_{C\equiv N}$ of cyano groups), 1640 ($\upsilon_{C=N}$ of picolinium moiety), 1571, 1450; TOF HRMS (ESI, DMF/Acetonitrile 1:1, m/z): 348.1776 $[M+H]^+$, 370.1608 $[M+Na]^+$, calculated value: 347.1798 $[M]^+$; UV-Vis: λ_{max} = 486 nm (DMF); TGA: T_d = 312 °C; Fluorescence emission 534 nm(excitation at 486 nm).

Synthesis of FCNE

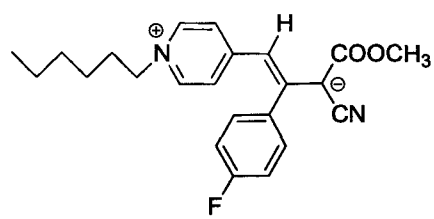

Under anhydrous and oxygen-free conditions, to a 50 mL round-bottomed flask methyl cyanoacetate (0.74 g, 7.5 mmol), sodium hydride (0.30 g, 60%, 7.5 mmol) and compound **4** (1.0 g, 2.6 mmol) in 20 mL of THF were added at 0 °C. The reaction was then warmed to room temperature. After 30 min, the insoluble inorganic salt was removed by filtration, and the filtrate solution was concentrated under reduced pressure. The residue was purified by mixture of acetone and hexane (1:1). The final product was

an orange-red crystal: 0.6 g, 61% yield. m.p: 204-206 °C; ^{1}H NMR (400 MHz, DMSO-d_6): δ 7.72 (2H, d, J = 6.7 Hz), 7.29 (2H, d, J = 8.5 Hz), 7.21 (2H, d, J = 8.5 Hz), 7.20 (1H, s), 6.16 (2H, d, J = 6.7 Hz), 3.88 (2H, t), 3.57 (3H, s), 1.65 (6H, t), 1.21(6H, m), 0.83 (3H, t); ^{13}C NMR (100 MHz, DMSO-d_6): 163.2, 160.7, 152.2, 139.3, 136.7, 129.9, 122.2, 118.6, 116.3, 116.1, 104.7, 75.1, 56.5 49.9, 30.4, 29.8, 24.9, 21.7, 13.7; IR (KBr, cm^{-1}): 2180 (C≡N), 1750 (C=O), 1639, 1505; MS (EI, m/z): 380 (M^+,100%); TOF HRMS (ESI, Acetonitrile, m/z): 381.1826 $[M+H]^+$, 403.1637 $[M+Na]^+$, calculated value: 380.1900 $[M]^+$.

Synthesis of FCNBen

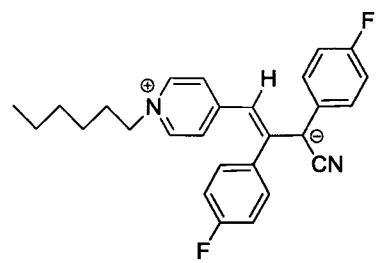

Under anhydrous and oxygen-free conditions, to a 50 mL round-bottomed flask, 4-fluorophenylacetonitrile (0.2 g, 0.5 mmol), sodium hydride (0.060 g, 60%, 1.5 mmol) and compound **2** (0.20 g, 0.44 mmol) in 5 mL of THF were added at 0 °C. Then the reaction was warmed to room temperature. After 30 min, the insoluble inorganic salt was removed by filtration, and the filtrate solution was concentrated under reduced pressure. The residue was purified by mixture of acetone and hexane (1:1). The final product was an orange-red crystal with 61% yield. m.p: 126-128 °C; IR (KBr, cm^{-1}): 2179 (C≡N), 1644, 1504; MS (EI, m/z): 416 (M^+, 100%); UV-Vis: λ_{max}= 484 nm (DMF).

2-Hydroxyethyl cyanoacetate

A mixture of 4.25 g (50.0 mmol) of cyanoacetic acid, 3.41 g (55.0 mmol) of ethylene glycol, and 0.2 g of TsOH in 15 mL of benzene was heated under reflux in a

round-bottom flask equipped with a Dean-Stark trap. After the calculated volume of water (0.9 mL) was distilled off, the solvent was evaporated then fractionation of the residue by vacuum distillation under nitrogen gave 2.58 g (40%) of 2-hydroxyethyl cyanoacetate. ^{1}H NMR (300 MHz, DMSO-d_6): δ (TMS, ppm) 3.52 (s, 2H, CH_2CN), 4.02 (m, 2H, CH_2OH), 4.4 (s, 1H, OH), 4.55 (m, 2H, $COOCH_2$); IR (NaCl, cm^{-1}): 3426 (OH), 2268 (C≡N), 1743(C=O), 1194.

Synthesis of FCNOH

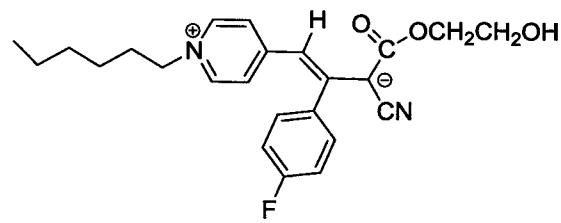

Under anhydrous and oxygen-free conditions, to a 50 mL round-bottomed flask, 2-hydroxyethyl cyanoacetate (0.99 g, 7.7 mmol), sodium hydride (0.30 g, 60%, 7.5 mmol) and compound **4** (1.0 g, 2.6 mmol) in 20 mL of THF were added at 0 °C. Then the reaction was warmed to room temperature. After 60 min, the insoluble inorganic salt was removed by filtration, and the filtrate solution was concentrated under reduced pressure. The residue was purified by mixture of acetone and hexane (1:1). The final product was a dark-red solid: 0.42 g, 40% yield. IR (KBr, cm^{-1}): 3387 (OH), 2934, 2175 (C≡N), 1637 (C=O), 1509; MS (EI, m/z): 410 (M^+, 100%); UV-Vis: λ_{max}= 496 nm (DMF). λ_{max}= 556 nm ($CHCl_3$). Negative solvatochromism of 60 nm was observed from $CHCl_3$ to DMF.

Synthesis of PpQDMs

1,4,4'-Trimethyl-2, 2'-dipyridylium iodide

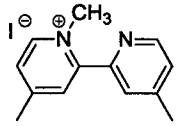

4, 4'-Dimethyl-2, 2'-dipyridyl (1.1 g, 6.0 mmol) was dissolved in 5 mL of methyl iodide. The mixture was refluxed at 40 °C for 20 h. The excess methyl iodide was removed by rotary evaporation. The solid residual was washed with acetone and hexane. An off-white powder was obtained: 1.85 g, 95%. melting point 201-202 °C. ^{1}H NMR (300 MHz, DMSO-d_6,TMS, ppm): δ 9.02 (1H, d, J = 6.2 Hz), 8.71 (1 H, d, J = 3.2 Hz), 8.16 (1H, s), 8.07 (1H, d, J = 6.2 Hz), 7.82 (1H, s), 7.56 (1H, d, J = 3.2 Hz), 4.21 (3H, s), 2.68 (3H, s), 2.52 (3H, s); MS (ESI, MeOH, m/z) (%): 199.3 (M^+,100%).

1-Benzyl -4, 4'-dimethyl-2, 2'-dipyridylium bromide

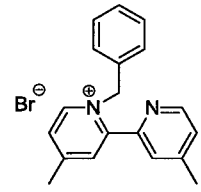

A similar procedure for the synthesis of 1,4,4'-trimethyl-2,2'-dipyridylium bromide: A mixture of 4, 4'-dimethyl-2, 2'-dipyridyl (8.832 g, 48.0 mmol) and benzyl bromide (5.7 mL, 48 mmol) were refluxed for 24 h and then cooled to room temperature. Then the cooled viscous mixture was slowly added into ether, and an off-yellow fine powder was precipitated out. The precipitate was filtered and dried in a vacuum oven .Yield 1.7 g (90%) with a melting point of 158 °C. ^{1}H NMR (300 MHz, $CDCl_3$, TMS, ppm): δ 9.66 (1H, d, J = 6.2 Hz), 8.61 (1 H, d, J = 6.2 Hz), 8.16 (1H, s), 8.07 (1H, d, J = 6.2 Hz), 7.82 (1H, s), 7.56 (1H, d, J = 3.2 Hz), 6.17 (2H, s), 2.70 (3H, s), 2.42 (3H, s); MS (ESI, MeOH, m/z) (%): 275.4 (M^+,100%).

1-Hydroxypropyl -4, 4'-dimethyl-2, 2'-dipyridylium bromide

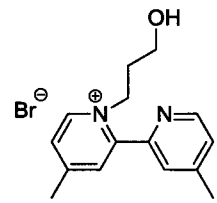

A similar procedure for the synthesis of 1-hydroxypropyl-4,4'-dimethyl-2,2'-dipyridylium bromide: 4,4'-dimethyl-2, 2'-dipyridyl (3.0 g, 16 mmol) was dissolved in 15 mL of 3-bromo-1-propanol. The mixture reacted at 55-60 °C for 72 h and then cooled to room temperature. Then the cooled viscous mixture was slowly added into ether, off-white fine powder was precipitated out. The precipitate was filtered and dried in vacuum oven. Yield 4.13 g (80%). ^{1}H NMR (300 MHz, $CDCl_3$):δ 8.71(1H, d, J = 6.4 Hz), 8.52 (1 H, d, J = 5.1 Hz), 7.88 (1H, d, J = 6.4 Hz), 7.84 (1H, s), 7.57 (1H, s), 7.48 (1H, d, J = 5.1 Hz), 4.55 (2H, t, J = 7.5 Hz), 3.39 (2H, t, J = 5.9 Hz), 2.61(3H, s), 2.43 (3H, s), 1.87 (2H, m); MS (ESI, MeOH, m/z) (%): 243.4 (M^+,100%).

Synthesis of the PpQDM-Met

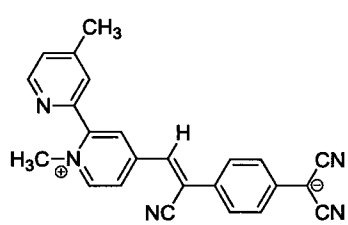

To a 30 mL methanol solution containing 1,4,4'-trimethyl-2,2'-dipyridylium iodide (3.3 g, 10 mmol), 200 mL of methanol solution of Li-TCNQ (4.22 g, 20.0 mmol) was added and the resulting green colored mixture was refluxed for 1 h. 5 mL of a methanol solution of 1-piperidineethanol (1.3 g, 10 mmol) was then added slowly over the course of 1 h. The reaction was monitored using the UV-Vis spectra of the reaction

mixture in DMF and typically the reaction can be finished within 48 h. Therefore, an aliquot of the reaction mixture was taken and dissolved in DMF for a UV-Vis measurement. The reaction was stopped until the CT band of the chromophore (~ 680 nm) was much stronger than the characteristic peaks of the radical anion (~ 420, 747 and 848 nm). The solution gradually turned to a blue color. After the reaction mixture was cooled to room temperature, the green precipitate was filtered and washed with methanol and ethyl ether. The final product was a green powder collected in 60% (2.28 g). ^{1}H NMR (400 MHz, DMSO-d_6): δ 9.01 (1H, d, J = 6.6 Hz), 8.72 (1H, d, J = 5.5), 8.39 (2H, d, J = 6.6 Hz), 8.38 (1H, s), 7.88 (1H, s), 7.80 (1H, s), 7.58 (2H, d, J = 8.7 Hz), 7.56 (1H, d, J = 5.5 Hz), 6.87 (2H, d, J = 8.7 Hz), 4.19 (3H, s), 2.48 (3H, s); ^{13}C NMR (75 MHz, DMSO-d_6): δ 152.28, 150.45, 150.00, 149.73, 147.78, 147.55, 128.16, 127.98, 127.13, 126.95, 125.59, 123.80, 123.47, 121.59, 120.36, 119.02, 118.79, 117.32, 46.80, 21.12; TOF HRMS (ESI, DMF/Acetonitrile 1:1, m/z) (%): 376.1615 $[M+H]^+$, 396.1422 $[M+Na]^+$, calculated value: 375.1484 $[M]^+$; IR (KBr, cm^{-1}): 2226, 2173 and 2137(C≡N), 1629, 1600 (C=C) ; UV-Vis (DMF): λ_{max} (nm) = 680 nm.

Synthesis of PpQDM-Ben

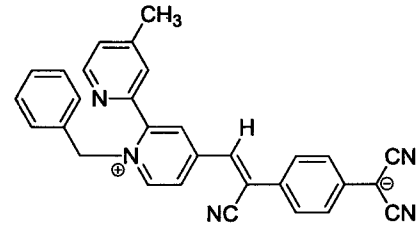

A similar procedure as PpQDM-Met: 1-benzyl-4,4'-dimethyl-2,2'-dipyridylium; bromide (3.55 g, 10.0 mmol) was used to afford 1.8 g of product (40% yield). ^{1}H NMR (300 MHz, DMSO-d_6): δ 9.15 (1H, d, J = 7.1), 8.68 (1H, d, J = 4.7), 8.46 (1H, d, J = 7.1

Hz), 8.36 (1H, s), 7.87 (1H, s), 7.59 (2H, d, J = 8.7 Hz), 7.51 (1H, d, J = 4.7 Hz), 7.28 (3H, m), 7.01 (2H, m), 6.87 (2H, d, J = 8.7 Hz), 5.94 (2H, s), 2.37 (3H, s); ^{13}C NMR (75 MHz, DMSO-d_6): δ 150.63, 150.40, 149.32, 147.54, 147.34, 146.58, 128.70, 128.61, 127.91, 127.72, 126.53, 126.51, 126.48, 125.12, 124.64, 124.44, 123.64, 123.55, 120.86, 118.71, 118.57, 117.33, 59.90, 20.44; TOF HRMS (ESI, DMF/Acetonitrile 1:1, m/z): 452.1701 $[M+H]^+$, calculated value: 451.1797 $[M]^+$; IR (KBr, cm^{-1}): 2214, 2176 and 2138 (C≡N), 1625, 1600 (C=C).

Synthesis of PpQDM-C3OH

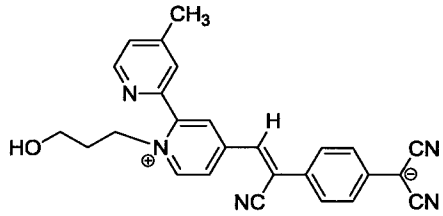

A similar procedure as PpQDM-Met: 1-hydroxypropyl-4,4'-dimethyl-2,2'-dipyridylium bromide (0.13 g, 0.40 mmol) was used to afford 0.067 g of product (40% yield). m.p. 248 °C from DSC. ^{1}H NMR (300 MHz, DMSO-d_6): δ 9.06 (1H, d, J = 6.8 Hz), 8.70 (1H, d, J = 5.0 Hz), 8.41 (1H, d, J = 6.8 Hz), 8.34 (1H, d, J = 2.1 Hz), 7.80 (1H, s), 7.87 (1H, s), 7.59 (2H, d, J = 8.8 Hz), 7.56 (1H, d, J = 5.0 Hz), 6.88 (1H, d, J = 8.8 Hz), 4.64 (2H, m), 4.62 (1H, s), 3.36 (2H, m), 2.49 (3H, s), 1.88 (2H, m); ^{13}C NMR (75 MHz, $CDCl_3$): δ 151.14, 149.68, 149.38, 149.03, 146.97, 145.94, 127.73, 127.10, 126.10, 126.03, 124.39, 122.98, 122.45, 120.72, 119.53, 118.11, 116.41, 56.88, 55.02, 32.52, 20.20; IR (KBr, cm^{-1}): 2218, 2175 and 2137 (C≡N), 1625, 1600 (C=C); TOF HRMS (ESI, DMF/Acetonitrile 1:1, m/z) (%): 420.1869 $[M+H]^+$, 442.1614 $[M+Na]^+$, calculated value: 419.1746 $[M]^+$.

2.5 References

(1) (a)Gorman, C. B.; Marder, S. R. *Proc. Natl. Acad. Sci. USA* **1993,** *90*, 11297. (b)Robin, B. H.; Dalton, L. R.; Harper, A. W.; Wang, F.; Zhang, C.; Todorova, G.; Lee, M.; Aniszfeld, R.; Garner, S.; Steier, W. H.; Houbrecht, S.; Persoons, A.; Ledoux, I.; Zyss, J.; Jen, A. K.-Y. *Chem Phys.* **1999**, *245*, 35. (c)Zhang, C.; Dalton, L. R.; Oh, M.; Zhang, H.; Steier, W. H. *Chem Mater.* **2001**, *13*, 3043.

(2) (a)Metzger, R. M.; Heimer, N. E.; Aswell, G. J. *Mol. Cryst. Liq. Cryst.* **1984**, *107*, 133. (b)Kay, A. J.; Woolhouse, A. D.; A. D.; Zhao, Y.; Clays, K.; *J. Mater. Chem.* **2004**, *14*, 1321.

(3) Ashwell, G. J. *Organic Materials for Nonlinear Optics*; Ashwell, G. J.; Bloor, D. Eds; Royal Soc. Chem.: Cambridge, 1993

(4) Metzger, R. M.; Heimer, N. E.; Aswell, G. J. *Mol. Cryst. Liq. Cryst.* **1984**, *107*, 133.

(5) Ashwell, G. J. *Thin Solid films* **1990**, *186*, 155.

(6) Kay, A. J.; Woolhouse, A. D.; A. D.; Clays, K.; *J. Mater. Chem.* **2004**, *14*, 1321.

(7) Metzger, R. M.; Ulf Hopfner, B. C.; Lakshmikanthanm, M. V.; Vuillaume, D.; Kawai, T.; Wu, X.; Tachibana, H.; Hughes, T. V.; Sakurai, H.; Baldwin, J. W.; Hosch, C.; Cava, M. P.; Brehmer, L.; Ashwell, G. J. *J. Am. Chem. Soc.* **1997**, *119*, 10455.

(8) Ashwell, G. J. Eur. Patent EP 0 391 631 A1, 1990.

(9) Weir, C. A. M.; Hadizad, T.; Beaudin, A. M. R.; Wang, Z. Y. *Tetrahedron Lett.* **2003**, *44*, 4697.

(10) Beaudin, A. M. R.; Song, N. H.; Bai, Y. W.; Men, L.; Gao, J. P.; Wang, Z. Y.; Szablewski, M; Cross, G.; Wenseleers, W. Campo, J.; Goovaerts, E. *Chem. Mater.* **2006,** *18,* 1079.

(11) (a)Wurther, F.; Yao, S. *Angew. Chem. Int. Ed.* **2000**, *39*, 1978. (b)Wurther, F.; Yao, S.; Debaerdemaeker, T.; Wortmann, R. *J. Am. Chem. Soc.* **2002**, *124*, 9431.

(12) Xiong, Y.; Tang, H.; Zhang, J.; Wang, Z. Y.; Campo, J.; Wenseleers, W.; Goovaerts, E. *Chem. Mater.* **2008,** *20*, 7465.

(13) Guseva, T. I.; Senchenya, N. G.; Golding, I. P.; Mager, K. A.; Gololobov, Y. G. *Russ. Chem. Bull.* **1993**, *42*, 478.

(14) Wu, Y.-L.; Bures, F.; Jarowski, P. D.; Schweizer, W. B.; Boudon, C.; Gisselbrecht, J.-P.; Diederich, F. *Chem. Eur. J.* **2010**, *16*, 9592.

(15) (a)Andreu, R.; Blesa, M. J.; Carrasquer, L.; Garin, J.; Orduna, J.; Villacampa, B.; Alcala, R.; Casado, J.; Delgado, M. C. R.; Navarrete, J. T. L.; Allain, M. *J. Am. Chem. Soc.* **2005**, *127*, 8835. (b)Kawase, T.; Wakabayashi, M.; Takahashi, C.; Oda, M. *Chem. Lett.* **1997**, 1055.

(16) Sutton, L. E. *Tables of Interatomic Distances and Configuration in Molecules and Ions, Special Publication No. 18*; Mitchell, A. D.; Somerfield, A. E.; Cross, L. C. Eds. The Chemical Society: London, 1965.

(17) Allen, F. H.; Kennard, O.; Watson, D. G.; Brammer, L.; Orpen, A. G.; Taylor, R. *J. Chem. Soc., Perkin Trans.* **1987**, *2*, S1.

(18) De Ridder, D. J. A.; Heijdenrijk, D.; Schenk, H.; Dommisse, R. A.; Lemiere, G. L.; Lepoivre, J. A.; Alderweireldt, F. A. *Acta Crystallogr.* **1990**, *C46*, 2197.

(19) Cole, J. C.; Cole, J. M.; Cross, G. H.; Farsari, M.; Howard, J. A. K.; Szablewski, M. *Acta Cryst.* **1997**, *B53*, 812.

(20) Wurthner, F.; Yao, S.; Debaerdemaeker, T.; Wortmann, R. *J. Am. Chem. Soc.* **2002**, *124*, 9431.

(21) (a)Wurthner, F.; Sens, R.; Etzbach, K.-H.; Seybold, G. *Angew. Chem., Int. Ed.* **1999**, *38*, 1649. (b)Wurthner, F. *Synthesis* **1999**, 2103. (c)Wurthner, F.; Yao, S.; Wortmann, R. *J. Inf. Rec.* **2000**, *25*, 69. (d)Wurthner, F.; Yao, S.; Schilling, J.; Wortmann, R.; Redi-Abshiro, M.; Mecher, E.; Gallego-Gomez, F.; Meerholz, K. *J. Am. Chem. Soc.* **2001**, *123*, 2810. (e)Mecher, E.; Gallego-Gomez, F.; Bra¨uchle, C.; Meerholz, K.; Wortmann, R.; Yao, S.; Sautter, A.; Wurthner, F. *Proc. SPIE* **2000**, *4104*, 118.

(22) Melby, L. R.; Harder, R. J.; Hertler, W. R.; Mahler, W.; Benson, R. E.; Mochel, W. E. *J. Am. Chem. Soc.* **1962**, *84*, 3374.

(23) (a)Albert, I. D. L.; Marks, T. J.; Ratner, M. A. *J. Am. Chem. Soc.* **1998**, *120*, 11174. (b)Albert, I. D. L.; Marks, T. J.; Ratner, M. A. *J. Am. Chem. Soc.* **1997**, *119*, 3155.

(24) Staneva, D.; Grabchev, I.; Soumillion, J. P.; Bojinov, V. *J. Photochem. Photobiol. A. Chem.* **2007**, *189*, 192.

(25) Reichardt, C. *Chem. Rev.* **1994**, *94*, 2319.

(26) Szablewski, M.; Thomas, P. R.; Thornton, A.; Bloor, D.; Cross, G. H.; Cole, J. M.; Howard, J. A. K.; Malagoli, M.; Meyer, F.; Bredas, J.; Wenseleers, W,; Goovaerts, E.; *J. Am. Chem. Soc.* **1997**, *119*, 3144.

(27) (a)Lu, L.; Lachicotte, R. J.; Penner, T. L.; Whitten, D. G. *J. Am. Chem. Soc.* **1999**, *121*, 8146. (b) Meech, S. R.; Phillips, D. *Chem. Phys.* **1983**, *80*, 317.

(28) Ying Xiong "Development of Zwitterinic Chromophores for Electro-Optic Applications", *Ph. D. Thesis*, Carleton University **2008**.

(29) Mes, G. F.; Jong, B.; Ramesdonk, H. J.; Verhoeven, J. W.; Warman, J. M.; Haas, M. P.; Horsman-van den Dool, L. E. W. *J. Am. Chem. Soc.* **1984**, *106*, 6524.

(30) (a)Weber, G.; Farris, F. J. *Biochemistry* **1979**, *18*, 3075. (b)Mes, G. F.; Jong, B.; Ramesdonk, H. J.; Verhoeven, J. W.; Warman, J. M.; Haas, M. P.; Horsman-vanden Dool, L. E. W. *J. Am. Chem. Soc.***1984**, *106*, 6524.

(31) Kawski, A**;** Bilot, L. *Acta Phys. Pol.* **1964**, *26*, 41.

(32) Kay, A. J.; Woolhouse, A. D.; Zhao, Y.; Clays, K.; *J. Mater. Chem.* **2004**, *14*, 1321.

(33) Szablewski, M.; Thomas, P.; Thornton, A.; Bloor, D.; Cross, G. H.; Cole, J.; Howard, J.; Malagoli, M.; Meyers, F.; Bredas, J.; Wenseleers, W.; Goovaerts, E. *J. Am. Chem. Soc.* **1997**, *119*, 3144.

(34) Cross, G. H.; Hackman, N. A.; Thomas, P. R.; Szablewski, M.; Palsson, L. O.; Bloor, D. *Opt. Mater.* **2003**, *21*, 29.

(35) Oudar, J. L.; Chemla, D. S. *Chem. Phys.* **1977**, *66*, 2664.

(36) Olmsted, J. *J. Phys. Chem.* **1979**, *83*, 2581.

(37) Benson, R. C.; Kues, H. A. *J. Chem. Eng. Data* **1977**, *22*, 379.

(38) Demas, J. N.; Crosby, G. *A. J. Phys. Chem.* **1971**, *75*, 991.

Chapter 3 Synthesis of Zwitterionic Nonlinear Optical Polymers

3.1 Introduction

As discussed in Chapter **1**, for EO applications, NLO chromophores are usually doped into or covalently bonded onto polymers, followed by poling under an externally applied electric field at the glass transition temperature (T_g) of the materials in order to achieve a noncentrosymmetric order. Therefore it is of importance to develop suitable host polymers that can impart efficiently the large hyperpolarizability of the NLO chromophores to a large and stable macroscopic EO activity. Grafting NLO chromophores onto polymer chains can effectively prevent the polar chromophores from forming aggregates while eliminating any possible phase separation.

In general, development of host polymers for highly polar zwitterionic chromophores needs to meet several critical requirements for device applications, including 1) the host polymer should be structurally compatible to form covalent bonds with the chromophore under proper reaction conditions; 2) good polarity compatibility with zwitterionic chromophores, the host polymer should be physically able to provide a desired polar or nonpolar medium; 3) high temporal stability to stabilize the oriented chromophores, which can be achieved by high T_g polymers or cross-linked organic networks; 4) optical transparency at telecommunication wavelengths. The host polymers should have a low content of C-H, N-H and O-H bonds. [1] These bonds are known to have overtone absorptions near the telecommunication wavelengths, which causes optical loss.

To choose a suitable host polymer for FDCN and PpQDM, these chromophores were first physically doped into various commercial available polymers to form guest-host systems for film-forming and compatibility tests. Then NLO chromophore grafted

polymers were prepared. To avoid the degradation of the fragile chromophores during the classical polymerization process for synthesis of zwitterionic NLO polymers, an approach of post-functionalization was employed. [2] First, the starting polymer is prepared. Then, NLO chromophores are attached to the polymer under a mild reaction condition in high yields with a minimum release of by-products. This strategy allows for optimization of the desired property, such as EO coefficients or thermal stability, through the large variety of different materials and synthetic conditions.

This chapter describes the design, synthesis and characterization of host polymers for FDCN and PpQDM chromophores, and the synthesis of FDCN-based NLO polymers and PpQDM-based crosslinkable NLO polyimides. EO properties of these two series of NLO polymers will be introduced in Chapter **4**.

3.2 Synthesis and Characterization of FDCN-based NLO Polymers

3.2.1 Synthesis of Cyanoacetate Containing MMA Host Polymers (A1)

A wide variety of polymer matrices have been exploited for development of EO materials and devices, such as poly(methyl methacrylate) (PMMA),[3] polycarbonate,[4] polyurethane,[5] polyimide,[6] polyethersulfone (PES),[7] sol-gel,[8] and polyvinylphenol,[9] etc. Among guest-host EO polymer systems, doping inorganic or NLO chromophores, such as disperse red one (DR1) into PMMA-based polymer materials have been widely studied[10], because of the flexibility and high transparency of the polymer, combined with the high thermal stability of organic chromophores; doping zwitterionic chromophores into PES have been extensively studied in our group [6b,6c,7b,7c,7e] and most of the doped PES films exhibited higher poling efficiency than those in other polymer matrices for PQDM and PeQDM chromophores.

Based on the preliminary study, PMMA and PES were selected as the host polymers for FDCN doping, due to their availability, processibility, and background knowledge. A relatively large amount of FDCN (5-10 wt %) was blended into PMMA and PES forming a red color film, no phase separation was observed. Functional PMMA was then designed and synthesized for grafting FDCN chromophore, PES was used to make FDCN-PES guest-host polymer films for EO coefficient measurement for comparison (In Chapter **4**).

Therefore, a series of cyanoacetate-containing MMA copolymers **A1** were designed (Scheme 3.1) as host polymers for FDCN chromophores. On the other hand, the cyanoacetate functionality in the MMA polymer offers a reactive site for the simple attachment of FDCN chromophores, which will be shown in the following section.

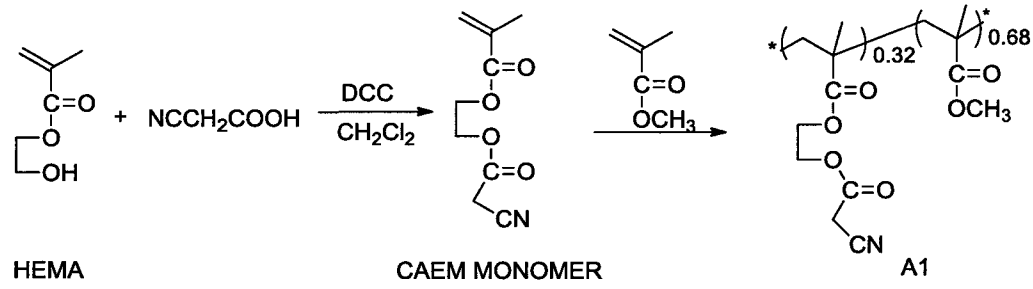

Scheme 3.1. Synthesis of CAEM and **A1** polymers.

First, the appropriate monomer, 2-cyanoacetoxyethyl methacrylate (CAEM) was prepared by esterification of 2-hydroxyethyl methacrylate (HEMA) with cyanoacetic acid using dicyclohexylcarbodiimide (DCC) as the coupling agent.[11]

Free radical copolymerization of CAEM with various amounts of MMA led to CAEM-MMA based copolymers **A1**. As an example, **A1-1** was synthesized by the copolymerization reaction of CAEM and MMA in dry toluene at 65-70 °C yielding a white powder in a low molecular weight (inherent viscosity of 0.22 dL/g), which has a T_g

of 83 °C and good thermal stability (220 °C for 5% weight loss) in nitrogen (Appendix B, Figures S3.1 and S3.2).

The ^{1}H NMR spectrum of **A1-1** demonstrated that 32 mol% of CAEM was incorporated into **A1-1** (Figure 3.1). This is in agreement with the composition expected from the monomer feed ratio. In both the **A1-1** and CAEM, $\upsilon_{C\equiv N}$ was at a high wavenumber (2264 cm^{-1}) with lower intensity, which is expected for cyano groups connected to the neutral saturated carbon atom (Figure 3.2).

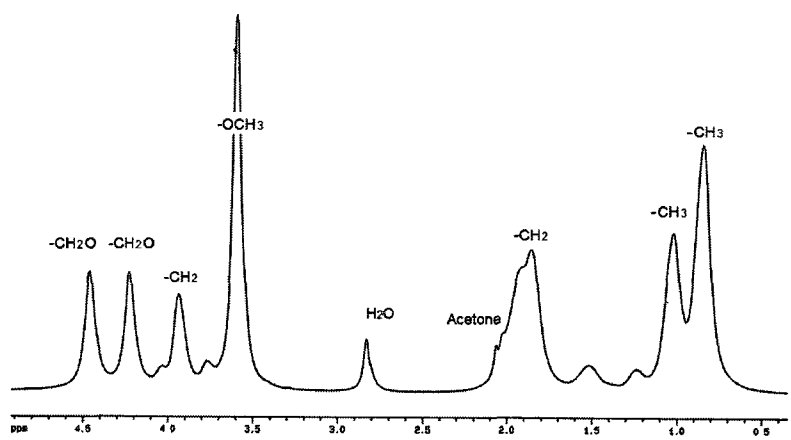

Figure 3.1. ^{1}H NMR spectrum of polymer **A1-1** in Acetone-d_6.

The polymer **A1-1** has good solubility in common organic solvents such as acetone, THF, and chloroform. Flexible and transparent films can be readily prepared on indium-tin oxide (ITO) coated glass by solution casting. **A1-1** was chosen as a host polymer for FDCN grafting due to its higher CAEM content, which is available for the adjustment of the content of FDCN. Although the T_g of **A1-1** is lower than the T_g of other common used EO polymers, grafting of FDCN chromophores onto the **A1-1** backbone was expected to bring the T_g up to a temperature suitable for electric poling.

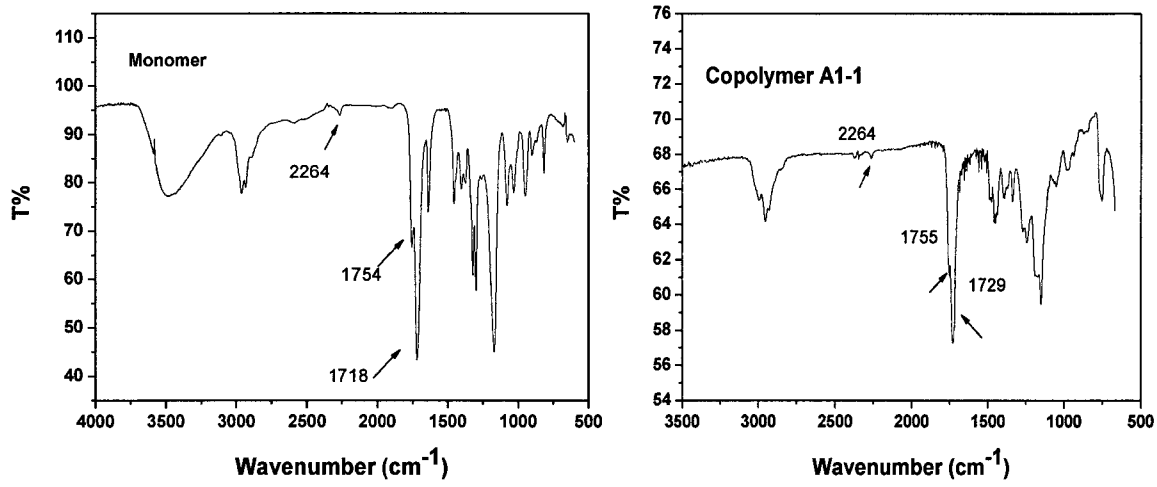

Figure 3.2. IR spectra of CAEM (left) and polymer **A1-1**(right).

3.2.2 Synthesis and Characterization of FDCN-A1 NLO Polymers (NA1)

Scheme 3.2 shows the general synthesis of the FDCN-**A1** NLO polymers, **NA1-a** to **NA1-d** (Table 3.1) using NaH/THF. Grafting of 2-(4-fluorophenyl)-3-pyridine-4-yl-acrylonitrile bromide salt (compound **4**, Chapter **2**) onto **A1-1** polymer was successfully performed at room temperature and confirmed by the IR spectrum of the resulting NLO polymer. The higher reactivity of the cyanoacetate group toward the reaction with compound **4** is expected in view of the electron withdrawing nature of the cyano group, which affects the acidity of the adjacent methylene protons.

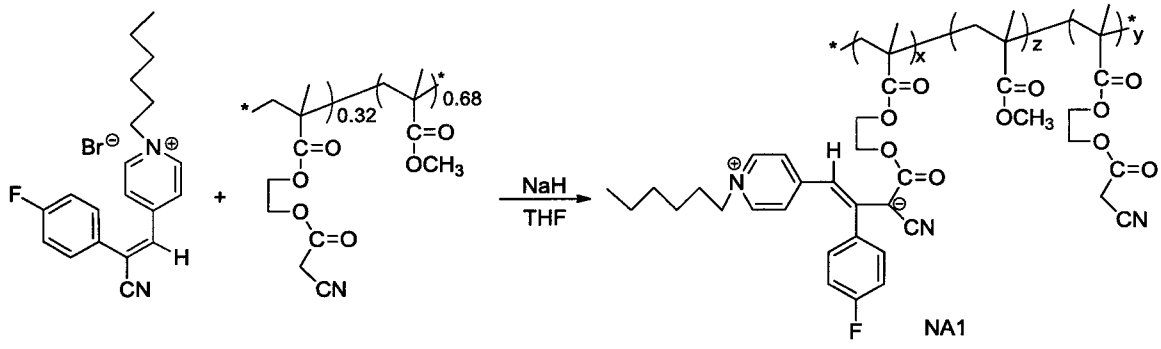

Scheme 3.2. Synthesis of NLO polymers **NA1**.

Table 3.1. Composition and properties of **NA1** NLO polymers

Polymer	X (mol%) [a]	Y	Z	T_g (°C) [b]	T_d (°C) [c]
NA1-a	0.5	31.5	68	85	245
NA1-b	1.0	31.0	68	86	243
NA1-c	2.0	30.0	68	88	240
NA1-d	5.0	27.0	68	93	238

[a] Concentration calculated from a calibration curve established by measuring the absorption of FDCN in THF; [b] Measured in nitrogen with a heating rate of 10 °C min^{-1}; [c] Onset temperature for 5% weight loss in nitrogen with a heating rate of 10 °C min^{-1}.

By comparing the IR spectrum of **NA1-a** (Figure 3.3) with that of **A1-1** (Figure 3.2, right), the position of cyano groups changed noticeably. In **A1-1**, $\upsilon_{C\equiv N}$ was at a high wavenumber (2264 cm^{-1}) with lower intensity, typical of cyano groups connected to the neutral saturated carbon atom; after the grafting, $\upsilon_{C\equiv N}$ moved to a lower wavenumber (2171 cm^{-1}) with higher intensity in **NA1-a**, due to the adjacent negatively charge carbon (characteristic of C≡N stretch in zwitterionic species).

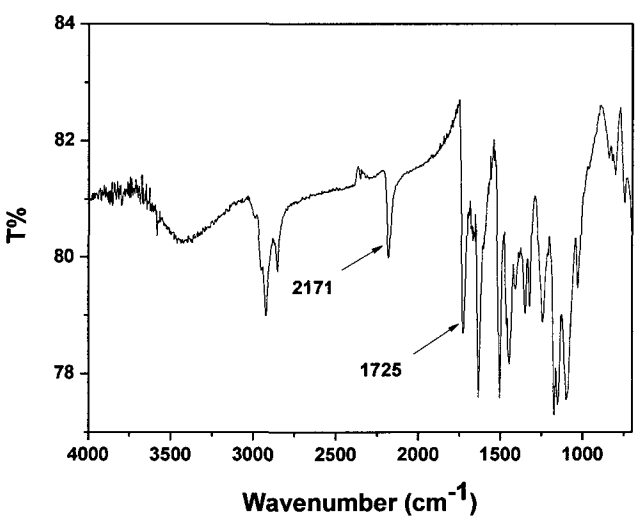

Figure 3.3. IR spectrum of NLO polymer **NA1-a**.

In comparison with the host copolymer **A1**, the solubility of NLO polymers **NA1** changed dramatically. The **NA1** were only soluble in THF, and therefore NMR spectra

could not be obtained. Transparent thin films were prepared, however, the films became brittle when the FDCN content was increased to above 10 mol%. EO coefficient was measured under the parallel electrode poling condition, and the r_{33} value is less than 15 pm/V. The main reason is that the small first hyperpolarizability and low number density of the chromophore in the films lead to the low EO signals.

3.2.3 Synthesis and Characterization of FDCN-MMA NLO Polymers (NA2)

To increase the glass transition temperature of the FDCN containing polymer, the flexible cyanoacetated HEMA unit must be eliminated from the polymer backbone. Therefore, FDCN functionalized acrylate was synthesized and copolymerized with MMA monomer. Accordingly, acrylate FDCN monomer (**A2**) was designed and synthesized by the reaction of FDCNOH, a hydroxyl containing FDCN chromophore with methacryloyl chloride (Scheme 3.3).

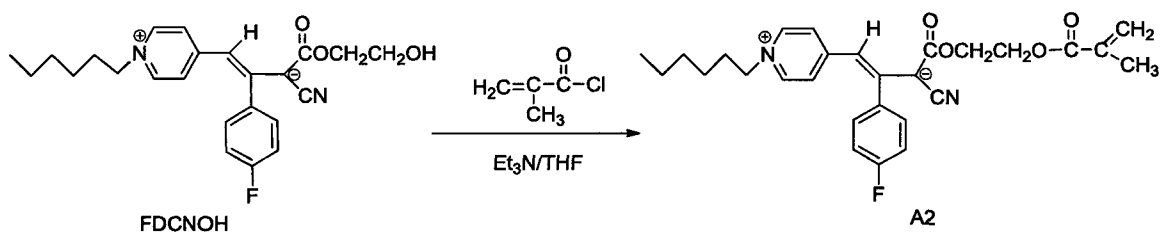

Scheme 3.3. Synthesis of acrylate FDCN monomer **A2**.

The yield of this reaction at room temperature is 70%. In the IR spectrum of **A2**, $\upsilon_{C\equiv N}$ showed at a low wavenumber (2177 cm^{-1}) with a high intensity (Figure 3.4). The maximal absorption of **A2** is at 556 nm in chloroform, and 496 nm in DMF (Appendix B, Figure S2.7). This negative solvatochromism indicates that this new FDCN chromophore has the same charge-separated ground state as that in the FDCNOH, which is consistent with the result obtained from IR study.

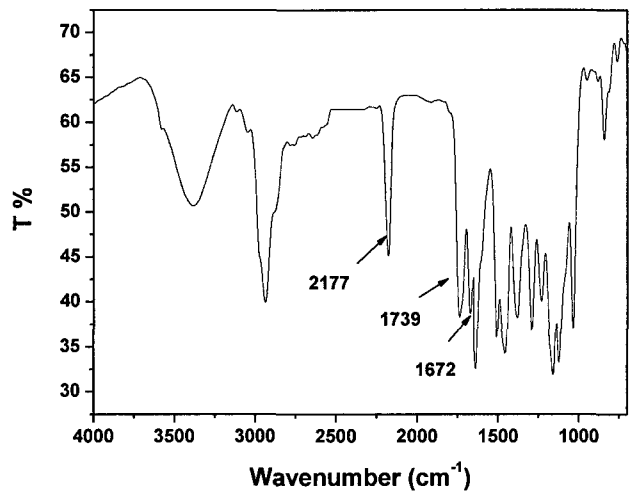

Figure 3.4. IR spectrum of **A2**.

The general synthesis of **NA2** using the polymerization reaction of **A2** and MMA is shown in Scheme 3.4. The synthesis and characterization of NLO polymers **NA2a** and **NA2b** are summarized in Table 3.2. **NA2a** and **NA2b** were obtained in 85-90% yields as light red in powders.

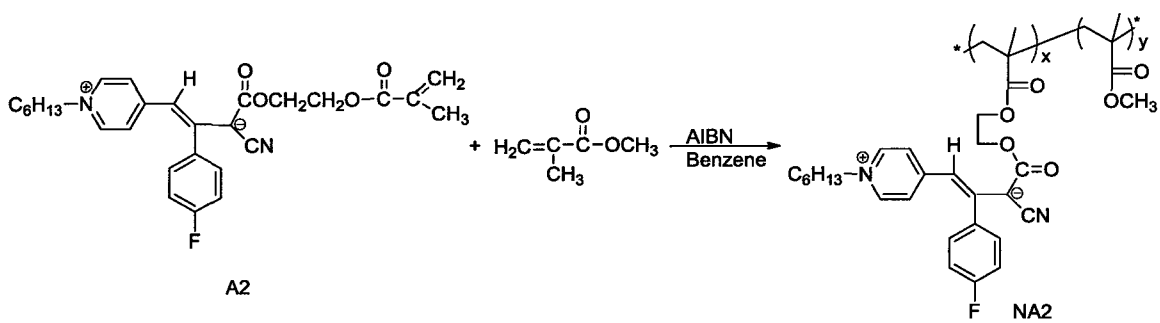

Scheme 3.4. Synthesis of NLO polymers **NA2**.

Table 3.2. Composition and properties of **NA2** polymers

NLO Polymer	X[a] (wt %)	Y (mol %)	λ_{max} (DMF, nm)	T_g[b] (°C)	T_d[c] (°C)
NA2a	7	95	502	95	264
NA2b	14	90	498	126	232

[a] Concentration calculated from a calibration curve established by measuring the absorption of FDCN in DMF; [b] Measured in nitrogen with a heating rate of 10 °C min^{-1} ; [c] Onset temperature for 5% weight loss in nitrogen with a heating rate of 10 °C min^{-1}.

The chemical structures of **NA2** polymers were consistent with their IR spectra, showing the characteristic peaks of the cyano groups at 2177 cm^{-1} (Appendix B, Figure S3.3); ^1H NMR spectra displaying the expected resonance associated with protons on the structures of both MMA and FDCN (Appendix B, Figure S3.4). The contents of FDCN in the resulting **NA2** polymers were calculated from the UV absorption calibration curve and found to be 7% and 14%. Negative solvatochromic of **NA2** was also obtained (e.g., the absorption of **NA2a** is at 558 nm in $CHCl_3$, 502 nm in DMF) (Figure 3.5).

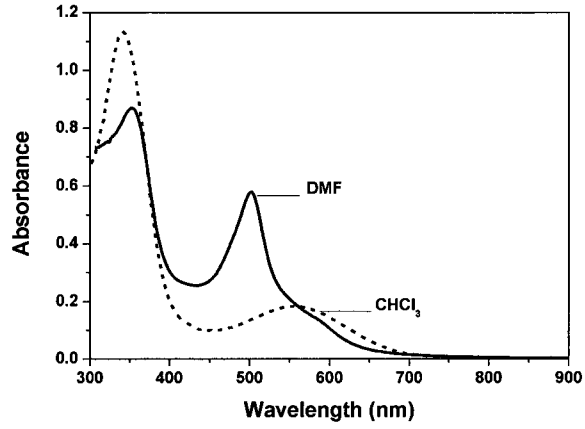

Figure 3.5. UV-Vis spectra of NLO polymers **NA2a** in DMF and chloroform.

The polymers **NA2a** and **NA2b** have good solubility in common organic solvents such as $CHCl_3$, benzene, ACN, DMF and have higher T_g and thermal stability (T_d > 232 °C) (Appendix B, Figures S3.5 and S3.6) than the **NA1** NLO polymers. Flexible and transparent high quality films were cast on ITO glass from their ACN solutions. The EO properties of these polymers will be discussed in Chapter **4** along with the PpQDM-based crosslinkable NLO polymers.

3.3 Synthesis of PpQDM-Based Crosslinkable NLO Polymers

3.3.1 Host Polymer Selection for Guest-Host System

In the search for a suitable host polymer for PpQDM chromophores, high T_g polymers such as APC, poly(4-hydroxystyrene) (PS-OH), polyvinyl-pyrrolidone (PVP) and PES (Chart 3.1) were screened in a doping test for compatibility with PpQDM. All of the polymers are amorphous and have good film-forming ability.

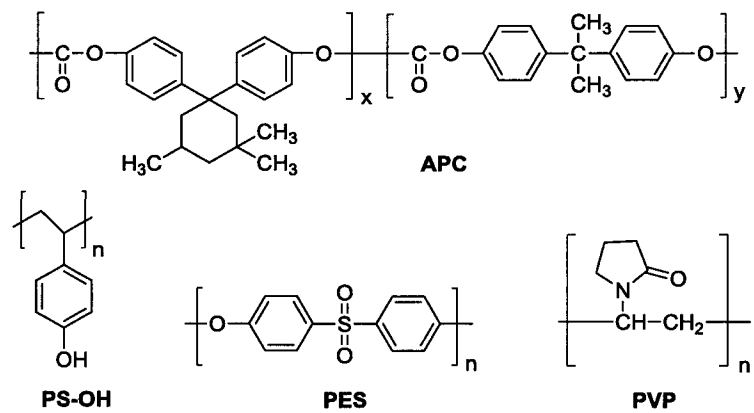

Chart 3.1. Chemical structures of the polymer materials.

PpQDM-Met was doped into these polymers and assessed. Film cracking and serious phase separation were observed in less polar PS-OH and APC (e.g., ε of APC is 3) (Figure 3.6); green color uniform film in PES was obtained ($\varepsilon = 3.5$), loading density of PpQDM-Met was lower than that in PVP ($\varepsilon = 4.5$). Among these polymers, the more polar PVP appeared to be the most promising host for high polar PpQDM chromophores. A relatively higher amount of PpQDM-Met (~ 3 wt %) could be blended into PVP (Molecular weight is around 1,300,000) forming a blue color film without showing phase separation.

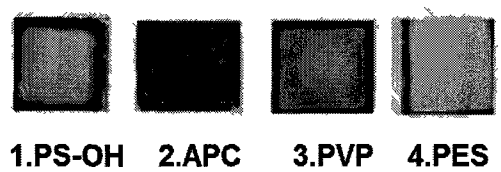

Figure 3.6. Films of PpQDM-Met in different polymers. (Color figure can be viewed in the Appendix C, Figure S4.5)

Host polymer selection for PpQDM was also determined by the absorption spectra (Figure 3.7). In comparison with the PpQDM-Met /DMF solution, the charge transfer absorption of PpQDM-Met in APC, PS-OH, PVP doped films underwent negative solvatochromism shifting from 680 nm to 628 nm, 644 nm and 640 nm, respectively.

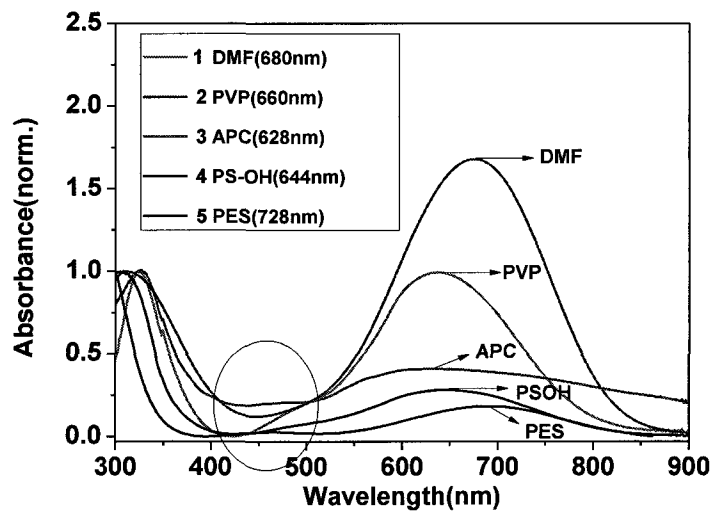

Figure 3.7. Absorption spectra of the films of PpQDM-Met in different polymers.

A red shift of the absorption band was observed for the PES doped film, this implies the existence of π–π stacking interactions between PpQDM-Met and the host polymer backbone. The broad absorption peaks in APC, PS-OH, PES films and the appearance of a new transition at shorter wavelength (450 nm) in APC, PS-OH and PES

confirm that the intermolecular aggregation occurred.[11] The absorption of PpQDM-Met doped PVP system is close to that in DMF solution, making PVP the best host polymer for PpQDM chromophores. Thus, for further EO measurement, PVP was chosen in our study as a host polymer for PpQDMs guest-host doping system.

3.3.2 Design and Synthesis of Polyimides for grafting PpQDM Chromophores

The first challenge for the development of polymers for PpQDM chromophores grafting is the instability of zwitterionic chromophores to some reaction conditions (e.g., acidic, Chapter **2**). Therefore, mild reaction conditions should be carefully chosen for grafting reaction. Secondly, PpQDM chromophores have extremely large dipole moments, host polymers with a proper spacer between the functional chromophores must be developed to reduce the electrostatic interactions between chromophores and to allow for good chromophore mobility during the poling process. Thirdly, the host polymers should contain some polar units in the structure and have moderate dielectric constants (e.g., 3.5-4.5). It is demonstrated that the relatively polar environment leads both to decrease intermolecular electrostatic interactions and to enhance the poling efficiency. Additionally, since PpQDM is ready functionalized with a hydroxyl group (e.g., PpQDM-C3OH), host polymers contains carboxylic acid groups is expected to allow for an efficient coupling reaction under mild reaction conditions.

A wide range of linear polyimides containing carboxylic acid with different glass transition temperatures and chain mobilities were designed and developed in our group. Among these polymers, poly(ether imide)s were promising host candidates for the highly polar PpQDM chromophores to obtain NLO polymers with large EO activity and good auxiliary properties. It was found that **PI-1** possessed good chain mobility, suitable T_g

(208-227 °C) and molecular weights ($[\eta]_{inh}$ = 0.22-0.37 dL/g) with good solubility, thermal stability, and film-forming ability. Most importantly, the dielectric constants of **PI-1s** were in the range of 3.5-4, [12] which meet the requirement of the polarity of the polymer matrix for PpQDM chromophores.

The reaction conditions were optimized by a former graduate (Dr. Naiheng Song) through investigating carefully the effect of backbone composition, end-capping groups and different feed ratios.[12] Using 1-(3-(dimethylamino)propyl)-3-ethylcarbodiimide (EDC) as a coupling agent, a series of NLO polyimides can be prepared.

The general synthesis of **PI-1** is shown in Scheme 3.5. The results of synthesis and characterization of **PI-1a - PI-1d** are summerized in Table 3.3. A relatively flexible diamine, 3, 5-bis (4-aminophenoxy) benzoic acid (DAPBA) was synthesized and polymerized with 4, 4'-(4, 4'-isopropylidenediphenoxy)bis(phthalic anhydride) (BPADPA) in the presence of phthalic anhydride (PA) (2-20 mol% relative to DAPBA) as an end-capping agent to afford the host **PI-1**.

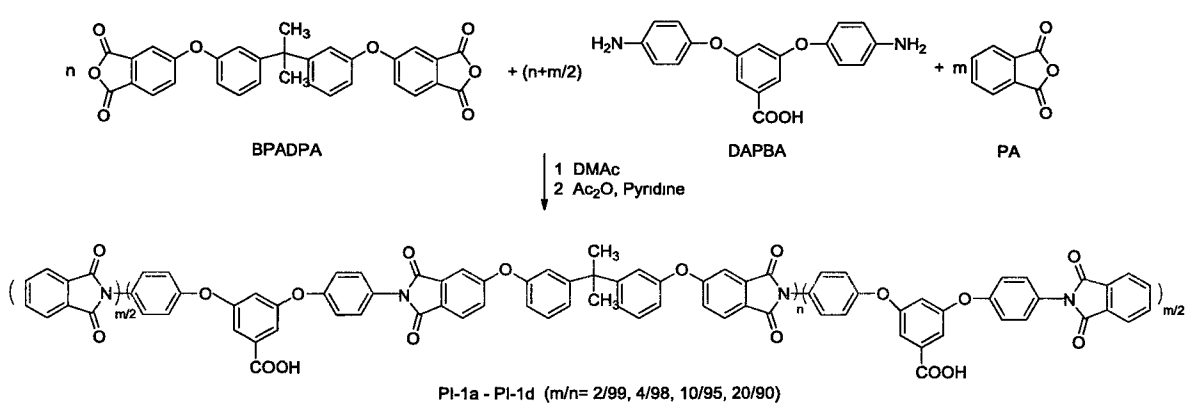

Scheme 3.5. Poly(ether imide) **PI-1** derived from DAPBA.

Table 3.3. Synthesis and characterization of poly (ether imide)s **PI-1**

Polymer	Feed Ratio (mol %)		T_g (°C)	$[\eta]_{inh}$ (dL/g)	T_d (°C)
	BPADPA	PA			
PI-1a	0.99	0.02	227	0.37	450
PI-1b	0.98	0.04	211	0.33	450
PI-1c	0.95	0.10	210	0.30	453
PI-1d	0.90	0.20	208	0.22	451

The polymerization was completed by a conventional two-step method, i.e., the formation of poly (amic acid)s and subsequent chemical imidization in the presence of acetic anhydride and pyridine. The ^{1}H NMR and IR spectra of **PI-1** were consistent with the polymer structure (Appendix B, Figures S3.7 and S3.8).

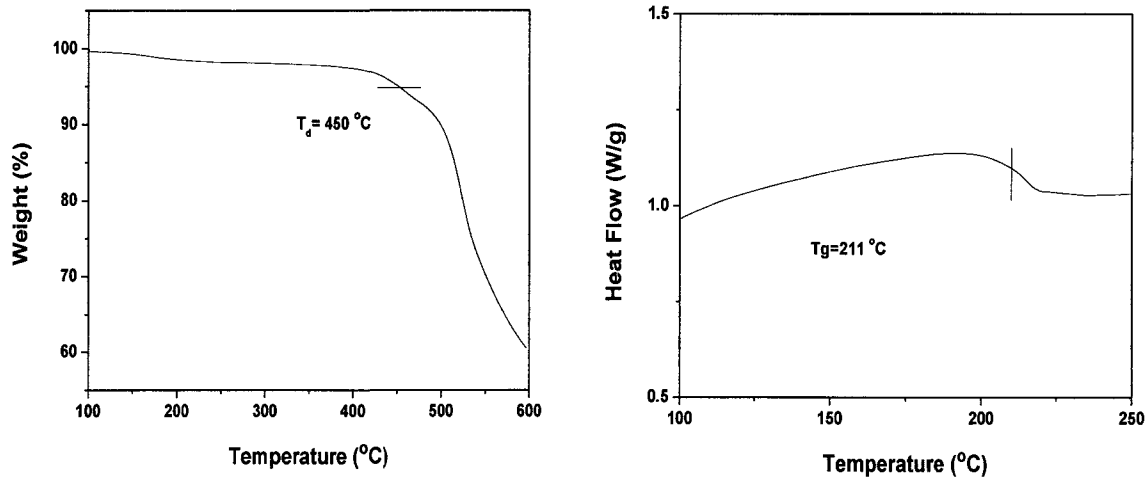

Figure 3.8. TGA (left) and DSC (right) traces of polyimide **PI-1b**.

PI-1b was chosen as the host polymer for chromophore grafting to prepare the NLO polymer due to the moderate T_g and good solubility. The molecular weight of **PI-1b** was not directly measured; it was estimated to be high enough with a high viscosity (0.33

dL/g). **PI-1b** can be precipitated from methanol as fibers and was readily soluble in THF, N, N-dimethylacetamide (DMAc), and DMF, and could be cast into flexible tough films on glass. TGA analysis indicated that **PI-1b** has a good thermostability with T_d of 450 °C for 5% weight loss in nitrogen (Figure 3.8 left) and a moderate T_g of 211 °C (Figure 3.8 right).

3.3.3 Design and Synthesis of PpQDM-Based Crosslinkable NLO Polymers

In general, noncentrosymmetric order in poled polymers tends to decay very quickly in low-T_g polymers at ambient to elevated temperatures. Accordingly, chromophores are usually incorporated into high-T_g polymers to improve temporal stability of EO activity. However, if the T_g of a polymer is too high, a higher poling temperature will be required which may cause chromophore decomposition. One of the most effective approaches to improve thermal stability of EO materials is to introduce covalent cross-linking system. Crosslinkable NLO polymers can be poled and cross-linked consecutively to lock-in the poling-induced nonlinearity.

In early studies of organic EO materials, such crosslinking was normally accomplished by utilizing condensation reactions to form polyurethane between the OH and NCO groups.[13] More recently, cycloaddition reactions have largely replaced these earlier methods. The two commonly utilized cycloaddition reactions include 1) reaction of fluorovinyl ether groups to form cyclobutyl crosslinks[14] and 2) Diels-Alder/retro-Diels-Alder reaction of dienes and dienophiles.[15] The latter has become very popular because of the wide range of diene and dienophiles available, which can be used to widely tune the glass transition temperatures of materials.

A new thermally reactive compound, 5-aminobenzocyclobutenone (BCBO), was developed by our group[16] and it has been demonstrated that the BCBO group in a variety of polymers or by itself can undergo a ring-opening reaction at temperatures above 200 °C to form a reactive vinylketene intermediate (Scheme 3.6). The subsequent dimerization of the vinylketene as side groups on polymer chain by self [4+2] cycloaddition and a 1,5-hydrogen shift lead to the polymer cross-linking or curing. [6b,7c] Therefore crosslinkable NLO polyimides can be obtained through grafting the hydroxyl-containing PpQDM and BCBO crosslinker onto the **PI-1b** backbones.

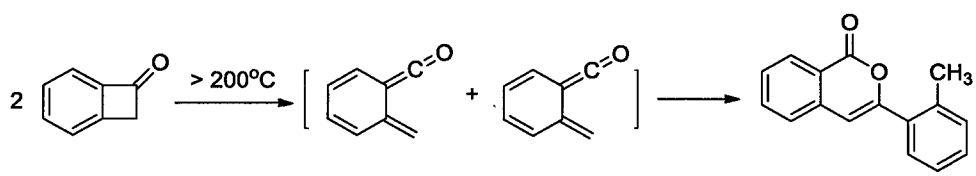

Scheme 3.6. Thermolysis and dimerization of BCBO.

3.3.3.1 Synthesis of PpQDM-Based Crosslinkable NLO Polymers

Grafting of PpQDM-C3OH onto **PI-1b** was performed by using EDC and 4-dimethylaminopyridine (DMAP).[17] Although PpQDMs are labile to acetic acid, they appeared to be stable to acid-containing polyimides, particularly in the presence of organic base such as pyridine or DMAP. Since covalently linking PpQDM-C3OH as a pendent group will largely increase the polarity of the polymer, [18] in addition with the strong interaction between the PpQDM chromophores, blocking groups with less polarity than PpQDM-C3OH should be introduced into the polymer to block the chromophore interaction to allow the NLO polymer to have a suitable T_g for poling without causing any decomposition. A preliminary study on the T_g of two NLO polymers with different ratio of PpQDM-C3OH, crosslinkable BCBO, and blocking pendent groups (methanol or

1-hexanol) was carried out in order to identify an appropriate composition for NLO polymers. The difference of the short and long aliphatic blocking groups is expected to affect the T_g of NLO polyimides.

Scheme 3.7 shows the general synthesis of NLO polyimides (**NPI-a-NPI-e**). The reactions were carried out at room temperature in DMAc by adding EDC to a mixture of **PI-1b**, PpQDM, BCBO, methanol or 1-hexanol. The structures of the synthesized PpQDM-grafted NLO polyimides, **NPI-a** to **NPI-d** are shown in Chart 3.2.

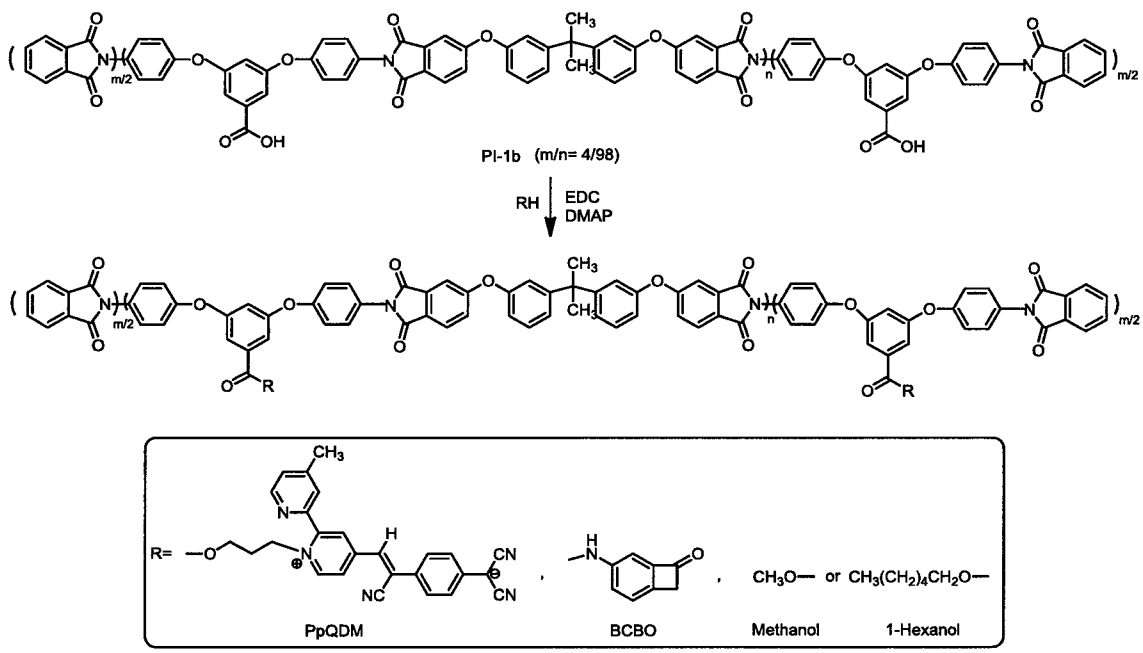

Scheme 3.7. Synthesis of NLO polyimides.

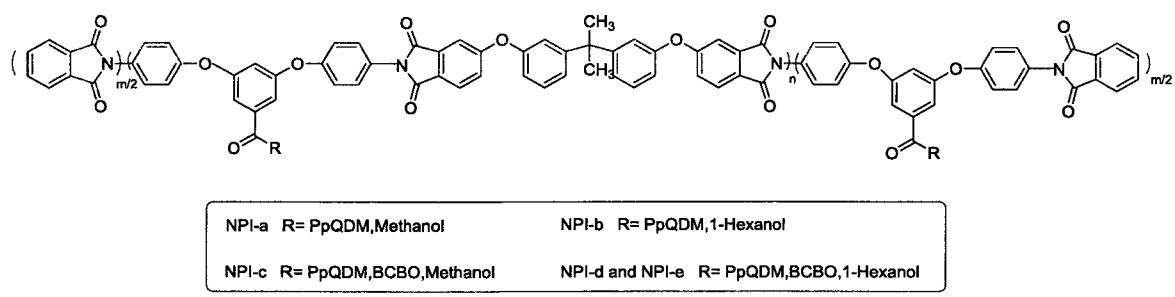

Chart 3.2. Structures of NLO polyimides **NPI-a** to **NPI-d**.

Table 3.4 summarizes the synthesis and characterization of NLO polyimides **NPI-a - NPI-e**. All NLO polymers were prepared from the same batch of host polyimide **PI-1b.** These NLO polymers differ in the PpQDM content, the thermally reactive BCBO unit content and the end-capping groups.

Table 3.4. Synthesis and characterization of crosslinkable NPI polymers

NLO Polyimide	PpQDM[c] (wt %)	BCBO[d] (mol %)	λ_{max} (DMF, nm)	T_g[e] (°C)	T_d[f] (°C)
NPI-a[a]	2.62	0	702	223	265
NPI-b[b]	4.71	0	695	185	264
NPI-c[a]	7.12	30	695	200	260
NPI-d[b]	7.59	5	694	163	255
NPI-e[b]	13.75	5	695	180	253

[a] The residual acid residues were blocked with methanol. [b] The residual acid residues were blocked with 1-Hexanol. [c] PpQDM content in weight percentage calculated from a calibration curve established by measuring the absorption of PpQDM-C3OH in DMF . [d] Molar ratio relative to the acid groups in the polymers. [e] Measured by DSC in nitrogen (10 °C min^{-1}). [f] Onset temperature for 5% weight loss measured by TGA in nitrogen.

Both **NPI-a** and **NPI-b** have high thermo stability with a decomposition temperature close to 265 °C, indicating both the methyl ester and hexyl ester bond are thermally stable. As expected, the T_g of **NPI-b** is much lower than that of **NPI-a,** by changing the length of the side chain, going from one carbon to six carbons, the T_g of the polymer decreases from 223 °C to 185 °C, despite the fact that **NPI-b** has higher rigid chromophore content than that of **NPI-a**. One can infer from this that introducing the softer long alkyl side chain can effectively lower the T_g of the NLO polymer. Therefore,

1-hexanol was chosen as the end-capping group for the synthesis of PpQDM-Based crosslinkable NLO polymers.

Previous studies indicated that a small amount of BCBO, such as 5 mol% introduced onto host polymers as a crosslinker can effectively form crosslinkable NLO polymers.[12,18] Therefore, the BCBO content was lowered from 30 mol % in **NPI-c** to 5 mol% in **NPI-d** and **NPI-e**. A suitable NLO polymer, **NPI-e,** was obtained with the highest chromophore content (13.8 wt %) and a high T_g (180 °C).

The NLO polyimides were obtained in 80-92% yields, **NPI-a** to **NPI-c** were light blue-green and **NPI-d** to **NPI-e** were deep blue. These crosslinkable polymers were characterized by IR, ^{1}H NMR and UV-Vis methods.

The change in chemical structure of **NPI-a** to **NPI-e** was consistent with their IR spectra. For **NPI-e,** Figure 3.9 showing the characteristic peaks of the cyano groups at 2178 and 2138 cm^{-1} and of the imides at 1777 and 1720 cm^{-1}.

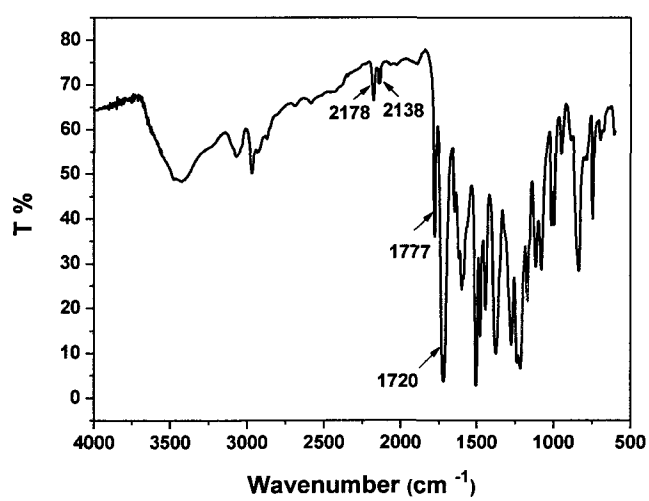

Figure 3.9. IR spectrum of **NPI-e** (KBr pellet).

^{1}H NMR spectra of NLO polyimides, displayed the expected resonance associated with protons on the structures of host polyimides, PpQDM, BCBO and ROH. In Figure 3.10, the unlabeled peaks represent the polymer main chain and the hexyl group in **NPI-e**. The total content of PpQDM in NLO polymers was estimated from the ^{1}H NMR spectra to be in the range of 5-26.25 mol % relative to the acid groups in the host polymers. The actual content was determined by UV-Vis analysis to be in the range of 2.6-13.8 wt %. The chromophore loading in **NPI-e** is higher than the guest-host system, in which the highest doping level of PpQDM chromophores in PVP is 5 wt %.

All the NLO polyimides were soluble in polar aprotic solvents such as DMF, DMAc, DMSO and NMP. Films of **NPI-a** - **NPI-e** in thickness of 1-3 μm can be readily prepared by casting of their solutions in DMF. Transparent films can be made on ITO glass. Good stability or dispersion of PpQDM in NLO polyimide films indicates a successful design of the host polymer in terms of achieving a high guest number density.

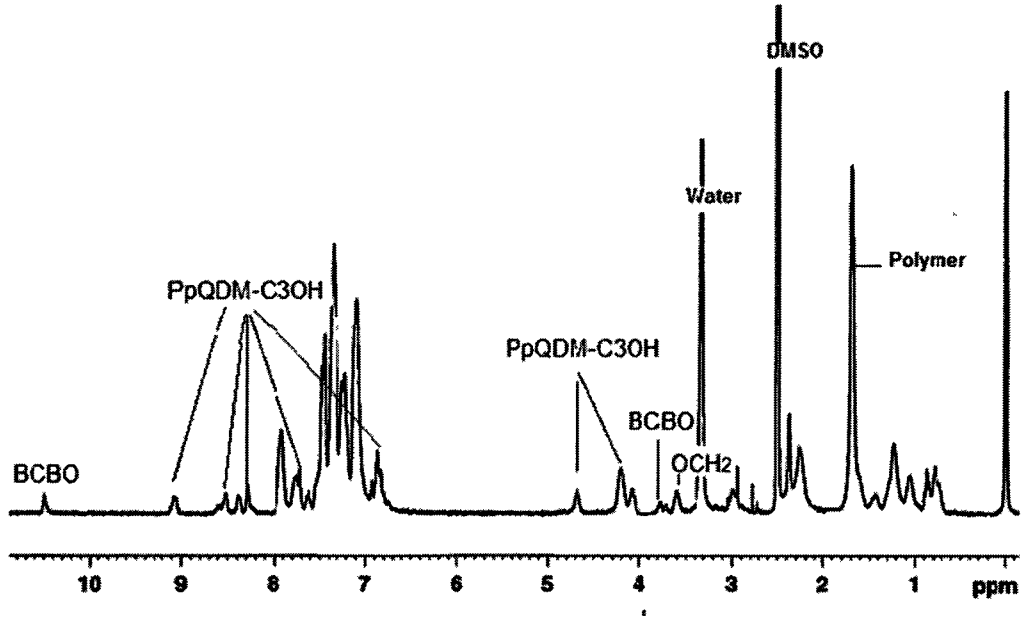

Figure 3.10. NMR spectrum of **NPI-e** in DMSO-d_6

3.3.3.2 Optical Absorption

A slight shift (10 -17 nm) of the charge transfer band to longer wavelengths was observed for the NLO polyimides in DMF solution when compared with that of PpQDM-C3OH (685 nm). For example, **NPI-b** in DMF solutions showed a bathochromic shift of about 10 nm in the CT absorption and **NPI-a** showed a larger shift of 17 nm (Figure 3.11, Table 3.4). Since the intramolecular CT absorption of organic molecules is related to the electronic environment, this red-shift in absorption may be due to less polar environment imparted by the polyimide backbones.

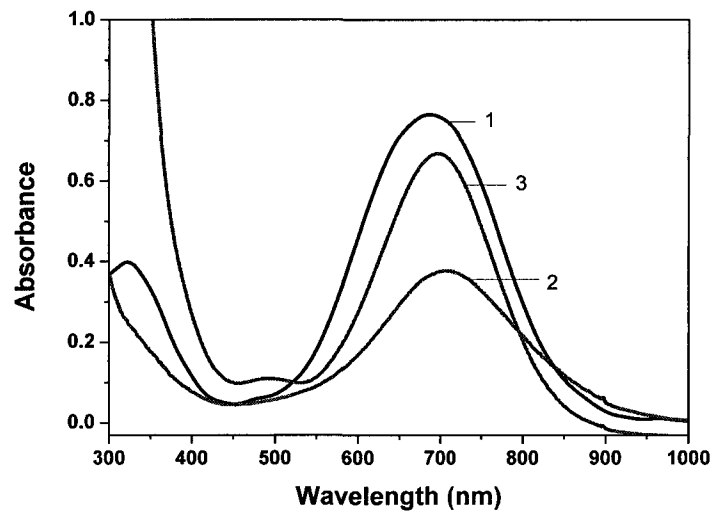

Figure 3.11. UV-Vis absorption spectra in DMF: 1) PpQDM-C3OH 2) **NPI-a** 3) **NPI-b**.

Although **NPI-a** to **NPI-e** show similar UV-Vis absorption spectra in DMF solution, the spectra of their corresponding films are apparently different. In comparison with the absorption of NLO polyimides in DMF solution, the CT absorption of NLO polyimide films showed a distinct peak broadening (~ 200 nm) and a bathochromic shift (Figure 3.12). The absorption peak of the NLO polymers is shifted to longer wavelengths as compared with the chromophore in DMF solution due to the lower polarity of the chromophore environment. The CT bond of **NPI-e** is much broader than that of **NPI-b**.

The broad peak is due to some J-aggregation of high loading of chromophores in less polar polymer environment.[18]

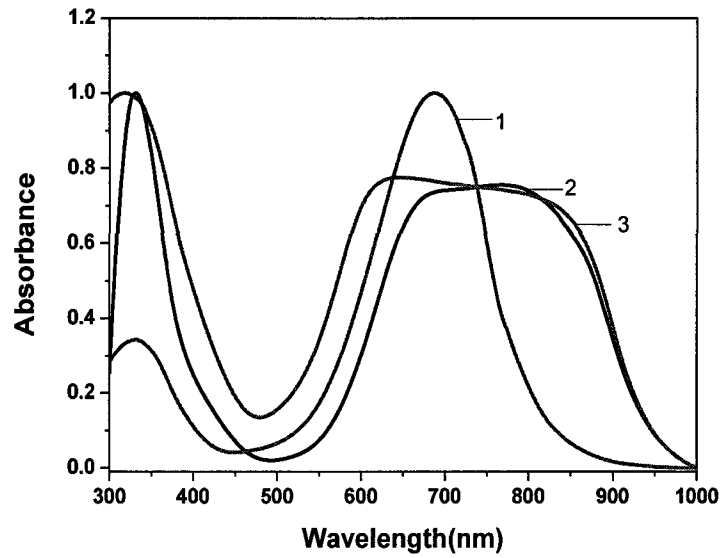

Figure 3.12. UV-Vis absorption spectra of a solution of PpQDM-C3OH in DMF (1), films of **NPI-b** (2) and **NPI-e** (3).

3.3.3.3 Thermal Analysis

In order to find applications in EO devices, NLO polymers must be thermally stable to the material processing temperature, poling temperature, and device processing and packaging temperatures. Thermal properties of **NPI-a** to **NPI-e** were measured by DSC. **NPI-c** containing higher BCBO content shows higher T_g (200 °C) compared to **NPI-d** (163 °C). The higher T_g of **NPI-e** compared to **NPI-d** is due to higher chromophore content. Figure 3.13 shows the DSC trace of **NPI-e,** after the glass transition, an endothermic process was found around 187 °C, followed by an exothermic process starting at 198 °C. The exothermic process is due to the ring-opening of the BCBO group.

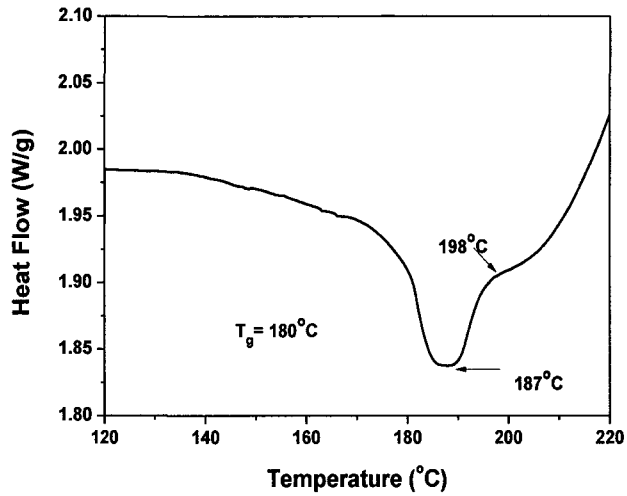

Figure 3.13. Representative DSC trace of **NPI-e** with a heating rate of 10 °C min^{-1}.

The thermal stability of **NPI-a** to **NPI-e** was determined by TGA in nitrogen. Figure 3.14 compares the TGA traces between PpQDM-C3OH and NLO polymer **NPI-a** to **NPI-c** and **NPI-e**. All the polymers showed good thermal stability with the T_d above 250 °C, which are comparable to that of PpQDM-C3OH (283 °C). These T_g and T_d data were used to determine the suitable poling temperature and decomposition point for the process of EO measurements.

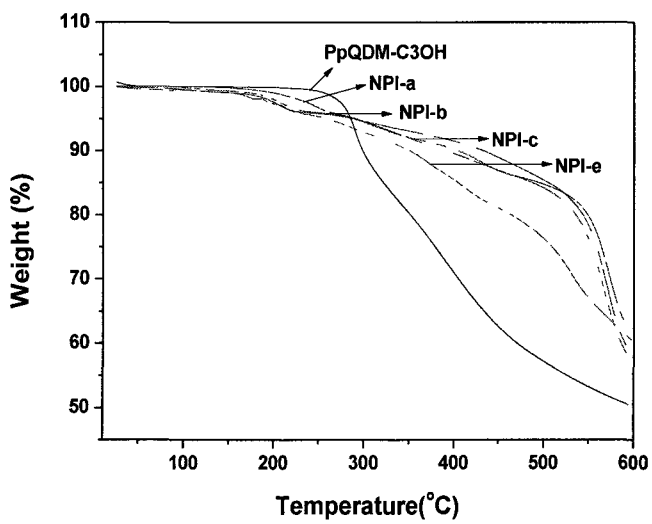

Figure 3.14. TGA traces of PQDM-C3OH, **NPI-a** - **NPI-c** and **NPI-e**.

3.4 Conclusions

Based on the results of preliminary compatibility test, PMMA and PES were selected to be the host polymers for the doping of FDCN. Two series of FDCN-based NLO polymers, **NA1** and **NA2** were prepared by either connecting the FDCN chromophores by a post-polymerization reaction or copolymerizing a FDCN containing monomer with MMA ,respectively. The solubility of **NA1** is limited to THF only and the films became brittle when increasing the content of FDCN chromophore to above 10%. EO coefficient was less than 15pm/V due to the low number density of the chromophore in the films and low T_g of the NLO polymers. In comparison with **NA1**, **NA2** has higher FDCN content (up to 14 wt %) and higher T_g. It has good solubility in common organic solvents such as $CHCl_3$, benzene, ACN and DMF. **NA2** can form high quality films for EO measurement and have high thermal stability (T_d > 232 °C).

Based on the comparative studies of chromophore doping in various polymers, PVP was selected to be the host polymer for doping the highly polar PpQDM chromophore. Poly(ether imide), **PI-1** was chosen for grafting with PpQDM chromophore. A series of acid-containing linear polyimides (**PI-1a** - **PI-1d**) having different T_g (208-227 °C) and molecular weights ($[\eta]_{inh}$ = 0.22-0.37 dL/g) were prepared. The acid groups in host polyimides allow for chemical grafting of the hydroxyl-containing PpQDM.

A series of PpQDM-based crosslinkable NLO polyimides (**NPI-a** - **NPI-e**) were synthesized in 80-92% yields through grafting PpQDM-C3OH onto **PI-1b**. The effect side chains on the T_g of the polymer and preliminary investigation into the chromophore loading are discussed. The reactive BCBO group was introduced to the side chains to

enable polymer crosslinking. Covalently grafting PpQDM-C3OH onto a polyimide can increase the chromophore loading level to a certain up to 13.8 wt % overall. Thermal crosslinking was performed at temperatures around 198 °C, which is higher or comparable to the T_g of most NLO polyimides. The T_g of **NPI-a** to **NPI-e** was observed to vary due to different pendant groups (methanol or 1-hexanol) and different PpQDM loading level. PpQDM-based crosslinkable NLO polymers were found to have good film-forming ability and high thermal stability (T_d > 250 °C).

3.5 Experimental Section

Materials. HEMA, DCC, cyanoacetic acid, CAEM, MMA, cyanoacetic acid, 2-hydroxyethyl alcohol, EDC and DMAP were purchased from Aldrich and used as receieved. AIBN was purchased from Aldrich and recrystallized from methanol. DMAc was dried over calcium hydride, vacuum distilled, and stored over 4 Å molecular sieves. Other chemical reagants were purchased from Aldrich and used as received.

Methods. Solubility tests were carried out by dissolving about 10 mg of polymer in 1 mL of studied solvent. For general characterization methods, such as ^1H and ^{13}C NMR, MS, IR, UV-Vis, DSC and TGA, refer to Chapter **2**.

Synthesis of CAEM

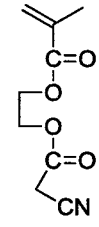

To a stirred solution of 2-hydroxyethyl methacrylate (6.5 g, 50 mmol) and cyanoacetic acid (4.45 g, 52.5 mmol) dissolved in dry CH_2Cl_2 (30 mL) under N_2 and

cooled with an ice bath was added DCC (10.8 g, 52.5 mmol) dissolved in CH_2Cl_2 (30 mL). A white precipitate formed, and the mixture was allowed to warm to room temperature and stir for an additional 18 h. The precipitate was removed by filtration and the crude product was purified by flash chromatography on silica gel, eluting with CH_2Cl_2 to provide 2-cyanoacetoxyethyl methacrylate as clear oil (9.0 g, 91%). Prior to use, the monomer was further purified by distillation, 90-92 °C at 0.3 mmHg. ^{1}H NMR ($CDCl_3$): δ 6.11 (s, CH, 1H), 5.59 (t, CH, 1H), 4.43 (m, CH_2O, 2H), 4.36 (m, CH_2O, 2H), 3.49 (s, CH_2CN, 2H), 1.92 (s, CH_3, 3H); ^{13}C NMR ($CDCl_3$): δ 166.2, 162.9, 135.2, 125.5, 112.9, 63.6, 61.3, 23.9, 17.4; IR (NaCl, cm^{-1}): 2964, 2264 (C≡N), 1754 (C=O), 1718 (C=O), 1637, 1170.

A typical synthesis of Copolymer A1-1

A solution of 2-cyanoacetoxyethyl methacrylate (2.50 g, 12.7 mmol), methyl methacrylate (4.0 g, 40 mmol), and AIBN (32.8 mg, 1.0 mol %) in dry toluene (14 mL) was heated under nitrogen at 65-70 °C for 20 h to provide a viscous solution. Solution was diluted with CH_2Cl_2 and precipitated twice into methanol to afford the copolymer as a white powder, and dried in a vacuum oven (1 mmHg) at 60 °C overnight (87%). ^{1}H NMR (Acetone-d_6): δ 4.5 (CH_2O), 4.3 (CH_2O), 3.9 (CH_2), 3.6 (CH_3O), 1.8-2.1 (CH_2), 0.8-1.1(CH_3); ^{13}C NMR (Acetone-d_6): δ 177.8-178.4, 164.8, 114.7, 64.2, 63.3, 53.0-55.1, 52.0, 45.2-45.7, 24.9, 19.4, 17.4; IR (NaCl, cm^{-1}) 2264 (C≡N), 1756 (C=O), 1729 (C=O), 1189, 1150; $[\eta]_{inh}$ = 0.22 dL/g (DMAc, c = 0.5 g/dL); T_g = 83 °C (DSC); T_d = 220 °C (TGA, nitrogen).

A typical synthesis of NLO polymers NA1-a

Under a anhydrous and oxygen-free condition, to a 50 mL round-bottomed flask were added copolymer **A1-1**(1.0 g, 7.6 mmol), sodium hydride (0.016 g, 60%, 0.40 mmol) and compound **4** (0.1 g, 0.2 mmol) in 10 mL of THF at 0 °C. Then the reaction was warmed to room temperature. After 6 h, purification of the crude product by flash chromatography on silica gel, eluting with THF to remove the insoluble inorganic salt, and the filtrate solution was concentrated under reduced pressure then precipitated twice into methanol to afford FDCN chromophore - copolymer as a red powder (77%).

Synthesis of A2

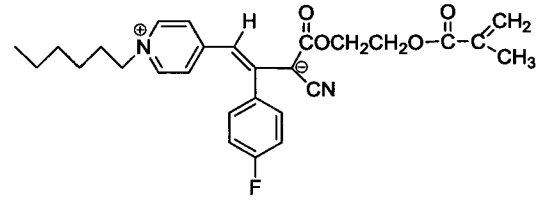

A Schlenk flask was charged with THF (23 mL), methacryloyl chloride (0.53 mL, 5.4 mmol), FDCNOH (1.86 g, 4.0 mmol), and Et_3N (0.76 mL, 5.4 mmol) and the mixture allowed to react with stirring at ambient temperature for 6 h. The reaction mixture was diluted with 200 mL of ether and the organic layer was washed with water (2 × 200 mL) and brine (200 mL) and then dried over K_2CO_3. The solvent was removed under reduced pressure, and the crude product was purified by an alumina column, eluting with CH_2C1_2. The red band was collected, and the solvent was removed to afford pure **A2** (1.52 g, 70%) without NMR measurement. IR: 2177 (C≡N), 1739 (C=O), 1672 (C=C), 1637 (C=O).

A typical synthesis of NLO polymers NA2a

A two-neck round bottom flask was charged with **A2** (0.105 g, 0.220 mmol), MMA (0.450 mL, 4.18 mmol), AIBN (3.0 mg) and 1mL of dry benzene. The reaction was heated to 80 °C under nitrogen for 18 h. Solution was diluted with benzene and

precipitated twice into methanol to afford the red NLO polymers **NA2a** (89%). ^{1}H NMR ($CDCl_3$): δ 8.5, 8.2, 7.5, 7.0, 4.3 (CH_2O), 3.6 (CH_3O), 1.3-1.5 (CH_2), 0.8-1.1(CH_3); IR (KBr, cm^{-1}): 2177 (C≡N), 1756 (C=O), 1731 (C=O), 1637, 1485, 1150; UV-Vis: λ_{max} = 502 nm (DMF), 558 nm ($CHCl_3$).

A typical synthesis of host polyimide PI-1b[12]

To a solution of DAPBA (1.05 g, 3.12 mmol) in anhydrous DMAc (13 mL) was added 4,4'-(4,4'-isopropylidene diphenoxy)bis(phthalic anhydride) (1.60 g, 3.06 mmol) and phthalic anhydride (0.0185 g, 0.125 mmol). The resulting solution was stirred at room temperature for 6 h and then acetic anhydride (1.6 mL) and pyridine (0.8 mL) were added. The reaction solution was stirred at room temperature for another 10 h and at 80 °C for 1 h. To the viscous solution was added slowly acetic acid (2 mL). After the resulting precipitate was dissolved at 60 °C with stirring, the polymer solution was poured slowly into methanol (200 mL). The precipitated white polymer product was collected by filtration, washed thoroughly with hot methanol, and dried in a vacuum (1 mmHg) oven at 120 °C overnight: 2.4 g (95% yield); $[\eta]_{inh}$ = 0.33 dL/g (DMAc, c = 0.5 g/dL); T_g = 217 °C (DSC); T_d = 450 °C (TGA, nitrogen); ^{1}H NMR (300 MHz, DMSO-d_6): δ 13.42 (s), 7.98 (d, J = 2.4 Hz), 7.52 (d, J = 7.2 Hz), 7.29-7.42 (m), 7.11-7.21 (m), 1.75 (s); IR (KBr, cm^{-1}): 1778, 1719 ($\upsilon_{C=O}$ of imide and carboxylic acid).

Synthesis of NPI-a

To an ice-cooled solution of **PI-1b** (0.204 g, 0.250 mmol), PpQDM-C3OH (0.0260 g, 0.0625 mmol) and DMAP (0.0335 g, 0.275 mmol) in anhydrous DMAc (4 mL) was added EDC (0.0575 g, 0.30 mmol). The solution was stirred at room temperature for

24 h, then 0.1 mL of methanol (excess), DMAP (0.067g, 0.55 mmol) and EDC (0.115 g, 0.60 mmol) were added to the mixture and the reaction continued for another 24 h at room temperature. The reaction solution was added dropwise slowly into methanol (250 mL) to precipitate the blue polymer. The blue polymer was re-dissolved into DMAc (4 mL) and then precipitated into methanol (200 mL). The blue polymer **NPI-a** was collected by filtration and dried at 100 °C under vacuum: 0.1 g (85% yield); PpQDM: 2.62 wt % in the polymer; ^{1}H NMR (300 MHz, DMSO-d_6): δ 10.45 (br s), 9.09 (br m), 8.70 (br m), 8.20 (br m), 8.09 (br m), 7.95 (br m), 7.88 (br s), 7.78 (br s), 7.68 (br m), 7.45-7.08 (br m), 6.93 (br m), 4.66 (br s), 3.73 (br s), 1.70 (br s); IR (KBr, cm^{-1}): 2178 and 2144 ($\upsilon_{C\equiv N}$ of cyano groups), 1777 and 1723 ($\upsilon_{C=O}$ of imide); T_g = 223 °C (DSC); T_d = 265 °C (TGA, nitrogen); UV-Vis: λ_{max} = 702 nm (DMF).

NPI-b: 90% yield; PpQDM: 4.71 wt % in the polymer; ^{1}H NMR (300 MHz, DMSO-d_6): δ 10.49 (br s), 9.07 (br s), 8.70 (br m), 8.74 (br m), 8.52 (br m), 8.38 (br m),8.29 (br m),7.93 (br s), 7.78 (br m), 7.73 (br s), 7.46-7.11 (br m), 6.88 (br m), 4.68 (br m), 4.22 (br m), 3.60(br m),1.70 (br s), 1.41(br m), 1.24 (br m), 0.88 (br m); IR (KBr, cm^{-1}): 2177 and 2142 ($\upsilon_{C\equiv N}$ of cyano groups), 1776 and 1722 ($\upsilon_{C=O}$ of imide); T_g = 185 °C (DSC); T_d = 264 °C (TGA, nitrogen); UV-Vis: λ_{max} = 695 nm (DMF).

Synthesis of NPI-c to NPI-e (with an example of NPI-e)

To an ice-cooled solution of **PI-1b** (0.204 g, 0.25 mmol), PpQDM-C3OH (0.031 g, 0.075 mmol), and DMAP (0.040 g, 0.33 mmol) in anhydrous DMAc (5 mL) was added EDC (0.0635 g, 0.33 mmol). After the solution was stirred at room temperature for 24 h, BCBO (0.00167 g, 0.0125 mmol) and additional DMAP (0.045 g, 0.23 mmol) and EDC

(0.0635 g, 0.33 mmol) were added to the mixture and the mixture was stirring at room temperature for 24 h; then 0.1 mL of 1-hexanol (excess), DMAP (0.045 g, 0.23 mmol) and EDC (0.0635 g, 0.33 mmol) were added and the reaction continued for another 24 h at room temperature. The reaction solution was added dropwise slowly into methanol (250 mL) to precipitate the blue polymer. The blue polymer was re-dissolved into DMAc (4 mL) and then precipitated into methanol (200 mL). After the product was dried at 100 ^{o}C under vacuum, a blue polymer **NPI-e** was obtained : 0.12 g (85% yield); PpQDM: 13.75 wt % in the polymer; ^{1}H NMR (300 MHz, DMSO-d_6): δ (TMS, ppm) 10.49 (br s), 9.07 (br m), 8.50 (br m), 8.38 (br m), 8.28 (br m), 7.92 (br s), 7.76 (br m), 7.73 (br m), 7.65-7.10 (br m), 6.83 (br m), 4.72 (br m), 4.21 (br m), 3.78 (br m), 3.59 (br m), 1.70 (br s), 1.23 (br m), 1.06 (br m), 0.88 (br m); IR (KBr, cm^{-1}): 2178 and 2144 ($\upsilon_{C\equiv N}$ of cyano groups), 1777 and 1723 ($\upsilon_{C=O}$ of imide); T_g= 180 ^{o}C (DSC); T_d = 253 ^{o}C (TGA, nitrogen); UV-Vis: λ_{max} = 695 nm (DMF).

NPI-c: 85% yield; PpQDM: 7.12 wt % in the polymer; ^{1}H NMR (300 MHz, DMSO-d_6): δ 10.45 (br s), 9.05 (br m), 8.52 (br m), 8.38 (br m), 8.37 (br m), 7.92 (br s), 7.77 (br m), 7.72 (br m), 7.45-7.10 (br m), 6.87 (br m), 4.68 (br m), 4.22 (br m), 3.78 (br s), 3.60 (br m), 1.70 (br s), 0.85 (br m) ; IR (KBr, cm^{-1}): 2178 and 2142 ($\upsilon_{C\equiv N}$ of cyano groups), 1773 and 1733 ($\upsilon_{C=O}$ of imide); T_g = 200 ^{o}C (DSC); T_d = 260 ^{o}C (TGA, nitrogen); UV-Vis: λ_{max} = 695 nm (DMF).

NPI-d: 80% yield; PpQDM: 7.59 wt % in the polymer; ^{1}H NMR (300 MHz, DMSO-d_6): δ 10.49 (br s), 9.07 (br m), 8.50 (br m), 8.38 (br m), 8.28 (br m), 7.92 (br s), 7.76 (br m), 7.73 (br m), 7.65-7.10 (br m), 6.83 (br m), 4.72 (br m), 4.21 (br m), 3.78 (br m), 3.59 (br

m), 1.70 (br s), 1.23 (br m), 1.06 (br m), 0.88 (br m); IR (KBr, cm^{-1}): 2178 and 2144 ($\upsilon_{C\equiv N}$ of cyano groups), 1777 and 1723 ($\upsilon_{C=O}$ of imide); T_g = 163 °C (DSC); T_d = 255 °C (TGA, nitrogen); UV-Vis: λ_{max} = 694 nm (DMF).

Determination of PpQDM Content

For the accurate determination of PpQDM content in NLO polyimides, a concentration calibration equation was established by measuring the absorption (*A*) of PpQDM-C3OH in DMF at six concentrations at 690 nm. By plotting the absorption against the concentration and by fitting the data with a straight line, the linear relationship between absorption and PpQDM concentration was defined as per the Beer-Lambert law:

$$A = 0.44318 \times C - 0.00469$$

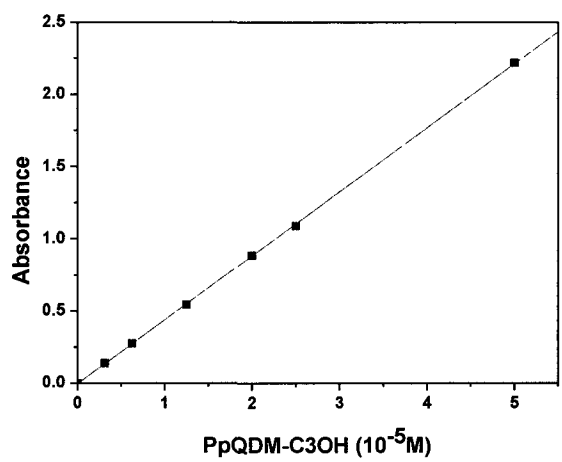

To determine the PpQDM-C3OH content in NLO polyimides, a polymer sample with known weight (1.8 mg) was dissolved in a certain volume of DMF (10 mL) and the intensity of CT absorption is recorded, from which the weight of PpQDM is calculated and used to estimate the weight percentage of PpQDM-C3OH in NLO polyimides.

3.6 References

(1) (a)Yesodha, S. K.; Sadashiva, C. K.; Pillaia, Tsutsumi, P. N. *Prog. Polym. Sci.* **2004,** *29*, 45. (b)Eaton, D. F. *Science* **1991**, *253*, 281. (c) Burland, D. M.; Miller, R. D.; Walsh, C. A. *Chem. Rev.* **1994,** *94*, 31. (d) Dalton, L. R.; Harper, A. W.; Ghosn, R.; Steier, W. H.; Ziari, M.; Fetterman, H.; Shi, Y.; Mustacich, R. V.; Jen, A. K.-Y.; Shea, K. J. *Chem. Mater.* **1995**, *7*, 1060.

(2) (a)Briers, D.; Koeckelberghs, G.; Picard, I.; Verbiest, T.; Persoons, A.; Samyn, C. *Macromol. Rapid Commun.* 2003, *24*, 841. (b) Lee, S. K.; Cho, M. J.; Jin, J.; Choi, D. H. *J. Polym. Sci. A: Polym. Chem.* **2007**, *45*, 531. (c)Scarpaci, A.; Cabanetos, C.; Blart, E.; Montembault, V.; Rodriguez, O. F. *J. Polym. Sci. A: Polym. Chem.* **2009**, *47*, 5652.

(3) (a)Shi, Y.; Zhang, C.; Zhang, H.; Bechtel, H.; Dalton, L. R.; Robinson, B. H.; Steier, W. H. *Scie*nce **2000**, *288*, 119. (b) Macchi, R.; Cariati, E.; Marinotto, D.; Roberto, D.; Tordin, E.; Ugo, R.; Bozio, R.; Cozzuol, M.; Pedron, D.; Mattei, G. *J. Mater. Chem.* **2010**, *20*, 1885. (c) Kajzar, F.; Krupka, O.; Pawlik, G.; Mitus, A.; Rau, I. *Mol. Cryst. Liq. Cryst.* **2010**, *522*, 180.

(4) Cheng, Y. J.; Luo, J. D.; Hau, S.; Bale, D. H.; Kim, T. D.; Shi, Z.; Tucker, N. M.; Tian, Y.; Dalton, L. R.; Reid, P. J.; Jen, A. K.-Y. *Chem.Mater.***2007**, *19, 1154.*

(5) Zhang, C.; Wang, C.; Dalton, L.R.; Zhang, H.; Steier, W. H. *Macromolecules* **2001**, *34*, 253.

(6) (a)Liang, Z.; Dalton, L. R.; Garner, S. M.; Kalluri, S.; Chen, A.; Steier, W. H. *Chem. Mater.* **1995**, *7*, 941. (b)Song, N. H. ; Men, L.; Gao, J. P.; Bai, Y.; Beaudin, A. M. R.; Yu, G.; Wang, Z. Y. *Chem. Mater.* **2004**, *16*, 3708. (c) Song, N. H. ; Men, L.; Gao, J. P.; Yu, G.; Beaudin, A. M. R.; Wang, Z. Y. *J. Nonlinear Opt. Phys. Mater.* **2005**, *14*, 367.

(7) (a)Garner, S. M.; Cites, J. S.; He, M.; Wang, J. *Appl. Phys. Lett.* **2004**, *84*, 1049. (b)Lu, Z.; Li, J.; Hua, J.; Li, X.; Qin, J.; Qin, A.; Ye, C. *Syn. Met.* **2005**, *152*, 217. (c)Bai, Y. W.; Song, N. H.; Gao, J. P.; Sun, X.; Wang, X.; Yu, G.; Wang, Z. Y. *J. Am. Chem. Soc.* **2005**, *127*, 2060. (d)Xiong, Y.; Tang, H.; Zhang, J.; Wang, Z. Y.; Campo, J.; Wenseleers, W.; Goovaerts, E. *Chem. Mater.* **2008**, *20,* 7465.

(8) Kalluri, S.; Shi, Y.; Steier, W. H.; Yang, Z.; Xu, C.; Wu, B.; Dalton, L. R.; *Appl. Phys. Lett.* **1994**, *65*, 2651.

(9) Kang, H.; Facchetti, A.; Jiang, H.; Cariati, E.; Righetto, S.; Ugo, R.; Zuccaccia, C.; Macchioni, A.; Stern, C. L.; Liu, Z.; Ho, S.-T.; Brown, E. C.; Mark A. Ratner, M. A.; Marks, T. J. *J. Am. Chem. Soc.* **2007**, *129*, 3267.

(10) (a)Jin, D.; Londergan, T.; Huang, D. **2004**, *4*, 44. (b) Drummond, J. P.; Clarson, S. J. ; Zetts, J. S.; Hopkins, F. K.; Caracci, S. J. *Appl. Phys. Lett.* **1999**, *74*, 18.

(11) Wurthner, F.; Yao, S.; Debaerdemaeker, T.; Wortmann, R. *J. Am. Chem. Soc.* **2002**, *124*, 9431.

(12) Naiheng Song: "Development of Zwitterinic Nonlinear Optical Polyimides for Electro-Optic Applications", *Ph. D. Thesis,* Carleton University **2004**.

(13) Mao, S. S. H.; Ra, Y.; Guo, L.; Zhang, C.; Dalton, L. R.; Chen, A.; Garner, S. M.; Steier, W. H. *Chem. Mater.* **1998**, *10*, 146.

(14) (a)Iacono, S. T.; Budy, S. M.; Jin, J.; Smith, D. W. *J. Polym. Sci., Part 1: Polym. Chem.* **2007**, *45*, 5706. (b)Budy, S. M.; Suresh, S.; Spraul, B. K.; Smith, D. W. *J. Phys. Chem. C* **2008**, *112*, 8089. (c)Luo, J. D.; Haller, M.; Li, H.; Kim, T.-D.; Jen, A. K.-Y. *Adv. Mater.* **2003**, *15*, 1635.

(15) (a)Sullivan, P. A.; Olbricht, B. C.; Akelaitis, A. J. P.; Mistry, A. A.; Liao, Y.; Dalton, L. R. *J. Mater. Chem.* **2007**, *17*, 2899. (b)Shi, Z.; Luo, J.; Huang, S.; Zhou, X. H.; Kim, T.-D.; Cheng, Y.-J.; Polishak, B. M.; Younkin, T. R.; Block, B. A.; Jen, A. K.-Y. *Chem. Mater.* **2008**, *20*, 6372. (c)Shi, Z.; Luo, J.; Hunag, S.; Cheng, Y.; Kim, T.; Polishak, B. M.; Zhou, X.; Tian, Y.; Jang, S.; Knorr, D. B., Jr.; Overney, R. M.; Younkin, T. R.; Jen, A. K.-Y. *Macromolecules* **2009**, *42*, 2438.

(16) (a)Wang, Z. Y. U.S. Patent 5,869,693. (b)Wang, Z. Y.; Suzzarini, L.; Gao, J. P. *Tetrahedron Lett.* **1997**, *38*, 5745. (c)Wang, Z. Y.; Kuang, L.; Meng, X. S.; Gao, J. P. *Macromolecules* **1998**, *31*, 5556.

(17) (a)Williams, A.; Ibrahim, I. T. *Chem. Rev.* **1981**, *81*, 589. (b)Hegarty, A. F.; McCormack, M. T.; Ferguson, G.; Roberts, P. J. *J. Am. Chem. Soc.* **1977**, *99*, 2016.

(18) Ying Xiong "Development of Zwitterinic Chromophores for Electro-Optic Applications", *Ph. D. Thesis,* Carleton University **2008**.

Chapter 4 Electro-Optic Properties of Nonlinear Optical Materials

4.1 Introduction

In NLO materials, the macroscopic electro-optic effect in terms of EO coefficient (r_{33}) is determined by the number density of the embedded NLO chromophores, their hyperpolarizability, and their degree of noncentrosymmetrical orientational order.

A number of techniques have been used to create the required noncentrosymmetry in EO polymers including photo-assisted poling,[1a] photothermal poling,[1b] and all optical poling,[1c] etc. However, the more common methods typically used are corona and parallel electrode poling.

Corona poling is advantageous because of its simplicity and the fast charging process as shown in Figure 4.1 (left). In corona poling, a sharp needle or wire is suspended above a polymer film and charged to several kilovolts to ionize the surrounding atmosphere and deposit charges on the surface of the films. Positive or negative charges can be deposited depending on the choice of electrode. Although high poling fields can be achieved in this way, the resulting strength can lead to dielectric damage to the polymer film surface resulting in optical losses after poling.[1d]

In the parallel electrode poling, the NLO polymer film was sandwiched between two electrodes (Figure 4.1, right), then the film subjected to heating up to the glass transition temperature while the poling field is applied.[1e] This method is advantageous to control the poling conditions, (such as voltage and the electric current monitored) and no damage to the surface of polymer films. The drawback of this technique is that the poling voltage is limited due to potential for dielectric breakdown in the polymer film. This

limitation can be alleviated by poling under vacuum, controlling polymer purity in synthesis and film forming.

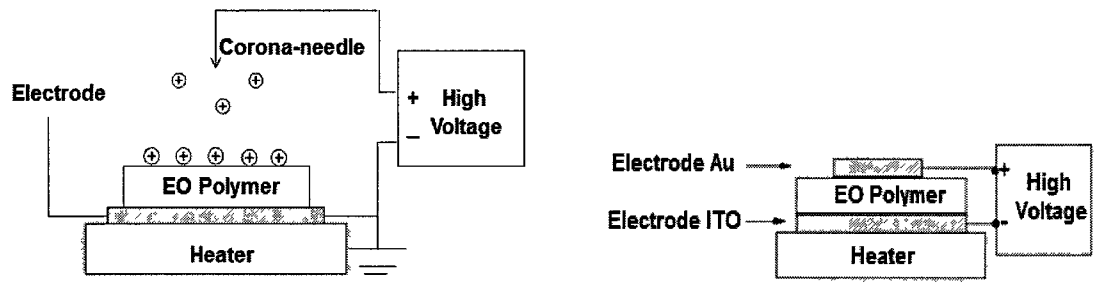

Figure 4.1. Schematic diagrams of the corona poling (left) and parallel electrode poling setup (right).

The net polar order of NLO materials in this research is achieved by electrode poling, since this process is commonly used in poling single-layer EO films to allow convenient characterization of NLO properties and screening of materials. The poling efficiency of NLO polymers is usually characterized as an order parameter of $\langle\cos^3\theta\rangle$. It depends on a number of factors, from both the material and technical aspects.

Usually, the maximum EO coefficient for a given polymer is achieved at the highest applicable poling field, often to a level where it nearly generates dielectric breakdown. Currently, medium electric field strengths (20 V/μm < E_{POL}< 100 V/μm) are widely used in the poling process,[2] electrode-poling voltages of around 100 V per micrometer are achievable for highly efficient NLO polymers.[3] Dalton and co-workers[4] systematically investigated the factors affecting the order parameter of poled polymers, showing that intermolecular electrostatic interactions associated with dipole moment, shape, and concentration of chromophores play an important role in lowering the maximum number density and poling efficiency.

Higher poling field usually produces higher EO coefficient. However, high poling voltage could induce local electrical discharges in low-density domains of the material or film defects (e.g., voids and impurities), and lead to high leak through currents (LTCs) that cause physical damages to the poled films.[5]

One of the most critical aspects in the poling of polymers is to obtain the maximum possible electric field without dielectric breakdown. Therefore, considerable research efforts have been spent on improving high field poling of NLO polymers. An effective approach to improve the poling of EO polymers is to insert a thin buffer layer of spin-on materials as a barrier between the electrode and the EO polymer layer to form a double-layer structure between the two poling electrodes (Figure 4.2).[6] Compared to a single-layer NLO film having intimate contact with two electrodes, the presence of an additional layer can delay the onset of dielectric breakdown, and effectively enhance the strength of the maximum applicable poling fields.

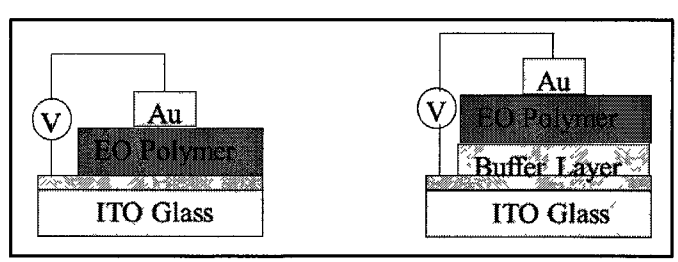

Figure 4.2. Sandwiched single-layer (left) and double-layer structures (right) for the poling of thin film EO materials.

The selection of buffer layer materials includes inorganic SiOx networks,[7] conducting polymer blends of poly(ethylene dioxythiophene):poly(styrenesulfonic acid) (PEDOT:PSS) with poly(vinyl alcohol)(PVA),[8] and sol-gel derived TiO_2.[9] It has been demonstrated that the application of a suitable barrier layer enhanced the r_{33} by 15-100%

on conventional NLO polymers, such as PMMA/DR1 and doped APC systems, compared to the results of poled single-layer films.[5a,7,8,9] For NLO polymers based on zwitterionic PQDM and PeQDM, strong inter-chromophore electrostatic interactions were found due to the very large dipole moments of those chromophores. PpQDM doped polymer systems with relatively high dielectric constants (e.g., in PVP) may attenuate the fields associated with intermolecular electrostatic interactions and alleviate the problem in achieving a high poling efficiency. The inter-chromophore electrostatic interactions effect regarding the FDCN-based NLO polymers are unclear. Barrier materials applied into making double layer structure device of zwitterionic chromophores have not been studied before, especially for the PpQDM-based NLO polyimides with much higher concentration of zwitterionic NLO chromophores.

Therefore, this chapter describes the EO property measurements of 1) FDCN doped PES guest-host polymers; 2) FDCN-MMA NLO polymers (**NA2**); 3) PpQDM doped PVP guest-host polymers; 4) crosslinkable PpQDM NLO polyimides (Chapter **3**). Detailed poling methods including conventional electrode poling and *in situ* poling and EO coefficient measurement method are introduced in the experimental section. The NLO chromophores loading and electrical properties of NLO polymer films are studied. The correlation studies of EO coefficients with the chromophore structures, poling conditions and NLO polymer film structures (e.g., single layer and double layer) will be also discussed.

4.2 Electro-Optic Properties of FDCN-Based NLO Polymers

4.2.1 Electro-Optic Properties of FDCN-PES Guest-Host Polymers

As discussed in Chapter **3**, PES represents a suitable host for FDCN guest-host system because of its high quality film-forming ability, film optical clarity, and high glass transition temperature of 225 °C, which could prevent or minimize the chromophore relaxation after poling. Therefore, guest-host FDCN NLO polymer films were prepared using FDCN chromophores and commercially available PES. FDCN chromophores and PES were dissolved in DMF to form 2 wt % FDCN/PES solution and stirred overnight at room temperature in the dark. After the solution was filtered through a 0.2 μm syringe filter, the filtered solution was cast onto ITO glass substrate (2.56 cm^2) to produce films of about 1~3 μm thickness and dried at 45 °C overnight under the protection of nitrogen. The films were further dried in a vacuum oven overnight at 85 °C to remove the residual solvent. A thin gold layer with a thickness of 100-150 nm was sputtered on the films. The ITO and gold layers were used as both poling and modulation electrodes.

FDCNs can be doped up to 10 wt % into PES and smooth thin films can be prepared by solution casting. The loading density of FDCN is higher than that of PQDM chromophores in PES system, which was limited to about 2 wt %, as larger concentrations led to phase separation, due to strong intermolecular interactions arising from the large dipole moments.[10]

The electrode poling process was carried out following a conventional way, under the protection of nitrogen in the dark in an electrode poling setup, the sample cells were gradually heated from room temperature to the poling temperature (e.g., 190 °C for

FDCN/PES) at a heating rate of 5 °C/min, and a direct current (DC) voltage applied across the polymer films was maintained between 60 and 70 V/μm.

During the poling process, the electric current was monitored to optimize poling efficiency and to control local electrical breakdown in the films. The increment of current should be dominantly ascribed to the chromophore alignment under the external electric field and the chain rearrangement of polymer, which is mostly accomplished around the T_g of the polymer. The monitoring of the current also enabled more efficient poling of the sample. Generally, the breakdown of the electric field through the polymeric film is accompanied by an abrupt overflow of the electric current. The current dropped slowly after it reached the maximum , and even under a constant poling field.

The poling temperature is about 5-10 °C below the T_g of the polymer films. After the films were held at the poling temperature for 20 min, the heating was turned off while keeping the poling field. At the same time, the current declined due to the remarkable increase in resistance of the polymeric films. After reaching room temperature, the poling voltage was taken off and the EO coefficients of the poled polymers were measured immediately at 1550 nm using the simple reflection technique (See experimental section 4.5.4).[11]

All samples possess very little absorbance at the measured wavelength of 1550 nm. Thus, we did not consider the absorption induced resonance enhancement. The EO coefficient, r_{33} was determined on a Teng-Man reflection setup. An alternate current (AC) voltage was applied to each sample to observe the modulated signal (I_m). The linear EO coefficient of the poled films was calculated by the following equation. The r_{33} value is directly proportional to I_m / I_c in eq 1. [11a]

$$r_{33} = \frac{3\lambda I_m}{4\pi V_m I_c n^2} \frac{(n^2 - \sin^2\theta)^{3/2}}{(n^2 - 2\sin^2\theta)} \frac{1}{\sin^2\theta} \quad \text{(eq.1)}$$

where n is the refractive index of the polymer materials and I_m is the amplitude of EO modulation. V_m is the modulating voltage applied to the sample and I_c is the half intensity of incident light. The molecular properties of FDCN chromophores and EO properties of FDCN doped NLO polymers are summarized in Table 4.1.

Although the FDCN series based on the picolium donor and dicyano acceptor exhibits moderate values of $\mu\beta$ (See Table 4.1), compared to PQDM, which $\mu\beta$ = 74,600 $\times 10^{-48}$ esu, more than ten times larger than that of FDCN, FDCN/PES thin films display almost the same EO coefficients as PQDM/PES thin films (21 pm/V of 1 wt % in PES),[10] due to its higher loading ability into PES (5 wt %) than the PQDM chromophores.

Table 4.1. The molecular properties of FDCN chromophores and EO properties of FDCN doped PES polymers

Chromophore	μ (D)	β (10^{-30}esu)	$\mu\beta$ (10^{-48}esu)	N (Polymer)	n (1.5 μm)	T_p (°C)	r_{33} (pm/V)
FDCN	21.6	-320	-6720	5%	1.6206	190	20
FCNE	11.4	-495	-5643	5%	1.6204	180	18

N: chromophore contents; n: refractive index at 1550 nm; T_p: poling temperature

The results indicated that the aromatic group attached perpendicular to the main axis of the FDCN chromophore leads to a larger EO coefficient compared to its plain analogue molecule PQDM in the same polymer matrix. This is attributed to the ability of the bulky aromatic side chain to keep neighboring molecules away from each other and thus reduce their intermolecular interactions. In addition, it suggested that PES is a proper polymer matrix with proper polarity for less polar FDCN than for the more polar PQDM

chromophore, because the EO coefficient is affected by different polymer densities and partially due to the influence of the polymer environment to the poling efficiency.

Compared with a neutral benchmark chromophore, namely CLD-1($\mu\beta$ = 14,065 × 10^{-48} esu, μ=13),[12] which EO coefficients are as high as 16 ~ 22 pm/V at 1550 nm for a 15 wt % chromophore loading in PMMA.[13] The FDCN series has relatively lower hyperpolarizabilities, but displays the same level of r_{33} with CLD-1 contributing to their large μ values, which is the significant zwitterionic molecular nature.

4.2.2 Electro-Optic Properties of FDCN-MMA NLO Polymers

In order to reduce relaxation of the EO signal and increase the number density of active chromophores in NLO polymer systems, the FDCN chromophore was covalently incorporated into an FDCN-MMA polymer system (**NA2**), which were expected to have higher r_{33} than that of the FDCN doped system.

For the poling studies, **NA2** polymer films with thickness of 1-3 μm on ITO glass were prepared by solution casting directly. The films were dried at 60-80 °C under vacuum (1 mmHg) for 24 h before sputtering a thin layer (~ 150 nm) of gold as a top electrode onto the polymer films for electrode poling. In a general experiment, the sample was mounted on the poling stage and the temperature was increased in several minutes up to around T_g. The poling field was then applied to the sample at a ramping rate of 10 V/min.

In comparison with FDCN doped PES system, **NA2** polymer films showed a better stability to high electric fields. A field above 70 V/μm was readily achieved for

these polymers, and the **NA2** polymers displayed large EO coefficients of 24 and 30 pm/V for the 7 and 14 wt % polymers, respectively (Table 4.2).

Table 4.2. Characterization of FDCN-MMA polymers

NLO polymer	FDCN (wt %)	T_g (°C)	Film thickness (μm)	n (1.5 μm)	T_p (°C)	r_{33} (pm/V)
NA2a	7	95	2.01	1.4972	90	24
NA2b	14	126	1.89	1.4970	120	30

The maximal level of chromophore loading was achieved around 14 wt % without showing any phase separation in solution-cast films, indicating the good compatibility of FDCN with PMMA. A higher number density of NLO chromophore in bulk polymers is highly desired to impart a large microscopic optical nonlinearity in NLO chromophores to a large macroscopic EO coefficient in NLO polymer, however, the higher number density in polymers may lead to either phase separation eventually or attenuation of the poling efficiency due to the increased intermolecular electrostatic interactions.[12] For example, the PQDM with a higher μβ value containing polyimides NLO polymers developed by our group, the optimal concentrations were below 11 wt %.[13]

As expected, the measured EO coefficient of the poled **NA2** polymer films with higher chromophore content, such as 14 wt % is much higher than that of the FDCN doped PES system (5 wt %) and reached values comparable to that of the bulk inorganic NLO single crystal lithium niobate ($LiNbO_3$, r_{33} = 31 pm/V), which is currently used in the commercial EO modulators, and even higher than those of FTC/CLD-based NLO polymers with similar number densities.[14, 15]

4.3 Electro-Optic Properties of PpQDM-Based NLO Polymers

4.3.1 Electric Poling of PpQDM/PVP Guest-Host Polymers

To investigate the potential of the PpQDM chromophores in EO applications, a doping study was carried out and the macroscopic EO activity of the poled NLO guest-host polymers was assessed. As discussed in Chapter **3**, PVP was chosen in our study as a host polymer for PpQDMs based on the absorption study of PpQDM-Met doped systems, good film forming ability and higher loading density of the PpQDM chromophores. For comparison, the EO properties of PpQDM/PES guest-host NLO polymer thin films were also studied.

PpQDM-Met and PpQDM-Ben were firstly doped into PES and PVP matrix materials in a host-guest way in the solvent of DMF with the chromophore contents of 1, 3 and 5 wt %, respectively; then visually clear PpQDM-Met polymer and PpQDM-Ben polymer films were prepared (See experimental section). These films were of high quality and pinhole free, and did not exhibit phase separation. These features are important to ensure successful poling without dielectric breakdown and to produce reproducible EO coefficients.

Table 4.3. Characterization of PpQDM guest-host polymer thin films

Chromophore	N (Polymer)	T_g (°C)	T_p (°C)	r_{33} (pm/V)
PpQDM-Met	1%(PES)	210	170	6
PpQDM-Met	3%(PVP)	165	140	16
PpQDM-Ben	1%(PES)	210	170	12
PpQDM-Ben	5%(PES)	210	170	25
PpQDM-Ben	5%(PVP)	165	140	40

A typical parallel electrode poling process and EO coefficient measurement was carried out as described in the 4.2.1 section; Table 4.3 collects the results from characterization of both PpQDM-Met and PpQDM-Ben guest-host polymer thin films.

4.3.2 Optimization of Poling Conditions

Poling Temperature

Typically, the electric poling of NLO polymers is carried out around the T_g, as the segmental chain relaxation of the polymers at such a temperature allows for good chromophore mobility. However, T_g is not the only factor governing the poling temperatures. Others like thermal stability and dielectric breakdown temperature under certain poling electric fields should also be considered.

To avoid degradation of the PpQDM chromophore during poling process, the thermal stability of the PpQDM-Ben/PVP thin films in nitrogen was evaluated by UV-Vis spectroscopy. As shown in Figure 4.3, when PpQDM-Ben/PVP thin film was heated at various temperatures below 120 ^{o}C for 30 min in nitrogen, the CT absorption band remained basically unchanged; when the film was heated at temperature above 140 ^{o}C, a rapid decrease in the CT absorption was observed, a second peak at 490 nm started appearing and kept increasing to the maximum value, while the CT absorption of PpQDM-Ben chromophore completely disappeared and the color of the film changed from blue to light pink.

The color bleaching behavior of PpQDM is similar with that of PQDM. The decomposition of PQDM in solution and in the solid state (guest-host in PES) has been investigated by a former graduate student in our group.[16] The results showed that PQDM chromophores are labile to the presence of oxygen, especially upon exposure to visible

light and heating. The same may also explain the color fading for the PpQDM-Ben/PVP film at high temperatures. Therefore, the poling was performed at 170 °C for PpQDMs/PES and 140 °C for PpQDMs/PVP, respectively, which are about 10 °C below the T_g of the corresponding polymer films.

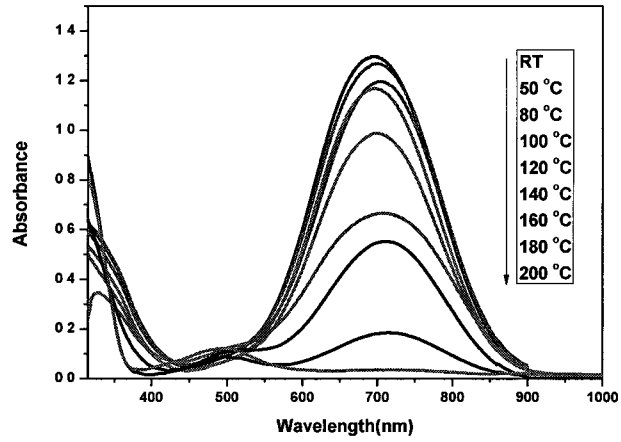

Figure 4.3. UV-Vis absorption spectra of thin film of PpQDM-Ben /PVP at elevated temperatures in nitrogen.

Poling Voltage

For the parallel electrode poling of NLO polymers, higher electric field is desired to afford a strong dipole-field interaction and a high order parameter. However, to simply pursue a high voltage is not appropriate, since dielectric breakdown may often occur. To obtain optimized electric field for poling, the EO coefficient of the sample was traced under various poling voltages. During the poling process, the electric current was monitored to optimize poling efficiency and to control local electrical breakdown in the films. It was found that a dielectric breakdown occurred at the high electric field of 80-100 V/μm, therefore relatively low electric fields, such as ~ 70 V/μm were utilized for the poling of the NLO polymers based on the various conductivity and achievable high

fields of different quality of polymer films.

Effect of Polymer Matrix

PpQDM-Ben/PVP (5 wt %) demonstrated the highest r_{33} value (~ 40 pm/V) among the tested guest-host NLO polymers, while PpQDM-Ben/PES, PpQDM-Met/PVP and PpQDM-Met/PES displayed lower r_{33} values of around 25, 16 and 6 pm/V, respectively (Table 4.3). These results indicated that the intermolecular aggregation of the chromophores in the more polar PVP polymer matrix was effectively reduced compared to PES and the poling efficiency of the PVP system was enhanced due to the relatively polar environment. For example, PpQDM-Ben/PVP (5 wt %) showed higher r_{33} value (~ 40 pm/V) than that of PpQDM-Ben/PES (5 wt % , ~ 25 pm/V) even though it was poled at a lower poling temperature (140 °C) compared with 170 °C in PES.

Effect of Chromophore Shape

It is interesting to find that PpQDM-Ben and PpQDM-Met have almost same $\mu\beta$ value, but higher compatibility with polymer host and higher corresponding r_{33} value were found in PpQDM-Ben than in PpQDM-Met. First, doping density of PpQDM-Ben in both PVP and PES can reach 5 wt % and are higher than that of PpQDM-Met (3 wt % and 1 wt %, respectively); second, PpQDM-Ben/PES (5 wt %) exhibited almost four fold higher r_{33} value than that of PpQDM-Met/PES (1 wt %) system due to the higher chromophore loading density. Even with the same amount of the chromophore inside, the r_{33} value of the PpQDM-Ben/PES (1 wt %) was two times higher than that of the PpQDM-Met/PES (1 wt %) system.

To investigate the difference of the chromophores' structure, the minimum energy conformations for three PpQDM-based chromophores such as PpQDM-Met, PpQDM-Ben, PpQDM-C3OH were determined by computer calculations using the MP6 method; in comparison, the minimum energy conformations of PQDM was also calculated. The optimized geometrical structures of these chromophores are illustrated in Figure 4.4.

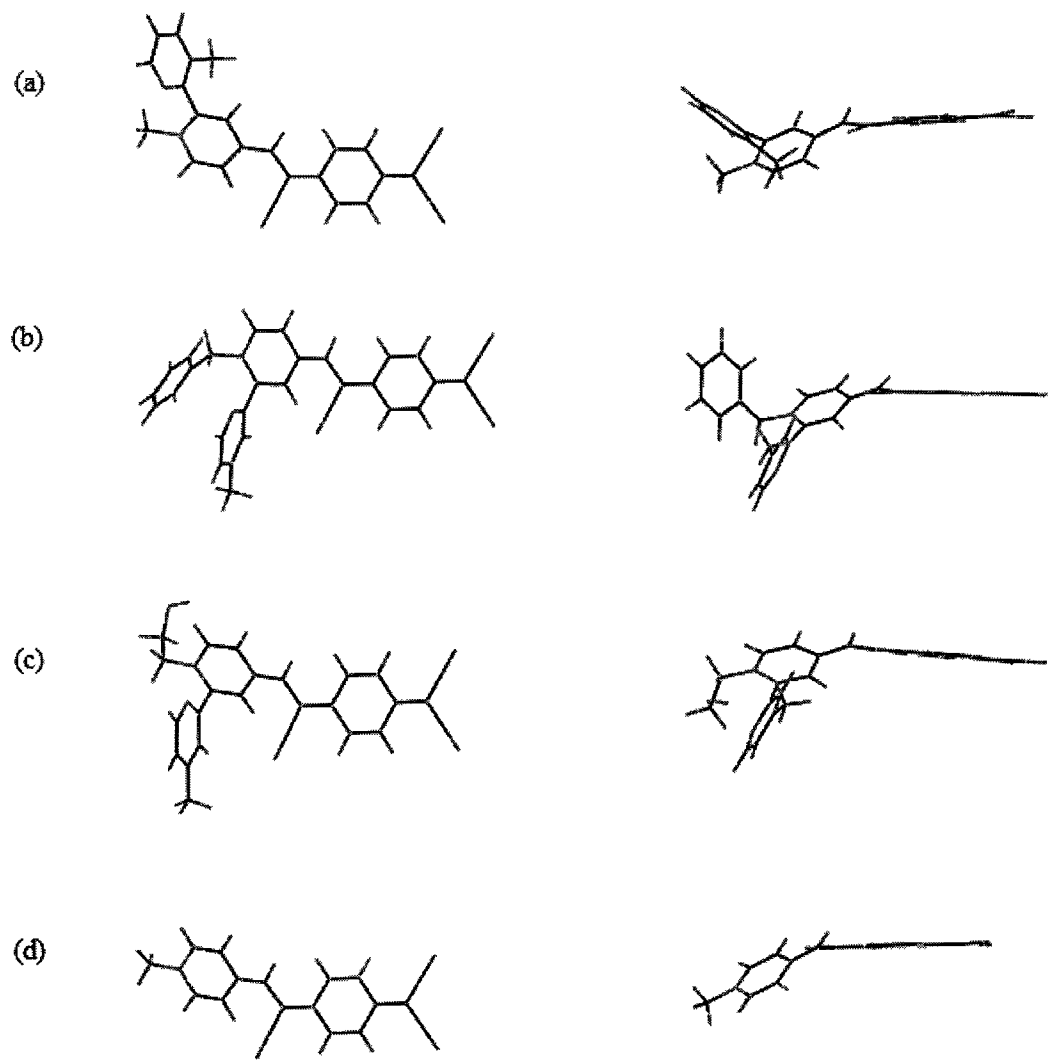

Figure 4.4. Geometries of chromophores: (a) PpQDM-Met (b) PpQDM-Ben (c) PpQDM-C3OH (d) PQDM-Met.

Both PQDM and PpQDM chromophores have plane structure, PQDM is more rigid and rod-like than PpQDM. The methyl pyridine in the PpQDM chromophores were aligned almost perpendicular to the long molecular axis of the chromophores.

Compared with PpQDM-Met, the donor group of PpQDM-Ben is encompassed by an additional bulky benzyl group in the PpQDM-Ben, it's plane is out of the molecular main chain plane, therefore the chromophores are more difficult to be interacted electrostatically, so that they are more labile to be poled. It is indicated that the bulky donor size and suitable molecular shape of PpQDM-Ben can lead to large r_{33} value.

For the practical application of NLO polymers, the long-term stability of the EO coefficient at elevated temperatures is important. The temporal stability of EO coefficient of the poled PpQDM-Ben/PVP film was investigated by measuring the r_{33} [r_{33} (t)/r_{33} (t_0)] as a function of time at 80 °C (operational temperature) in the dark. Figure 4.5 shows the temporal stability of EO coefficient for the poled PpQDM-Ben/PVP film. The r_{33} value decreased around 10% of the initial value after the first 160 h in the dark and under nitrogen atmosphere. This large drop of the EO coefficient at the beginning of thermal treatment may arise as a result of the relaxation of the ordered state, i.e. from the recovery of bond angle and bond length of the oriented chromophores. [17]

The r_{33} value maintains constant around 15% relaxation of the initial value after the second 160 h in air. The results show high stabilities of NLO responses at elevated temperatures, and PVP polymer matrix have proper polarity to hold the oriented chromophores, thus restricting the local movement of the chromophores and reducing orientation relaxation.

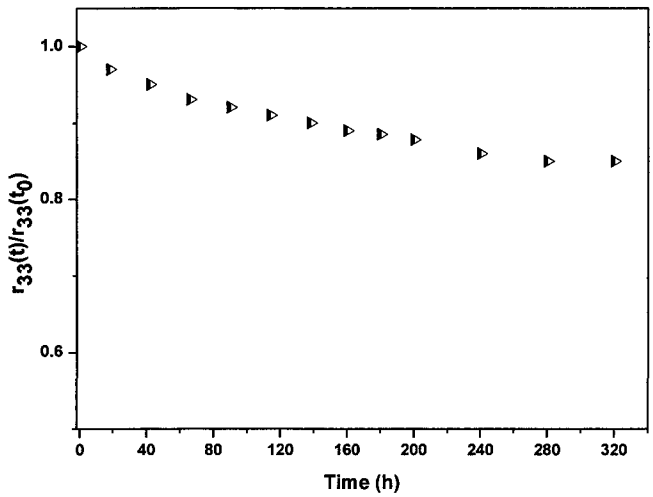

Figure 4.5. Temporal stability of the r_{33} for the poled PpQDM-Ben/PVP at 80 °C.

4.3.3 *In situ* Poling of PpQDM-PVP Guest-Host Polymers

To explore the intrinsic EO properties of the PpQDM series chromophores, the *in situ* EO coefficient measurement of poled PpQDM-PVP guest-host materials at the laser wavelength of 1550 nm was performed by a modified Teng-Man reflection technique.[18] In this measurement, r_{33} signals were collected during the process of heating and cooling in the presence of a poling field. Overlaying a DC poling field with an AC voltage, real time monitoring of the ratio I_m / I_c allowed direct evaluation of optimal r_{33} values under the controlled experimental parameters such as temperature and applied voltage.

A representative *in situ* poling process using PpQDM-Ben doped PVP polymer system is shown in Figure 4.6. The loading concentration of the chromophore is 5 wt %. In a general experiment, the sample was mounted on the poling stage and the temperature was increased in several minutes up to around T_g. The poling field was then applied to the sample at a ramping rate of 10 V/min. Since no electric current was monitored during our *in situ* poling process, the ramping of the poling field at 50 °C and 80 °C was

recorded to investigate the maximum poling voltage (Table 4.4), a linear dependence of the r_{33} values versus the poling voltages has been observed.

Table 4.4. EO coefficient (pm/V) of PpQDM-Ben/PVP (5 wt %) under various temperature and poling fields

NLO polymer	T_p (°C)	Poling Field (V/μm)			
		35	50	60	70
PpQDM-Ben	50	5.5	15.5	19.8	33.0
PpQDM-Ben	80	6.2	16.4	25.2	40.1

Since the poled films show the largest r_{33} values of 33 and 40 pm/V in the poling field around 70 V/μm at 50 °C and 80 °C, respectively, the ramping of the *in situ* poling field of PpQDM-Ben/PVP (5 wt %) NLO polymers was ceased and maintained at 70 V/μm to achieve excellent poling efficiency by considering the stability of the film. The highest r_{33} values of the films PpQDM-Met and PpQDM-Ben were obtained with the chromophore concentrations of 3 and 5 wt %, respectively. The resultant EO properties of PpQDM doped NLO polymers under the optimal poling condition are summarized in Table 4.5.

Table 4.5. Characterization of PpQDM Guest-host polymers under *in situ* poling

Chromophore	N (Polymer)	T_g (°C)	T_p (°C)	V_p (V/μm)	r_{33} (pm/V)
PpQDM-Met	3%(PVP)	170	120	70	36
PpQDM-Met	3%(PVP)	170	140	70	40
PpQDM-Ben	5%(PVP)	170	50	70	33
PpQDM-Ben	5%(PVP)	170	80	70	40
PpQDM-Ben	5%(PVP)	170	120	70	50
PpQDM-Ben	5%(PVP)	170	140	70	70

Figure 4.6 (c) indicates that the r_{33} varied simultaneously with the applied voltage and temperature then reached its maximum of 75 pm/V at the poling field of 70 V/μm. The EO signal increases slowly as temperature is raised. Such a value levelled off under the continuous poling field at 140 °C, resulting in poling efficiency of 1.07 $(nm/V)^2$, which is defined as the ratio of r_{33} and V_p.

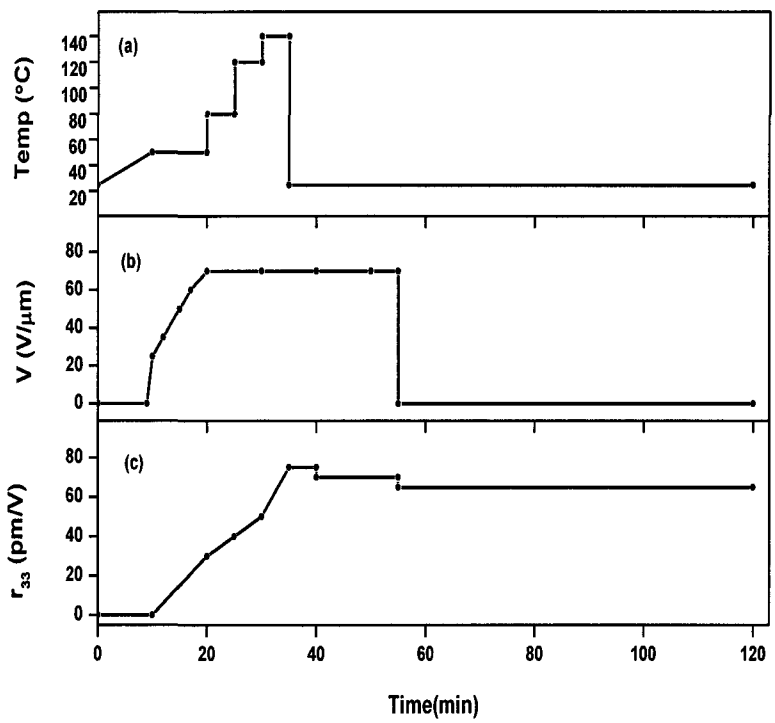

Figure 4.6. In situ poling process plot of 5% PpQDM-Ben/PVP NLO polymer film. (a) Poling temperature (b) Applied poling field (c) EO coefficient (r_{33}) value

The sample was then cooled to room temperature with the poling field maintained. During the rapid cooling process, there was a notable relaxation phenomenon of the molecular ordering as the total EO signal decreased by 13%. Eventually, r_{33} of 65-70 pm/V was realized at room temperature for the poled PpQDM-Ben/PVP guest-host film after removing the poling field. Poling efficiency of 1.0 $(nm/V)^2$ was estimated for PpQDM-Ben/PVP.

In situ measurement indicate that materials based on chromophore PpQDMs have larger EO coefficient compared with the FDCNs and PQDM chromophores, especially the chromophore PpQDM-Ben, which contains an additional large benzyl group in the donor part and a suitable shape which leads to a large r_{33} value. This value is the highest value obtained for chromophore PpQDMs in guest-host polymers. All the data indicated that the increased donor strength, and suitable shape of the chromophores could significantly increase their macroscopic EO activities.

4.3.4 EO Properties of PpQDM-Based Crosslinkable NLO Polyimides

According to the enhanced molecular hyperpolarizabilities for chromophores PpQDM-Met and PpQDM-Ben compared with PQDM, an improvement of macroscopic EO property for the PpQDM-based crosslinkable NLO polyimides is expected.

The synthesized NLO polyimides, **NPI-a** to **NPI-e** offer good processability, and optical quality thin films can be easily prepared by casting onto ITO glass from DMF solution. The polyimides give smooth and physically stable films with thicknesses ranging from 1.4 to 2.2 μm.

To avoid degradation of the NLO active chromophore during poling, an UV-Vis spectrophotometer was utilized to trace the chromophore in the polymer. Figure 4.7 shows the absorption characteristics of the NLO polyimides **NPI-d** film after thermal treatment at various temperatures for 30 min. A sharp decrease of the chromophore absorbance was observed when temperatures were higher than 160 °C. This indicates that NLO chromophore is capable of enduring thermal treatment under 160 °C.

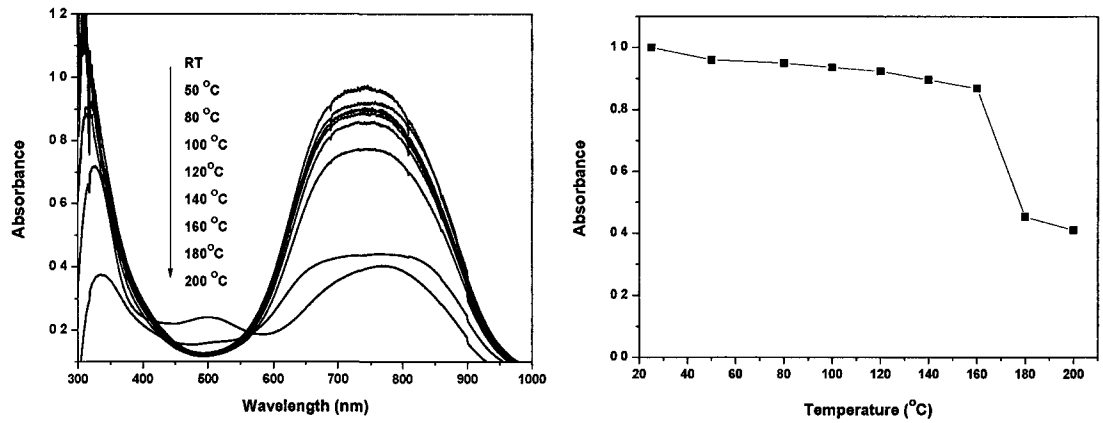

Figure 4.7. UV spectra (left) and thermal stability (right) of NLO polyimide **NPI-d** thin films.

To evaluate the EO activities of **NPI-d** and **NPI-e**, the polymer films were electric poled to induce noncentrosymmetric polar order. To avoid the damages of thermal treatment, electric discharge and the negative effect of crosslinking on the chromophore orientation, electric poling practically involves a process that begins at low temperatures over a long time. For example, **NPI-d** and **NPI-e** were initially held at 155 °C and 160 °C respectively for 20 min under a poling voltage around 70 V/μm. Electric poling ends with holding at higher temperatures above 170 °C for around 10 min while keeping the electric field to complete the crosslinking reaction. The EO coefficients of **NPI-d** and **NPI-e** were measured by the simple reflection technique at 1550 nm. **NPI-d** and **NPI-e** give 25 and 30 pm/V of r_{33} value, respectively (Table 4.6).

Table 4.6. Characterization of PpQDM-based crosslinkable NLO polyimide films

NLO polymer	PpQDM (wt %)	n (1.5 μm)	Film thickness (μm)	T_g (°C)	T_p (°C)	V_p (V/μm)	r_{33} (pm/V)
NPI-d	7.59	1.572	1.91	163	155	70	25
NPI-e	13.75	1.597	2.09	180	160	70	30

The higher density of chromophore in **NPI-e** did not lead to much higher r_{33} value compared to **NPI-d** with less chromophore, and also the lower EO coefficients of the crosslinkable NLO polyimides compared to PpQDM-Ben doped PVP obtained (r_{33} = 70 pm/V) is mainly due to the chromophore aggregations, as evident by their broader absorptions (See Chapter **3**).

Initially, the chromophores might tend to pack with each other to form dimeric aggregates at a relatively low temperature. When the poling temperature was increased, the aggregated chromophores partially dissociated. However, the poling temperature is close to the onset of the crosslinking temperature, partial crosslinking may have taken place, as evident that when the films were heated at 170 °C for 5 min, they could not be completely dissolved in DMF, which indicate that partial crosslinking occurred in the polymers. This makes it harder for the dissociation of the aggregated chromophores due to the limited mobility of chromophores especially in the high chromophore loading polymers. Moreover, lower poling temperature was applied due to the limitation of the thermal stability of the chromophores, leading to the lower poling efficiency.

In order to improve the poling efficiency of the PpQDM-based crosslinkable NLO polyimides, a conductive polymer, PEDOT: PSS thin film was investigated as the barrier layer for poling the NLO polymers.

In general, for practical optical guided-wave devices application, the NLO polymer layer usually needs to be sandwiched between two cladding layers. The basic requirements for these claddings are: 1) relatively low optical loss, 2) must have refractive indices that are less than that of the active guiding layer, 3) the resistance of the cladding should be significantly smaller than that of the active layer, to make the

poling voltage in the active layer is nearly equal to the external applied voltage, 4) should be compatible with the processing of the active EO layer. In addition, these cladding layers also act as buffer layers, delaying the onset of dielectric breakdown in the active layer.

The PEDOT: PSS thin film, with thickness around 500 nm on top of the ITO glass was selected due to its beneficial properties, such as much higher electrical conductivity and dielectric constant, excellent thin film processibility,[19] and the ability to smooth and pacify rough surfaces such as ITO, reducing charge localization.[20] To achieve highly transparent and conductive films, a blended system of PEDOT:PSS (Aldrich corporation) in polyvinylalcohol (PVA) was chosen. Solutions of 9 wt % PVA in water was prepared under 50 °C first. Then PEDOT: PSS and PVA solutions were mixed at weight ratios varying from 10:100 to 50:100. Solutions were filtered and spin coated onto ITO glass. The resulting films had uniform thickness of approximately 500 nm and exhibited good transparency. These samples were dried in a vacuum oven at 45 °C for 48 h.

Transmission was measured because the transparency of the materials used in EO application is critically important. The PEDOT: PSS/PVA films were found to have low absorption in the visible range of the spectrum and had an increased absorption in the infrared range from 1100 to 1500 nm. Figure 4.8 shows that there is a slight decrease in transmission with increasing PEDOT: PSS doping in the blended samples. However, lightly doped samples, 15 wt % of PEDOT: PSS/PVA had more than 90% transmission across the measured spectrum.

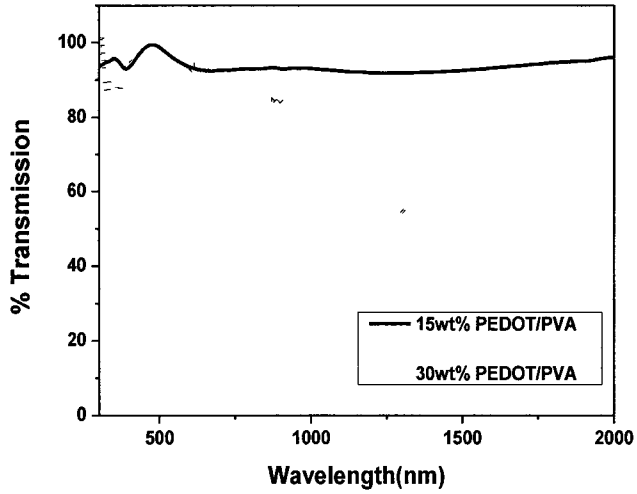

Figure 4.8. UV-Vis-NIR spectra showing optical transparency for PEDOT: PSS/PVA thin films (Thinkness: 500 nm).

Therefore, thin films containing 15 wt % PEDOT: PSS in PVA were prepared on ITO glass for testing as barrier layers for the poling of NLO polymers. Around 2 μm of PpQDM-based crosslinkable polyimides were casted on the top of PEDOT: PSS/PVA film as a second layer.

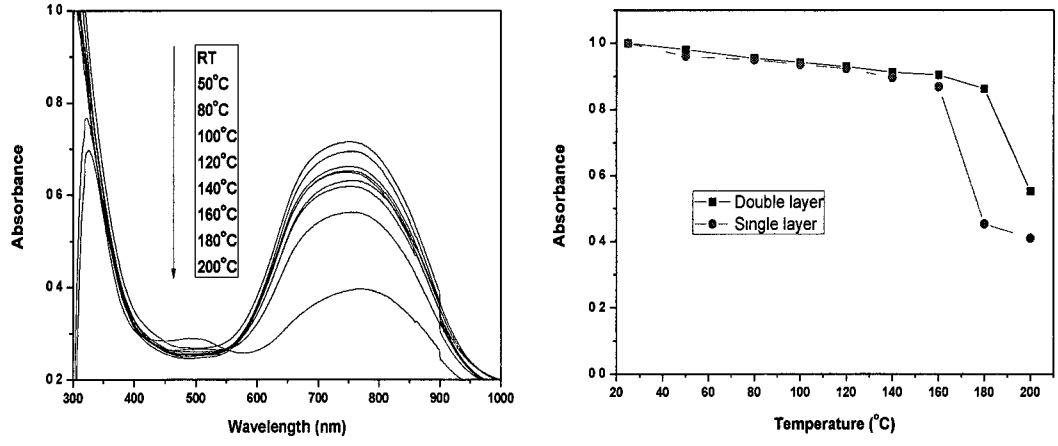

Figure 4.9. UV spectra of **NPI-d** double layer films (left); thermal stability comparison of the **NPI-d** in the single and double layer films (right).

Thermal stability of the chromophores in the double layer films was also tested by UV-Vis absorption. Figure 4.9 (left) shows the absorption characteristics of the **NPI-d** film after thermal treatment at various temperatures for 30 min. No sharp decrease of the chromophore absorbance was observed till the temperatures reach to 180 °C. This indicates that the NLO chromophores can endure higher temperatures compared with that in the single layer films (Figure 4.9 right).

For comparison, the double layer films were electric poled, the EO coefficients were measured by the simple reflection technique at 1550 nm as described as the single layer films and the results are summarized in Table 4.7.

Table 4.7. Characterization of PpQDM NLO polymer /PEDOT: PSS/PVA films

NLO polymer	PpQDM (wt %)	Film thickness (μm)	T_p (°C)	V_p (V/μm)	r_{33} (pm/V)
NPI-d	7.59	1.82	170	100	35
NPI-e	13.75	1.75	170	100	40

Up to 100 V/μm effective poling fields (defined as the total external applied voltage divided by the thickness of the NLO polymer layer only) were achieved across the NLO polymer layer of the double layer films, while the single layer films could not be poled above 70 V/μm without encountering dielectric breakdown. Thus, more than 40% increase in effective poling field could be achieved through the use of the PEDOT: PSS/PVA layers.

The r_{33} value of **NPI-d** and **NPI-e** are 35 and 40 pm/V, respectively. With the PEDOT:PSS buffer, the maximum achievable r_{33} values can be enhanced in ~ 30%

higher for both **NPI-d** and **NPI-e** NLO polyimides in the double layer films over that observed in the single layer films. The PEDOT: PSS layer which was labeled as conductive in this experiment is much more resistive than electrode such as ITO and gold. This provides a less conductive interface with the active layer than a direct interface with the ITO electrode. Thus the interfacial surface between the NLO polymer and this buffer layer is a relatively low conductivity surface, which diminishes the formation of charge avalanches and reduces the probability of dielectric breakdown.

4.4 Conclusions

EO properties of zwitterionic chromophores FDCN and PpQDM, and their corresponding NLO polymers, FDCN-MMA (**NA2**) and PpQDM-based crosslinkable polyimides have been studied. This work demonstrates that an effective way to reduce the formation of aggregates for FDCN chromophores is by adding a bulky aromatic group side chain perpendicular to the conjugated backbone of the molecule.

The optimum poling conditions for the PpQDM-Ben doped PVP system were studied according to the electrical properties of NLO chromophores and various factors such as polymer matrix, poling temperature and electric poling field. An excellent long-term stability of the induced EO activity of PpQDM-Ben/PVP at 80 ^{o}C was demonstrated.

In situ poling method was established to explore the intrinsic large EO properties of PpQDM series of chromophores. This dynamic EO measurement indicates that the PpQDM-Ben doped PVP NLO materials have the largest EO coefficient (60-70 pm/V). This result demonstrates that the presence of longer conjugation, stronger acceptor and bulky donor groups in PpQDM significantly enhanced CT interactions, leading to larger

μβ value than PQDM; also the PVP polymer host has a large enough dielectric constant which favors the dispersion of the polar zwitterionic chromophores.

The poling efficiency of high chromophore concentration crosslinkable NLO polyimides in this study is found to be very sensitive to both temperature and the actual applied field strength. Further modification for PpQDM to become more thermally stable in polymer host is critical to achieve higher poling efficiency.

In this work, a buffer layer (PEDOT: PSS/PVA) was successfully introduced into the double layer device for zwitterionic NLO polymers and improvement of the poling efficiency of NLO polymer systems was demonstrated. More than a 40% increase in effective poling field was achieved through the use of the buffer layers, also the r_{33} values were enhanced to ~ 30% higher for both **NPI-d** and **NPI-e** NLO polymers in the double layer films compared with that in the single layer films. The buffer layer provides a relatively low conductivity interface with the active NLO layer in comparison to a direct interface with the ITO electrode, which effectively reduces the probability of dielectric breakdown. By further careful selection of buffer materials, this additional layer will be used to more effectively block the excessive LTC and suppress the onset of dielectric breakdown to enhance the maximum applicable poling field.

4.5 Experimental Section

4.5.1 Materials

See Chapters **2** and **3** for the synthesis of zwitterionic chromophores and NLO polymers, respectively. PMMA, PVP, PVA and PEDOT: PSS 2.8 wt % dispersed in H_2O were purchased from Aldrich. PES (commercial trade name: Ultrason E, T_g = 225 ^oC)

was obtained from BASF. The $LiNbO_3$ wafer was purchased from Thorlabs, Inc. (New Jersey, USA) and used to calibrate the Teng-Man setup.

4.5.2 Thin Film Preparation for EO Study

Doping NLO chromophore FDCNs and PpQDMs into PES and PVP matrix materials in host-guest system with 1, 3 and 5 wt % chromphore contents; for the cast films, a 2 wt % DMF solution containing chromophore doped polymers or NLO polymers such as **NA2** polymers and crosslinkable NLO polyimides **NPI-d** to **NPI-e** was stirred overnight at room temperature in darkness. After the solution was filtered through a 0.2 μm syringe filter, it was casted onto ITO glass (2.56 cm^2) to produce films of about 1~3 μm thickness and baked at 45 °C overnight under the protection of nitrogen. The films were further baked in a vacuum oven overnight at 85 °C to remove the residual solvent. Then a thin gold layer with a thickness of 100-150 nm was sputtered or vacuum deposited on the films as the top electrode for electric poling.

4.5.3 General Methods

Refractive indices were measured using a Metricon 2010 prism coupler. An alpha-step 200 surface profiler was used for measuring the thin film thickness. EO coefficients of the poled samples were measured at the laser wavelength of 1550 nm using the simple reflection technique and a modified Teng-Man reflection method. The Teng-Man setup was calibrated with a commercial $LiNbO_3$ crystals (r_{33} = 31pm/V at 1550 nm) before use. For the UV-Vis, IR spectrometry, TGA and DSC methods refer to Chapter **2**.

4.5.4 Poling Process and EO Coefficient Measurement

Parallel Electrode Poling Station

The parallel electrode poling setup (Figure 4.1, right) is equipped with a hot plate, whose temperature is sensed by a thermocouple and controlled digitally (±1 °C), and a high voltage supply (0–3 kV) (Bertan Associates, INC. Model 215) (See Appendix C, Figure S4.1). All the components are assembled in a sealed box, through which an inert gas such as nitrogen can flow to remove the air for a high temperature poling. In order to lower the probability of electrical breakdown due to film defects, a half-dumbbell configuration of the gold electrode was made, which has a smaller area than a round disk (See Appendix C, Figure S4.2). During poling and EO measurements, the electrode contact is positioned at the small gold area (diameter d = 2 mm), while the incident light is directed at the big gold part (d = 6 mm). A resistor with impedance of 10^7 Ω is connected in series with the polymer circuit to regulate the poling current.

Teng-Man Setup

Several techniques are available to evaluate the EO coefficients of poled polymer films. These included attenuated total reflection (ATR), [21] simple reflection, [11a] transmission[22] techniques and so on. In this research work, the simple reflection technique established by Teng and Man was used (Figure 4.10). The principle of the Teng-Man setup is based on the relative phase shift difference between the *s*- and *p*-polarized waves of a single laser beam reflected from the sample when a modulating voltage is applied across two parallel plate electrodes.

The Teng-Man setup was equipped with a 1550 nm laser (ILX Lightwave LDC 3724B), a Soleil-Babinet compensator (Thorlabs Inc. SBC-IR), a Lock-in amplifier (Standford Research Systems SR830 DSP), a detector (Newport 1830-C), a frequency generator (AVTECH AV-151B-C), an oscilliscope (LeCory 9400A) and other optical components such as a polarizer and an analyzer (See Appendix C, Figure S4.3).

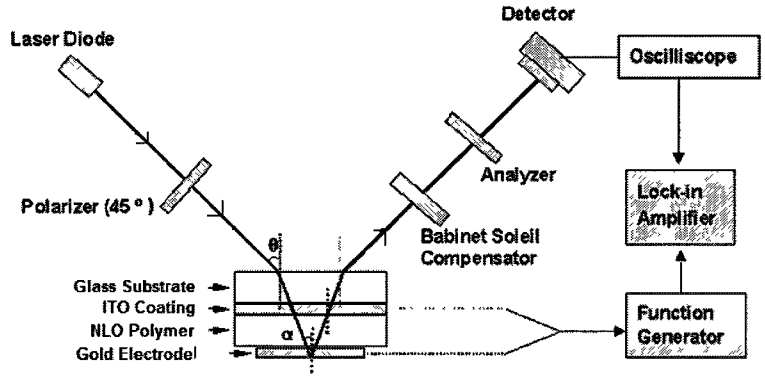

Figure 4.10. Schematic diagram of the simple reflective Teng-Man setup.

EO Coefficient Measurement

For general measurements of EO coefficient (r_{33}), the laser beam (1550 nm) travels through a polarizer, where the incident angle (θ) was set to be 20°, then passes through the transparent conducting ITO top electrode , and then the EO polymer thin film before being reflected by the bottom gold electrode. The reflected laser beam travels through a compensator and then an analyzer, which is cross-polarized with respect to the polarizer. The modulating voltage (V_m) is 48.5 V and the signal frequency is 1 KHz in this experiment. The signals are collected by a detector and then monitored with an oscilloscope and a lock-in amplifier. The intensity of modulated signal (I_m) and the half intensity of incident light (I_c) are recorded.

For *in situ* EO coefficient measurement, the sample film is mounted under an N_2 flow on a temperature-controlled heated stage with good thermal contact to apply the voltage combined of DC and AC components. An AC voltage was added to the DC voltage for the simultaneous poling and probing of the EO signal (I_m/I_c). In this measurement, r_{33} signals were collected during the process of heating or cooling in the presence of a poling field (See Appendix C, Figure S4.4).

4.6 References

(1) (a)Sekkat, Z.; Dumont, M. *Nonlinear Opt.* **1992**, *2*, 359. (b)Date, M.; Furukawa, T.; Yamaguchi, T. Kojima, A.; Shibata, I. *IEEE Trans Dielect. El. In.* **1989**, *24*, 537. (c)Charra, F.; Kajzar, F.; Nunzi, J. M.; Raimond, P.; Idiart, E. *Opt. Lett.* **1993**, *18*, 941. (d)Sprave, M.; Blum, R.; Eich, M. *Appl. Phys. Lett.* **1996**, *69*, 2962. (e) Burland, D. M.; Miller, R. D.; Walsh, C. A. *Chem. Rev.* **1994**, *94*, 31.

(2) Shutoa, Y.; Amano, M.; *J. Appl. Phys.* **1995**, *77*, 4632.

(3) (a)Luo, J. D.; Haller, M.; Li, H.; Tang, H.-Z.; Jen, A. K.-Y.; Jakka, K.; Chou, C.-H.; Shu, C.-F. *Macromolecules***2004**, *37*, 248. (b)Jen, A. K.-Y.; Liu, Y.; Zheng, L.; Liu, S.; Drost, K. J.; Zhang, Y.; Dalton, L. R. *Adv. Mater.***1999**, *11*, 452.

(4) (a)Robinson, B. H.; Dalton, R. L. *J. Phys. Chem.* 2000, *104*, 4785. (b)Dalton, L. *Adv. Polym. Sci.*2002,*158*,1.

(5) (a)Sprave, M.; Blum, R.; Eric, M. *Appl. Phys. Lett.* **1996**, *69*, 2962. (b)Chen, H.; Chen, B.; Huang, D.; Jin, D.; Luo, J. D.; Jen, A. K.-Y.; Dinu, R. *Appl. Phys. Lett.***2008**, *93*, 43507.

(6) Luo, J. D.; Huang, S.; Shi, Z.; Polishak, B. M.; Zhou, X-H.; Jen, A. K-Y. *Chem. Mater.***2011**, *23,544*.

(7) Blum, R.; Sprave, M.; Sablotny, J.; Eich, M. J. *Opt. Soc. Am. B* **1998**, *15*, 318.

(8) Drummond, J. P.; Clarson, S. J.; Zetts, J. S.; Hopkins, F. K. ; Carraci, S. *J. Appl. Phys. Lett.***1999**, *74,368*.

(9) Huang, S.; T.-D.; Luo, J. D.; Hau, S. K.; Shi, Z. W.; Zhou, X.-H.; Yip, H.-L.; Jen, A. K.-Y. *Appl. Phys. Lett.* **2010**,*96*,2433.

(10) Beaudin, A. M. R.; Song, N. H.; Bai, Y; Men, L.; Gao, J. P.; Wang, Z. Y.; Szablewski, M.; Cross, G.; Wenseleers, W. Campo, J.; Goovaerts, E. *Chem. Mater.* **2006,***18*,1079.

(11) Teng, C. C.; Man, H. T. *Appl. Phys. Lett.* **1990**, *56, 1734*. (b)Shuto, Y.; Amano, M. *J. Appl. Phys.* **1995**,*77*,4632.

(12) Robinson, B. H.; Dalton, R. L. *J. Appl. Phys. A* **2000**, *104*, 4785.

(13) Naiheng Song "Development of Zwitterinic Nonlinear Optical Polyimides for Electro-Optic Applications", *Ph. D. Thesis*, Carleton University **2004**.

(14) Zhang, C.; Dalton, L. R. *Chem. Mater.* **2001**,*13*,3043.

(15) Liakatas, I.; Cai, C.; Bosch, M.; Jager, M.; Bosshard, Ch.; Gunter, P.; Zhang, C.; Dalton, L. R. *Appl. Phys. Lett.* **2000**,*76*,1368.

(16) Cara Weir "Synthesis and Stability Studies of Z- -(1-Substituted-4-Pyridinium)-Cyano-4-Styryldicyano methanide Nonlinear Optical Chromophores", *M.Sc. Thesis*, Carleton University **2003.**

(17) (a)Tsai, H. C.; Yu, I. C.; Chang, P.H.; Yu, D. C.; Hsiue, G. H. *Macromol. Rapid Commun.* 2007,*28*,334. (b)Centore, R.; Riccio, P.; Fusco, S.; Carella, A.; Quatela, A.; Schutzmann, S. *J. Polym. Sci. Part A Polym. Chem.***2007**,*45*,2719.

(18) Dalton, L. R.; Sullivan, P. A.; Denise H. Bale, D. H. *Chem. Rev.* **2010,** *110,* 25.

(19) Drummond, J. P.; Clarson, S. J. *Appl. Phys. Lett.* **1999**, *74*, 368. (b) Grote, J. G.; Zetts, J. S.; Nelson, R. L.; Hopkins, F. K.; Dalton, L. R.; Zhang, C.; Steier, W. H. *Opt. Eng.***2001**, *40, 2464.*

(20) Carter, S. A.; Angelopoulos, M.; Karg, S.; Brock, P. J.; Scott, J. C. *Appl. Phys. Lett.* **1997**, *70, 2067.*

(21) Dentan, V.; Levy, Y.; Dumont, M.; Robin, P.; Chastaing, E. *Opt.Commun.***1989**, *69,*379.

(22) Ma, C. B.; Xu, D.; Ren, Q.; Lv, Z. H.; Yang, H. L.; Meng, F. Q.; Zhang, G. H.; Guo, S. Y.; Sang, L.X.; Wang, Z. G. *J. Mater. Sci. Lett.***2003**, *22*, 49.

Chapter 5 Applications of Zwitterionic Chromophores as Near Infrared Chemosensor

5.1 Introduction

The high sensitivity and abundance of fluorophores makes fluorescence one of the most promising tools for chemosensor development. Numerous chemical and biochemical analytes can be detected by fluorescence methods such as cations, [1] anions, neutral molecules and gases. [2] However, the selectivity of fluorescent chemosensors for metal ions remains a significant challenge; also there remains still a need for sensors, which operate and offer minimum perturbation to the microenvironment being probed. Moreover, there is potential for progress in the development of NIR fluorescent sensors for biochemical analytes such as amino acids, coenzymes and nucleotides.

Three series of functional NIR probes have been reported to detect cations over the past decades: Akkaya and Turkyilmaz [3a] developed a squaraine-based probe for calcium (Ca^{2+}), Akkaya and co-workers[3b] also developed a bis(2-pyridiyl)-substituted boratriazaindacene (AzaBODIPY)-based NIR fluorescent probe for mercury (Hg^{2+}), and a series of tricarbocyanine derivatives, synthesized by Kazuki Kiyose, [3c] were developed into a zinc (Zn^{2+}) probe that operates in the NIR region. To the best of our knowledge, no NIR probe has been reported to apply to the detection of both Fe^{2+} and Cu^{2+}.

PpQDMs are a new series of zwitterionic chromophores, in this thesis their basic photophysical properties were investigated in organic solvents of different polarity (Chapter **2**). It is known that these kinds of zwitterionic chromophores are sensitive to protons because of the static affinity between protons and the negative carbon center of

the chromophore. Therefore, it is predicted that these chromophores might also be sensitive to metal ions.

This chapter will focus on the influence of metal ions on the photophysical properties of PpQDM-Met and application of this chromophore/copper complex as a NIR fluorescent molecular probe for the selective detection of the amino acid- Cysteine.

Part of the work presented in this chapter was published: Hao, W.; McBride, A.; McBride, S.; Wang, Z. Y. "Colorimetric and near-infrared fluorescence turn-on molecular probe for selective detection of cysteine in human plasma", *J. Mater. Chem.* **2011**, *21*, 1040.

5.2 Influence of Metal ions on the Optical Properties of PpQDM-Met

The investigation of the photophysical properties of PpQDM-Met (**M1**) as a ligand in the presence of different metal ions has been of particular interest. Its capability to sense the presence of metal ions has been evaluated by monitoring spectrophotometrically the changes in both the absorbance and fluoresence intensity in DMF solution, with regard to potential applications as a NIR metal sensor. DMF was chosen as the solvent for all the measurements since it guarantees a good solubility of the metal salts, ligand used and the respective complexes. The behaviour of **M1** has been tested in the presence of different metal ions including Li^+, Na^+, K^+, Ag^+, Mg^{2+}, Ba^{2+}, Mn^{2+}, Fe^{2+}, Co^{2+}, Ni^{2+}, Cu^{2+}, Zn^{2+}, Pb^{2+}, Hg^{2+}, Fe^{3+}, Eu^{3+} and Er^{3+}.

The fluorescence of **M1** (2×10^{-5} M) is distinguished sensitive to the presence of $Fe^{2+}$and Cu^{2+}. For example, a strong decrease of the fluorescence is observed when 2×10^{-5} M of Fe^{2+} was added. Raising the concentration of the Fe^{2+} up to 20×10^{-5} M induces further decrease in the fluorescence up to 85% (Figure 5.1).

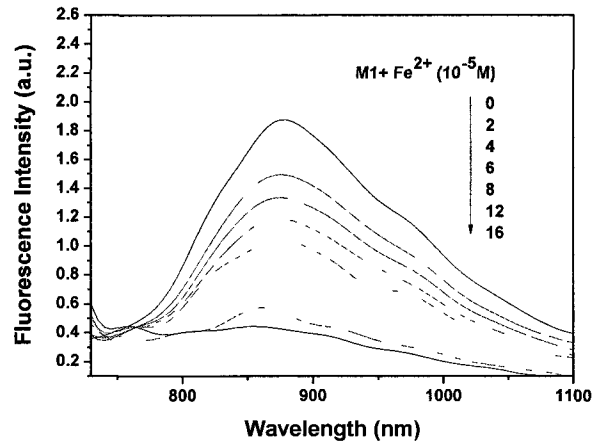

Figure 5.1. Fluorescence spectra of **M1** (2×10^{-5} M) in DMF at various concentrations of Fe^{2+}. The concentrations of Fe^{2+} are increasing from 0 to 1.6×10^{-4} M.

The UV-Vis spectrum of **M1** in DMF is characterized by a very intense band centered at 680 nm which is responsible for the blue color of the solution. The absorption at 680 nm decreased sharply with the gradual addition of Fe^{2+} to the solution of **M1**. A new absorption band centered at 480 nm increased prominently with an isosbestic point at 560 nm, characteristic of the **M1**-iron (II) complexation. Such a large blue-shift (200 nm) makes the color of the solution change from blue to brown-yellow (Figure 5.2).

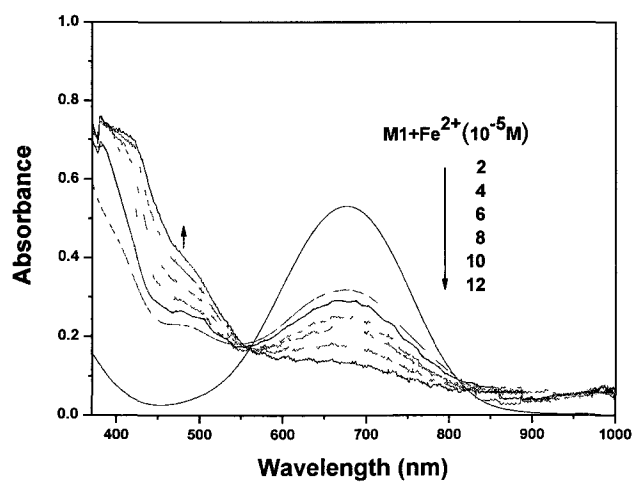

Figure 5.2. Changes in the UV-Vis spectra of **M1** (2×10^{-5} M in DMF) upon titration by $FeCl_2$ from 2×10^{-5} to 12×10^{-5} M.

The fluorescence spectra show that the nature of the metal ions determines the behavior of **M1** in the complex formation process. The dependence of the metal ions on the fluorescence quenching is presented in Figure 5.3.

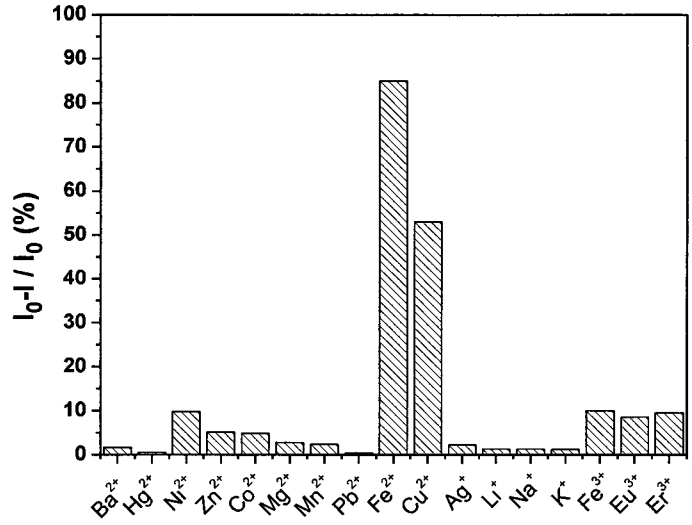

Figure 5.3. Fluorescence responses of **M1** (2×10^{-5} M) in the presence of different metal ions (2×10^{-4} M) in DMF solution. Excitation wavelength: 670 nm.

The fluorescence quenching factor (I_0-I/I_0) was determined from the ratio of maximum fluorescence intensity of **M1** before metal ion addition minus the fluorescence intensity after addition of metal ion divided by the maximum fluorescence intensity before addition. The highest fluorescence quenching effect was determined in the presence of Fe^{2+} and Cu^{2+} ions (85% and 53% at 2×10^{-4} M, respectively).

There was nearly no difference between the fluorescence intensity of **M1** in the presence and absence of alkali (Na^{+}, K^{+}) and alkaline earth metal ions (Ba^{2+}, Mg^{2+}). In the case of Ni^{2+}, Co^{2+}, Mn^{2+}, Zn^{2+}, Hg^{2+}, Fe^{3+}, Pb^{2+}, Ag^{+}, Li^{+}, Eu^{3+} and Er^{3+}, the changes in the fluorescence intensity was also negligible.

A possible explanation for this effect may be that the ICT process from the donor carbon atom on the negative carbon center to the acceptor bipyridium nitrogen was disturbed by Fe^{2+} and Cu^{2+} ions, due to the characteristics of these ions (ionic diameter, charge density, coordination number, hardness of metal ions, etc.). This would weaken the electron density of the negative carbon, causing a fluorescence quenching. The result showed clearly that only Fe^{2+} and Cu^{2+} ions were effectively detected.

It is known that most of the identified iron chelators exhibit demonstrably higher affinity for Fe^{3+} than Fe^{2+} in physiological conditions,[4] but selectivity for a particular metal valency cannot always be achievable by metal sensing probes. A commercially available fluorophore, Calcein, with an EDTA-like chelating moiety for metal ion binding, has been applied as turn-off sensor for Fe^{2+} ion; [5] a 46% decrease in Calcein fluorescence was observed upon addition of excess Fe^{2+}, whereas Fe^{3+} produces a 6% emission turn-off. Compared with Calcein, large difference between the fluorescence decrease around 90% for Fe^{2+} and only 7% for Fe^{3+} in **M1**, making **M1** a potentially useful NIR turn-off sensor for Fe^{2+} ion detection in biosystems. However, Fe (II) compounds are not stable in ambient conditions as they tend to be oxidized to Fe (III) compounds in air, preventing differentiation between these two oxidation states.

Therefore, the following research turned to focus on the formation of **M1** copper complex, then investigated whether the complex could offer some advantages in terms of affinity and selectivity, next attempted to employ the complex as metal-containing receptor for the detection of natural amino acids in the NIR region.

5.3 Binding Study of M1 with Cu^{2+}

Copper is third most abundant (after Fe^{3+} and Zn^{2+}) among the essential heavy metals in the human body and plays an important role in various physiologic processes.[6] In addition, copper is one of the major components of heavy metal pollution in the environment. It has been found in the range of 7.86×10^{-7} M in non-contaminated environmental samples and up to 62 mM in polluted samples.[7] The design and synthesis of chemosensors in NIR region for copper ions has become a very active area of research for more sensitive and selective chemosensors for in vitro and in vivo detection.[8]

The binding behaviour of **M1** with Cu^{2+} in a solution of DMF and methanol (99:1 v/v) was studied using spectroscopic methods. The UV-Vis absorption spectra of a set of solutions containing a constant concentration of **M1** (2×10^{-5} M) and different amounts of the copper ion were recorded at 25.0 ± 0.1 °C (Figure 5.4). Upon gradual addition of Cu^{2+}, the CT band of **M1** at 680 nm decreased dramatically which corresponds to a more intense cation complexation by the – C $(CN)_2$ moiety similar to the effect of protonation. A new absorption band centered at 435 nm (indicative of the d-d* transition of Cu^{2+} center)[9] increased noticeably with a tight isosbestic point at 500 nm, characteristic of the formation of the **M1-Cu** complex in DMF solution. A very intense band below 350 nm can be assigned to the metal ligand charge transfer (MLCT). A large spectral change (245 nm) between **M1** and **M1-Cu** complex or a sharp color change from blue to yellow is ideal for colorimetric detection.

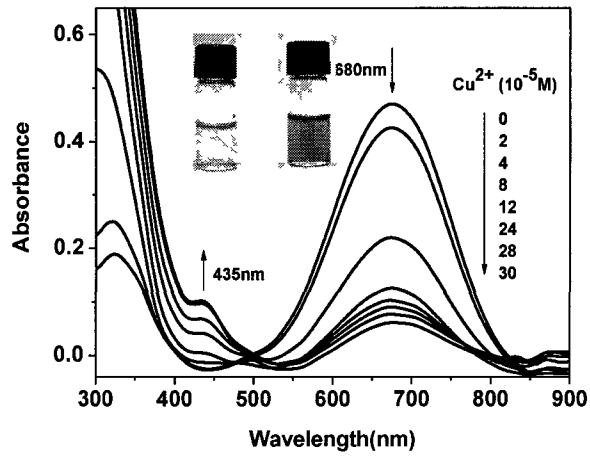

Figure 5.4. Changes in the absorption spectra of **M1** in DMF (2×10^{-5} M) upon addition of $CuCl_2$ (0 to 30×10^{-5} M).

The fluorescence of **M1** is also very sensitive to the presence of Cu^{2+}. The fluorescence of **M1** (2×10^{-5} M) was observed to decrease at a low concentration of Cu^{2+} (4×10^{-5} M) and leveled off when 12 equiv. of Cu^{2+} were added (Figure 5.5 left). A hypsochromic shift in the maximum emission wavelength from 875 nm to 850 nm ($\Delta\lambda_F$ = 25 nm) was observed upon addition of Cu^{2+}, along with significant fluorescence quenching.

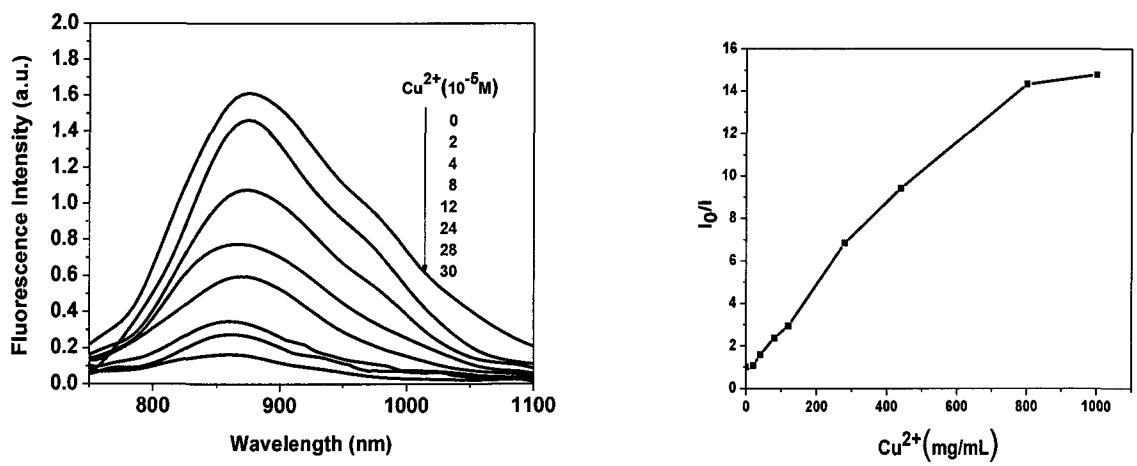

Figure 5.5. Changes in the fluorescence spectra of **M1** in DMF (2×10^{-5} M) upon addition of $CuCl_2$ (0 to 30×10^{-5} M).

The influence of other metal ions to the sensing of Cu^{2+} was also investigated. Figure 5.6 presents the fluorescence spectra of **M1** taken in the presence of metal ions (Ni^{2+}, Co^{2+}, Mn^{2+}, Zn^{2+}, Hg^{2+}, Fe^{3+}, Pb^{2+}, Ag^{+}, Li^{+}, Eu^{3+}, Er^{3+}, Sr^{2+} and Mg^{2+}) each at concentration of 2×10^{-5} M. The fluorescence intensity in this case is slightly lower than that of the solution free of metal ions. The addition of Cu^{2+} at concentration of 20×10^{-5} M to the same solution causes a dramatic decrease in fluorescence intensity. The data prove that other metal ions resulted in nearly no disturbance to the selective sensing of **M1** toward Cu^{2+} in the NIR region.

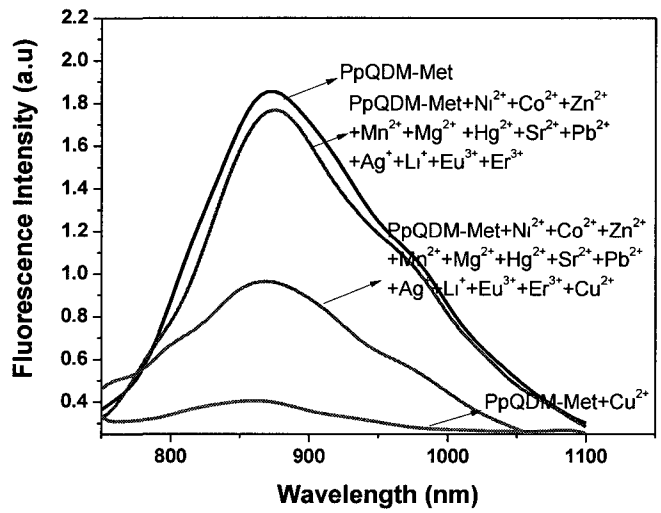

Figure 5.6. Fluorescence spectra of **M1** (2×10^{-5} M) in DMF at various metal ions.

5.4 Formation and Characterization of M1-Cu Complex

In order to confirm the formation of the **M1-Cu** complex found in the binding study of **M1** with Cu^{2+}, the **M1-Cu** complex was synthesized and characterized by UV, IR and MS methods.

The synthesis of **M1-Cu** complex was fairly straightforward and was done simply by mixing a DMF solution of **M1** with copper chloride in methanol (Figure 5.7). After

continuous stirring for 2 hours at room temperature, a yellow complex precipitated out from the solution gradually and was filtered and washed with ethanol and anhydrous ethyl ether. It was isolated as air-stable off-yellow powder in good yield. The complex could be re-dissolved in DMF, affording a yellow color solution with a maximum absorption at 435 nm (Appendix D, Figure S5.1) but no detectable PL in a range of 700-900 nm.

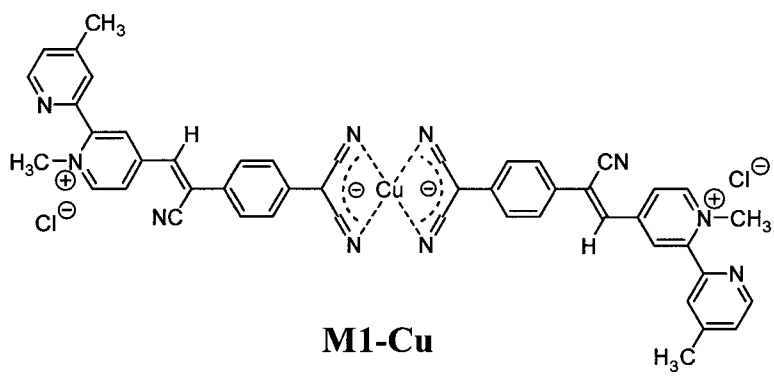

M1-Cu

Figure 5.7. Proposed structure of the **M1-Cu** complex.

The formation of the **M1-Cu** complex was confirmed by IR spectroscopy. In the IR spectrum of **M1-Cu**, only a single, relatively weak peak at 2017 cm^{-1} was observed compared with those two strong absorption peaks at 2173 and 2137 cm^{-1} in IR spectrum of **M1**[10] (Figure 5.8). The lower intensity of cyano groups in the complex is a consequence of the lower charge intensity on the negative carbon center, indicating charge delocalization through the two cyano groups and possibly onto the empty orbitals of the Cu^{2+} ion. The significant difference of the C≡N stretching vibration between the IR spectra of **M1** and **M1-Cu** complex strongly implies that the nitrogen of –CN groups in **M1** are involved in binding with the copper ion. The presence of only one C≡N stretching vibration at 2017 cm^{-1} in the isolated **M1-Cu** complex indicates identical

bonding of the two cyano groups to the copper in the complex and the relatively lower frequency of the cyano groups further confirms a strong binding with the copper ion.[11]

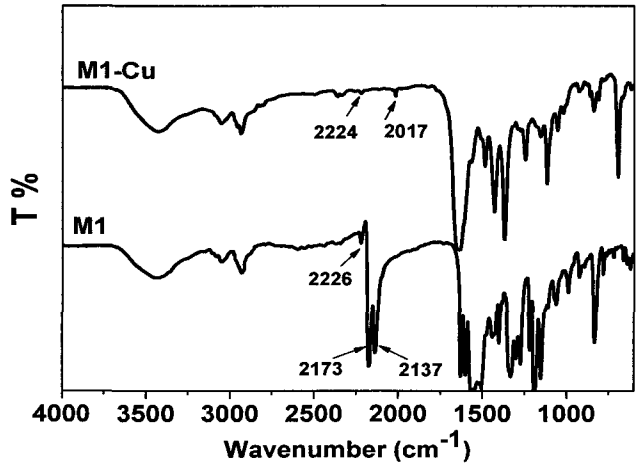

Figure 5.8. Baseline corrected IR spectra (4000-600 cm^{-1}) of **M1** and **M1-Cu**.

To determine the stoichiometry between **M1** and Cu^{2+}, time-of-flight electrospray ionization mass spectrometry (TOF-ESI-MS) was conducted on the isolated complex. In the ESI mass spectrum, a molecular ion peak at *m/z* 882.964 corresponding to a 2:1 complex $[2\mathbf{M1}+CuCl_2]^+$ (calculated value 883.182) was clearly observed (Appendix D, Figure S5.2). In addition, fragment peaks at *m/z* 375.042 (calculated value 375.15), 849.119 (calculated value 848.201), and 407.081 (calculated value 406.611) corresponding to $[\mathbf{M1}]^+$, $[2\mathbf{M1}+CuCl]^+$ and $[2\mathbf{M1}+Cu]^{2+}$ were also present, respectively. Therefore this result confirms the stoichiometry of **M1-Cu** complex to be 2:1.

5.5 Design of NIR Fluorescence Turn-On Molecular Probe for Cysteine Detection

Cysteine (Cys, Chart 5.1), a sulfur containing amino acid, facilitates crosslinking of bio-macromolecules through the formation of disulfide bonds in a biological system, which is important in both the structure and function of secondary order proteins.[12] A

deficiency of Cys is related to many medical conditions including slow growth, hair depigmentation, edema, liver damage, muscle and fat loss, hematopoiesis decrease, leucocyte loss, psoriasis and skin lesions.[13] Elevated levels of Cys are associated with neurotoxicity, which has been demonstrated in vivo in animals with immature blood-brain barriers and in cultured neurons in vitro. Cys-induced hypoglycemic brain damage has also been studied as an alternative mechanism to excitotoxicity.[14] In light of the important roles that Cys plays in a variety of fundamental physiological processes in organisms, there are considerable interests in detecting Cys in biological systems. [15]

The most common determination methods of Cys in human plasma and urine have been developed in conjugation with HPLC, capillary electrophoresis, and gas chromatography, followed by fluorescence or electrochemical detection, and often require time consuming sample separation and preparation.[16] Because Cys possesses a very low molar extinction coefficient and lacks a suitable chromophore, derivatization with fluorescent reagents are typically used for detection. Most of these fluorescent-labeling reagents contain a functional group, e.g., N-substituted maleimide, reactive halide or aziridine, which reacts with the thiol group in general, and thus are not specific to Cys.[17] Recent studies have focused on the development of direct fluorescent methods for detection of Cys and other biological thiols, aiming at high sensitivity, remote operation, and suitability as a fluorescent tag for labeling or as an imaging tool for diagnostics.[18] A fluorescent molecular probe for Cys and homocysteine (Hcy, Chart 5.2) was reported by the Strongin group, [19] which uses an aldehyde containing xanthene dye to form a thiazolidine by the reaction with N-terminal Cys and Hcy under alkaline conditions resulting in fluorescence quenching. Unlike fluorescence quenching,

fluorescence turn-on, either increase in fluorescence intensity or a new PL at a different wavelength, is typically more reliable and sensitive method for signaling in detection.[20]

To date, a few research groups have reported fluorescence turn-on sensors for Cys and Hcy. In 2004, Tanaka *et al* [21] used a fluorogenic aldehyde as a probe, which reacts with Cys to form a thiazolidine, resulting in an increase in fluorescence at a rather short wavelength of 380 nm. Recently, Huang's group has reported a 588 nm fluorescence turn-on probe based on the reaction of 8-oxo-8H-acenaphtho[1,2-b]pyrrole-9-carbonitrile with the thiol group in Cys and Hcy. [22]

Clearly, all the reported methods require the chemical reaction of the probing molecule with Cys under specific conditions to form a new product for detection by fluorescence in the visible region. However, the presence of Cys in biological systems and its distribution in cellular processes should ideally be detected quickly, selectively and directly, without any chemical derivatization, by a fluorescence turn-on signaling process in the NIR spectral region.

It is known that among many amino acids, Cys shows the strongest binding ability to Cu^{2+} over other metal ions, [23] which suggests its capacity to act as a powerful ligand over others in competitive complexation with Cu^{2+}. Therefore, a fluorescence turn-on probe can be conceptually recognized by the design of a non-florescent complex of Cu^{2+} and a fluorophore. This probe works simply by release of the fluorophore from its copper complex as a result of ligand exchange with Cys. In addition, the fluorophore should be ideally NIR fluorescent and forms a non-fluorescent copper complex with a relatively weaker binding constant than Cys.

Zwitterionic chromophore **M1** was found to be blue color and NIR fluorescent (875 nm). Due to the presence of the two cyano groups, binding to Cu^{2+} produced a non-fluorescent complex and resulted in an immediate color change from blue to brown-yellow. Thus, if Cys is able to replace the fluorophore in the copper complex, it should trigger a sharp turn-on signal of NIR fluorescence and a colorimetric signal due to the presence of released fluorophore (Scheme 5.1). Herein we describe the study of **M1-Cu** complex as a fluorescence turn-on probe for direct, fast, sensitive and selective detection of Cys.

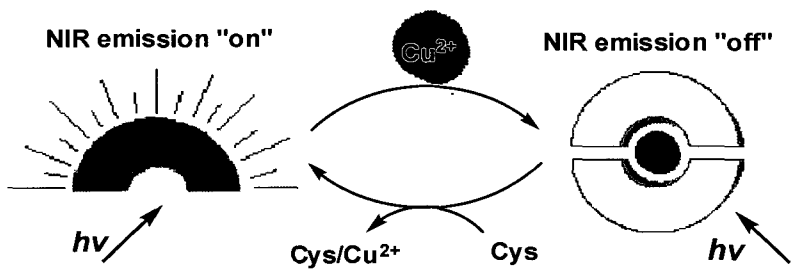

Scheme 5.1. Conceptual design of colorimetric and NIR fluorescence turn-on probe for detection of cysteine, based on the complexation and de-complexation of NIR fluorophore and copper ion.l

Based on the confirmed stoichiometry of a 2:1 (**M1**:Cu^{2+}) complex and the fluorescence titration data, the binding constant of **M1** with Cu^{2+} in DMF was calculated to be 4.44×10^8 M^{-1} (In experimental section). It is important for the **M1-Cu** complex to have an appropriate binding constant to work as a highly sensitive and selective probe for detection of Cys. Its binding constant should be ideally lower than that of Cys-Cu but higher than those of Cu^{2+} and many other amino acids and biologically important thiols.

5.6 Detection of Cysteine in Solution

High sensitivity of **M1-Cu** towards Cys was revealed by fluorescence spectroscopic titration experiments. Figure 5.9 displays the changes in NIR fluorescence of **M1** (as a control sample) and **M1-Cu** in DMF solution at different concentrations of Cys. The fluorescence intensity increases gradually with the increase of the Cys concentration from 0 to 20×10^{-5} M and has a decent signal-to-noise ratio. The release of **M1** (2×10^{-5} M) due to competitive binding of Cys with Cu^{2+} is evident by the fluorescence turn-on and the fluorescence recovery percentage (FRP), which is defined as the ratio ($I/I_0 \times 100$) of the maximum fluorescence intensity (I) after addition of Cys and the fluorescence intensity (I_0) of free dye **M1**, and correlates well to the concentration of Cys. At the Cys concentration of 4×10^{-5} M, the FRP of **M1** was 50%, which reached the maximum value of 89% when 20×10^{-5} M of Cys was added (Inset of Figure 5.9). A 25-nm bathochromic shift in the maximum emission wavelength from 850 nm to 875 nm was also observed upon addition of Cys, which suggested that nearly all **M1** was released from **M1-Cu**.

In order to calculate the detection limit (DL) of **M1-Cu** for Cys, the intensity values (Figure 5.9) were normalized between the minimum (without Cys) and the maximum intensity (20×10^{-5} M). The point at which the line fitting the six values (20×10^{-5} M-6×10^{-5} M) in Figure 5.10 crosses the horizontal ordinate axis is taken as the DL of **M1-Cu** for Cys, which is approximately 4.07×10^{-6} M (Appendix D).[24]

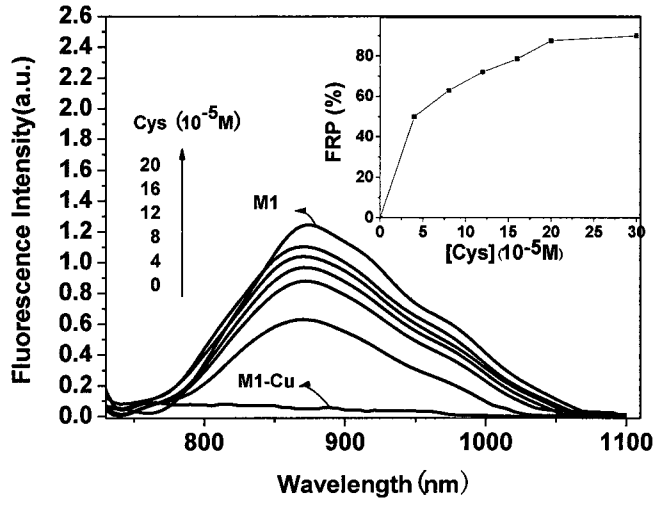

Figure 5.9. Fluorescence spectra of **M1-Cu** (**M1** = 2×10^{-5} M) upon addition of Cys (4×10^{-5} -20×10^{-5} M) in comparison with the fluorescence spectrum of **M1** (2×10^{-5} M). Excitation wavelength = 670 nm. Inset: FRP versus the concentration of Cys.

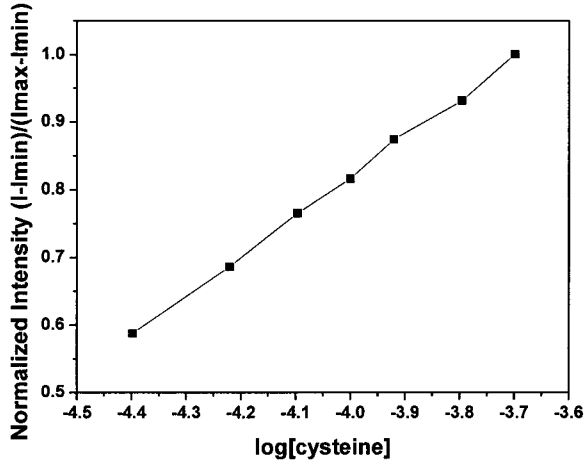

Figure 5.10. Fluorescence intensity of **M1-Cu** versus Cys concentration.

The **M1-Cu** response time vs. Cys concentrations is plotted in Figure 5.11. The response time is defined as the time required for the fluorescence signal to reach 90% of the saturation value after Cys is in contact with **M1-Cu.** As shown in Figure 5.11, the response time is as short as 10 s when **M1-Cu** is exposed to 20×10^{-5} M of Cys, which is,

to our knowledge, the fastest response of all the reported optical sensors for Cys.[20c,23b,25,26]

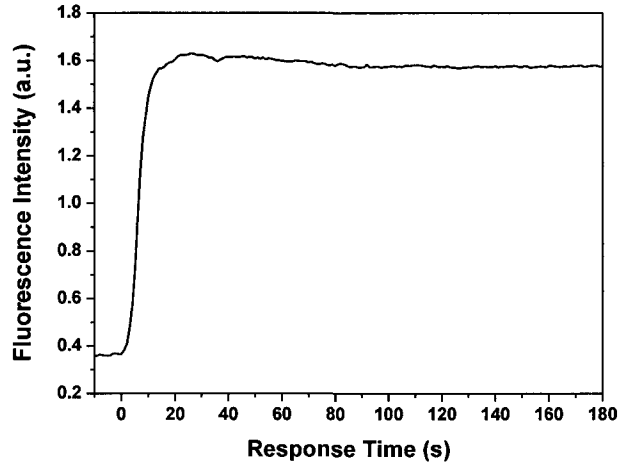

Figure 5.11. Response time measurement for a step change in Cys concentration from 0 to 20×10^{-5} M.

The absorption and color changes upon addition of Cys were monitored (Figure 5.12). The absorbance of **M1-Cu** at 435 nm decreased gradually while the band at 680 nm of **M1** reappeared with increase of Cys. Similar to the fluorescence experiment, the absorbance at 680 nm reached a maximum when 10 equiv. Cys was introduced. The color changed clearly from brown-yellow to blue and could be observed visually even at the concentration of Cys as low as 4×10^{-5} M.

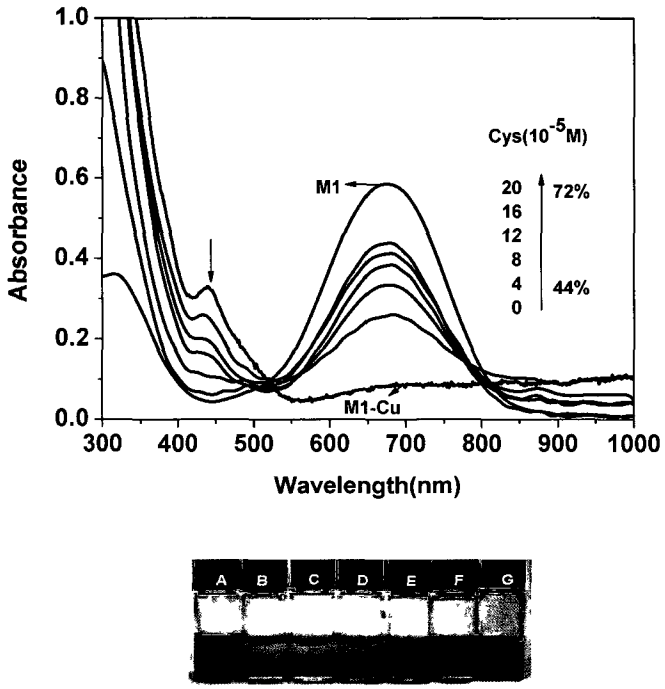

Figure 5.12. Changes in the absorption spectra of **M1-Cu** (**M1** = 2×10^{-5} M) upon addition of Cys (4×10^{-5} M to 20×10^{-5} M) in comparison with the spectrum of **M1** (2×10^{-5} M). Photographs of **M1** (A: 2×10^{-5} M), **M1-Cu** (B) and **M1-Cu** containing Cys (C: 4×10^{-5} M, D: 8×10^{-5} M, E: 12×10^{-5} M, F: 16×10^{-5} M and G: 20×10^{-5} M) in DMF, taken under daylight.

5.6.1 Selective Detection of Cys in the Presence of other Amino Acids

Selective detection of Cys in the presence of other amino acids was investigated. Possible interference from naturally occurring α-amino acids were first investigated by measuring the absorption and fluorescence spectra of solutions containing these α-amino acids (4×10^{-5} M) with and without Cys (3×10^{-5} M) (Figure 5.13). Among all the α-amino acids tested, histidine (His), glycine (Gly), serine (Ser), threonine (Thr), methionine (Met), proline (Pro), alanine (Ala), phenylalanine (Phe), arganine (Arg), lysine (Lys), aspargine (Asp), glutamine (Gln), leuine (Leu), isoleucine (Ile), tyrosine

(Tyr), glutamate (Glu) and valine (Val), Cys gave the highest response toward the **M1-Cu** probe.

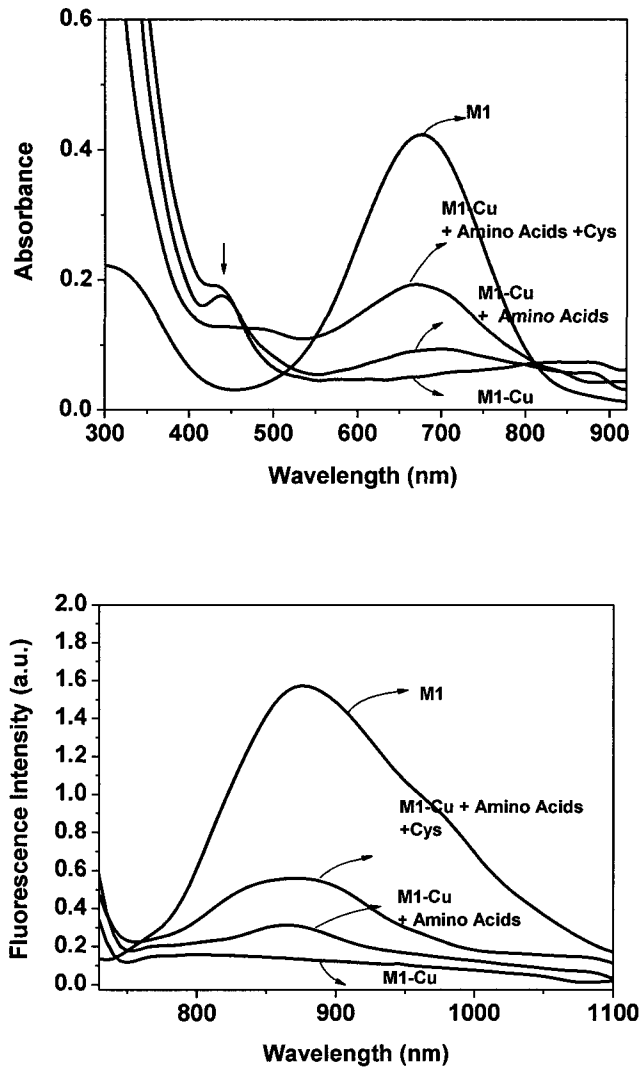

Figure 5.13. Changes in absorption (top) and fluorescence spectra (bottom) of **M1-Cu** (**M1** = 2×10^{-5} M) in DMF upon addition of α-amino acids (4×10^{-5} M) including His, Gly, Ser, Thr, Met, Pro, Ala, Phe, Arg, Lys, Asp, Gln, Leu, Ile, Tyr, Glu and Val, with Cys (3×10^{-5} M) or without Cys, in comparison with **M1** (2×10^{-5} M).

As shown by the NIR fluorescence changes (Figure 5.14 and Appendix D, Figure S5.3.1 to Figure S5.3.3), the FRP of **M1** was the highest at 65% for Cys at the

concentration as low as 4×10^{-5} M, 30% and 15% for His and Met, respectively, and below 10 % for the rest α-amino acids. The observed order of selectivity towards **M1-Cu**, Cys > His > Met > other amino acids, is consistent with a trend of ability of the different ligands in biomaterials (-S > -N > -O) that can bind to Cu^{2+}.[23] The high selectivity is likely due to co-operative effect of the thiol-amino-carboxylic acid moiety in Cys as a ligand to Cu^{2+}.[26]

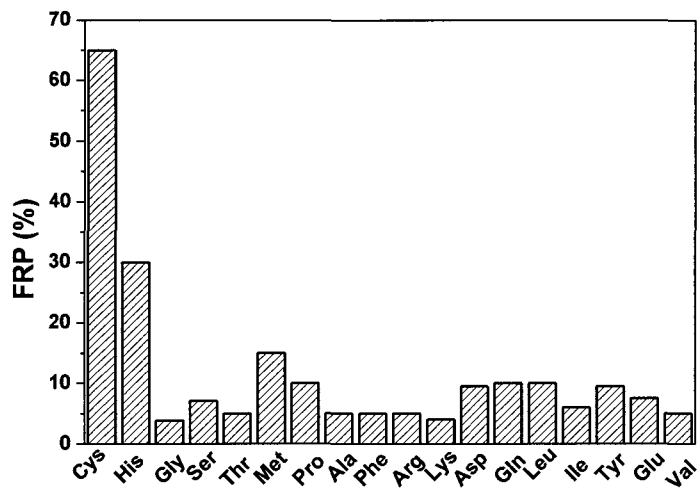

Figure 5.14. Fluorescence recovery percentage (FRP) of **M1-Cu** (**M1** = 2×10^{-5} M) towards various natural α-amino acids (4×10^{-5} M) (Excitation at 670 nm, emission at 875 nm).

A relatively stronger binding ability of Cys towards Cu^{2+} over **M1** in the probe of **M1-Cu** clearly contributes to high sensitivity in detection of Cys and is also responsible for good selectivity over other amino acids. According to the linear Benesi-Hildebrand expression,[27] the measured fluorescence intensity $[I_0/(I - I_0)]$ at 875 nm varied as a function of 1/[amino acid]^2 in a linear relationship, further confirming 2:1 stoichiometry between the amino acids and Cu^{2+} (Appendix D, Figure S5.4). The binding constants for

amino acids /Cu^{2+} interactions were then calculated and found to be in accordance with the observed selectivity trend (Table 5.1). The binding constant of Cys/Cu^{2+} (5.91×10^8 M^{-2}) is larger than that of **M1**/Cu^{2+} and those of other amino acids with Cu^{2+}. Therefore, **M1-Cu** just has an appropriate affinity relative to Cu^{2+} in comparison with Cys and other amino acids and is able to selectively discriminate Cys among other analogs.

Table 5.1. Binding constants of Cys and some amino acids with copper ion

Compound	Binding Constant (M^{-2})
M1	4.44×10^8
Cys	5.91×10^8
His	5.54×10^7
Met	2.63×10^7
Gly	8.01×10^5

5.6.2 Effect of Amines and other Biothiols

Since significant fluorescence changes occur only when Cys is present among other amino acids, the role of the -SH and -NH_2 in Cu^{2+} binding was further investigated by studying the fluorescence response of **M1-Cu** with some amines, (e.g., propylamine) and some sulfur-containing compounds such as L-Cystine, ethanethiol and ethyl sulfide (Chart 5.1) with or without the presence of Cys (4×10^{-5} M).

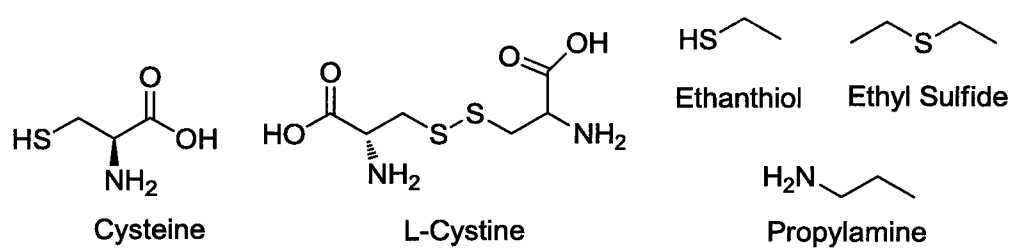

Chart 5.1. Structures of selected competitive chemicals.

Experimentally, Cys still triggered an insignificant fluorescence increase even when the above potential interfering agents were added in 40-fold higher concentration than Cys (Figure 5.15). As the precursor of Cys in biosystem, L-cystine does not show any interference in detection. Thus, this experiment clearly confirms that Cu^{2+} mainly interacts through the co-operative effect of the thiol-amino-carboxylic acid function of Cys, the single functional group such as $-NH_2$, -SH and -S-S- do not bind to Cu^{2+} effectively, which further explains the high selectivity of the **M1-Cu** probe towards Cys.

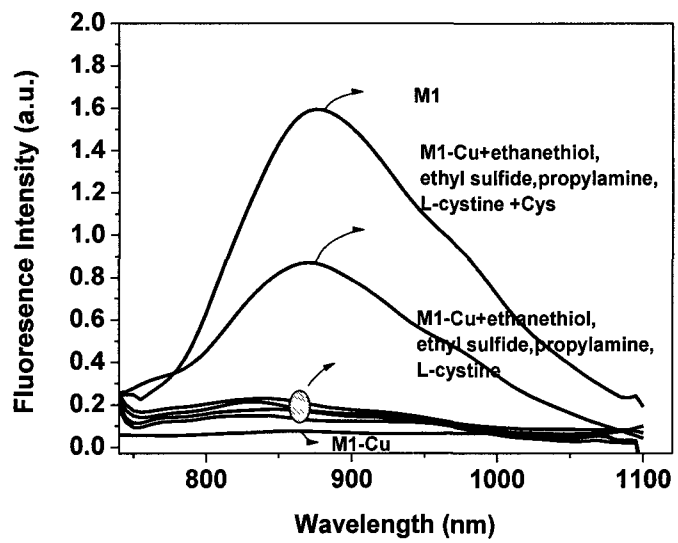

Figure 5.15. Changes in fluorescence spectra of **M1-Cu** (**M1** = 2×10^{-5} M) in DMF with various other chemicals including L-cystine, ethanethiol, ethyl sulfide and propylamine (4×10^{-5} M) with and without Cys (4×10^{-5} M) in comparison with the fluorescence spectrum of **M1** (2×10^{-5} M) in DMF.

5.7 Detection of Cysteine in Human Plasma

To further demonstrate the potential application of the **M1-Cu** complex in biological samples, the **M1-Cu** complex was further studied as a probe to detect Cys in human plasma. It was confirmed that a trace amount of Cys in human plasma can be

easily detected using **M1-Cu** by colorimetric, absorption and fluorescence methods. The changes of absorption spectra were observed upon adding human plasma samples spiked with Cys to **M1-Cu** solution and particularly the intensity of the peak at 680 nm for **M1** was monitored and compared with that of free **M1** (Figure 5.16) as a measure for detection limit. With 4×10^{-5} M of Cys present in human plasma, the peak at 680 nm increased to 40% intensity of **M1** (2×10^{-5} M); with 20×10^{-5} M of Cys, the intensity reached to 65% and at the same time the original blue color of **M1** appeared. The overall sensitivity of **M1-Cu** to Cys in human plasma was only 10% less than that of in water solution. Similarly, the fluorescence signals were turned on and the emission intensity at 875 nm increased with an increase of Cys in human plasma (Appendix D, Figure S5.5). The FRP value was found to be 75% when 20×10^{-5} M of Cys was present. Therefore, the detection limit of **M1-Cu** for Cys in human plasma is calculated to be 4.37×10^{-6} M (Appendix D, Figure S5.6).

In colorimetric experiments, human plasma samples containing Cys and other α-amino acids were tested using the **M1-Cu** probe. Visually, only the one containing Cys (4×10^{-5} M) in human plasma displayed a distinct blue color that is the same as the standard solution of **M1** (Photograph 5.1). The rest samples containing various amino acids remained the original light yellow color like **M1-Cu**. Therefore, Cys in human plasma as low as 4×10^{-5} M can be readily detected by colorimetric method using the **M1-Cu** probe.

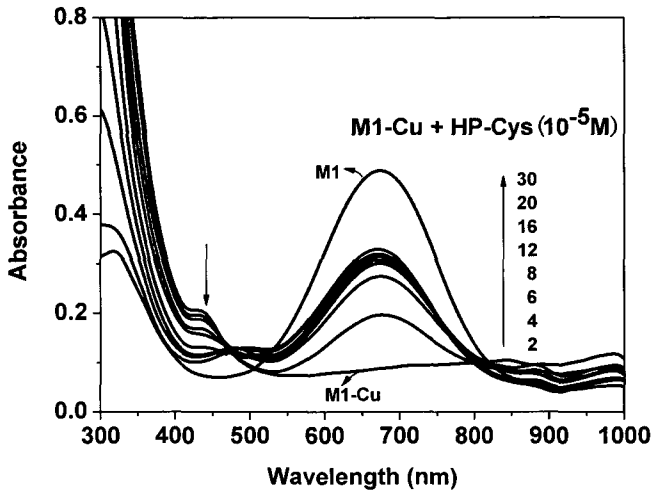

Figure 5.16. Changes in the absorption spectra of **M1-Cu** (**M1** = 2×10^{-5} M) upon addition of human plasma with Cys (HP-Cys) in concentrations of 2×10^{-5} M to 30×10^{-5} M in comparison with the absorption spectrum of **M1** (2×10^{-5} M).

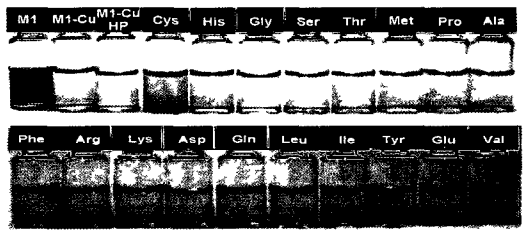

Photograph 5.1. Solutions of **M1** (2×10^{-5} M), **M1-Cu** (**M1** = 2×10^{-5} M), **M1-Cu** in human plasma (**M1-Cu** HP), and **M1-Cu** in human plasma samples containing Cys and various amino acids, taken under daylight. The concentration of each amino acid is fixed at 12×10^{-5} M.

Selective detection of Cys in human plasma with various α-amino acids was experimentally confirmed by titration of **M1-Cu** with human plasma solutions spiked with various amino acids with or without of Cys over a range of 0 to 30×10^{-5} M (Figure 5.17). The ratio of amino acids to Cys is varied and the concentrations of Cys in human plasma samples are also varied as 0 M (HPAA), 10×10^{-5} M (HP21), 15×10^{-5} M (HP11), 20×10^{-5} M (HP12) and 25.8×10^{-5} M (HP13). There was a negligible change in

both absorption and fluorescence spectra when human plasma with other amino acids (HPAA, 30×10^{-5} M) without Cys was added to **M1-Cu** in DMF solution. For the sample of HP21, there was a small change in both absorbance and fluorescence emission. As the concentration of Cys increases, both absorbance and fluorescence were further enhanced. The FRP of **M1** with HP13 sample (25.8×10^{-5} M of Cys) was higher than that standard sample of human plasma containing only Cys (20×10^{-5} M) (Figure 5.17, Right). Therefore, this probe can be used to selectively detect Cys in relatively more complex native human plasma.

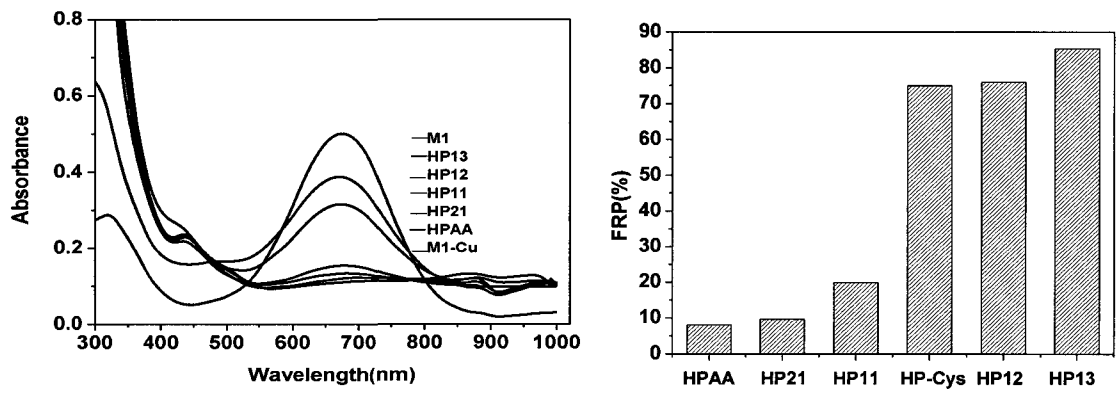

Figure 5.17. Left: UV-Vis absorption spectra of **M1** (2×10^{-5} M), **M1-Cu** (**M1** = 2×10^{-5} M) and the titration of **M1-Cu** with deproteinized plasma solutions spiked with various amino acids with or without of Cys. Total amino acids concentration is fixed at 30×10^{-5} M. The ratio of amino acids to Cys is varied in plasma samples: HPAA = human plasma with amino acids (His, Gly, Ala, Val, Ile, Pro, Met, Asp, Ser, Phe, Thr, Glu, Lys, Arg, Gln, Leu and Tyr) (30×10^{-5} M) without Cys; HP21 = 2:1 (Cys =10×10^{-5} M), HP11 = 1:1 (Cys = 15×10^{-5} M), HP12 = 1:2 (Cys = 20×10^{-5} M), and HP13 = 1:3 (Cys = 25.8×10^{-5} M). Right: Fluorescence recovery percentage at 875 nm (excitation at 670 nm) of the **M1-Cu** probe (**M1** = 2×10^{-5} M) with the above deproteinized plasma solutions HPAA, HP21, HP11 and HP13. The concentration of Cys in human plasma for the control sample of HP-Cys is 20×10^{-5} M.

Finally, detection of Cys among other biologically important thiol compounds, such as Hcy, L-glutathione (GSH) and N-acetylcysteine (N-Acys) was studied (Chart 5.2). Cys can be obtained as the final product of the transsulfuration pathway through Hcy metabolism. Hcy is a risk factor for disorders including cardiovascular[28] and Alzheimer's disease.[29] Unlike Hcy, the relatively more common biological thiols, GSH is widely distributed in animal tissues and plasma, which plays essential roles in the maintenance of the integrity of thiol moieties of protein and other compounds, is typically associated with beneficial antioxidant activity.[30]

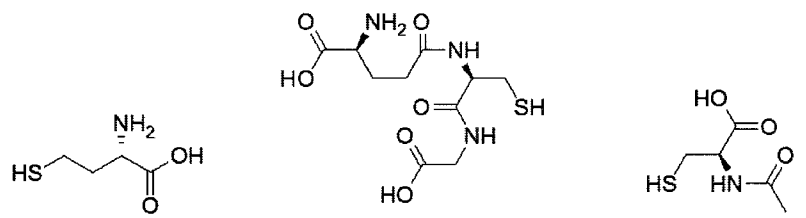

Chart 5.2. Structures of selected bioactive thiols.

Therefore, it is of interest to exam the sensitivity and selectivity of the **M1-Cu** probe for detection of Cys, Hcy, N-Acys and GSH. Comparative fluorescence studies of Cys and bioactive thiols at a concentration level of 4×10^{-5} M indicated a relative sensitivity for detection with **M1-Cu** in the following order: Cys > GSH > Hcy > N-Acys (Appendix D, Figure S5.7). Without the active amino group, N-Acys is the most inert towards the probe among the four biothiols. It is known that in healthy human plasma the total Hcy concentration is less than ca. 12-15 μM, and Cys concentration is typically 20-30 times that of Hcy[19] and 10 times that of GSH.[30] Since the **M1-Cu** probe can selectively monitor Cys in a range of 10^{-4}-10^{-5} M, Hcy only becomes detectable by the same probe when its concentration reaches a dangerous level of 1.3×10^{-4} M.[19b] Therefore,

the **M1-Cu** probe is potentially useful for sensitive and selective detection of Cys in biological system.

5.8 Conclusions

A new zwitterionic NIR fluorophore, **M1** has been synthesized and investigated. The influence of metal ions (Cu^{2+}, Fe^{2+}, Ni^{2+}, Co^{2+}, Mn^{2+}, Zn^{2+}, Hg^{2+}, Fe^{3+}, Pb^{2+}, Ag^{+}, Li^{+}, Eu^{3+}, Er^{3+}, Mg^{2+} and Sr^{2+}) on the fluorescence intensity has been studied to test the capacities of **M1** as both a NIR fluorescence and a naked eye sensor for these ions in the environment. The data obtained shows that the new **M1** is capable of detecting selectively Cu^{2+} and Fe^{2+} ions in DMF solution. The detection is based on both colorimetric detection and the quenching of ICT processes in the **M1** fluorophore.

A rational strategy for the development of a zwitterionic-metal dependent optical sensing material was demonstrated. The unique ability of **M1** to form a copper complex has led to the design and development of the first colorimetric and NIR fluorescence turn-on molecular probe, **M1-Cu**, for sensitive and selective detection of Cys in human plasma, in the presence of various amino acids and biologically active thiol compounds. The **M1-Cu** probe offers high-contrast colorimetric and unique NIR fluorescence turn-on methods for Cys detection with a detection range of 10^{-5}-10^{-4} M within a normal physiological level.

5.9 Experimental Section

Materials. All organic solvents were of spectroscopy grade and used without further purification. Salts of metals were purchased from Aldrich Chemical Co., The British Drug House LTD., Bioshop Canada Inc. including anhydrous copper (II) chloride, nickel

(II) chloride hexahydrate , cobalt (II) acetate tetrahydrate, manganese (II) acetate, zinc nitrate, mercuric chloride, iron (II) chloride tetrahydrate, iron (III) chloride, lead (II) acetate trihydrate, barium acetate, magnesium sulfate , silver nitrate, lithium bromide , sodium chloride, potassium chloride, europium chloride and Erbium chloride. Amino acids, L-cystine, propylamine, ethanethiol, ethyl sulfide and other chemicals were purchased from Aldrich Chemical Canada. Pooled human plasma (sodium citrate as an anticoagulant) was purchased from Bioreclamation Inc. (U.S.A.) and was stored at -20°C until analysis. Distilled water was used in all experiments.

Methods. The UV-Vis absorbance spectrophotometric investigation was performed on a Perkin-Elmer Lambda 900 UV-Vis-NIR spectrometer. Fluorescence emission spectra were measured on a PTI fluorescence system. The absorption and fluorescence emission spectra of all the samples were taken in DMF/MeOH solution in a quartz cuvette with a path length of 10.0 mm.

Fluorescence and UV-Vis absorption titration of M1 with Cu^{2+}. A solution of **M1** (2×10^{-5} M) in DMF and a solution of $CuCl_2$ (2×10^{-1} M) in MeOH were prepared and used for all of the following experiments. The titration was carried out by sequentially adding 1 μL of aliquots of Cu^{2+} solution to 10 mL of the **M1** solution. The solutions of **M1** with Cu^{2+} were stirred for 1 minute and were placed in a quartz cuvette. The absorption and fluorescence spectra were recorded at room temperature each time (excitation wavelength = 670 nm).

Determination of binding constant of M1-Cu^{2+}. To determine the binding strengths of the **M1-Cu** complex, a series of the **M1** solutions at a fixed concentration were mixed with the Cu^{2+} solutions at various concentrations. Absorbance of the resultant mixtures at

680 nm was measured. Fluorescence emission intensity of the resultant mixtures at 875 nm was measured. All measurements were carried out in DMF: Methanol = 99:1 (v/v). Same conditions are used for all of the fluorescence emission intensity measurement. The binding constant of the **M1** with Cu^{2+} was calculated according to the B-H equation for spectrofluorometric titration.

Selectivity of M1-Cu to Cys Measurements. The concentration of **M1** in **M1-Cu** is 2×10^{-5} M. Amino acids were added in portions (2-35 μL) to 10 mL of **M1-Cu** solution. The fluorescence intensity changes were recorded at room temperature each time. Amino acids (2×10^{-1} M in water) used in experiments are Cys, His, Gly, Ala, Val, Ile, Pro, Met, Asp, Ser, Phe, Thr, Glu, Lys, Arg, Gln. Leu (8×10^{-2} M) and Tyr (8×10^{-3} M) were used.

Response Time Measurement. The response characteristic of **M1-Cu** probe was measured in DMF: Methanol = 99:1 (v/v) solution, concentration of **M1** in **M1-Cu** was 2×10^{-5} M. After addition of 20×10^{-5} M of Cys, the fluorescent signal was monitored.

Determination of Cu^{2+}-amino acid binding constant. For the determination of binding strengths of the various Cu^{2+}-amino acid adducts, a series of **M1-Cu** complex solutions at a fixed concentration were mixed with the amino acid solutions at various concentrations. Absorption of the resultant mixtures at 680 nm and fluorescence intensity of the resultant mixtures at 875 nm were measured.

Binding constants of Cu^{2+} with amino acids using the Benesi-Hilderbrand method. Binding constants, K_B, were estimated from the ratio between the *y*-intercept and the slope of the linear line of best fit. The 1:2 donor-acceptor interactions were analyzed according to the B-H equation for spectrofluorometric titration (eq.1).

$$\frac{I_0}{I-I_0}=\left(\frac{c}{d-c}\right)^2\left(\frac{1}{K_B[substrate]^2}+1\right) \quad \text{(eq. 1)}$$

where I_0 and I are luminescence intensity of **M1-Cu** at 875 nm, in the absence and presence of amino acids, respectively; c, d are constants. [substrate] is the concentration of the titrants (various amino acids). Binding constant calculation for representative amino acids were shown in Appendix D, Figure S5.4.

Preparation of Human Plasma Samples. Pooled human plasma was thawed and deproteinized by adding 3 mL of acetone to 1 mL of plasma sample. After vortex-mixing for 10 s, the mixture was centrifuged at 10,000 rpm for 5 min (Mikro 22R refrigerated centrifuge, Hettich, Germany) to precipitate protein, and the supernatants obtained were concentrated by evaporation to ca. 1/3 of the total volume under nitrogen flow. A human plasma with Cys solution (1×10^{-1} M) was prepared by doping 1 mL of Cys (2×10^{-1} M in distilled water) into 1 mL of the deproteinized human plasma.

Absorption and Fluorescence Titration of M1-Cu with Cys in Human Plasma Samples. A solution of $CuCl_2$ in methanol (40 μL, 2×10^{-1} M) was added to 10 mL of **M1** solution (2×10^{-5} M) to form **M1-Cu** and quench the fluorescence. The **M1** and **M1-Cu** solution were placed in a quartz cuvette, respectively. Both the fluorescence and absorption spectra were then recorded. The solution of human plasma with Cys was introduced in portions (2-35 μL) to 10 mL of **M1-Cu** (**M1** = 2×10^{-5} M) in DMF and the intensity changes in absorption and the fluorescence spectra were recorded 1 min after Cys addition at room temperature .

Preparation of solutions of L-cystine, propylamine, ethanethiol, ethyl sulfide, homocysteine, L-glutathione and N-acetylcysteine. 5 mmol of each compound was dissolved in distilled water (25.0 mL) to afford a 2×10^{-1} M aqueous solution, except for L-cystine (2×10^{-3} M).

Flourescence titration of M1-Cu with L-cystine, propylamine, ethanethiol and ethyl sufide. The solution of Cu^{2+} (2×10^{-1} M, 40 μL) was added to 10 mL of **M1** (2×10^{-5} M in DMF) solution to quench the fluorescence. The solutions of L-cystine, propylamine, ethanethiol or ethyl sulfide were introduced to the above **M1-Cu** solution in portions up to 40 equiv. of Cys (2×10^{-1} M) and the fluorescence intensity changes were recorded at room temperature each time.

5.10 References

(1) (a)Kramer, R. *Angew. Chem., Int. Ed.* **1998**, *37*, 772. (b)*Chemosensors of Ion and Molecule Recognition*; Desvergne, J. P., Czarnik, A. W., Eds.; NATO ASI Series; Kluwer Academic Publishers: Dordrecht, 1997. (c)De Silva, A. P.; Nimal Gunaratne, H. O.; Gunnlaugusson, T.; Huxley, A. J. M.; McCoy, C. P.; Rademacher, J. T.; Rice, T. E. *Chem. Rev.* **1997**, *97*, 1515. (d)*Topics in Fluorescence Spectroscopy*; Lakowicz, J. R., Ed.; Plenum Press: New York, 1994.

(2) (a)Lakowicz, J. R. *Principle of Fluorescence Spectroscopy*, Kluwer Academic / Plenum Publishers: New York, 1999. (b)*Fluorescent Chemosensors for Ion and Molecule Recognition*; Czarnik, A. W., Ed.; ACS Symposium Series 538, American Chemical Society: Washington, DC, 1993.

(3) (a)Akkaya, E. U.; Turkyilmaz, S. Tetrahedron Lett. **1997**, *38*, 4513. (b)Coskun, A.; Yilmaz, M. D.; Akkaya, E. U. *Org. Lett.* **2007**, *9*, 607. (c) Kiyose, K.; Kojima, H.; Urano, Y.; Nagano, T. *J. Am. Chem. Soc.* **2006**, *128*, 6548.

(4) Esposito, B. P.; Breuer, W.; Cabantchik, Z. I. *Biochemical Society Transactions* **2002**, *30*, 729.

(5) Breuer, W.; Epsztejn, S.; Milgram P.; Cabantchik, Z. I. *Am. J. Physiol. Cell Physiol.* **1995**, *268*, C1354.

(6) Zheng, Y.; Huo, Q.; Kele, P.; Andreopoulos, F. M.; Pham, S. M.; Leblanc, R. M. *Org. Lett.* **2001**, *3*, 3277.

(7) Bush, A. I. *Curr. Opin. Chem. Biol.* **2000**, *4*, 184.

(8) (a)Bhattacharya, S.; Thomas, M. *Tetrahedron Lett.* **2000**, *41*, 10313. (b)Torrado, A.; Walkup, G. K.; Imperiali, B. *J. Am. Chem. Soc.* **1998**, *120*, 609. (c)DeSantis, G.; Fabbrizzi, L.; Licchelli, M.; Mangano, C.; Sacchi, D.; Sardone, N. *Inorg. Chim. Acta* **1997**, *257*, 69.

(9) (a)Solomon, E. I.; Penfield, K. W.; Wilcox, D. E.; *Structure Bonding*; Springer-Verlag: New York, 1993. (b)Wallace, K. J.; Cordero, S. R.; Tan, C. P.; Lynch, V. M.; Anslyn, E.V. *Sens. Actuators B* **2007,** *120*, 362.

(10) (a)Bai, Y. W.; Song, N. H; Gao, J. P.; Sun, X; Wang, X. M.; Yu, G. M.; Wang, Z. Y. *J. Am. Chem. Soc.* **2005**, *127*, 2060. (b)Ashwell, G. J. *Thin Solid Films* **1990**,

186, 155. (c) Bell, N. A.; Broughton, R. A.; Brooks, J. S.; Jones, T. A.; Thorpe, S. C.; Ashwell, G. J. *J. Chem. Soc., Chem.Commun.* **1990**, 325.

(11) Chow, C. F.; Lam, M. H.W.; Wong, W. Y. *Inorg. Chem.* **2004**, *43*, 8387.

(12) Voet, D.; Voet, J. G. *Biochemistry*, 2nd ed.; John Wiley & Sons: New York, 1995.

(13) Shahrokhian, S. *Anal. Chem.* **2001**, *73*, 5972.

(14) (a)Klingman, J. G.; Choi, D. W. *Neurology* **1989**, *39*, 397. (b)Janaky, R.; Varga, V.; Hermann, A.; Saransaari, P.; Oja, S. S. *Neurochem. Res.* **2000**, *25*, 1397. (c) Gazit, V.; Coleman, R.; Weizman, A.; Katz, Y. *Amino Acids* **2004**, *26*, 163.

(15) (a)Vandeberg, P.; Johnson, D. C. *Anal. Chem.* **1993**, *65*, 2713. (b)Pelletier, S.; Lucy, C. A. *Analyst* **2004**, *129*, 710. (c)Sudeep, P. K.; Shibu Joseph, S. T.; Thomas, G. K. *J. Am. Chem. Soc.* **2005**, *127,* 6516. (d)Andrabi, S. M. Z.; Khan, Z. *Colloid Polym. Sci.* **2007**, *285*, 389. (e)Prasad, K.S.; Muthuraman, G.; Zen, J. M. *Electroanalysis* **2008**, *20*, 1167.

(16) (a)Nekrassova, O.; Lawrence, N. S.; Compton, R. G. *Talanta* **2003**, *60*, 1085. (b) Bai, Y. H.; Xu, J. J.; Chen, H. Y. *Biosensors and Bioelectronics* **2009**, *24*, 2985. (c) Li, S.; Dong, S. J. *Biosensors and Bioelectronics* **2009**, *24*, 1569. (d)Pastore, A.; Massoud, R.; Motti, C.; Russo, A.; Fucci, G.; Cortese, C.; Federici, G. *Clin. Chem.***1998**, *44*, 825.(e)Refsum, H.; Smith, A.D.; Ueland, P. M.; Nexo, E.; Clarke, R.; McPartlin, J.; Johnston, C.; Engbaek, F.; Schneede, J.; McPartlin, C.; Scott, J. M. *Clin. Chem.* **2004**, *50, 3.*

(17) (a)Chwatko, G.; Bald, E. *Talanta* **2000**, *52*, 509. (b)Shimada, K; Mitamura, K. *J. Chromatogr. B* **1994**, *659*, 227. (c)Pastore, A.; Massound, R.; Motti, C.; Russo, A. L.; Fucci, G.; Cortese, C.; Federici, G. *Clin. Chem.* **1998,** *44*, 825. (d)Winters, R. A.; Zukowski, J.; Ercal, N.; Matthews, R. H.; Spitz, D. R. *Anal. Biochem.* **1995**, *227*, 14. (e) Haugland, R. P. *Handbook of Fluorescent Probes and Research Products*, 9th ed.; Molecular Probes: Eugene, OR. 2002.

(18) (a)Chen, S. J.; Chang, H. T. *Anal. Chem.* **2004**, *76*, 3727. (b)Negi, D. P. S.; Chanu, T. I. *Nanotechnology* **2008**, *19*, 465503. (c)Ros-Lis, J.V.; Garci, B.; Jimenez, D.; Martinez-Manez, R.; Sancenon, F.; Soto, J.; Gonzalvo, F.;

Valldecabres, M. C. *J. Am. Chem. Soc.***2004**, *126*, 4064. (d)Sreejith, S.; Divya, K.P.; Ajayaghosh, A. *Angew. Chem. Int. Ed.* **2008**,*47*,7883.

(19) (a)Rusin, O.; Luce, N. N. S.; Agbaria, R. A.; Escobedo, J. O.; Jiang, S.; Warner, I. M.; Dawan, F. B.; Lian ,K.; Strongin, R. M. *J. Am. Chem. Soc.*, **2004**, *126*, 438. (b)Wang, W. O.; Rusin, X.; Xu, K.; Kim, K.; Escobedo, J. O.; Fakayode, S. O.; Fletcher, K. A.; Lowry, M.; Schowalter, C. M.; Lawrence, C. M.; Fronczek, R. I.; Warner, M.; Strongin, R. M. *J. Am. Chem. Soc.* **2005**, *127*, 15949.

(20) (a)McQuade, D. T.; Hegedus, A. H.; Swager, T. M. *J. Am. Chem. Soc.* **2000**, *122*, 12389. (b)Rudzinski, C. M.; Hartmann, W. K.; Nocera, D. G. *Coord. Chem. Rev.***1998**, *171*, 115. (c)Mortellaro, M. A.; Nocera, D. G. *J. Am. Chem. Soc.* **1996**, *118*,7414.

(21) (a)Tanaka, F.; Mase, N.; Barbas, C. F. *Chem. Commun.* **2004**,*15*,1762. (b) Tanaka, F.; Mase, N.; Barbas, C. F. *J. Am. Chem. Soc.*, **2004**, *126*, 3692.

(22) Zhang, M.; Yu, M. X.; Li, F.Y.; Zhu, M. W.; Li, M. Y.; Gao, Y. H.; Liu, Z. Q.; Zhang, D. Q.; Yi, T.; Huang, C. H. *J. Am. Chem. Soc.* **2007**, *129*, 10322.

(23) Frausto da Silva, J. J. F.; Williams, R. J. P. *The Biological Chemistry of Elements*; Clarendon, Oxford, UK. 1991.

(24) Shortreed, M.; Kopelman, R.; Hoyland, B. *Anal. Chem.* **1996**, *68*, 1414.

(25) (a)Shang, L.; Yin, J.Y.; Li, J.; Jin, L.; Dong, S. J. *Biosens. Bioelectron.* **2009**, *25*, 269. (b)Li, H. L.; Fan, J. L.; Wang, J.Y.; Tian, M. Z.; Du, J. J.; Sun, S. G.; Sun, P. P.; Peng, X. J. *Chem. Commun.***2009**, 5904.

(26) Everin, K.; Bergs, R.; Beck, W. *Angew. Chem. Int. Ed.***1998**, *37*, 1635.

(27) (a)Benesi, H. A.; Hildebrand, J. H. *J. Am. Chem. Soc.* **1949**, *71*, 2703. (b)Chow, C. F.; Lam, M. H. W.; Wong, W. Y. *Inorg. Chem.* **2004**, *43, 8387.*

(28) Refsum, H.; Ueland, P. M.; Nygard, O.; Vollset, S. E. *Annu. Rev. Med.* **1989**, *49*, 31.

(29) Seshadri, S.; Beiser, A.; Selhub, J.; Jacques, P. F.; Rosenberg, I. H.; D'Agostino, R. B.; Wilson, P. W. F. *N. Engl. J. Med.* **2002**, *346*, 476.

(30) Yoshida, Y.; Ohiwa, Y.; Shimamura, M.; Izumi, T.; Yoshida, S.; Takahashi, K.; Miyairi, S.; Makimura, M.; Naganuma, A. *J. Health Sci.***2003**, *49,527.*

Contribution to Knowledge

1. A new series of zwitterionic NLO chromphores, dicyanodimethane-based (FDCN) and their corresponding chromophore-polymers were designed and synthesized. Incorporation of bulk groups onto the central part of the FDCN chromophore was demonstrated as an effective strategy to minimize dipole-dipole molecular interaction.
2. Second series of zwitterionic chromophores, PpQDM with dipyridylium electron donors and strong tricyanoquino-dimethane electron acceptors were prepared and grafted onto host polyimides to yield a new series of NLO polyimides.
3. A large EO coefficient of 70 pm/V at the telecommunication wavelength of 1550 nm has been obtained with a 5 wt % PpQDM-Ben doped PVP polymer using an *in situ* poling measurement technique.
4. A buffer layer (PEDOT: PSS/PVA) was first successfully introduced into the double layer device for zwitterionic NLO polymers, and improvement of the poling efficiency of NLO polymer systems was demonstrated.
5. PpQDMs is found to be NIR fluorescent with a large Stokes shift.
6. PpQDM-Met/copper complex was demonstrated to be the first high-contrast colorimetric and NIR fluorescence turn-on molecular probe for sensitive and selective detection of cysteine.

Publications:

1. **Hao, W.;** Wang, Z. Y. "Synthesis, crystal structures, and photophysical properties of second-order nonlinear optical zwitterionic 1-substituted-4-pyridinium-fluorophenyl-dicyanomethanide chromophores" (In preparation.)

2. **Hao, W.;** Wang, Z. Y. "1-hexyl-4-pyridinium-fluorophenyl-dicyanomethanide" (To be submitted to *Acta crystollographic*)
3. Ma, J.; Chiniforooshan, Y.; Chen, J. H.; Bock, W. J.; **Hao, W.;** Wang, Z. Y. "Recapturing Lost Evanescent Power by Tuning Endface-TIR-Capable Tunneling Modes at a Roughened Fiber Endface" (Submittited to *Optical Letter* July, 2011)
4. **Hao, W.;** McBride, A.; McBride, S.; Wang, Z. Y. "Colorimetric and near-infrared fluorescence turn-on molecular probe for selective detection of cysteine in human plasma" *J. Mater.Chem.***2011**, *21*, 1040.
5. Ma, J.; Bock, W. J.; Wang, Z. Y.; **Hao, W.;** MacKinnon, S. M. "Investigation of a large-core photonic crystal fiber sensor for enhancement of fluorescent light collection of polymer membrane" *Proceedings of SPIE-The International Society for Optical Engineering* **2005**, 5970 (Pt. 1, Photonic Applications in Devices and Communication Systems), 597006/1-597006/6
6. Ma, J.; Bock, W. J.; Wang, Z. Y.; **Hao, W.;** MacKinnon, S. M. "Fiber-optic membrane fluorescent sensor based on photonic crystal fiber with a glass rod in the fiber end" *IEEE Sensors* 2005, [IEEE Conference on Sensors], 4th, Irvine, CA, United States, Oct. 30-Nov. 3, 2005 **2005**, *2*, 1096-1099.
7. Ma, J.; Bock, W. J.; Wang, Z. Y.; **Hao, W.** MacKinnon, S. M. "Towards optimum sample probe spectrometer system design by adjusting receiving fiber end face position and probe-membrane sample separation" *Optics express* **2005**, *13*, 9492.

Conference presentations

1. **Hao, W.**; Wang, Z. Y. "Development of Zwitterionic Chromophores and Polymers for Electro-Optic Application" *34th Canadian High Polymer Forum*, Hôtel Mont Gabriel, Ste-Adèle, Québec, Aug. 18-20, **2010** (Oral Presentation)
2. Wang, Z. Y.; Gao, J. P.; Zhang, J.; Tang, H.; LeClair, G.; Xun, S.; Xiong, Y.; **Hao, W.**; Volland, S. "Infrared Organic Materials for Optoelectronic and Sensor Applications" *32nd Canadian High Polymer Forum*, Aylmer, Quebec, Aug.19-21, **2005** (Oral Presentation)
3. Song, N. H.; Bai, Y. W.; Xiong, Y.; **Hao, W.**; Volland, S.; Wang, X.; Sun, X.; Yu, G.; Men, L.; Gao, J. P.; Wang, Z. Y. "A New Approach to Highly Electro-Optically Active Polymers Using Cross-Linkable, Hyperbranched Chromophore Containing Oligomers as Macromolecular Dopants" *88th Canadian Chemistry Conference and Exhibition*, Saskatoon, SK, Canada, May 28-June 1, **2005** (Award Presentation)

Appendix A X-ray data for FDCN

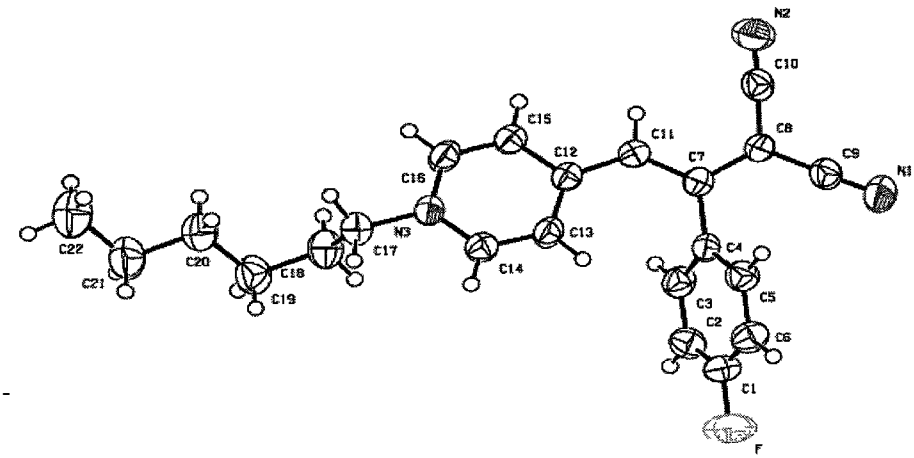

Table 1. Crystal data and structure refinement for FDCN

Identification code	P237
Empirical formula	C22 H22 F N3
Formula weight	347.43
Temperature	293 (2) K
Wavelength	0.71073 Å
Crystal system	Monoclinic
Space group	P 2(1)/c
Unit cell dimensions	a=10.485(3)Å b=8.809(2)Å c=21.313(5)Å α=90.00° β=100.628(4)° γ= 90.00 °
Volume	1934.7(8) $Å^3$
Z	4
Density (calculated)	1.193 Mg/m^3
Absorption coefficient	0.08 mm^{-1}
F(000)	736.0
Crystalsize	0.437 ×0.217 ×0.056 mm^3
Theta range for data collection	1.94 to 28.68°
Index ranges	-13 =< h =< 10 -11 =< k =< 11 -26 =< l =< 27
Reflections collected	11920
Independent reflections	4589
Completeness to theta=28.68°	92%
Absorption correction	Semi-empirical from equivalents
Max. and Min. transmission	0.9956 and 0.9667
Refinement method	Full-matrix least-squares on F^2
Data/restrains/parameters	4589/0/236
Goodness-of-fit on F^2	0.991
Final R indices [I>2sigma(I)]	R=0.0505
R indices (all data)	R1=0.1084, wR2=0.0902
Largest diff. peak and hole	0.153 and -0.165 e. $Å^{-3}$

Table 2. Atomic coordinates ($\times 10^4$) and equivalent isotropic displacement parameters ($Å^2 \times 10^3$) for FDCN. U (eq) is defined as one third of the trace of the orthogonalized U^{ij} tensor

Atom	x	y	z	U^{ij}(eq)
F	95(1)	3228(1)	1471(1)	89(1)
N1	5246(2)	19(2)	2192(1)	76(1)
N2	7935(2)	489(2)	868(1)	70(1)
N3	3170(1)	4945(2)	-1432(1)	44(1)
C1	1227(2)	2873(2)	1278(1)	54(1)
C2	1180(2)	1996(2)	752(1)	54(1)
C3	2329(2)	1660(2)	552(1)	46(1)
C4	3509(2)	2197(2)	886(1)	38(1)
C5	3499(2)	3064(2)	1427(1)	45(1)
C6	2351(2)	3428(2)	1626(1)	54(1)
C7	4744(2)	1794(2)	678(1)	38(1)
C8	5674(2)	1016(2)	1123(1)	41(1)
C9	5426(2)	482(2)	1713(1)	50(1)
C10	6925(2)	696(2)	989(1)	48(1)
C11	4969(2)	2106(2)	71(1)	42(1)
C12	4302(2)	3065(2)	-414(1)	39(1)
C13	3342(2)	4151(2)	-359(1)	47(1)
C14	2814(2)	5041(2)	-856(1)	481(1)
C15	4656(2)	3023(2)	-1022(1)	47(1)
C16	4093(2)	3923(2)	-1507(1)	49 (1)
C17	2554(2)	5899(2)	-1975(1)	49(1)
C18	1528(2)	5046(2)	-2425(1)	59(1)
C19	772(2)	6054(2)	-2945(1)	67(1)
C20	1555(2)	6747(2)	-3398(1)	62(1)
C21	729(2)	7591(2)	-3947(1)	75(1)
C22	1493(2)	8187(2)	-4426(1)	872(1)

Table 3. Bond lengths [Å] and angles [°] for FDCN

F - C (1)	1.362(2)
N (1) - C (9)	1.147(2)
N (2) - C (10)	1.151(2)
N (3) - C (14)	1.349(2)
N (3) - C (16)	1.352(2)
N (3) - C (17)	1.480(2)
C (1) - C (2)	1.355(2)
C (1) - C (6)	1.363(2)
C (2) - C (3)	1.382(2)
C (3) - C (4)	1.392(2)
C (4) - C (5)	1.386(2)
C (4) - C (7)	1.487(2)
C (5) - C (6)	1.386(2)
C (7) - C (11)	1.384(2)
C (7) - C (8)	1.408(2)
C (8) - C (9)	1.411(2)
C (8) - C (10)	1.420(2)
C (11) - C (12)	1.416(2)
C (12) - C (13)	1.409(2)
C (12) - C (15)	1.413(2)
C (13) - C (14)	1.352(2)
C (15) - C (16)	1.349(2)
C (17) - C (18)	1.504(2)
C (18) - C (19)	1.525(2)
C (19) - C (20)	1.508(2)
C (20) - C (21)	1.516(2)
C (21) - C (22)	1.503(2)
C (14) - N (3) - C (16)	118.3(1)
C (14) - N (3) - C (17)	121.44(14)
C (16) - N (3) - C (17)	120.25(14)
C (2) - C (1) - F	118.76(17)
C (2) - C (1) - C (6)	123.4(2)
F - C (1) - C (6)	117.83(18)
C (1) - C (2) - C (3)	118.52(16)
C (2) - C (3) - C (4)	120.83(16)
C (5) - C (4) - C (3)	118.1(2)
C (5) - C (4) - C (7)	121.38(14)
C (3) - C (4) - C (7)	120.48(15)
C (6) - C (5) - C (4)	121.54(16)
C (1) - C (6) - C (5)	117.59(17)
C (11) - C (7) - C(8)	120.66(15)
C (11) - C (7) - C(4)	122.66(14)
C (8) - C (7) - C (4)	116.63(14)
C (9) - C (8) - C (7)	123.0(2)
C (7) - C (8) - C (10)	120.83(14)
C (9) - C (8) - C (10)	116.16(14)
N (1) - C (9) - C (8)	178.3 (2)
N (2) - C (10) - C (8)	177.25(20)
C (7) - C (11) - C (12)	130.85(15)
C (13) - C (12) - C (15)	114.0(2)
C (13) - C (12) - C (11)	127.46(15)
C (15) - C (12) - C (11)	118.45(15)

C (14) - C (13) - C (12)	121.64(15)
N (3) - C (14) - C (13)	122.25(16)
C (16) - C (15) - C (12)	122.34(16)
C (15) - C (16) - N (3)	121.46(15)
N (3) - C (17) - C (18)	111.85(14)
C (17) - C (18) - C (19)	112.78(15)
C (20) - C (19) - C (18)	115.47(16)
C (19) - C (20) - C (21)	113.02(16)
C (22) - C (21) - C (20)	113.23(17)

Symmetry transformations used to generate equivalent atoms

Table 4. Anisotropic displacement parameters ($Å^2$) for FDCN. Anisotropic displacement factor exponent takes the form: $-2\pi^2 [h^2 a^{*2} U^{11} + ... + 2 h k a^* b^* U^{12}]$

Atom	U^{11}	U^{22}	U^{33}	U^{23}	U^{13}	U^{12}
F	0.0578(8)	0.1138(11)	0.1017(9)	-0.0069(8)	0.0344(7)	0.0152(7)
N1	0.0951(14)	0.0947(14)	0.0430(10)	0.0155(10)	0.0217(9)	0.0315(10)
N2	0.0523(11)	0.0930(14)	0.0629(11)	-0.0080(9)	0.0075(8)	0.0117(9)
N3	0.0491(9)	0.49451(15)	0.0354(8)	0.0046(7)	0.0079(6)	0.0016(7)
C1	0.0470(12)	0.2873(2)	0.0576(12)	0.0065(11)	0.0220(10)	0.0102(10)
C2	0.0410(11)	0.0649(13)	0.0527(12)	0.0034(10)	0.0028(9)	-0.0037(9)
C3	0.0487(12)	0.0532(12)	0.0366(10)	-0.0040(8)	0.0057(8)	-0.0028(9)
C4	0.0422(11)	0.0409(10)	0.0303(9)	0.0037(8)	0.0066(8)	0.0008(8)
C5	0.0457(11)	0.0470(11)	0.0410(10)	-0.0027(9)	0.0044(8)	-0.0001(8)
C6	0.0625(13)	0.0565(13)	0.0451(11)	-0.0083(9)	0.0163(10)	0.0070(10)
C7	0.0417(10)	0.0373(10)	0.0343(9)	-0.0034(8)	0.0064(8)	-0.0033(8)
C8	0.0418(11)	0.0490(11)	0.0320(10)	-0.0016(8)	0.0077(8)	0.0034(8)
C9	0.0548(12)	0.0588(13)	0.17131(8)	-0.0011(9)	0.0048(9)	0.0132(9)
C10	0.0525(12)	0.0522(12)	0.0351(10)	-0.0032(8)	0.0001(9)	0.0033(9)
C11	0.0431(10)	0.0463(11)	0.0383(10)	0.0001(8)	0.0107(8)	0.0058(8)
C12	0.0402(10)	0.0413(10)	0.0350(9)	-0.0011(8)	0.0079(7)	-0.0036(8)
C13	0.0586(12)	0.0506(11)	0.0327(10)	0.0016(9)	0.0141(8)	0.0059(9)
C14	0.0548(12)	0.0508(11)	0.0407(11)	-0.0004(9)	0.0141(8)	0.0079(9)
C15	0.0522(11)	0.0492(12)	0.0415(10)	0.0048(9)	0.0157(8)	0.0082(8)
C16	0.0604(13)	0.0566(12)	0.0356(10)	0.0024(9)	0.0174(9)	0.0019(10)
C17	0.0550(12)	0.0479(11)	0.0416(10)	0.0066(9)	0.0058(8)	0.0011(9)
C18	0.0684(13)	0.0556(13)	0.24246(8)	0.0008(10)	0.0015(9)	0.0088(10)
C19	0.0627(14)	0.0831(16)	0.0495(12)	0.0046(11)	0.0045(10)	0.0051(11)

C20	0.0696(14)	0.0663(14)	0.0469(12)	0.0001(10)	0.0028(10)	0.0007(11)
C21	0.0811(16)	0.7591(2)	0.0518(13)	0.0126(12)	0.0001(11)	0.0052(12)
C22	0.1042(19)	0.0917(19)	0.0603(14)	0.0088(13)	0.0011(12)	0.0128(14)

Table 5. Hydrogencoordinates ($\times 10^4$) and isotropic displacement parameters ($Å^2 \times 10^3$) for FDCN

Atom	x	y	z	U^{ij}(eq)
H (2)	393	1629	530	54
H (3)	2313	1067	189	46
H (5)	4281	3411	1662	45
H (6)	2348	4029	1985	54
H (11)	5678	1601	-36	42
H (13)	3066	4259	29	47
H (14)	2182	5742	800	48
H (15)	5301	2351	-1091	47
H (16)	4344	3839	-1902	50
H (17A)	3213	6252	-2206	49
H (17B)	2166	6783	-1814	49
H (18A)	928	4590	-2183	59
H (18B)	1936	4232	-2622	59
H (19A)	78	5457	-3192	67
H (19B)	373	6868	-2743	67
H (20A)	2030	5949	-3569	62
H (20B)	2185	7444	-3163	62
H (21A)	58	6915	-4162	74
H (21B)	305	8435	-3777	74
H (22A)	2175	8834	-4214	87
H (22B)	929	8755	-4748	87
H (22C)	1861	7352	-4620	87

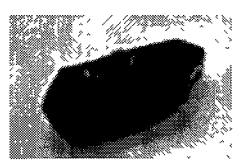

Appendix B Spectra of Synthesized Products of Chapter 2 and 3

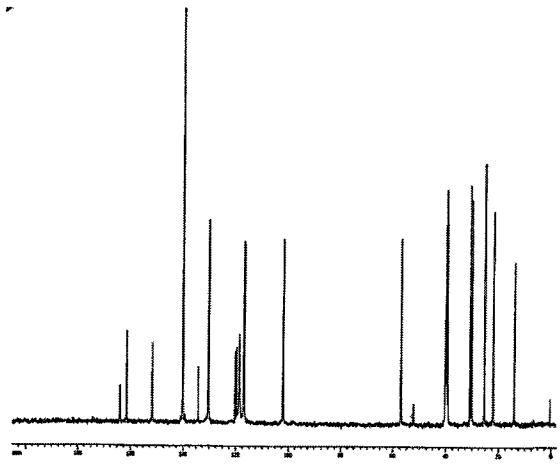

Figure S2.1. ^{13}C NMR of FDCN.

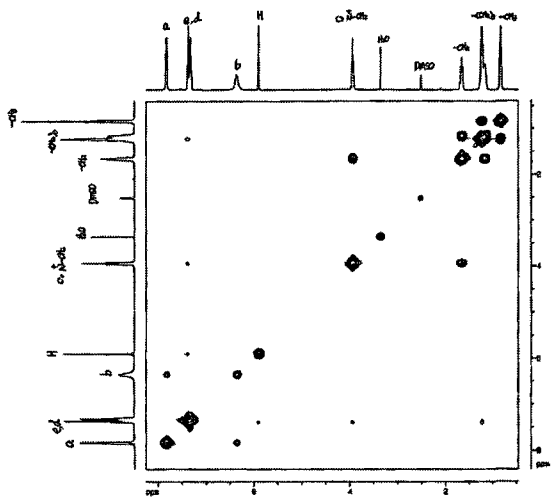

Figure S2.2. 2D cosy of FDCN.

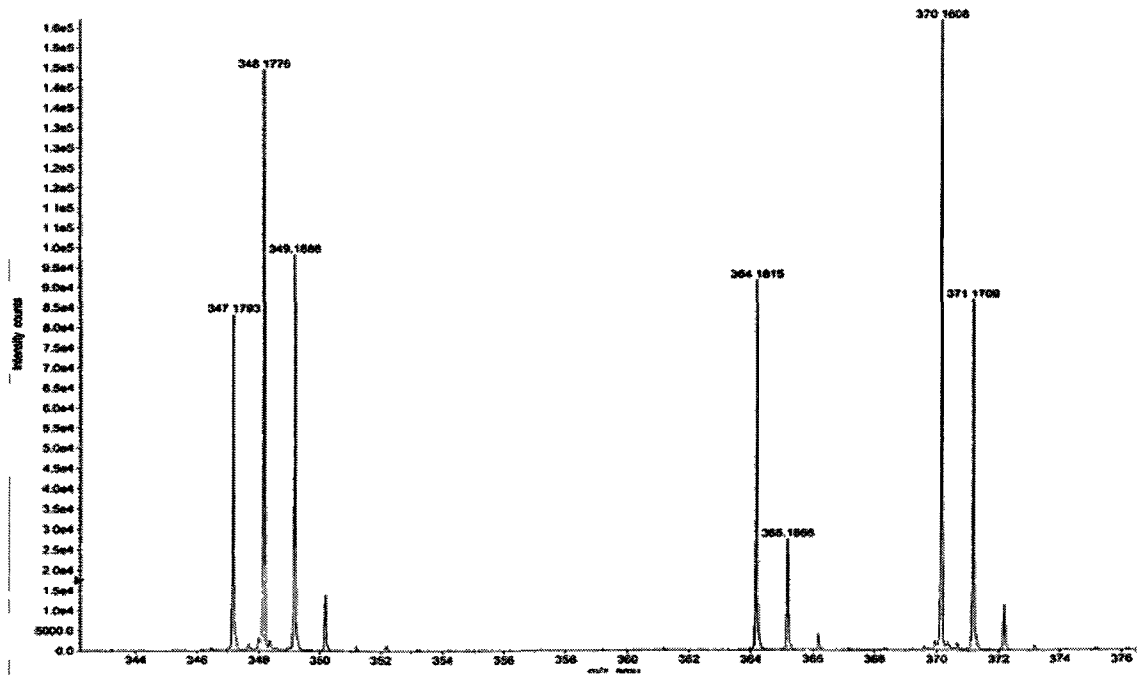

Figure S2.3. MS spectrum of FDCN.

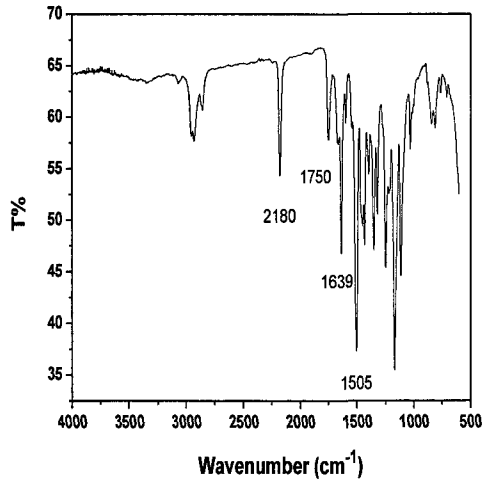

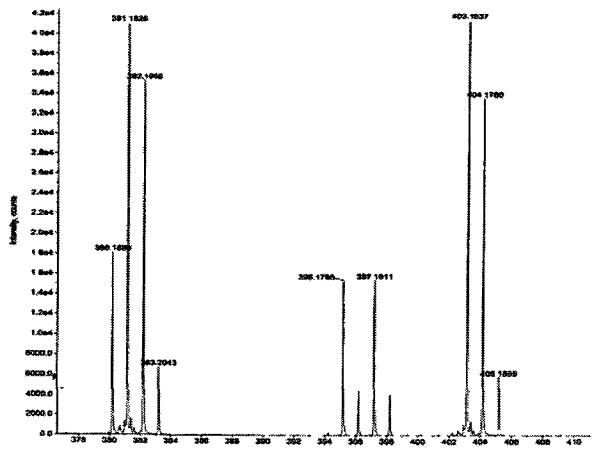

Figure S2.4. IR spectrum of FCNE (KBr pellet). Figure S2.5. MS spectrum of FCNE.

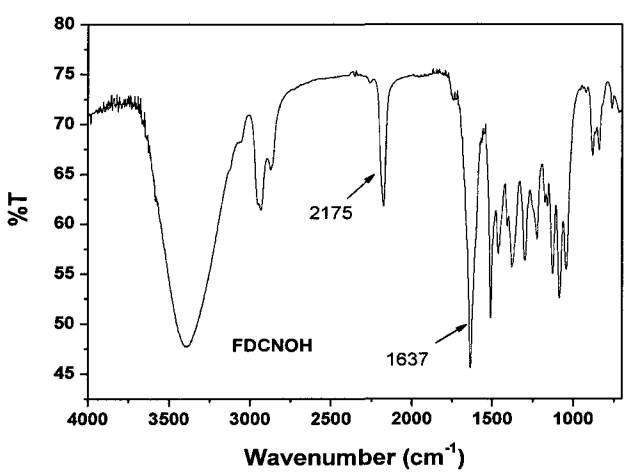

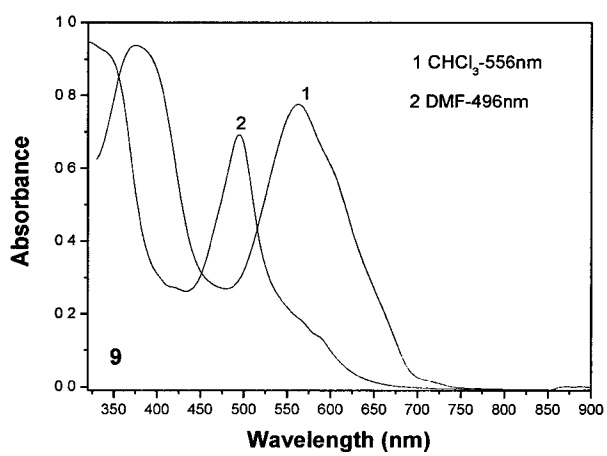

Figure S2.6. IR spectrum of FDCNOH (KBr pellet). Figure S2.7. UV spectra of **A2** in DMF and chloroform.

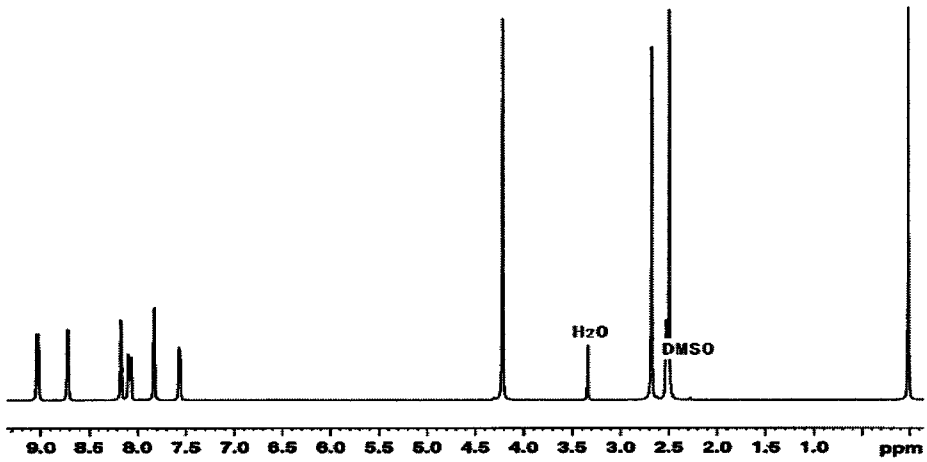

Figure S2.8. ^{1}H NMR of 1,4,4'-trimethyl-2, 2'-dipyridylium iodide.

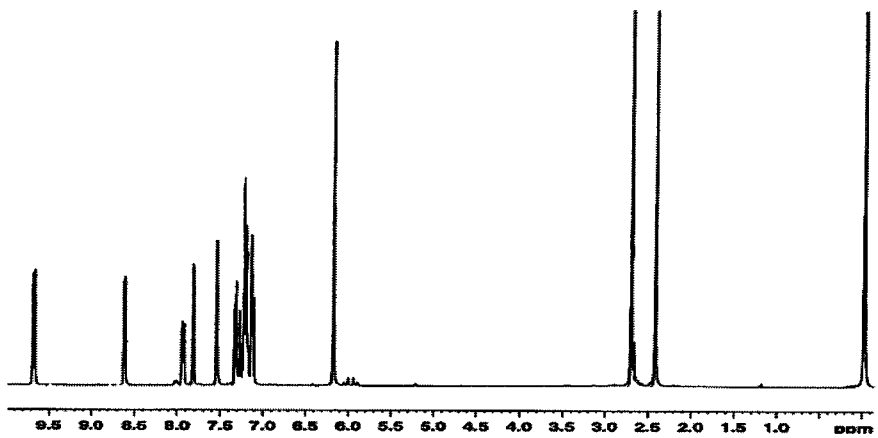

Figure S2.9. ^{1}H NMR of 1-benzyl -4,4'-trimethyl-2, 2'-dipyridylium bromide.

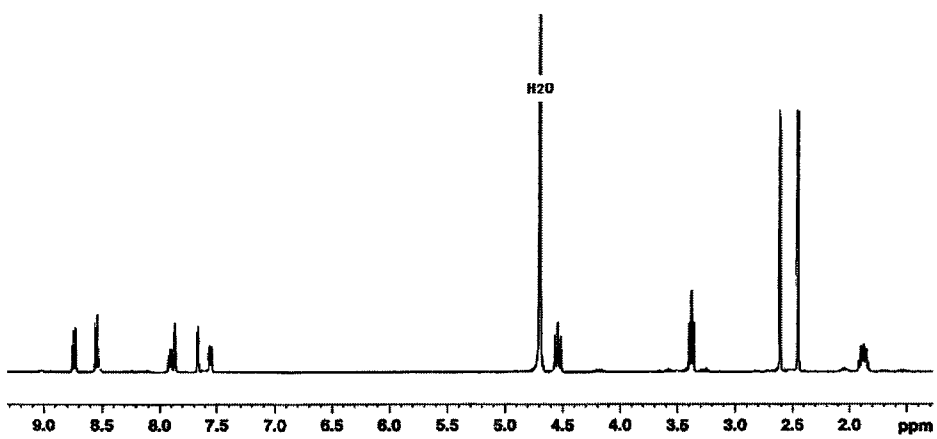

Figure S2.10. ^{1}HNMR of 1-hydroxypropyl -4, 4'-trimethyl-2, 2'-dipyridylium bromide.

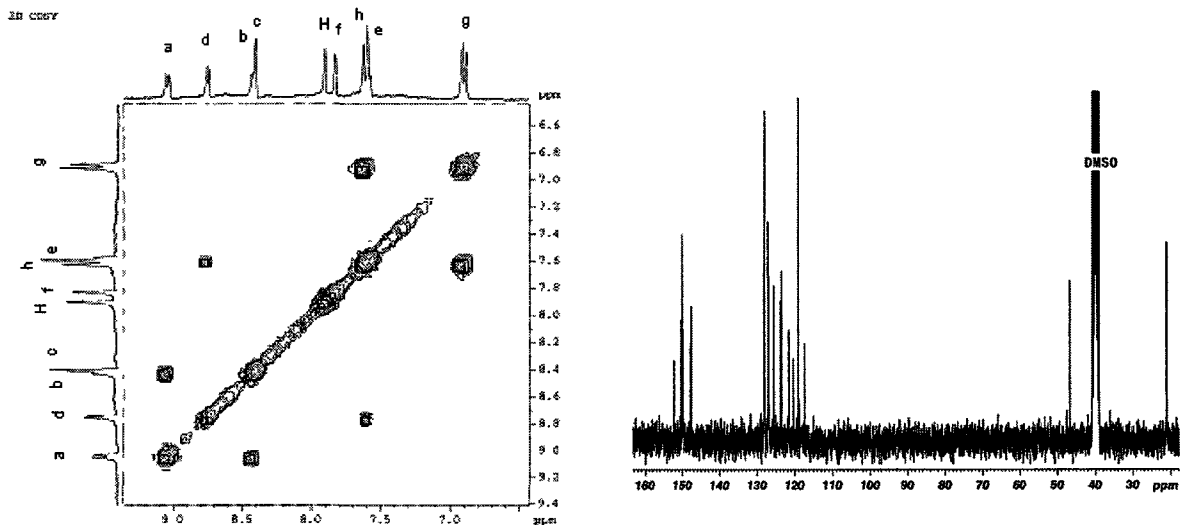

Figure S2.11. ^{1}H NMR (2D COSY) spectrum of aromatic protons of PpQDM-Met in DMSO-d_6 (left) and Figure S2.12. ^{13}C NMR of PpQDM-Met (right).

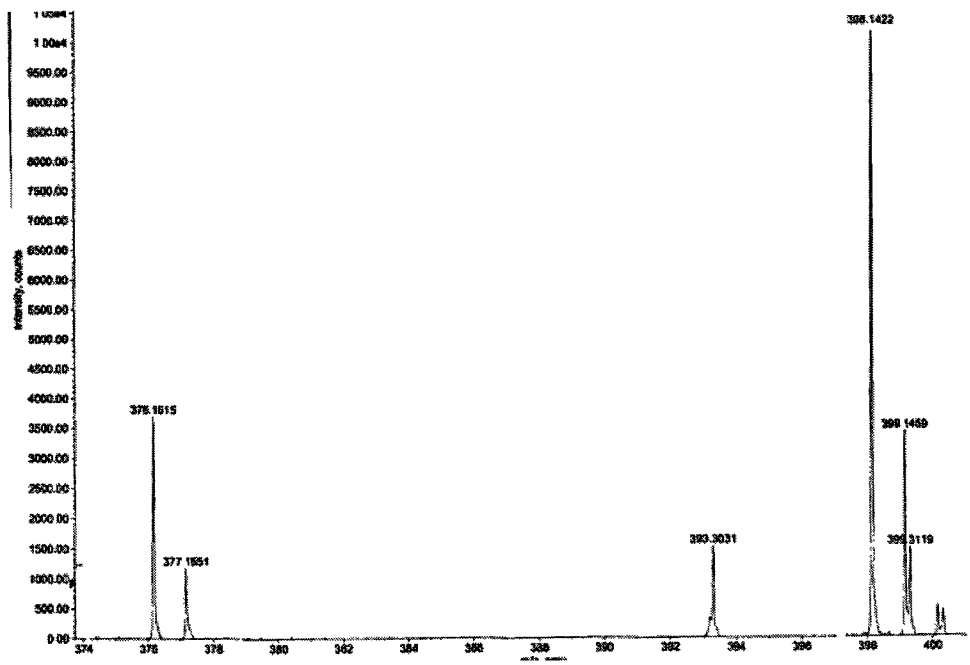

Figure S2.13. ESI mass spectrum of PpQDM-Met.

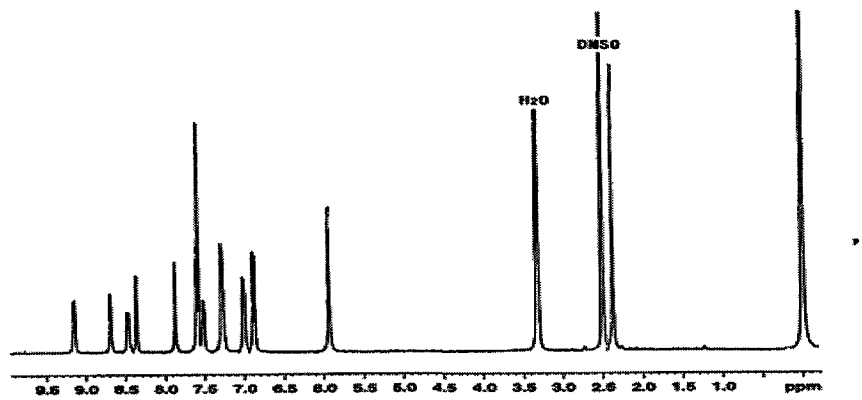

Figure S2.14. ^{1}HNMR of PpQDM-Ben in DMSO-d_6.

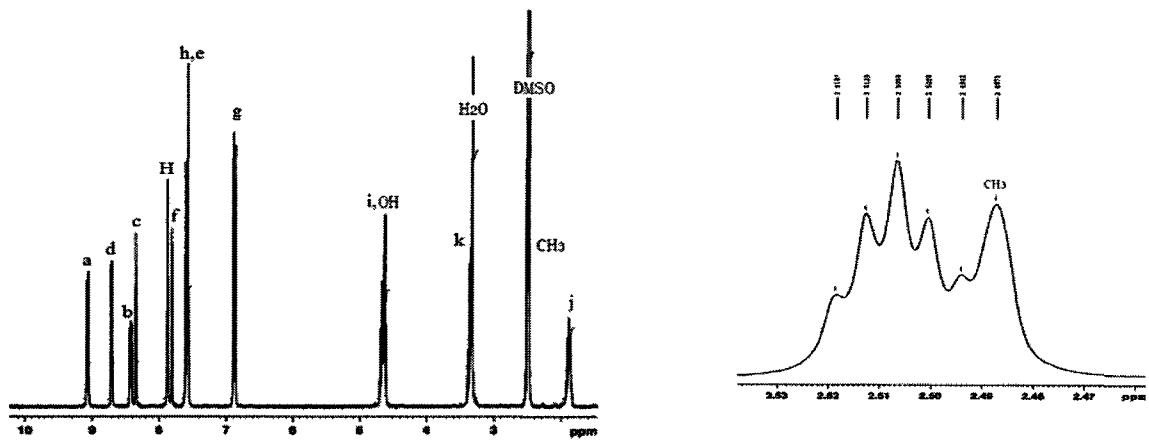

Figure S2.15. ^{1}HNMR of PpQ DM-C3OH in DMSO-d_6.

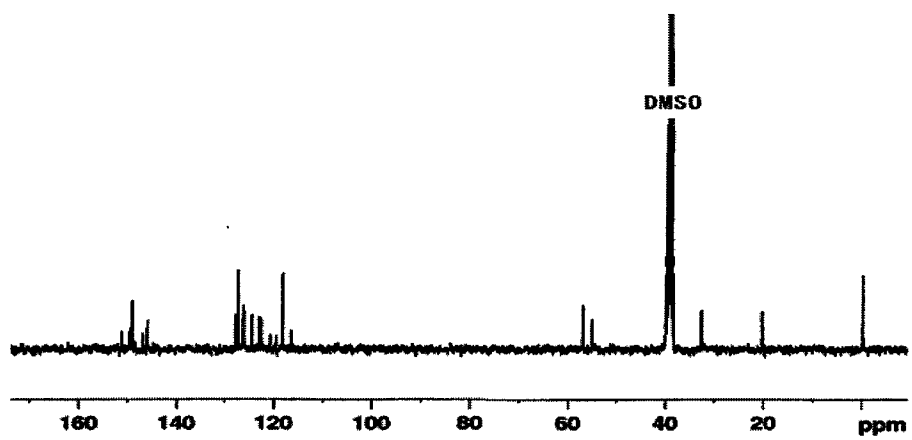

Figure S2.16. ^{13}CNMR of PpQDM-C3OH.

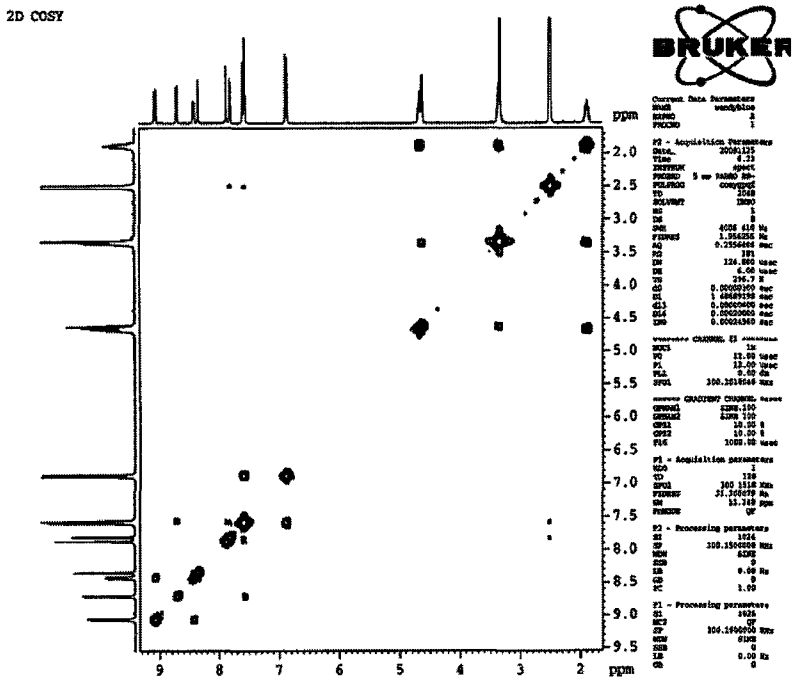

Figure S2.17. 2D cosy NMR of PpQDM-C3OH.

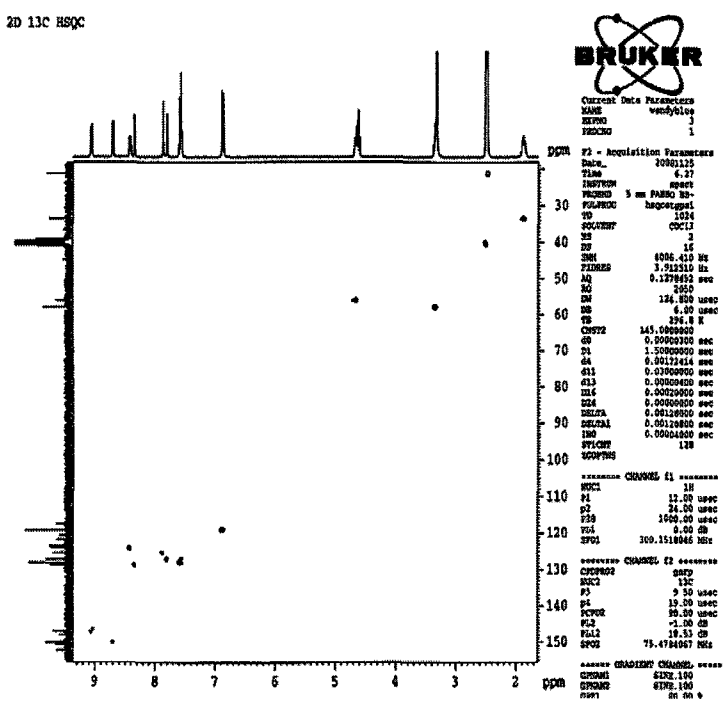

Figure S2.18. 2D 13C HSQC NMR of PpQDM-C3OH.

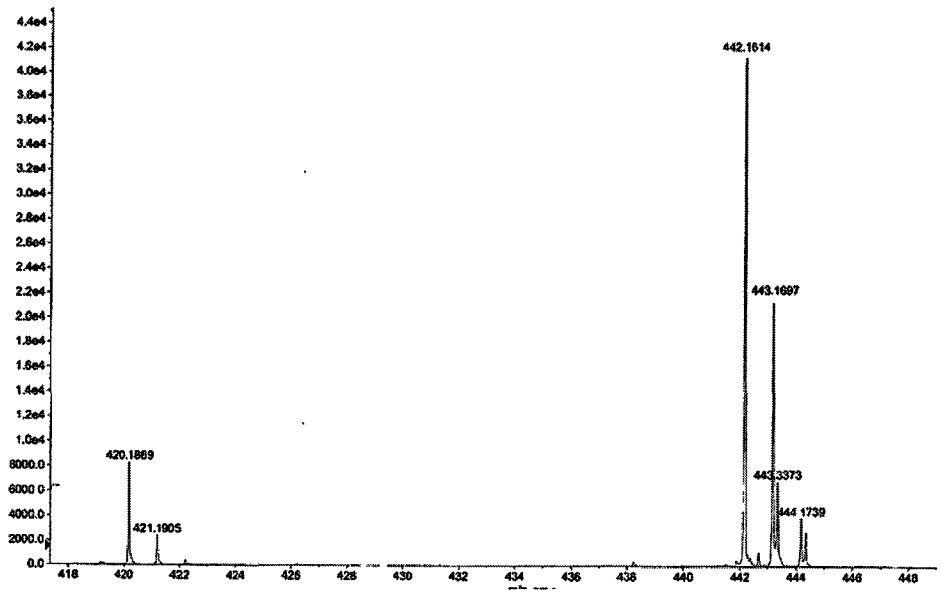

Figure S2.19. ESI mass spectrum of PpQDM-C3OH.

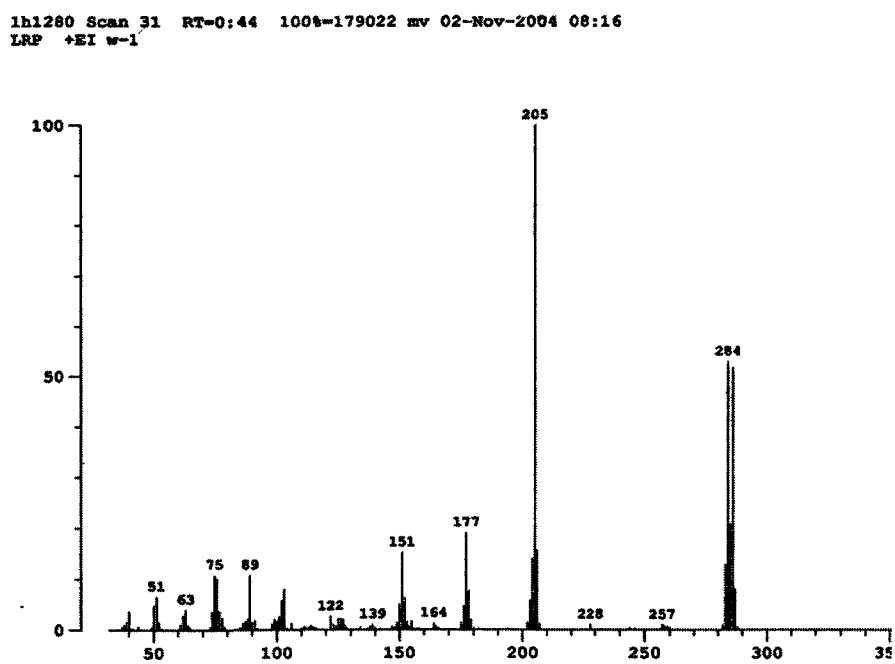

Figure S2.20. EI mass spectrum of compound 1.

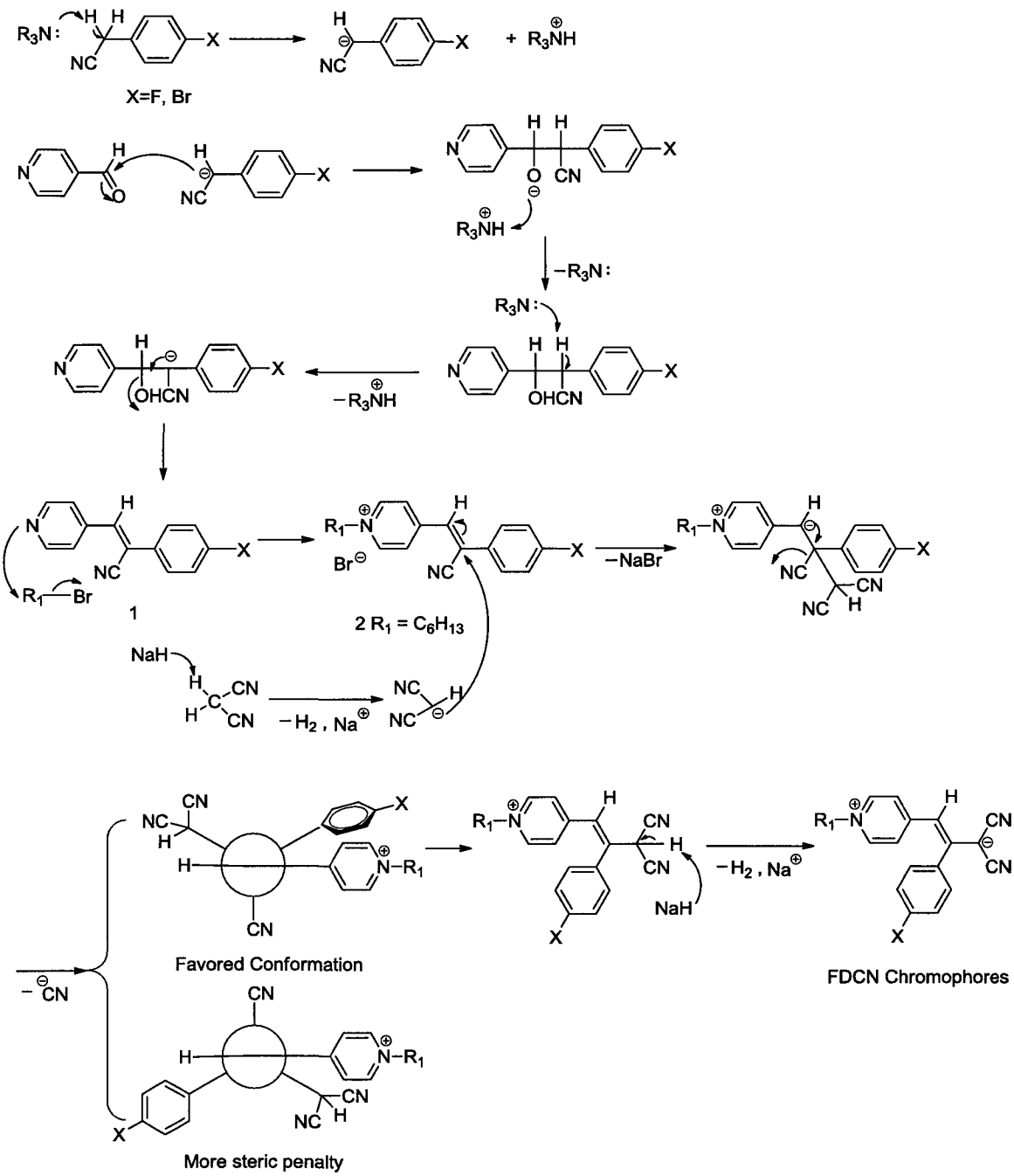

Scheme S2.1. Proposed reaction mechanism for the formation of compound 1 and FDCN chromophores

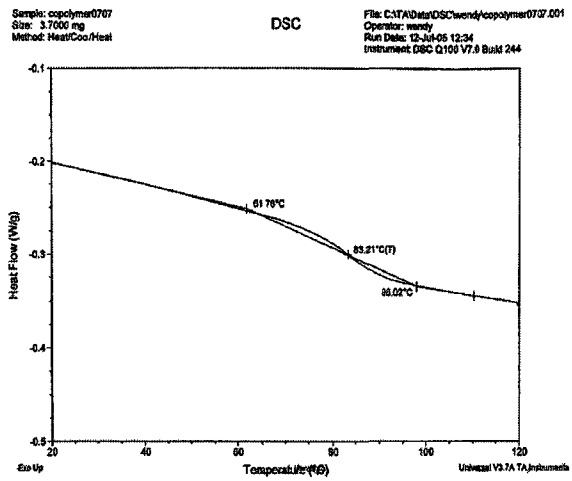

Figure S3.1. DSC trace of **A1-1**.

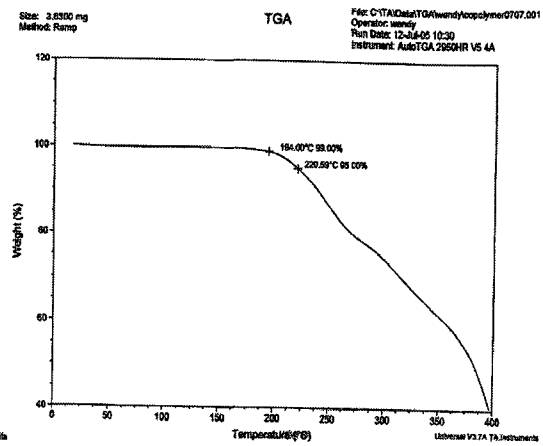

Figure S3.2. TGA trace of **A1-1**.

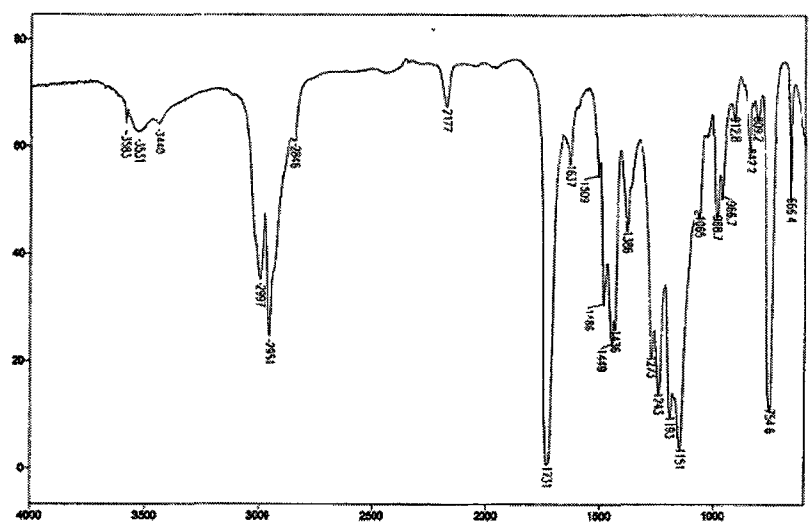

Figure S3.3. IR spectrum of NLO polymer **NA2b**.

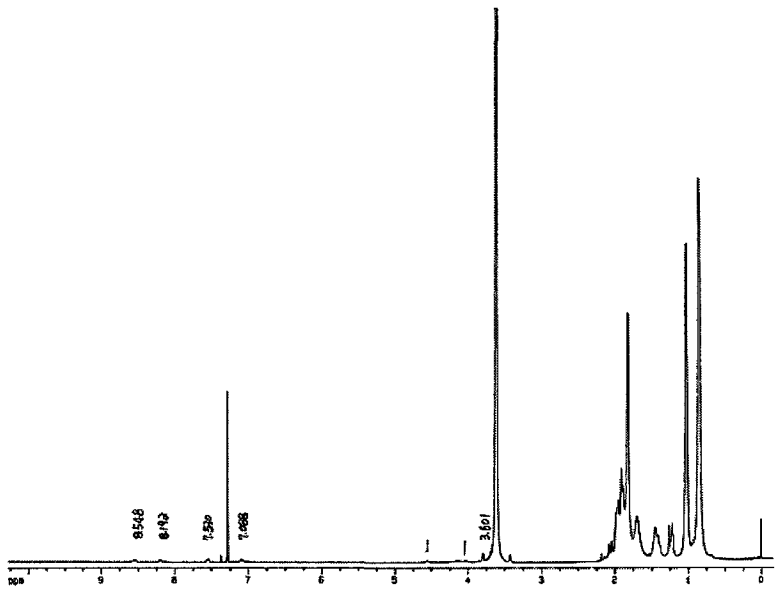

Figure S3.4. NMR spectrum of NLO polymer **NA2b**.

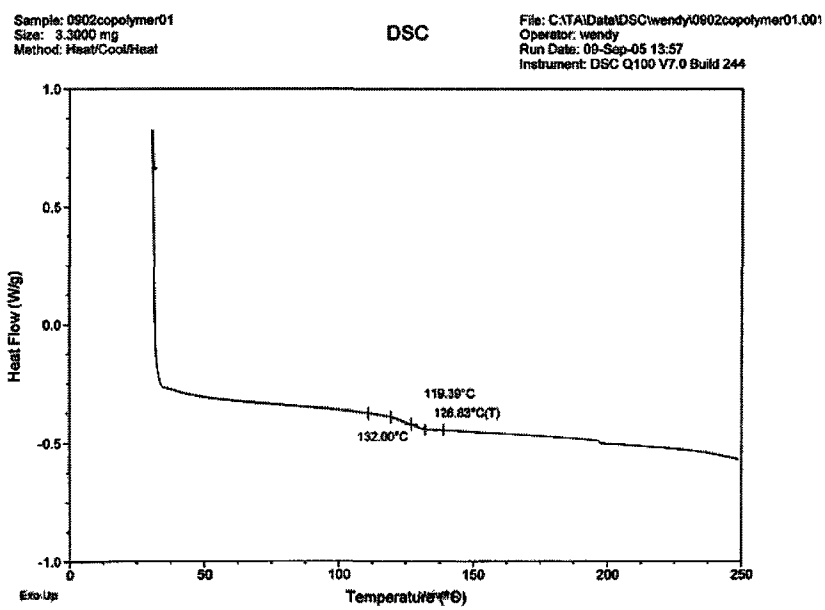

Figure S3.5. DSC trace of NLO polymer **NA2b**.

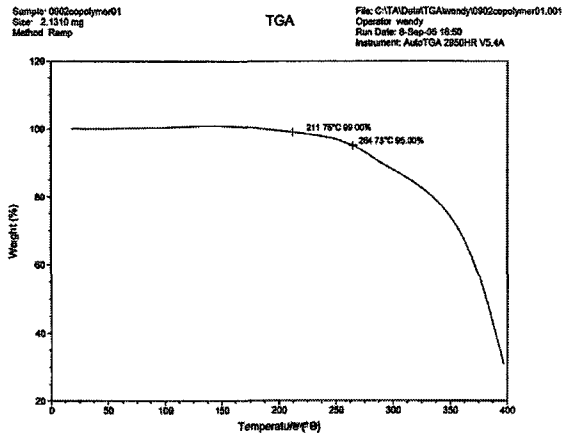

Figure S3.6. TGA trace of polymer **NA2b**.

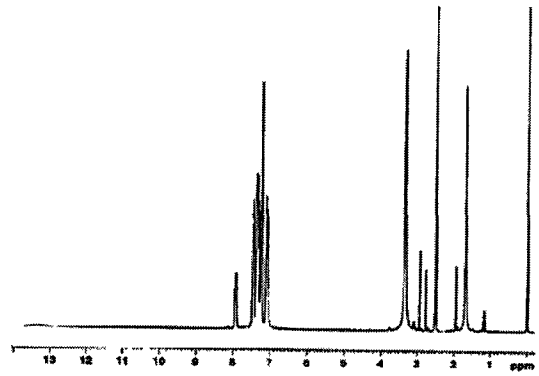

Figure S3.7. NMR spectrum of **PI-1b**.

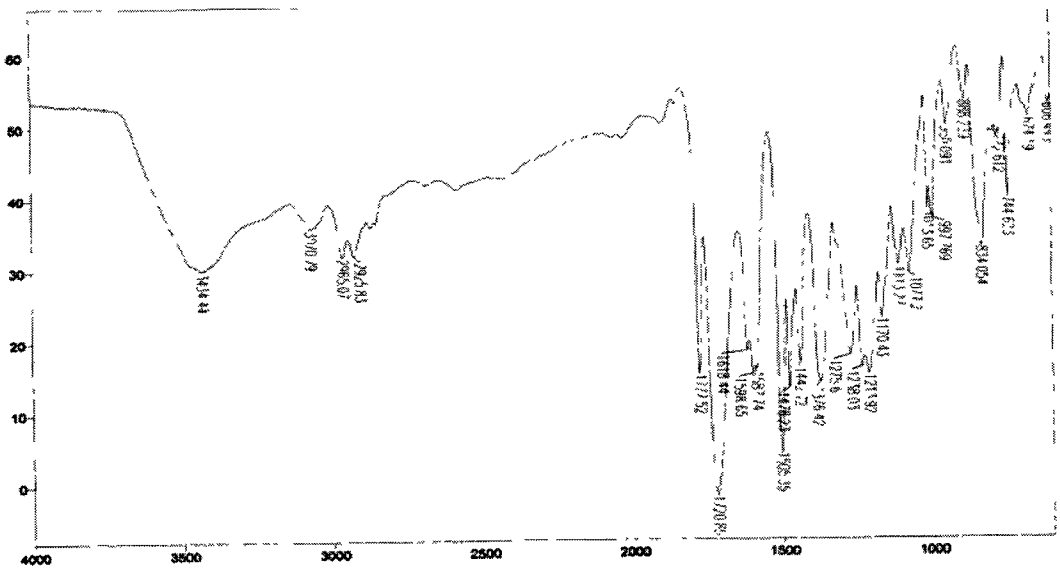

Figure S3.8. IR spectrum of polyimide **PI-1b**.

Appendix C Supporting Information of Chapter 4

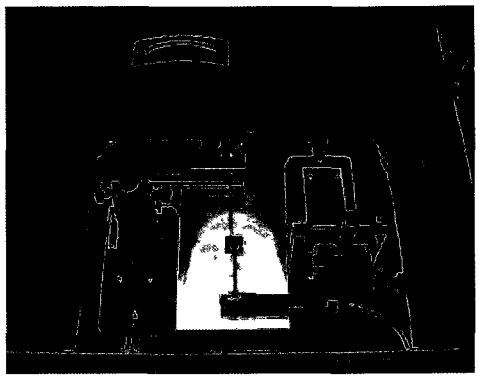

Figure S4.1. Electro-thermal poling station.

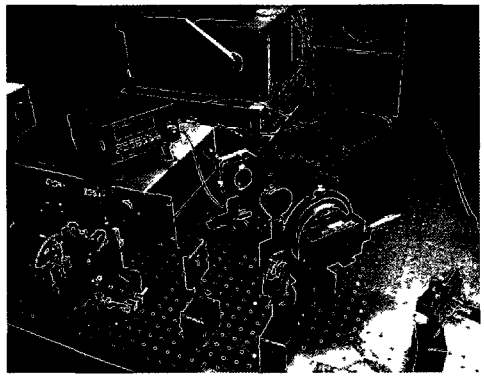

Figure S4.3. Teng-Man Setup.

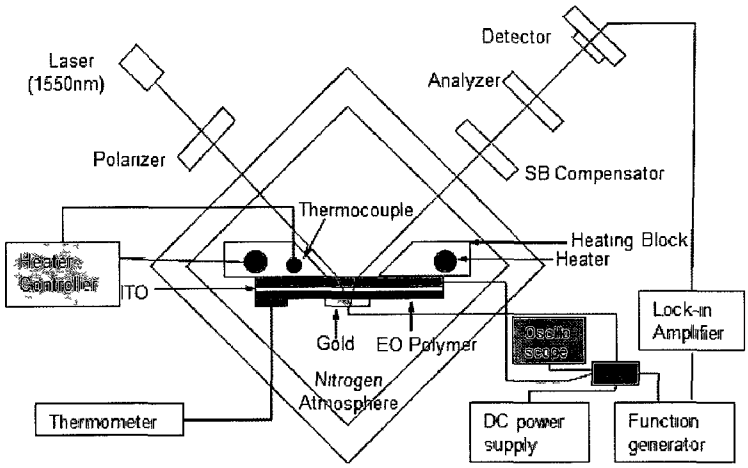

Figure S4.4. The modified reflection ellipsometry apparatus for *in situ* monitoring of r_{33} during electric field poling.

Figure S4.2. Films of FDCN/PES (left) and NPI-d (right) on ITO with gold.

Figure S4.5. Films of PpQDM-Met in different polymers.

Appendix D Supporting Information of Chapter 5

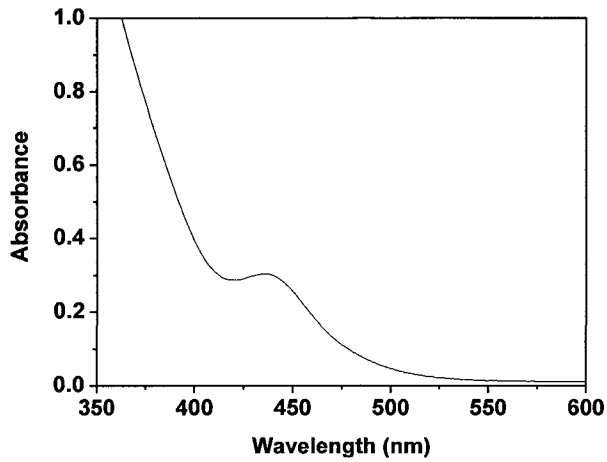

Figure S5.1. UV-Vis spectrum of **M1-Cu**.

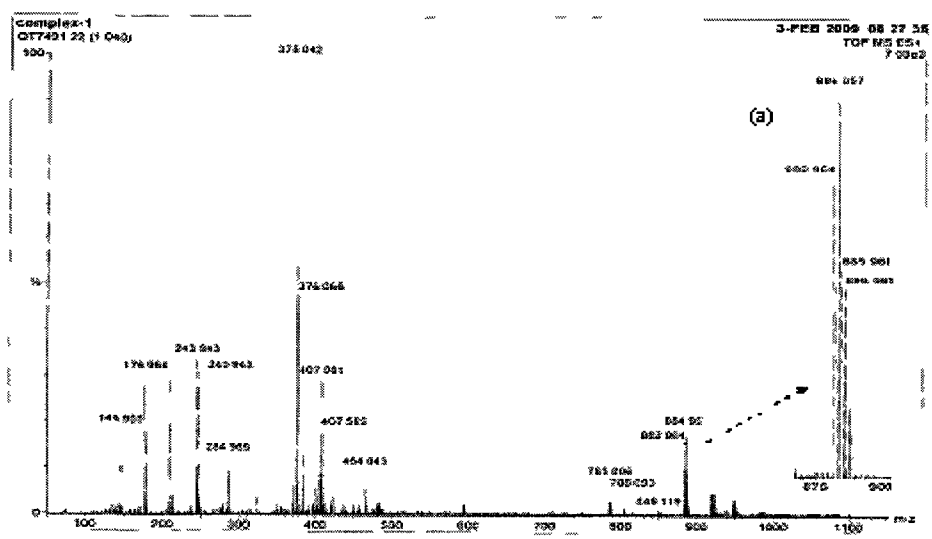

Figure S5.2. ESI mass spectrum of **M1-Cu**. Inset: (a) expanded peak of the complex.

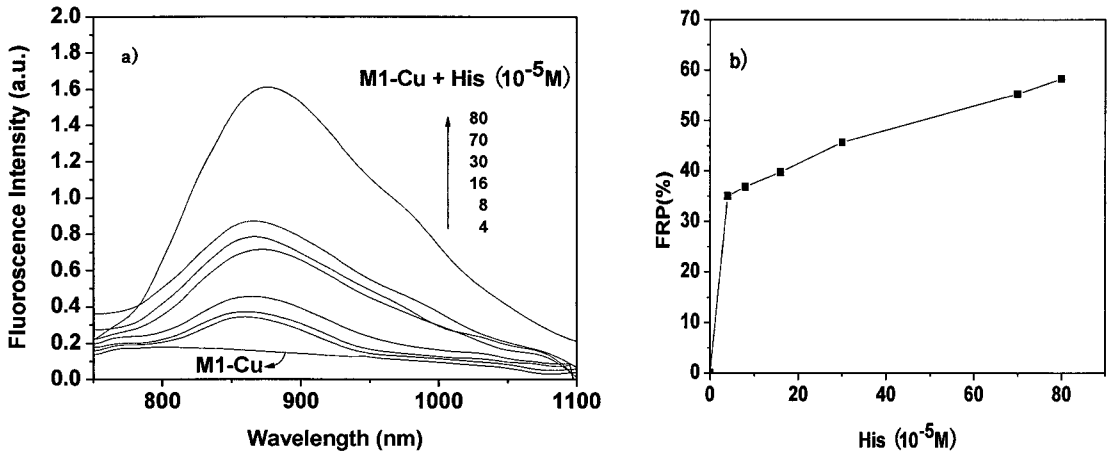

Figure S5.3.1 a) Changes in the fluorescence emission spectra of **M1**, **M1-Cu** and fluorescence titration of **M1-Cu** with increasing amounts of His. The concentration of **M1** is fixed at 2×10^{-5} M. Excitation wavelength (nm): 670. b) FRP versus the concentration of His. Each spectrum is acquired 1 min after His addition.

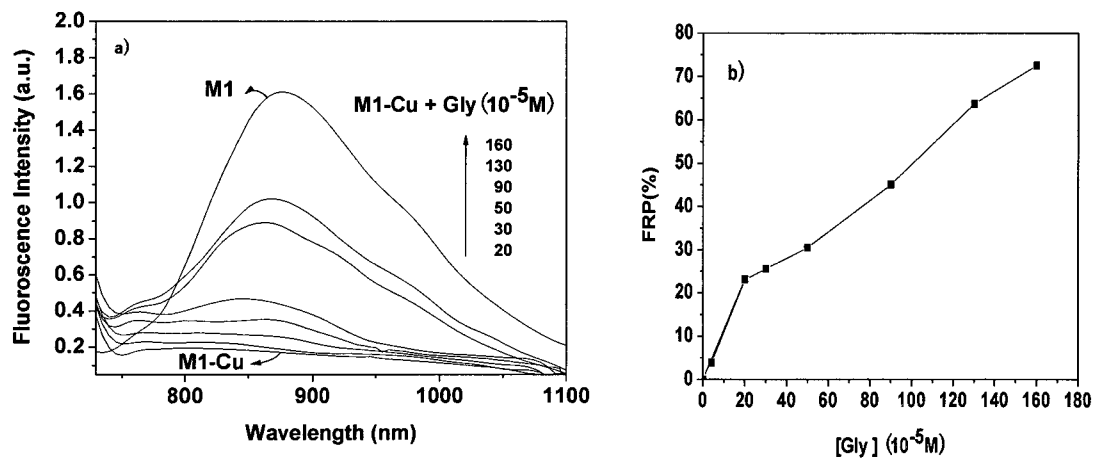

Figure S5.3.2. a) Changes in the fluorescence emission spectra of **M1**, **M1-Cu** and fluorescence titration of **M1-Cu** with increasing amounts of Gly. The concentration of **M1** is fixed at 2×10^{-5} M. Excitation wavelength (nm): 670. b) FRP versus the concentration of Gly. Each spectrum is acquired 1 min after Gly addition.

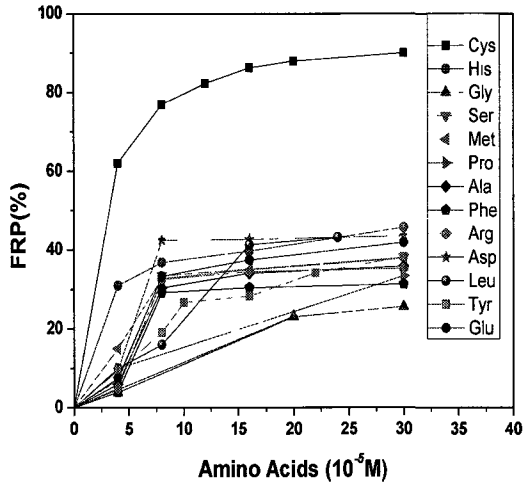

Figure S5.3.3. FRP with respect to the concentration of different α-amino acids.

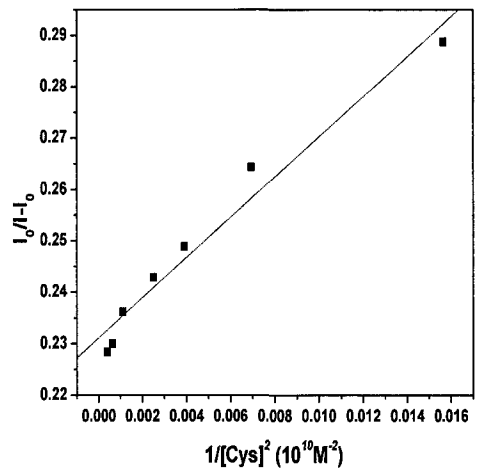

Figure S5.4. B-H plot of **M1-Cu** with Cys.

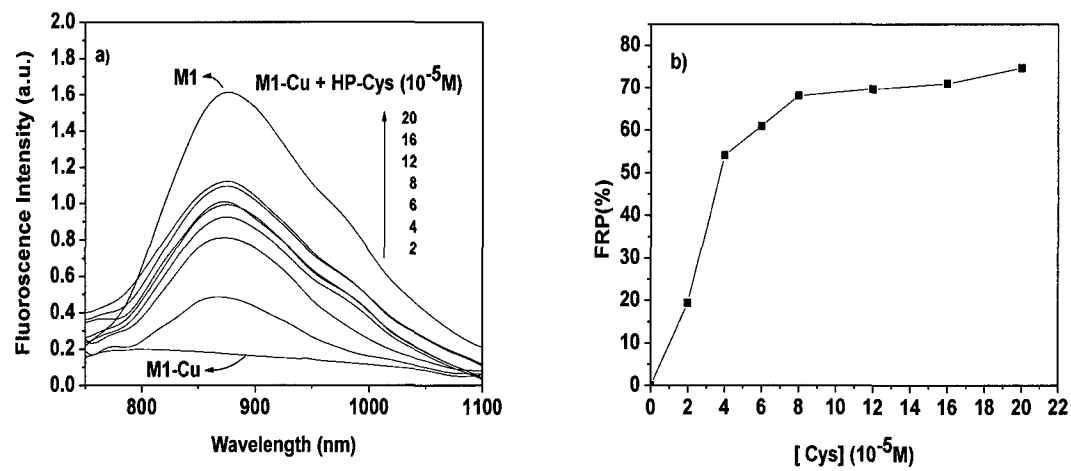

Figure S5.5. a) Changes in the fluorescence emission spectra of **M1**, **M1-Cu** and fluorescence titration of **M1-Cu** with increasing amounts of human plasma with Cys. The concentration of **M1** is fixed at 2×10^{-5} M. Excitation is at 670nm. b) FRP versus the concentration of human plasma with Cys.

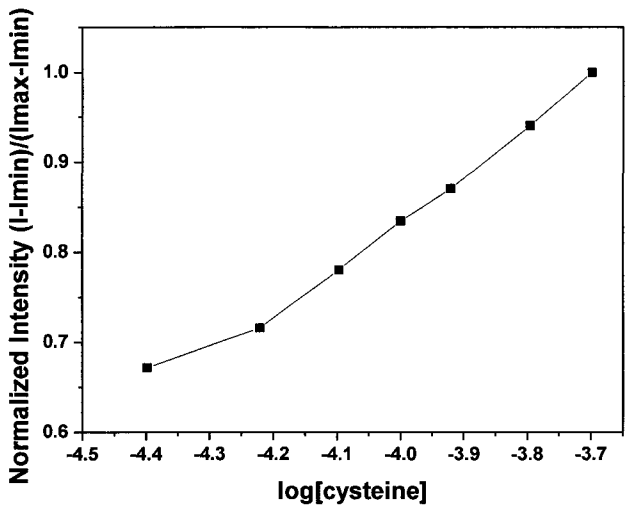

Figure S5.6. Fluorescence intensity of the **M1-Cu** probe at each concentration of Cys in human plasma, normalized between the minimum fluorescence intensity, found at zero Cys and the maximum fluorescence intensity, found at 20×10^{-5} M Cys in human plasma. The excitation at 670 nm and the emission at 875 nm.

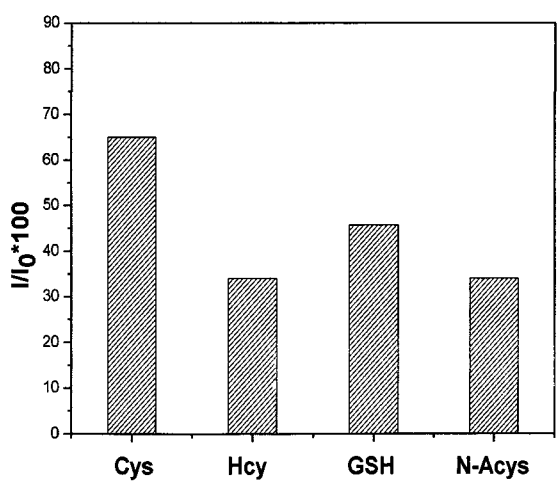

Figure S5.7. Fluorescence emission response of **M1-Cu** towards various bioactive thiols. Concentration of **M1** is 2×10^{-5} M; concentration of bioactive thiols is 4×10^{-5} M.